UNIVERSITE PARIS XIII –SORBONNE PARIS NORD
École doctorale Sciences, Technologies, Santé Galilée

Detection and elimination of Chromium(VI) Application to the removal of industrial liquid effluents

---

THÈSE DE DOCTORAT
présentée par

Son Truong NGUYEN

Laboratoire des Sciences des Procédés et des Matériaux
LSPM-CNRS, UPR 3407, Villetaneuse

pour l'obtention du grade de
DOCTEUR EN SCIENCES POUR L'INGENIEUR

soutenue le 31 Mars 2022 devant le jury d'examen constitué de :

HAMDAN Ahmad, Université de Montréal, Rapporteur

MAGUREANU Monica,National Institute for Lasers,Plasma and Radiation Physics de Bucarest, Rapporteure

HONG Dumpin, Université d'Orléans, Examinateur

SANTOS SOUSA João , Université Paris-Saclay, Examinateur

VEGA GONZALEZ Arlette, Laboratoire des Sciences, des Procédés et des Matériaux , Examinatrice

ROND Cathy, Université Sorbonne Paris Nord , Encadrante

DUTEN Xavier, Université Sorbonne Paris Nord, Directeur de thèse

FORGET Sébastien, Université Sorbonne Paris Nord, Co-directeur de thèse

Acknowledgments

First of all, I want to thank my director of the thesis, Prof. Xavier DUTEN, and Sebastien FORGET for giving me the opportunity to work with them on this Ph.D. project. It has been an educative experience in which I have gained much scientific knowledge in multidisciplinary research fields. Furthermore, it has been an experience that allowed me to develop myself personally.

I would like to thank Arlette VEGA for the best she has given me during my thesis work. She is always ready to help me whenever I need it, and most of all, her contributions have been very valuable to me in completing this work. She also always taught me the skills that I lacked during my work and helped me to grow up and gain more experience. Once again, I would like to express my deep gratitude to Arlette.

I extend my sincerest thanks to my super excellent professor Cathy ROND. Thank you for helping me during the past four years, from the day I arrived in France to do my internship until I finished this doctoral thesis. She is always enthusiastic about guiding me whenever I have difficulties in both life and work. It's challenging to find a professor as enthusiastic as her. She is also an excellent example for me to learn about working and reasoning. Her frankness in work helps me grow up and learn many valuable things. I am very fortunate to work under her guidance. Once again, I would like to thank her for all the wonderful things she has given me and for helping me to complete this thesis.

I would like to thank to RABAT Hervé for his help during the study in the discharge characterization. He is one of the very nice guys, even in life or work. His guidance led me better understand the “black box” in my work, which is not easy to understand.

It would not be possible to perform experiments without the technical assistance of Nicolas FAGNON, Ludovic WILLIAM, and Noël GIRONDON-BOULANDET. Therefore, I want to thank them for their effort in helping me with designing and developing the experimental setup as a very important step of this Ph.D. work.

I want to thank Ovidiu BRINZA for his advice and help during the electrodes characterization process.

I also want to thank the members of the Ph.D. committee, Dunpin HONG, Monica MAGUREANU, Ahmad HAMDAN, Joao SANTOS SOUSA, for their time and valuable comments on my Ph.D. work.

Lastly, I would like to thank the administration, permanents, students, and technicians at LSPM for their kindness and personal support.

I also would like to thank to ANR (Agence Nationale de la Recherche), and CGI (Commissariat à l’Investissement d’Avenir) are gratefully acknowledged for their financial support of this work through Labex SEAM (Science and Engineering for Advanced Materials and devices), ANR-10-LABX-0096 and ANR-18-IDEX-0001

Lời cảm ơn

Thiêng liêng và trân quý nhất xin gửi tặng niềm vui và lời cảm ơn tới hai người bà yêu quý của tôi. Người đã cho tôi những niềm tin, những bài học làm người quý giá và luôn động viên tôi trong suốt những năm tháng tôi hoàn thiện bản thân mình. Ở một nơi xa nào đó tôi biết rằng người vẫn đang dõi theo từng bước chân của tôi trên đường đời và chung vui với niềm vui nhỏ này của tôi.

Xin gửi lời cảm ơn chân thành đến gia đình, những người luôn cho tôi niềm tin và động lực để vượt qua những khó khăn. Cảm ơn hai người ông đáng kính đã luôn dạy dỗ tôi và cho tôi những lời khuyên để tôi nên người. Cảm ơn bố mẹ, người đã sinh tôi ra và dành tất cả những điều tốt đẹp nhất trên cuộc đời này cho tôi. Cảm ơn anh chị em trong gia đình luôn ở bên tôi và động viên tôi. Cảm ơn gia đình đã luôn tin tưởng và hy vọng ở tôi.

Xin cảm ơn em người đã gắn bó với tôi trong suốt những chặng đường tôi đi, người đã cùng tôi vượt qua những khó khăn trong cuộc sống, người đã thấu hiểu và sẻ chia với tôi những niềm vui nỗi buồn. Hơn tất cả xin cảm ơn vì những hy sinh của em cho tôi, xin cảm ơn em đã luôn là hậu phương vững chắc cho tôi yên tâm hoàn thành công việc. Tôi xin gửi lời cảm ơn và chia vui tới người con gái tôi yêu nhất cuộc đời.

Xin gửi lời cảm ơn đến thầy Đỗ Hoàng Tùng, Nguyễn Văn Hảo, những người đã đặt nền móng cho tôi trên con đường và sự nghiệp khoa học, hơn thế nữa thầy luôn dành cho tôi những kiến thức bổ ích giúp tôi có thể giải quyết những khó khăn trong công việc.

Tôi không thể hoàn thành tốt luận án này nếu không có những người anh, người chị, người bạn của tôi ở trường Paris 13 (Sorbonne Paris Nord). Cảm ơn chị Phượng, như người mẹ thứ 2 đối với tôi, chị luôn quan tâm tới các thành viên trong hội và trong đó có cả tôi. Chị luôn động viên và mang những năng lượng tích cực cho tôi. Chị luôn sẵn sàng ở bên tôi lắng nghe tôi chia sẻ mọi niềm vui nỗi buồn. Chị là người gắn kết chúng tôi, từ những con người xa lạ lại có cơ hội để trở thành một hội nhóm mang đầy tình cảm như anh chị em trong nhà. Xin cảm ơn và dành những điều tốt đẹp nhất đến với chị.

Xin gửi lời cảm ơn đến các anh chị bạn bè ở trường Paris 13: Hoàn-Huyền , Việt-Ý , Thái-Hòa, Hiếu, Tuân, Nhật, Thủy, Ky, Trâm, Quang, Long, Thảo, những người đã cho tôi những giây phút vui vẻ hạnh phúc và luôn sát cánh bên tôi.

Xin cảm ơn anh Thi và Thiện, đã cùng tôi trải qua những điều tuyệt vời nhất suốt những năm tháng học tập xa nhà. Hai anh là người anh, người bạn, đã cho tôi nhiều lời khuyên bổ ích và luôn ở bên tôi những khi vui buồn. Cảm ơn đã cho tôi những kỷ niệm thật đáng nhớ nơi đất khách quê người, cho tôi cảm giác của gia đình những khi tôi cần và hơn hết là cho tôi động lực để hoàn thành luận án.

Cuối cùng xin cảm ơn những người bạn của tôi ở châu âu: Dương Trang, Bình Minh, Fodeke, Diệu Thúy, những người đã góp thêm động lực cho tôi và cả những kỷ niệm khó quên.

Contents

Abstract 11

Résumé 12

List of figures 14

List of tables 21

Chapter 1 Introduction and purpose of the work 27

Chapter 2 Bibliographic study and state of the art 31

2.1 General information on Chromium 31

2.1.1 Properties and applications 31

2.1.2 Toxicity and regulation of Chromium VI 33

2.1.3 Chromium VI remediation technologies 34

a. Ion exchange 34

b. Adsorption 35

c. Electrochemical treatment 35

d. Chemical precipitation 37

e. Summary 37

2.1.4 Detection methods 38

a. Atomic absorption spectrometry (AAS) 39

b. High-performance liquid chromatography (HPLC) 39

c. Inductively coupled plasma mass spectrometry (ICP-MS) 40

d. Photometric method 41

e. Summary 42

2.2 Electric discharge in liquid 44

2.2.1 Plasma and electric discharge 44

a. Generalities on Plasma-Liquid Interactions (PLI) 45

b. Plasma discharge above the liquid phase 46

c. Plasma discharges in the liquid phase 47

d. Plasma discharge in multi-phase system 48

2.2.2 Physical and chemical processes in direct PLI 49

a. Physical processes 49

b. Chemical processes in aqueous solution 52

2.3 Chromium (VI) reduction in plasma discharge liquid systems 55

2.3.1 Influence of the chemical parameters 58

a. Initial concentration of hexavalent chromium 58

b. Initial pH 58

c. Effect of OH scavenger 59

d. Influence of hydrogen peroxide 60

2.3.2 Influence of physical parameters 60

2.4 Conclusion 62
Chapter 3 Description of the experimental systems and applied methods 63
3.1 The experimental setup 64
3.1.1 Overall experimental configuration 64
3.1.2 Reactor and electrodes 65
3.2 Data collection and analysis 67
3.2.1 Electrode analysis 67
3.2.2 Shadowgraphy measurements 68
3.2.3 Electrical measurements 69
3.2.4 Chemical analysis 71
a. Colorimetric diagnostics 71
b. Concentration of Cr(VI) 72
c. Concentration of hydrogen peroxide 74
3.3 Reproducibility of the experiments 76
3.3.1 Standard deviation 76
3.3.2 Estimation of uncertainty in repeated measurements 77
3.4 Conclusion 81
Chapter 4 Characterization of the discharge 83
4.1 Single-pulse discharge in water 84
4.1.1 Discharge descriptions using shadowgraphy 84
4.1.2 Electrical waveforms 85
4.1.3 High conductivity results 86
4.2 Discharge in Cr(VI) solution 87
4.2.1 Effect of multi-pulse 90
4.2.2 Effect of applied voltage 93
a. In the case of No breakdown 93
b. In the case of Breakdown 96
4.2.3 Effect of the interelectrode gap 97
4.2.4 Effect of pulse duration 99
a. In the Case of NOBK: 100
b. In the Case of BK 101
4.3 Conclusion 103
Chapter 5 Preliminary studies: discharges in water 105

5.1 Comparison of methods for measuring H_2O_2 106
5.2 Effect of applied voltage on H_2O_2 production 108
5.2.1 Electrical characteristics of the discharge 108
5.2.2 H_2O_2 measurements 109
5.3 Effect of the pulse frequency on the H2O2 production 113
5.4 Effect of pulse duration on the H2O2 production 115
5.5 Effect of Electrode Parameters on H2O2 Formation 117
5.5.1 Effect of different electrode materials on H_2O_2 formation 117
5.5.2 Effect of different electrode diameters and lengths on H_2O_2 production 119
5.6 Effect of the electrolytes on the production of H_2O_2 122
5.7 Erosion of Electrodes 126
5.7.1 In situ length measurements 126
5.7.2 SEM analysis 128
5.8 Conclusion 131
Chapter 6 Reduction of Cr(VI) by PLI 133
6.1 Study of electrode geometry (length & diameter) 135
6.1.1 Effect of electrode parameters on Cr(VI) reduction 135
6.1.2 Effect of electrode parameters on the distribution of BK/NOBK 136
6.1.3 Effect of electrode parameters on the injected energy 138
6.1.4 Effect of electrode parameters on the chemical properties 140
6.1.5 Conclusion 141
6.2 Influence of injected energy 142
6.2.1 Effect of the applied voltage 142
a. Influence of the applied voltage on Cr(VI) reduction for 2 mm gap 142
b. Influence of the applied voltage on Cr(VI) reduction for 5 mm gap 147
c. Conclusion 150
6.2.2 Influence of the gap 150
6.2.3 Effect of pulse frequency 154
6.3 Effect of pulse duration 158
6.3.1 Influence of the pulse duration on Cr(VI) reduction for 2 mm gap 158
6.3.2 Influence of the pulse duration on Cr(VI) reduction for 5 mm gap 162

6.3.3 Comparison and analysis of the results 164
6.4 Comparison of the energy yield with the literature 168
6.5 Conclusion 170
Chapter 7 H_2O_2 formation in Cr(VI) solution 175
7.1 Influence of the applied voltage 176
7.1.1 Influence of the applied voltage on H_2O_2 production for 2 mm gap 176
7.1.2 Influence of the applied voltage on H_2O_2 production for 5 mm gap 178
7.1.3 Comparison and analysis 180
7.2 Influence of applied pulse duration 182
7.2.1 Influence of the pulse duration on H_2O_2 production for 2 mm gap 182
7.2.2 Influence of the pulse duration on H_2O_2 production for 5 mm gap 184
7.2.3 Comparison and analysis 185
7.3 Conclusion 188
Chapter 8 Conclusion & perspectives 189
8.1 Characterization of the discharge 189
8.1.1 Pulse plasma discharge in water 190
8.1.2 H_2O_2 production 190
8.1.3 Electrode erosion 190
8.2 Pulse plasma discharge in Cr(VI) solution 191
8.2.1 Reduction of Cr(VI) 191
8.2.2 Production of H_2O_2 in Cr(VI) solution 192
8.3 Improvement of the detection method 193
8.4 Outlook 194
Annex 195
References 245

Abstract

Chromium is found in many industrial applications, including the production of stainless and refractory steel, pigments, surface treatment, leather tanning. However, this extensive application leads to serious pollution of water sources by Cr(VI), which is considered a CMR agent even at very low concentrations. Therefore, the thorough treatment and accurate measurement of Cr(VI) concentration in our environment is an important and very current issue. Then this project aims to develop a green method for reducing Cr(VI) in an aqueous solution and a high-performance and economical technology to determine [Cr(VI)].

First, we develop a plasma-liquid process to efficiently reduce Cr(VI). It consists of a pin-to-pin electrodes system under high pulsed voltage (about 9 kV, 500 µs, 50 Hz) immersed in the solution to be treated. The electrical discharge initiates the generation of reactive reducing species such as (e_{aq}^-, H^o, H_2O_2), which can diffuse into the liquid phase and reduce dissolved Cr(VI) elements. The experimental setup has been first tested in water to study the production of H_2O_2. Then the reduction of Cr(VI) is studied by varying different physical parameters (applied voltage, inter-electrode distance, applied frequency, and pulse duration). Moreover, to better understand the reduction process of Cr(VI), the production of hydrogen peroxide in Cr(VI) solution is studied. The results show that Cr(VI) is completely reduced after 90 minutes for reference conditions (9 kV, 0.5 mm gap, 50 Hz, and 500 µs) with an energy yield of 4.7×10^{-4} g/kJ. The reduction of Cr(VI) increases with the increase of injected energy (by increasing applied voltage), the number of pulses, the number of breakdowns and the pulse duration. Finally, the more H_2O_2 generated, the higher the Cr(VI) reduction. However, the results also suggest that H_2O_2 is not the only responsible for the reduction process of Cr(VI) by the PLI method.

The second objective of this thesis is to develop an innovative method for measuring Cr(VI) at low concentrations. The approach is based on measuring the absorbance of Cr(VI) using a LED source at 365 nm. The results show that using this method allows analyzing the concentration of Cr(VI) in real-time and *in situ* during the treatment process. Moreover, this method can also define when Cr(VI) is completely reduced.

Résumé

Le chrome est présent dans de nombreuses applications industrielles, notamment la production d'acier inoxydable et réfractaire, les pigments, le traitement de surface, le tannage du cuir. Toutefois, cette application extensive entraîne une grave pollution des sources d'eau par le Cr(VI), qui est considéré comme un agent CMR même à très faible concentration. Par conséquent, le traitement et la mesure précise de la concentration de Cr(VI) dans notre environnement est une problématique actuelle très importante. Ainsi ce projet vise à développer une méthode verte pour réduire le Cr(VI) dans une solution aqueuse et une technologie performante et économique pour mesurer le [Cr(VI)].

Tout d'abord, nous développons un procédé de plasma dans un liquide pour réduire efficacement le Cr(VI). Il s'agit d'un système d'électrodes pointe-pointe sous haute tension pulsée (environ 9 kV, 500 µs, 50 Hz) immergé dans la solution à traiter. La décharge électrique initie la génération d'espèces réductrices réactives telles que (e_{aq}^-, H^o, H_2O_2), qui peuvent diffuser dans la phase liquide et initier la réduction des éléments dissous de Cr(VI). Le dispositif a d'abord été utilisé dans l'eau pour étudier la production de H_2O_2. Puis une étude paramtérique de la réduction du Cr(VI) est réalisée sur différents paramètres physiques (tension appliquée, distance inter-électrodes, fréquence et durée d'impulsion). De plus, pour mieux comprendre le processus de réduction du Cr(VI), la production de peroxyde d'hydrogène dans une solution de Cr(VI) est étudiée. Les résultats montrent que le Cr(VI) est complètement réduit après 90 minutes pour les conditions de référence (9 kV, 0,5 mm d'écart, 50 Hz et 500 µs) avec un rendement énergétique de $4{,}7\times10^{-4}$ g/kJ. La réduction du Cr(VI) a augmenté avec l'augmentation de l'énergie injectée (en augmentant la tension appliquée), le nombre d'impulsions, le nombre de claquages et la durée des impulsions. Enfin, plus la quantité de H_2O_2 générée était importante, plus la réduction du Cr(VI) était élevée. Cependant, les résultats suggèrent également que H_2O_2 n'est pas la seule responsable de la réduction du Cr(VI).

Le second objectif de cette thèse est de développer une méthode de mesure innovante pour mesurer le Cr(VI) à de faibles concentrations. L'approche est basée sur la mesure de l'absorbance du Cr(VI) à l'aide d'une source LED à 365 nm. Les résultats montrent que l'utilisation de cette méthode permet de mesurer la concentration de Cr(VI) en temps réel et *in situ* pendant le processus de traitement. De plus, cette méthode permet également de définir le moment où le Cr(VI) est complètement réduit.

List of figures

Figure 2.1 Contributing sectors to chromium fluxes to water in 2017[9] 32
Figure 2.2 Cr(VI) speciation in an aqueous environment as a function of pH [17] 33
Figure 2.3 Utilization of various analytical techniques for the determination of hexavalent chromium since 2006, *i.e.* Flame atomic absorption spectrometry (FAAS), Graphite furnace atomic absorption spectroscopy (GFAAS), Electrothermal atomic absorption spectroscopy (ETAAS), High-performance liquid chromatography/gas chromatography (HPLC/GC), and Inductively coupled plasma (ICP) [63] 38
Figure 2.4 Atomic absorption spectrometer block diagram [55] 39
Figure 2.5 High-Performance Liquid Chromatography [HPLC] system [84] 40
Figure 2.6 Basic instrument components of the ICP-MS [95] 41
Figure 2.7 Types of discharge above the liquid phase: (a) pin-to-water, (b) multi-pin-to-water, (c) wire-to-water, (d) plasma jet [143] 46
Figure 2.8 Types of plasma discharge inside liquid reactors: (a) pin-to-pin, (b) pin-to-plate, (c) multi-pin-to-plate, (d) brush-to-plate [143] 47
Figure 2.9 Schematic illustration of solution plasma and their chemical species [149] 48
Figure 2.10 Types of bubble discharge reactors: (a) upward nozzle electrode-to-plate, (b) upward nozzle containing needle electrode-to-plate, (c) hole containing needle electrode-to-plate, (d) downward nozzle electrode-to-plate [143] 49
Figure 2.11 Images of typical streamers modes [169] 51
Figure 3.1 Schematic diagram of the experimental setup. 64
Figure 3.2 Schematic diagram of the optical diagnostics in water with IDS camera [202] 67
Figure 3.3 Schematic diagram of the optical diagnostics in Cr(VI) 68
Figure 3.4 (a) Voltage and current signals and (b) a zoom of a pin-to-pin discharge in Cr(VI) solution ([Cr(VI)]=47 mg/L; σ=4 mS/cm; pH=2.4) monitored for applied voltage of 10 kV, Δt = 500 µs and gap=2 mm 69
Figure 3.5 Energy per pulse of a pin-to-pin discharge in Cr(VI) solution ([Cr (VI)]=47 mg/L; σ=4 mS/cm; pH=2.4) monitored for applied voltage of 10 kV, Δt= 500µs and gap=2 mm 70
Figure 3.6. Illustration of a cuvette explaining the Beer-Lamberts law [204] 71
Figure 3.7 UV-vis absorption spectrum of Cr(VI) solution ([Cr(VI) = 40 mg/L) 72
Figure 3.8 UV-vis absorption spectrum of the complex of Cr(VI) ([Cr(VI) = 0.01 mg/L) with DPC 73
Figure 3.9 Schematic diagram of the experimental setup for direct *in situ* [Cr(VI)] measurement 74
Figure 3.10 Concentration of Cr(VI) as a function of time with several repeated experiments. U = 9 kV, Δt = 500 µs, f =50 Hz, 2 mm gap, electrodes length = 0 ± 10 µm, (47 mg/L,σ=4 mS/cm,pH=2.4) 78
Figure 3.11 Realtion of [Cr(VI)] uncertainty as a function of concentration obtained by several repeated experiements. U = 9 kV, Δt = 500 µs, f =50 Hz, 2 mm gap, electrodes length = 0 ± 10 µm, (47 mg/L,σ=4 mS/cm,pH=2.4) 79

Figure 4.1 Time-resolved schlieren measurements of a pin-to-pin discharge obtained in water (σ=100 μS/cm) for 9 kV and 12 kV - the voltage pulse duration equals 1 ms, and the camera resolutions are 128x32 pixels and Δt=1.75 μs [175]. 84
Figure 4.2 Voltage and current signals of a single pin-to-pin discharge in water (σ=100μS/cm) monitored for applied voltages of 500 μs (a) 9 kV and (b) 12 kV [175] 85
Figure 4.3 Schlieren images for double regime obtained for σ = 1500 μS/cm (U = 12 kV) (exposure time 1 μs)[177] 86
Figure 4.4 Examples of case NOBK and case BK of a pin-to-pin single discharge obtained in Cr(VI) solution (47 mg/L,σ=4 mS/cm,pH=2.4) for 11 kV, Δt=500 μs, gap = 2 mm, electrodes length = 0±10 μm, the camera resolutions are 128x80 pixels and Δt=2.7 μs. 88
Figure 4.5 Voltage and current signals for (a) case 1 NOBK and a zoomand (b) case 2 BK and a zoom of a pin-to-pin single discharge obtained in Cr(VI) solution (47 mg/L,σ=4 mS/cm,pH=2.4) for 11 kV, Δt=500 μs, gap = 2 mm, electrodes length = 0±10 μm 89
Figure 4.6 Pin-to-pin single discharges obtained in Cr(VI) solution (47 mg/L,σ=4 mS/cm,pH=2.4) for BK experiments (U=12,5 kV) with three successive imaging measurements. V = 100 mL, gap = 2 mm, electrodes length = 0±10 μm. 90
Figure 4.7 Time-resolved shadowgraphy measurements of multi-pulse and single-pulse with NOBK and BK of a pin-to-pin discharge obtained in Cr(VI) solution (47 mg/L, σ=4 mS/cm,pH=2.4) for 11 kV , V = 100 mL, Δt = 500 μs, gap = 2 mm, electrodes length = 0±10 μm, f = 50 Hz for multi-pulse 91
Figure 4.8 Voltage and current signals for (a) case 1 NOBK and a zoom, (b) case 2 BK and a zoom for multi-pulse and single-pulse modes, of a pin-to-pin discharge obtained in Cr(VI) solution (47 mg/L,σ=4 mS/cm,pH=2.4) for 11 kV, V = 100 mL, Δt = 500 μs, gap = 2 mm, electrodes length = 0±10 μm, f = 50 Hz for multi-pulse 92
Figure 4.9 Time-resolved shadowgraphy measurements of a pin-to-pin discharge obtained in Cr(VI) solution (47 mg/L,σ=4 mS/cm,pH=2.4) for 7, 9, 10 and 11 kV, V = 100 mL, Δt = 500 μs, gap = 2 mm, electrodes length = 0±10 μm, f = 50 Hz and the camera resolutions are 128x80 pixels and Δt=2.7 μs. The red star presents the maximum size of the bubbles. 94
Figure 4.10 (a) Voltage and (b) current signals of a pin-to-pin discharge for case NOBK in Cr(VI) solution (47 mg/L,σ=4 mS/cm,pH=2.4) for 7, 9, 10, and 11 kV. V = 100 mL, Δt = 500 μs, gap = 2 mm, electrodes length = 0±10 μm, f = 50 Hz. (See annex 4.2.2 (a) for the signals with high time resolution). 95
Figure 4.11 Time-resolved ombroscopy measurements of a pin-to-pin discharge obtained in Cr(VI) solution (47 mg/L,σ=4 mS/cm,pH=2.4) for 7, 9, 10 and 11 kV respectively, V = 100 mL, Δt = 500 μs, gap = 2 mm, electrodes length = 0±10 μm, f = 50 Hz and the camera resolutions are 128x80 pixels and Δt=2.7 μs. 96
Figure 4.12 (a) Voltage and current signals and (b) a zoom of a pin-to-pin discharge in Cr(VI) solution (47 mg/L,σ=4 mS/cm,pH=2.4) for 9, 10, and 11 kV, V = 100 mL, Δt = 500 μs, gap = 2 mm, electrodes length = 0±10 μm, f = 50 Hz. (See annex 4.2.2 (b) for signals with high time resolution) 97

Figure 4.13 The time-resolved shadowgraphy measurements of a pin-to-pin discharge obtained in Cr(VI) solution (47 mg/L,σ=4 mS/cm,pH=2.4) for 7 kV and 11 kV and 2 different gaps V = 100 mL, Δt = 500 µs, electrodes length = 0±10 µm, f = 50 Hz.....98
Figure 4.14 Voltage and current signals of a pin to pin discharge in Cr(VI) solution (47 mg/L,σ=4 mS/cm,pH=2.4) for (a) 7 kV and (b) 11 kV with gap of 2 and 5 mm, V = 100 mL, Δt = 500 µs, electrodes length = 0±10 µm, f = 50 Hz. (See annex 4.2.3 for signals with high time resolution)99
Figure 4.15 The time-resolved shadowgraphy measurements of a pin-to-pin discharge obtained in Cr(VI) solution (47 mg/L,σ=4 mS/cm,pH=2.4) for different pulse durations with U = 9 kV V = 100 mL, gap = 5 mm, electrodes length = 0±10 µm, f = 50 Hz. Red stars identify the maximum radius.....100
Figure 4.16 (a) Voltage and current signals and (b) a zoom of 9 kV discharge in Cr(VI) solution (47 mg/L,σ=4 mS/cm,pH=2.4) for different pulse durations with U = 9 kV, V = 100 mL, gap = 5 mm, electrodes length = 0±10 µm, f = 50 Hz. (See annex 4.2.4 (a) for signals with high time resolution) 101
Figure 4.17 The time-resolved shadowgraphy measurements of a pin-to-pin discharge obtained in Cr(VI) solution (47 mg/L,σ=4 mS/cm,pH=2.4) for different pulse duration with U = 11 kV V = 100 mL, gap = 2 mm, electrodes length = 0±10 µm, f = 50 Hz. Red stars show the maximum radius.....101
Figure 4.18 (a) Voltage and current signals and (b) a zoom of 11 kV discharge in Cr(VI) solution (47 mg/L,σ=4 mS/cm,pH=2.4) for different pulse duration. V = 100 mL, gap = 2 mm, electrodes length = 0±10 µm, f = 50 Hz.....102
Figure 5.1 H_2O_2 concentration as a function of time measurement by two different methods using NH_4VO_3 (Vasko's method) and $TiOSO_4$ (Eisenberg's method). V=200 mL, f=50 Hz, Δt=500 µs, 2 mm of gap, Voltage = 6 kV, σ=200 µS/cm. Uncertainty of H_2O_2 concentration is 15 %.....107
Figure 5.2 Typical electrical waveforms of pin-to-pin discharge generated in water V = 200 mL, f = 50 Hz, Δt = 500 µs, 2 mm of gap, and σ = 200 µS/cm); (a) Voltage and Current signals and (b) Time evolution of the energy per pulse [202].....109
Figure 5.3 Hydrogen peroxide concentration for three different cases (applied voltages). (a) Concentration of H_2O_2 as a function of time. (b) Final concentration of H_2O_2 as a function of total injected energy (measured after 30 min) (V = 200 mL, f = 50 Hz, Δt = 500 µs, 2 mm of gap, σ = 200 µS/cm). Uncertainties of [H_2O_2] and energy are 15 % and 10%, respectively.....110
Figure 5.4 H_2O_2 concentration according to the total energy for 2 different cases of pin-to-pin discharge generated in water (V = 200 mL, Δt = 500 µs, 2 mm of gap, σ = 200 µS/cm) – couples "frequency-applied voltage" are reported. Uncertainties of [H_2O_2] and energy are 15 % and 10%, respectively.....113
Figure 5.5 H_2O_2 production measured for different pulse durations (Δt =50, 100, 500 µs) and reported for 2 different cases of pin-to-pin discharge generated in water. V = 200 mL, f = 50 Hz, 2 mm of gap, σ= 200 µS/cm, Time of process 30 min. Uncertainty of [H_2O_2] is 15 %.....115
Figure 5.6 The effect of electrode material on the production of H_2O_2 by pin-to-pin discharge generated in water (V = 200 mL, f = 50 Hz, Δt = 500 µs, 2 mm of gap, σ = 200 µS/cm). HV means anode, and GND is for the cathode. Duration is 30 min except for Platinum 6 and 9 kV (10 min). Uncertainty on [H_2O_2] is 15 %.....118

Figure 5.7 Hydrogen peroxide concentration for different applied voltages (6 and 9 kV) with different electrodes (lengths and diameter) after 30 minutes of pin-to-pin discharge generated in water. V = 200 mL, f = 50 Hz, Δt = 500 µs, 2 mm gap σ = 200 µS/cm, Ø = 100 µm for W electrodes with the length = 400 µm, Ø = 200 µm for Pt electrodes with the length = 0 µm). Uncertainty of [H_2O_2] (15 %) 120
Figure 5.8 Distribution of energy per pulse of pin-to-pin discharge generated in water at 9 kV for different conductivities and electrolytes, V = 100 mL - σ = 200 µS/cm adjusted by NaCl, V = 200 mL - σ = 4 mS/cm adjusted by NaCl and H_2SO_4 0.1 M. f = 50 Hz, 2 mm of gap, Δt = 500 µs, HV-0-Pt and GND-0-Pt, Ø = 200 µm 123
Figure 5.9 Time evolution of H_2O_2 concentration for two different electrolyte solutions. The red curve presents the results of the solution with H_2SO_4, and the black curve for the solution with NaCl. V=100 mL, f = 50 Hz, Δt = 500 µs, 2 mm of gap, Voltage = 9 kV, σ = 4 mS/cm). HV-0-Pt and GND-0-Pt, Ø = 200 µm (HV means anode, and GND is for cathode). Uncertainty of H_2O_2 concentrations is 15 % 125
Figure 5.10 Variation of normalized length of anode and cathode electrodes as a function of time, (a) tungsten electrodes, (b) platinum electrodes (V = 150 mL, f = 50 Hz, Δt = 500 µs, 2 mm of gap, σ = 200 µS/cm). Uncertainty of equipment is not discernable (2 %)..... 127
Figure 5.11 SEM images of the eroded tip of tungsten and platinum electrodes after the electrical discharge obtained for (a) case 1 (4 kV), (b) case 2 (6 kV) and (c) case 3 (9 kV), anode and cathode are shown on left and right respectively (V = 150 mL, f = 50 Hz, Δt = 500 µs, 2 mm of gap, and σ = 200 µS/cm) with a ×500 magnification 129
Figure 5.12 SEM images of the eroded tip of tungsten and platinum electrodes after the electrical discharge obtained for (a) case 1 (4 kV), (b) case 2 (6 kV) and (c) case 3 (9 kV), anode and cathode are shown on left and right respectively (V = 150 mL, f = 50 Hz, Δt = 500 µs, 2 mm of gap, and σ = 200 µS/cm) with a ×1000 magnification..... 130
Figure 6.1 Concentration of Cr(VI) as a function of time for different electrodes lengths (0, 100, 400 µm) and for two diameters (a) Ø = 100 µm and (b) Ø = 200 µm. Cr(VI) solution (47 mg/L,σ=4 mS/cm,pH=2.3), V = 100 mL , U = 9 kV, f = 50 Hz, Δt = 500 µs, gap = 2 mm..... 135
Figure 6.2 Time evolution of injected energy per pulse for the HV-0, GND-0, (a) Ø = 100 µm and (b) Ø = 200 µm. Cr(VI) solution (47 mg/L,σ=4 mS/cm,pH=2.3), V = 100 mL , U = 9 kV, f = 50 Hz, Δt = 500 µs, gap = 2 mm. 137
Figure 6.3 Concentration of Cr(VI) as a function of time of a pin-to-pin discharge obtained in Cr(VI) solution (47 mg/L,σ=4 mS/cm,pH=2.3) for 2, 7, 9, 10, 11 and 12 kV, V = 100 mL, Δt = 500 µs, gap = 2 mm, electrodes length = 0±10 µm, f = 50 Hz. 143
Figure 6.4 Time evolution of the injected energy per pulse for the different applied voltage from 7 kV to 12 kV. Cr(VI) solution (47 mg/L,σ=4 mS/cm,pH=2.3), V = 100 mL, Δt = 500 µs, gap = 2 mm, electrodes length = 0±10 µm, f = 50 Hz 143

Figure 6.5 Concentration of Cr(VI) as a function of time of a pin-to-pin discharge obtained in Cr(VI) solution (47mg/L, σ=4 mS/cm,pH=2.4) for 7, 8, 9, and 10 kV respectively, V = 100 mL,Δt = 500 μs, gap = 2 mm, electrodes length = 0±10 μm, f = 50 Hz. 148
Figure 6.6 Time evolution of the injected energy per pulse for the different applied voltages from 7 kV to 10 kV. Cr(VI) solution (47 mg/L,σ=4 mS/cm,pH=2.3-2.4), V = 100 mL, Δt = 500 μs, gap = 5 mm, electrodes length = 0±10 μm, f = 50 Hz..... 149
Figure 6.7 Concentration of Cr(VI) as a function of time of a pin-to-pin discharge obtained in Cr(VI) solution (σ=4 mS/cm) for differents gaps, U= 9 kV, Cr(VI) solution (47 mg/L,σ=4 mS/cm,pH=2.4), V = 100 mL, Δt = 500 μs, electrodes length = 0±10 μm, f = 50 Hz. The uncertainty of [Cr(VI)] is 20 %. It is noted that last values for 1 and 1.5 mm are given for 110 min. 151
Figure 6.8 Time evolution of the injected energy per pulse for the different gaps from 0.5 mm to 5 mm. U= 9 kV, Cr(VI) solution (47 mg/L,σ=4 mS/cm,pH=2.4), V = 100 mL, Δt = 500 μs, electrodes length = 0±10 μm, f = 50 Hz..... 152
Figure 6.9 Concentration of Cr(VI) as a function of time (a) and pulse number (b) of a pin-to-pin discharge obtained in Cr(VI) solution (47 mg/L,σ=4 mS/cm,pH=2.4) for different pulse frequencies, U = 8 kV, V = 100 mL, Δt = 500 μs, gap = 2 mm, electrodes length = 0±10 μm. 154
Figure 6.10 Time evolution of the injected energy per pulse for the different frequencies from 10 Hz to 70 Hz. U= 8 kV, (47 mg/L,σ=4 mS/cm,pH=2.4), V = 100 mL, Δt = 500 μs, electrodes length = 0±10 μm, gap = 2 mm. The different times correspond to the same number of pulses equal to 324000 for 10 Hz and 315000 for 25, 50 and 70 Hz. 155
Figure 6.11 Concentration of Cr(VI) as a function of time of a pin-to-pin discharge obtained in Cr(VI) solution (47 mg/L,σ=4 mS/cm,pH=2.4) for different pulse durations, U = 9 kV, V = 100 mL, gap = 2 mm, electrodes length = 0±10 μm, f = 50 Hz. 159
Figure 6.12 Time evolution of the injected energy per pulse for the different pulse duration from 10 μs to 1 ms. U = 9 kV, Cr(VI) solution (47 mg/L,σ=4 mS/cm, pH=2.4) V = 100 mL, Δt = 500 μs, gap = 2 mm, electrodes length = 0±10 μm. 159
Figure 6.13 Concentration of Cr(VI) as a function of time of a pin-to-pin discharge obtained in Cr(VI) solution (47 mg/L, σ=4 mS/cm, pH=2.3) for different pulse durations, U = 9 kV, V = 100 mL, gap = 5 mm, electrodes length = 0±10 μm, f = 50 Hz. 162
Figure 6.14 Time evolution of the injected energy per pulse for the different pulse durations from 10 μs to 1 ms. U = 9 kV, Cr(VI) solution (47 mg/L, σ=4 mS/cm, pH=2.3), V = 100 mL, Δt = 500 μs, gap = 5 mm, electrodes length = 0±10 μm, f = 50 Hz. 163
Figure 6.15 Energy yield versus pulse duration (a) and log scale (b) for 2 and 5 mm gap of a pin-to-pin discharge obtained in Cr(VI) solution (47 mg/L, σ=4 mS/cm, pH=2.4) U = 9 kV, V = 100 mL, f = 50 Hz, electrodes length = 0±10 μm. 166
Figure 6.16 Final solution conductivity versus pulse duration for 2 and 5 mm gap of a pin-to-pin discharge obtained in Cr(VI) solution (47 mg/L, σ=4 mS/cm, pH=2.4) U = 9 kV, V = 100 mL, f = 50 Hz, electrodes length = 0±10 μm 166

Figure 7.1 The concentration of (a) H_2O_2 and (b) Cr(VI) as a function of time of a pin-to-pin discharge obtained in Cr(VI) solution (47 mg/L, σ = 4 mS/cm, pH = 2.4) for 7, 9, and 10 kV, V = 100 mL, Δt = 500 μs, gap = 2 mm, electrodes length = 0±10 μm, f = 50 Hz. The uncertainty of [H_2O_2] is 15 %. 176
Figure 7.2 The concentrations of (a) H_2O_2 and (b) Cr(VI) as a function of time of a pin-to-pin discharge obtained in Cr(VI) solution (47 mg/L, σ = 4 mS/cm, pH = 2.4) for 7, 8, 9, and 10 kV, respectively, V = 100 mL, Δt = 500 μs, gap = 5 mm, electrodes length = 0±10 μm, f = 50 Hz. The uncertainty of [H_2O_2] is 15 %. 179
Figure 7.3 Concentration of Cr(VI) as a function of [H_2O_2] for different applied voltages and gaps by pin-to-pin discharge in Cr(VI) solution (47 mg/L, σ = 4 mS/cm, pH = 2.4). V = 100 mL, Δt = 500 μs, electrodes length = 0±10 μm, f = 50 Hz - measurements performed at 15, 45, 90 and 120 minutes.....181
Figure 7.4 The concentrations of (a) H_2O_2 and (b) Cr(VI) as a function of time of a pin-to-pin discharge obtained in Cr(VI) solution (47 mg/L, σ = 4 mS/cm, pH = 2.4) for different pulse durations after 120 minutes. U = 9 kV, V = 100 mL, gap = 2 mm, electrodes length = 0±10 μm, f = 50 Hz. The uncertainty of [H_2O_2] is 15 %,.....183
Figure 7.5 The concentration of (a) H_2O_2 and (b) Cr(VI) as a function of time of a pin-to-pin discharge obtained in Cr(VI) solution (47 mg/L, σ = 4 mS/cm, pH = 2.4) for different pulse durations after 120 minutes. U = 9 kV, V = 100 mL, gap = 5 mm, electrodes length = 0±10 μm, f = 50 Hz. The uncertainties of [Cr(VI)] and [H_2O_2] are 20 % and 15 %, respectively 184
Figure 7.6 Concentration of H_2O_2 versus pulse duration for 2 and 5 mm gap of a pin-to-pin discharge obtained in Cr(VI) solution (47 mg/L, σ = 4 mS/cm, pH = 2.4) after 120 minutes. U = 9 kV, V = 100 mL, electrodes length = 0±10 μm, f = 50 Hz. The uncertainties of [H_2O_2] is 15 % 186
Figure 7.7 Cr(VI) concentration as a function of H_2O_2 formation by pin-to-pin discharge in Cr(VI) solution (47 mg/L, σ = 4 mS/cm, pH = 2.4) for different pulse durations and gaps. U = 9 kV, V = 100 mL, electrodes length = 0±10 μm, f = 50 Hz - measurements performed at 15, 45, 90 and 120 minutes are reported.....186

List of tables

Table 2.1 The reduction efficiency of Cr(VI) for different activated carbons based on size and shape - PAC=powder-activated carbon, GAC=granular-activated carbon, ACF=activated carbon fibers 35
Table 2.2 Advantages and disadvantages of various Cr(VI) removal techniques 37
Table 2.3 The advantages, disadvantages, and limitations of various analytical techniques to the determination of chromium 43
Table 2.4 Application of non-thermal plasma for reduction of Cr(VI) (*these values are recalculated in this work using Equation 11) 57
Table 3.1 Standard deviation and uncertainty of repeated experiments for Cr(VI) experiments. U = 9 kV, Δt = 500 µs, f =50 Hz, 2 mm gap, electrodes length = 0±10 µm, ([Cr(V)] = 47 mg/L,σ=4 mS/cm,pH=2.4) 80
Table 3.2 Standard deviation and uncertainty of repeated experiments for [H_2O_2] measurement. U = 9 kV, Δt = 500 µs, f =50 Hz, 2 mm gap, electrodes length = 400±30 µm, (in water, σ=200 σS/cm,pH=5.9) 80
Table 4.1 Distribution of cases BK / NOBK according to the applied voltage of multi-pulse pin-to-pin discharges obtained in Cr(VI) solution (47 mg/L,σ=4 mS/cm,pH=2.4) Δt=500 µs, gap = 2 mm, electrodes length = 0±10 µm, f = 50 Hz. 93
Table 5.1 Average energy per pulse and total injected energy after 30 minutes for three different cases of pin-to-pin discharge generated in water. V = 200 mL, f = 50 Hz, Δt = 500 µs, 2 mm of gap, and σ = 200 µS/cm 109
Table 5.2. Hydrogen peroxide production rate and energy yields for three different cases after 30 minutes of pin-to-pin discharge generated in water. V = 200 mL, f = 50 Hz, Δt = 500 µs, 2 mm of gap, and σ = 200 µS/cm 111
Table 5.3 Initial and final solution parameters obtained from ex situ pH and conductivity measurements for three different cases after 30 minutes of pin-to-pin discharge generated in water. V = 200 mL, f = 50 Hz, Δt = 500 µs, 2 mm of gap, and σ = 200 µS/cm. 112
Table 5.4 Initial and final solution parameters obtained from ex situ pH and conductivity measurements for case 2 and case 3 with different applied frequencies after 30 minutes of pin-to-pin discharge generated in water. V = 200 mL, Δt = 500 µs, 2 mm of gap, and σ = 200 µS/cm 114
Table 5.5 Initial and final solution parameters obtained from ex situ pH and conductivity measurements for cases 2 and 3 with different applied pulse duration after 30 minutes of pin-to-pin discharge generated in water. V = 200 mL, f = 50 Hz, 2 mm of gap, and σ = 200 µS/cm. 116
Table 5.6 Initial and final solution parameters obtained from ex situ pH and conductivity measurements for 4,6 and 9 kV after 30 minutes of pin-to-pin discharge generated in water. V = 200 mL, f = 50 Hz, 2 mm of gap, and σ = 200 µS/cm, HV-Pt and GND-W (HV means anode and GND is for cathode) 119
Table 5.7 Initial and final solution parameters obtained from ex situ pH and conductivity measurements for 6 and 9 kV after 30 minutes of pin-to-pin discharge generated in water. V = 200 mL, f = 50 Hz, 2 mm

of gap, and σ = 200 µS/cm Δt = 500 µs, Ø = 100 µm for W with the length = 400 µm ,Ø = 200 µm for Pt electrodes with the length = 0 µm (HV means anode and GND is for cathode)..... 121
Table 5.8 Initial and final solution parameters obtained from ex situ pH and conductivity measurements according to the electrolytes. The final values are obtained after 30 minutes of pin-to-pin discharge generated in water. (a) V = 200 mL σ = 200 µS/cm , (b) and (c) V = 100 mL and σ = 4 mS/cm. f = 50 Hz, 2 mm of gap, U = 9 kV , Δt = 500 µs 122
Table 5.9 Effect of the conductivity on H_2O_2 production of pin-to-pin discharge generated in water at 9 kV after 30 minutes, f = 50 Hz, 2 mm of gap, Δt = 500 µs, HV-0-Pt and GND-0-Pt, Ø = 200 µm (a) σ = 200 µS/cm adjust by NaCl, V= 200 mL (b) σ = 4 mS/cm adjust by NaCl, V = 100 mL (b) and (c) σ = 4 mS/cm adjust by H_2SO_4 0.1 M, V= 100 mL, HV means anode and GND is for cathode)..... 124
Table 6.1 Concentration of Cr(VI) species in the initial solution. Estimated by Visual Minteq[246] software with the initial concentration of Cr(VI) = 47 mg/L (9×10^{-4} mol/L), pH = 2.4. 133
Table 6.2 Reduction efficiency after 120 minutes for the discharge with different electrodes lengths and diameters. Cr(VI) solution (47 mg/L, σ=4 mS/cm, pH=2.3), V = 100 mL , U = 9 kV, f = 50 Hz, Δt = 500 µs, gap = 2 mm. 136
Table 6.3 Ratio of BK/ NOBK after 120 minutes for the discharge with different lengths and diameters of the electrodes. Cr(VI) solution (47 mg/L,σ=4 mS/cm,pH=2.3). V = 100 mL , U = 9 kV, f = 50 Hz, Δt = 500 µs, gap = 2 mm 137
Table 6.4 Part of the electrodes HV/GND eroded after 120 minutes (in %) for the discharge with different lengths and diameters of the electrodes. Cr(VI) solution (47 mg/L,σ=4 mS/cm,pH=2.3), V = 100 mL , U = 9 kV, f = 50 Hz, Δt = 500 µs, gap = 2 mm 138
Table 6.5 The total injected enery after 120 minutes for the discharge with different lengths and diameters of the electrodes. Cr(VI) solution (47 mg/L,σ=4 mS/cm,pH=2.3). V = 100 mL, U = 9 kV, f = 50 Hz, Δt = 500 µs, gap = 2 mm..... 139
Table 6.6 Energy yield in g/kJ after 120 minutes for the discharge with different lengths and diameters of the electrodes. Cr(VI) solution (47 mg/L,σ=4 mS/cm,pH=2.3), V = 100 mL , U = 9 kV, f = 50 Hz, Δt = 500 µs, gap = 2 mm 139
Table 6.7 Initial and final (after 120 minutes) solution parameters obtained from ex situ pH and conductivity measurements for 9 kV with different lengths and diameters. Cr(VI) solution (47 mg/L,σ=4 mS/cm,pH=2.3), V = 100 mL, f = 50 Hz, Δt = 500 µs, gap = 2 mm..... 140
Table 6.8 Characteristics of the experiments Ø = 200 µm - HV-0 - GND-0 after 120 minutes Cr(VI) solution (47 mg/L,σ=4 mS/cm,pH=2.3), V = 100 mL , U = 9 kV, f = 50 Hz, Δt = 500 µs, gap = 2 mm 141
Table 6.9 Influence of applied voltage on Cr(VI) reduction efficiency and the discharge characteristics. Cr(VI) solution (47 mg/L,σ=4 mS/cm,pH=2.3), V = 100 mL, Δt = 500 µs, gap = 2 mm, electrodes length = 0±10 µm, f = 50 Hz. * these values are calculated with different durations (1:105 min, 2:90 min, and 3: 70 min)..... 144

Table 6.10 Initial and final solution parameters obtained from ex situ pH and conductivity measurements for the different applied voltages. Cr(VI) solution (47 mg/L,σ=4 mS/cm,pH=2.3-2.4),. V = 100 mL, Δt = 500 μs, gap = 2 mm, electrodes length = 0±10 μm, f = 50 Hz 147
Table 6.11 Influence of applied voltage on Cr(VI) reduction efficiency and the discharge characteristic after 120 minutes. Cr(VI) solution (47 mg/L,σ=4 mS/cm,pH=2.4), V = 100 mL, Δt = 500 μs, gap = 5 mm, electrodes length = 0±10 μm, f = 50 Hz 149
Table 6.12 Initial and final solution parameters obtained from ex situ pH and conductivity measurements for the different applied voltages. Cr(VI) solution (47 mg/L,σ=4 mS/cm,pH=2.4) V = 100 mL, f = 50 Hz, Δt = 500 μs, for 5 mm of gap. 150
Table 6.13 Influence of the gap on Cr(VI) reduction efficiency and the discharge characteristic after 90 minutes. U= 9 kV, Cr(VI) solution (47 mg/L,σ=4 mS/cm,pH=2.4), V = 100 mL, Δt = 500 μ, electrodes length = 0±10 μm, f = 50 Hz 153
Table 6.14 Initial and final solution parameters obtained from ex situ pH and conductivity measurements for the different gaps. Cr(VI) solution (47 mg/L,σ=4 mS/cm,pH=2.4), U = 9 kV, V = 100 mL, f = 50 Hz, Δt = 500 μs. 153
Table 6.15 Influence of applied pulse frequencies on Cr(VI) reduction efficiency and the discharge characteristic. U= 8 kV, (47 mg/L,σ=4 mS/cm,pH=2.4), V = 100 mL, Δt = 500 μs, electrodes length = 0±10 μm, gap = 2 mm, number of pulses of 315 000 (except for 10 Hz that is 324 000) 156
Table 6.16 The distribution of BK/NOBK during first 30 minutes of time of a pin-to-pin discharge obtained in Cr(VI) solution (47 mg/L, σ=4 mS/cm, pH=2.4) for different pulse durations, U = 9 kV, V = 100 mL, gap= 2 mm, electrodes length =0±10 μm, f = 50 Hz 160
Table 6.17 Influence of pulse duration on Cr(VI) reduction efficiency and the discharge characteristics. U = 9 kV, Cr(VI) solution (47 mg/L, σ=4 mS/cm, pH=2.4), V = 100 mL, Δt = 500 μs, gap = 2 mm, electrodes length = 0±10 μm, f = 50 Hz. 160
Table 6.18 Initial and final solution parameters obtained from ex situ pH and conductivity measurements for the different pulse duration after 120 minutes. Cr(VI) solution (47 mg/L, σ=4 mS/cm, pH=2.4) U = 9 kV, V = 100 mL, f = 50 Hz, gap = 2 mm, electrodes length = 0±10 μm 161
Table 6.19 Influence of pulse duration on Cr(VI) reduction efficiency and the discharge characteristic after 120 minutes. Cr(VI) solution (47 mg/L, σ=4 mS/cm, pH=2.3), U = 9 kV, V = 100 mL, gap =5 mm, electrodes length = 0±10 μm, f = 50 Hz 164
Table 6.20 Initial and final solution parameters obtained from ex situ pH and conductivity measurements for the different pulse duration after 120 minutes. Cr(VI) solution (47 mg/L, σ=4 mS/cm, pH=2.3) U = 9 kV, V = 100 mL, f = 50 Hz, gap = 5 mm, electrodes length = 0±10 μm. 164
Table 6.21 Energy efficiency for Cr(VI) reduction using the non-thermal plasma method (*these values are recalculated by using Equation 11) 169
Table 7.1 Influence of applied voltage on the formation of H_2O_2 by pin-to-pin discharge in Cr(VI) solution (47 mg/L, σ = 4 mS/cm, pH = 2.4) after 105 minutes. V = 100 mL, Δt = 500 μs, gap = 2 mm, electrodes length = 0±10 μm, f = 50 Hz 178

Table 7.2 Influence of applied voltage on the formation of H_2O_2 by pin-to-pin discharge in Cr(VI) solution (47 mg/L, σ = 4 mS/cm, pH = 2.4) after 120 minutes. for 7, 8, 9, and 10 kV, respectively, V = 100 mL, Δt = 500 μs, gap = 5 mm, electrodes length = 0±10 μm, f = 50 Hz. 180
Table 7.3 Influence of pulse duration on the formation of H_2O_2 by pin-to-pin discharge in Cr(VI) solution (47 mg/L, σ = 4 mS/cm, pH = 2.4) after 120 minutes. U = 9 kV, V = 100 mL, gap = 2 mm, electrodes length = 0±10 μm, f = 50 Hz. 183
Table 7.4 Influence of pulse duration on the formation of H2O2 by pin-to-pin discharge in Cr(VI) solution (47 mg/L, σ = 4 mS/cm, pH = 2.4) after 120 minutes. U = 9 kV, V = 100 mL, gap = 5 mm, electrodes length = 0±10 μm, f = 50 Hz..... 185

Chapter 1
Introduction and purpose of the work

Hexavalent chromium (Cr(VI)) is extremely toxic to the health of humans due to its mutagenic and carcinogenic properties. It is also known to be water soluble throughout the wide pH range. For these reasons, the European regulation have tried to reduce the use of Cr(VI) compounds in the industry. For example, the European REACH regulation (for "Registration, Evaluation, Authorisation and Restriction of Chemicals") has scheduled the ban on hexavalent chromium for 2024. However, the European Commission has recently extended the authorization for the use of hexavalent chromium for the Connectors Manufacturers Group from 4 to 12 years (due to a lobbying group of European connector manufacturers). Moreover, this regulatory ban, restricted to manufacturing in the European zone only, does not concern American or Asian manufacturers or customers.

Uncontrolled Cr(VI) wastewater leads to widespread chromium contamination of the environment around the world. Even if regulations limit the future use of Chromium VI in industry, there are problems due to old use or pollution present in industrial wastelands. As an example, recently in Marseille (France)[1,2], groundwater analyses of a residential area show pollution levels 500 times higher than the norms. The pollution came from a company that used Chromium VI, six years ago, for the surface coating of metal parts (aerospace industry).

Currently, the treatment of liquid waste containing Cr(VI) is carried out mainly according to a few techniques such as ion-exchange, electrochemical treatment, or chemical precipitation. However, neither of them is completely satisfactory due to several disadvantages. For example, the electrochemical treatment method requires a strongly acidic environment and involves producing sludge containing the second pollution and high cost.

Electrical discharge processes have already been tested for the treatment of Cr(VI) in a liquid phase[3–6]. Experimental results showed that Cr(VI) can be significantly eliminated within 15-30 minutes in all cases reported. These studies demonstrate the importance of plasma processes for the removal of Cr(VI). They represent a promising first step but also bring many questions about the best technological solution to optimize energy costs and processing time. Indeed, most of these studies have favored the use of gas phase plasma in contact with the solution to be treated, a simple but less effective method than the immersed discharges we propose to use in this project.

As part of the work of this thesis, the objectives of the 3PE team (PolyPhasic Plasma and Environment) were proposed to develop a clean, economical and efficient process based on immersed plasma-liquid technology to reduce Chromium VI. In order to achieve this general goal, the work described in this thesis has been organized to provide the following **specific objectives**:

- Simple process - which does not require many steps
- "Green" – A process, which does not require very toxic and hazardous reactants. Moreover, it does not produce a second pollution.
- Cost-effective - A process performed with low energy consumption. Furthermore, it does not require a lot of additional equipment.

This Ph.D. thesis is structured in eight chapters.

In this **first chapter**, a brief introduction to the thesis is given concerning the goals and structure of the thesis.

The **second chapter** is devoted to a literature review and state of the art, highlighting the technological and scientific challenges as well as the fundamental aspects of Cr(VI) reduction and detection, non-thermal plasma generation, and plasma-liquid interaction and reaction pathways. Then a summary of the recent work on the reduction of Cr(VI) using the PLI method.

Chapter 3 describes the pulsed discharge reactor and the methodology used in this work to analyze the data. Finally, the reproducibility of the experiments is investigated.

Chapter 4 presents the discharge characterization in water solution and in Cr(VI) solution with parametric studies such as applied voltage, pulse duration, and the gap between two electrodes.

Chapter 5 includes a description of the study of H_2O_2 formation in water after plasma discharge. The effect of some parameters such as applied voltage, pulse frequency, pulse width, and electrode material on the formation of H_2O_2 is studied. Along with that, the erosion of the electrode is analyzed.

The main results obtained in this work are presented in **Chapter 6**, which itself is divided into three parts:

- The first part discusses the first study of the influence of the electrode geometry on the reduction of Cr(VI) to estimate the best electrode configuration.
- The second part presents the effect of energy on reducing Cr(VI) by changing the applied voltage, the gap, and the pulse frequency.
- The third part shows the effect of pulse duration on the Cr(VI) reduction

Chapter 7 presents exciting results on the measurement of H_2O_2 formation in Cr(VI) to better understand the reduction process.

Finally, **Chapter 8** contains the general conclusions and future works.

Another technical problem involved by the tightening of the legislation concerns the detection of Cr(VI). There is a need to be able to detect low concentration because low threshold. In the frame of this PhD, we start working on that point by developing an optical setup (based on Absorption spectroscopy) in order to perform *in situ*, real time measurement of low concentration. Because it is the first approach and this manuscript already presents a lot of results about reduction, this very interesting part is detailed in annex.

Chapter 2

Bibliographic study and state of the art

2.1 General information on Chromium

2.1.1 Properties and applications

Louis Nicolas Vauquelin discovered the element of chromium (Cr) in the mineral crocoite (lead chromate) in 1797. The element's name is derived from the Greek word “chroma,” meaning color, due to its property on mineral pigmentation [7]. Chromium can’t be found in its elemental state in nature, but it is commonly found in the mineral chromite such as the complex of iron chromium oxide ($FeCr_2O_3$) and or magnesiochromite ($MgCr_2O_4$). Cr is a chemical element belonging to the metal transition group in the periodic table with the atomic number of 24. Cr is one of the most important and indispensable industrial metals because of its hardness and resistance to corrosion. Through refining processes, mineral chromite produces both ferrochromium and metallic chromium [8]. It exists in several oxidation states, but primarily in the following stable forms: trivalent Cr(III) and hexavalent Cr(VI).

Both Cr(III) and Cr(VI) are present in the environment by natural processes but also by human activities. Since the 19th century, due to the explosion of industrial zones accompanied by inefficient waste treatment processes, a large amount of chromium compounds (including Cr(III) and Cr(VI)) is released into the environment, mainly towards the aquatic environment (around 94 % of total emissions in European in 2020) [9]. **Figure 2.1** shows the industrial activities dealing with energy sector, waste wastewater management, production and processing of metal, and chemical industry that produce the highest chromium-containing liquid effluents.

Cr(III) and Cr(VI) have drastically different physical and chemical properties and then different toxicity.

Cr(III) is the most common form of naturally occurring chromium and is relatively stable. This element is not dangerous as traces; it is an essential element for the metabolism of glucose and lipids [10]. In addition to insulin, it is responsible for reducing blood glucose levels, and it is used to control certain cases of diabetes. It has also been found to reduce blood cholesterol levels by diminishing the concentration of low-density lipoprotein [11]. Cr(III) has low solubility in aqueous solutions, it is largely immobile in the subsurface at typical environmental conditions (pH 6-9), thus it can be easily removed by filter and precipitation method.

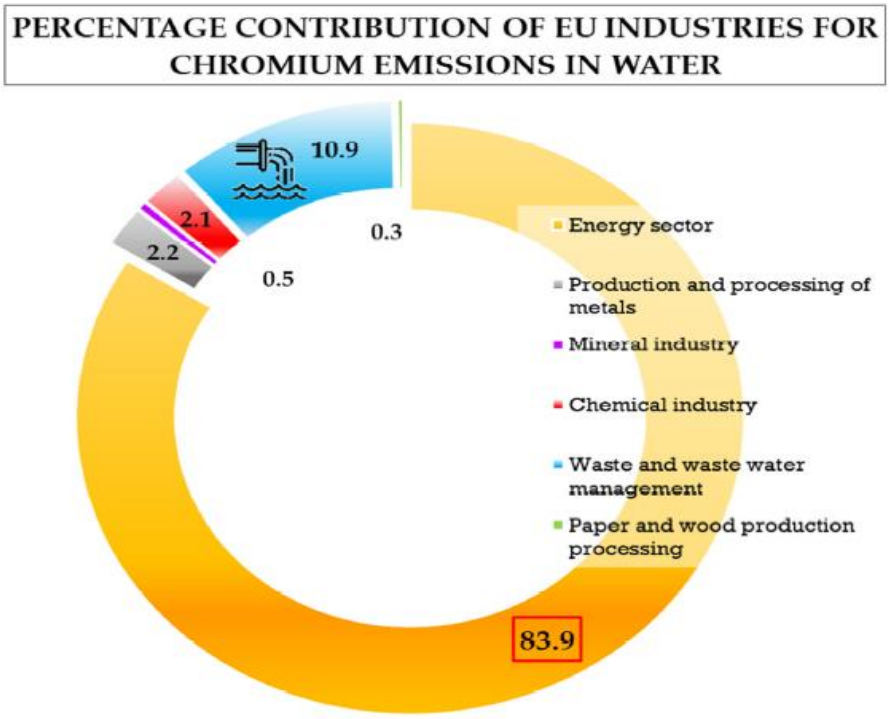

Figure 2.1 Contributing sectors to chromium fluxes to water in 2017[9]

On the opposite, Cr(VI) exerts extremely hazardous effects on biochemical systems. Cr(VI) is considered as one of the most toxic chemicals and is classified as Carcinogenic, Mutagenic, Reprotoxic [10,12]. Due to its high solubility, Cr(VI) readily enters and damages cells. The toxicity of hexavalent chromium is mainly due to its compounds' high oxidative potential and solubility [13,14]. Acute exposure to Cr(VI) causes nausea, diarrhea, liver, kidney damage, internal hemorrhage, and respiratory problems (ulceration of the nasal septum and asthma). Skin contact may result in systematic poisoning damage, dermatitis, or even severe burns, and interference with the healing of cuts or scrapes [12,15,16]. In aqueous systems, hexavalent chromium can be present in different species: primarily as chromic acid [H_2CrO_4] and its salts, hydrogen chromate ion [$(HCrO_4)^-$] and chromate ion [$(CrO_4)^{2-}$]. The speciation of Cr(VI) is affected by the pH values according to the equilibria [6]:

$H_2CrO_4 \rightleftarrows H^+ + HCrO_4^-$	pKa = 1.2	**Reaction 1**
$HCrO_4^- \rightleftarrows H^+ + CrO_4^{2-}$	pKa = 6.5	**Reaction 2**
$2HCrO_4^- \rightleftarrows Cr_2O_7^{2-} + H_2O$	pKa = 2.05	**Reaction 3**

Figure 2.2 presents Cr(VI) speciation in an aqueous medium depending on the pH environment. The dominant form of Cr(VI) at low pH is H_2CrO4; then, with increasing the pH the form of Cr(VI) shifts to $HCrO_4^-$ and CrO_4^{2-}.

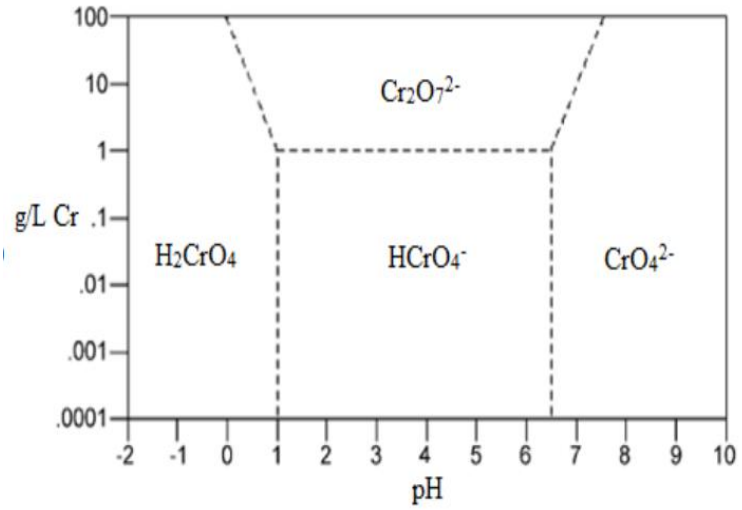

Figure 2.2 Cr(VI) speciation in an aqueous environment as a function of pH [17]

2.1.2 Toxicity and regulation of Chromium VI

Cr(VI) compounds in water can easily penetrate the groundwater and cause serious impacts on human life and ecosystems on earth. Fan *et al.* [18] have shown that the mobility of Cr(VI) in water has caused severe pollution. Lindberg *et al.* [19] have concluded that 8 hr mean exposure exceeding ***2×10^{-6} mg/L*** of Cr(VI) to humans may cause a transient decrease in lung function and that short-term exposure to at least ***2×10^{-5} mg/L*** of Cr(VI) may causes septal ulceration and perforation. Until now, there have been only a few human studies addressing oral exposure to Cr(VI) and its adverse health effects. Zhang *et al.* [20] have reported an increase in stomach cancer mortality in the residents of small villages in the Liaoning province of China where the drinking water was heavily contaminated with the concentration of Cr(VI) > ***0.5 mg/L***. Linos *et al.* [21] studied the mortality in the Greek Oinofita region, where the water has been contaminated with Cr(VI) (***from 41 to 156 µg/L***), showing high mortality due to liver-related disease, lung and kidney cancer. Studies performed by Sazakli *et al.* [22] in Greece and Sharma *et al.* [23] in India point to a relationship between exposure to Cr(VI) in drinking water and some hematological and biochemical parameters. These studies have been performed from high concentrations of Cr(VI) (~ ***20 mg/L***) in India to the small amount of Cr (VI) in the range ***5-90 µg/L*** in Greece.

The current drinking water guideline has been set to ***50 µg/L*** total chromium by the World Health Organization (WHO) and the European Community [24]. In July 2014, the California state of USA established a more stringent Maximum Contaminant Level of ***10 µg/L*** for Cr(VI) [25]. Italian law limits for groundwater (CSC – Contamination Threshold Concentrations) are equal to ***50 µg/L*** for total chromium and ***5 µg/L*** for hexavalent chromium [26]. There is a lack of uniformity from limiting the concentration of

Cr(VI) in wastewater from medical organizations in the world but they are all pointing to the idea that concentrations of Cr(VI) have to be controlled.

Thus, due to the high toxicity of Cr(VI) and its significant presence in industrial wastewaters, selective detection and elimination of Cr(VI) are important objectives to provide control of this highly poisonous substance for humans and environmental concerns.

2.1.3 Chromium VI remediation technologies

As detailed above, the discharge of hexavalent chromium into the environment can result in damaging the ecosystem and adversely affecting human health. Therefore, it is necessary to limit the Cr(VI) concentration in wastewater from industries to below the prescribed level. Hexavalent chromium-containing wastewater needs to be treated before being discharged. Different techniques can be used: classical methods such as physical, chemical, or thermal methods can be applied as waste treatment. The most effective classical methods used are ion exchange, adsorption, electrochemical treatment, and chemical precipitation [27]. These classical methods are shortly presented below.

a. Ion exchange

Ion-exchange processes have been widely used to remove heavy metals from wastewater due to their many advantages, such as high removal capacity, high elimination efficiencies, and fast kinetics [27,28]. Ion exchange is a physical separation process in which the exchanged ions are not changed chemically [29]. Synthetic resins are commonly used as ion exchangers since easy to reuse. Resins can be divided into cations or anions exchangers based on the charges of the exchanged ions [28–31]. When the solution contaminated with the metals flows through ion exchangers (resins), the positively charged metal cations, possibly toxic, which affect the purity of the water, such as chrome ions, are interchanged with the resins' positively charged ions, such as hydrogen and sodium ions in equivalent amounts in the solution [28,30,31]. The same process happens with the negatively charged undesirable anions present in the wastewater solution, such as hydroxyl and chloride ions, which are replaced by the sulfate, nitrate, and chromate ions released by the resins.

Kumar *et al.* [27] have studied the removal of hexavalent chromium ions from aqueous solutions by an anion-exchange resin. It was noticed that the sorption process was rapid during the first 20 minutes, and the maximum adsorption efficiency of Cr(VI) was 99 % for an initial concentration of Cr(VI) of ***100 mg/L***. Using the same method, Petruzzelli *et al.* [32] and Shi *et al.* [33] also showed a 99 % reduction in Cr (VI) in solution from tanning factories.

Although this method shows a high effect on the removal of Cr(VI), it has certain limitations such as the high cost of equipment and chemicals, time, and samples-consuming.

b. Adsorption

Adsorption is the method by which molecules are concentrated on the surface of an adsorbent. Species/materials in gaseous or liquid form (the adsorptive) become attached to a solid or liquid surface (the adsorbent) and form the adsorbate [34]. Activated carbon is the most popular adsorbent in use because of its high surface areas, well-developed internal micro-porosity structure, and the presence of a wide spectrum of surface functional groups like the carboxylic group [35]. As a consequence, the removal rate is more than 99 % for certain metal ions treatment [30].

Adsorbents such as activated carbon, carbon nanotubes, metal oxides, and many agricultural and bio adsorbents have been tested and proven to be successful in removing Cr(VI) from wastewater. The most studied in adsorption of Cr(VI) is found to be the activated carbon [36,37]. As an example, Pérez-Candela *et al.* [38] have reported that a 100 % reduction of Cr(VI) has been obtained at pH 1.0 using different types of activated carbons prepared from different raw materials. They have also shown that the adsorption process depends on the pretreatment of activated carbon and that the highest removal performance was obtained with prepared by physical activation. **Table 2.1** summarized some of the reported adsorption capacities for activated carbons of different sizes and shapes.

Activated Carbon	Initial concentration of Cr(VI) mg/L	Reduction rate (%)	Time duration of process (hours)	pH	Reference
PAC	7500	100%	300h	2.0	[38]
GAC	53.19	99%	5h	2.0	[39]
ACF	53	100%	3h	4	[40]

Table 2.1 The reduction efficiency of Cr(VI) for different activated carbons based on size and shape - PAC=powder-activated carbon, GAC=granular-activated carbon, ACF=activated carbon fibers

However, many researchers are still working on improving the cost of using activated carbon in removing Cr(VI). Since the industrial carbon sources become exhausted and the activated carbon materials are non-reusable, the cost of carbon adsorbents is increasing every day.

c. Electrochemical treatment

Electrochemical treatment techniques are becoming an alternative wastewater treatment method because they constitute more cost-effective methods [41]. Cr(VI) can be completely removed via different electrochemical methods such as electrocoagulation, electrochemical precipitation, and membrane electrolysis [28]. Among the reported electrochemical treatments, Cr(VI) in the solution can be reduced by two pathways: through direct reduction, which involves the exchange of electrons directly with electrode

surface, and indirect reduction, which proceeds through the generation and consumption of some strong reductive species [42–44].

- **Electrocoagulation** (EC) involves the creation of metal ions *in situ* by dissolving ions electrically from the electrode surface [45–47]. The metal ion production takes place at the anode, and hydrogen gas is delivered from the cathode. The hydrogen vapor can help to float the flocculated particles out of the water [46]. Cr(VI) was proposed to be reduced first to Cr(III) at the cathode before precipitating as hydroxide [28]. Several researchers have reported the effect of electrocoagulation for the elimination of Cr(VI) by using a steel electrode [45,47,48]. It was found that the electrocoagulation process for the reduction of Cr(VI) required the following steps:

  The first step was the formation of Fe^{2+}, by the oxidation of a steel electrode by a DC power supply:

  $$Fe^0 + 2H_2O \rightarrow Fe^{2+} + 2H_2 + O_2 + 2e^- \qquad \textbf{Reaction 4}$$

  The second step was the reaction between Fe^{2+} and chromium (VI) described in **Reaction 5** in a low pH environment ($0.5 < pH < 6.5$) and **Reaction 6** in the high pH environment ($pH > 6.5$) :

  $$6Fe^{2+} + Cr_2O_7^{2-} + 14H^+ \rightarrow 6Fe^{3+} + 2Cr^{3+} + 7H_2O \qquad \textbf{Reaction 5}$$

  $$3Fe^{2+} + CrO_4^{2-} + 4H_2O \rightarrow 3Fe^{3+} + 2Cr^{3+} + 8OH^- \qquad \textbf{Reaction 6}$$

  As an example, Lu *et al.* [48] have reported that the concentration of Cr(VI) decreases more than 50 % after 40 minutes at pH = 6 by using electrocoagulation with multi irons plate electrode with an initial Cr(VI) concentration of ***106 mg/L***.

- **Membrane electrolysis** is a chemical process driven by an electrolytic potential. The electrical potential is applied across an ion exchange membrane, and then a reduction-oxidation reaction takes place at the electrodes [49]. By using the carbon aerogel electrodes, Rana *et al.* [50] have investigated the removal of Cr(VI) from industrial wastewater in an electrochemical bath. It was found that the concentration of Cr(VI) from the wastewater can be reduced by 98.5 % under high charge (0.8 Ah) in acidic conditions (pH = 2), with the initial concentration of Cr(V) was ***2 mg/L***.

- Some researchers have used **electrochemical precipitation** (ECP), which results from the conjugation of an electrochemical process with a precipitation process, to remove Cr(VI) from electroplating wastewater[49]. As an example, Kongsricharoern *et al.*[51] have performed the electrochemical precipitation process with two steel plates for electrodes. The result has shown that 85 % of Cr(VI) have been removed after 10 minutes with an initial Cr(VI) concentration of ***100 mg/L*** at a pH of 4.5.

d. Chemical precipitation

The process is performed by using chemical reactions with ions of heavy metals like chromium, copper, nickel, zinc present in the wastewater to form insoluble precipitates of the heavy metals involved, such as hydroxide, carbonate, sulfide, and phosphate, depending on the chemicals used for the precipitation. The formed precipitates are then removed as sludge by multi-step as coagulation, flocculation, sedimentation, and filtration [28,30,52]. Chemical precipitation is most commonly used to remove Cr(VI) in the wastewater treatment industry for the large-scale unit without requiring specialized skills [28].

Minas *et al.* [53] have used the chemical precipitation method for chromium removal from tannery wastewater in Ethiopia. The results showed that removal efficiencies of the Cr(VI) using different precipitating agents (NaOH, $Ca(OH)_2$, and MgO) are more than 99 %, and they do not depend on the variation of pH environment with a very high initial concentration of Cr(VI) was ***5010 mg/L***. Even though the process is fairly simple, effective, and can be low cost compared to other removal technologies but the major drawback of the process is the production of a large amount of concentrated and toxic sludge.

e. Summary

As we have presented, various treatments such as ion exchange, chemical precipitation, and electrochemical method can be handled to remove hexavalent chromium from contaminated wastewater, but each one has some limitations, as summarized in **Table 2.2**

Methods	Advantages	Disadvantages
Ion exchange	Energy-efficient Low maintenance High regeneration of materials Metal selective	High cost Less number of metal ions remove Solution concentration must be monitored
Adsorption	Fast kinetics High efficiency Most of the metal can be removed	Expensive: the higher the quality, the greater the cost Performance is dependent on the type of carbon used No regeneration
Electrochemical treatment	Highly efficient Pure metals can be achieved Large scale	High cost Production of sludge containing the second pollution Need of acidic environment to increase the efficiency
Chemical precipitations	Simple Inexpensive Most of the metal can be removed	A large amount of sludge produced Chemicals consuming Disposal problem

Table 2.2 Advantages and disadvantages of various Cr(VI) removal techniques

It is also to notice that with the development of science and technology, biological methods have also been studied and showed certain benefits but they also include drawbacks due to the cost and time consumption, hardness to develop into a large scale and requirement of a special technique [54].

Recently, a promising method based on physicochemical phenomena has been studied; it consists of **plasma discharge in contact with liquid**. In plasma discharge in contact with liquid, highly energetic electrons are generated from plasma discharges to dissociate water molecules into radicals (O, H, OH) and ions (H_2O^+, O_2^-). These reactive species are involved in reducing Cr(VI) to Cr(III) in solution. The section **2.2** will mention a more detailed description of this method, representing the method developed in this work.

2.1.4 Detection methods

The development of analytical methods capable of determining Cr(VI) concentration in environmental samples at trace levels has received considerable attention in the last few years. The determination of [Cr(VI)] has traditionally been carried out by UV-vis absorption spectrophotometry. Powerful analytical tools like atomic absorption spectrometry (AAS) [55], high-performance liquid chromatography (HPLC) [56,57], inductively coupled plasma mass spectrometry (ICP-MS) [58,59], and inductively coupled plasma-optical emission spectrometry (ICP-OES) [60–62], are also widely used techniques in laboratories. **Figure 2.3** shows the percentage of papers describing the various analytical techniques used to determine the hexavalent chromium in different samples [63]. It is clear to see that most of the researchers used atomic absorption spectroscopy techniques (over 50 %).

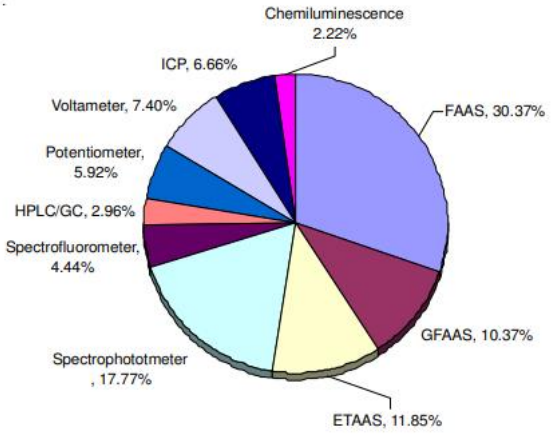

Figure 2.3 Utilization of various analytical techniques for the determination of hexavalent chromium since 2006, *i.e.* Flame atomic absorption spectrometry (FAAS), Graphite furnace atomic absorption spectroscopy (GFAAS), Electrothermal atomic absorption spectroscopy (ETAAS), High-performance liquid chromatography/gas chromatography (HPLC/GC), and Inductively coupled plasma (ICP) [63]

a. Atomic absorption spectrometry (AAS)

Atomic absorption spectrometry (AAS) is an analytic technique used for the qualitative and quantitative measurement of chemical elements, especially in trace element analysis. The process is based upon the absorption of radiant energy, usually in the ultraviolet and visible region of electromagnetic radiation [55,64,65]. It requires standards with known analyte content to establish the relation between the measured absorbance and the analyte concentration, which relies on Beer-Lambert Law [66,67]. **Figure 2.4** shows the basic principle of the atomic absorption spectrometer.

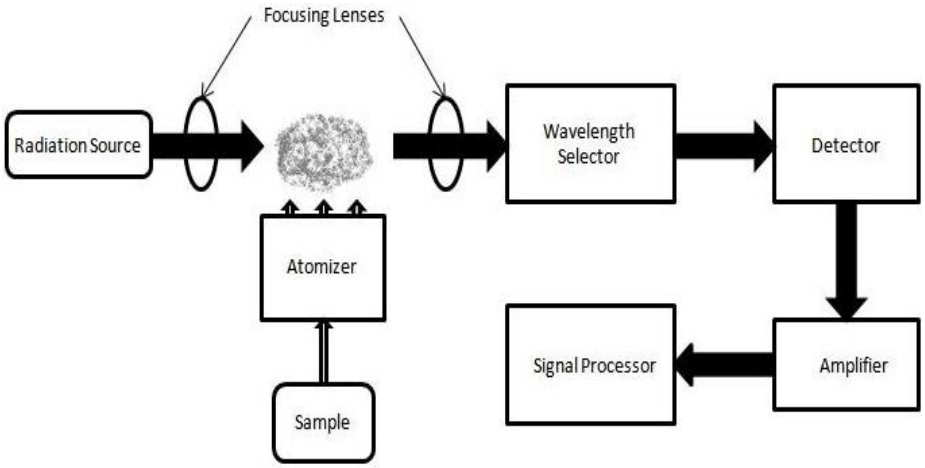

Figure 2.4 Atomic absorption spectrometer block diagram [55]

Studies of the detection of Cr(VI) in waste water using AAS have been completed by many scientists with different types of atomizers and also different kinds of radiation sources [68–71]. The atomizers most commonly used nowadays are (spectroscopic) flames and electrothermal (graphite tube) atomizers. The two common types of radiation sources are line source AAS (LS AAS) and continuum source AAS (CS AAS) [64]. Most reports indicate that AAS can be used to detect low concentrations of Cr(VI) in industrial wastewater. Depending on the technique, the limits of detection can range from ng/mL to μg/mL. However, this method still has certain limitations. The use of this method requires having a high level of operator skill and high samples consumption [65].

b. High-performance liquid chromatography (HPLC)

High-performance liquid chromatography (HPLC) is a popular analytical technique used to separate, identify, and quantify each constituent of a mixture (**Figure 2.5**). Chromatography can be described as a mass transfer method including adsorption [72,73]. The sample to be analyzed is introduced in a small volume to the mobile phase stream and is retarded by specific chemical or physical interactions with the stationary phase [72–75]. Retention time (when a specific analyte comes out of the column) varies depending on the interactions between the stationary phase, the molecules being analyzed, and the solvent(s) used.

Typical solvents used include any miscible combinations of water or organic liquids (the most common are methanol and acetonitrile) [76–82]. The most commonly used adsorbents are Silica and Alumina. In particular, for Cr (VI), the most commonly used is Silica gel- C18 [83].

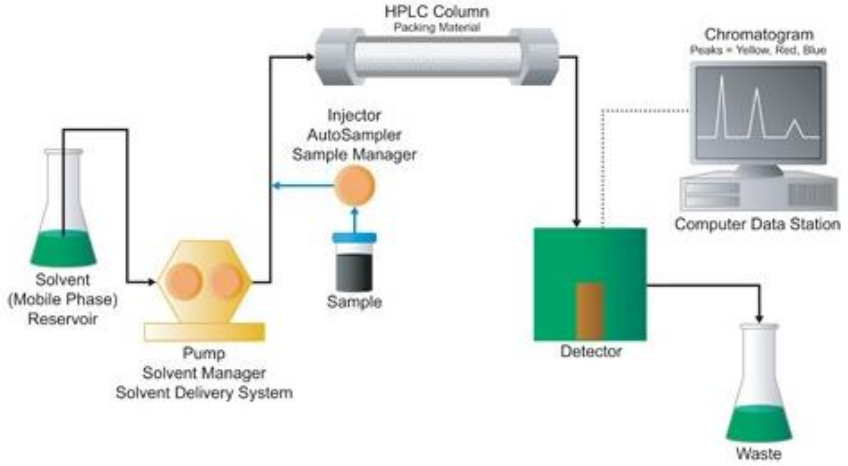

Figure 2.5 High-Performance Liquid Chromatography [HPLC] system [84]

Numerous studies on the use of HPLC to analyze the amount of Cr (VI) in industrial wastewater have been reported [56,83,85–87]. The use of HPLC gives very accurate results even in complex solutions. As an example, Wang *et al.* [85] have studied the ability of high-performance liquid chromatography for speciation of Cr(III) and Cr(VI) in environmental sediment samples. It was found that the concentration of Cr(VI) in sediments of Chaohu Lake is in the range ***18-53 mg/L*** and these results demonstrate that the concentration of Cr(VI) exceeds the WHO regular value (***50 µg/L***). They also showed that the limit of this method was ***7.5 µg/L*** for Cr(III) and ***3.5 µg/L*** for Cr(VI), respectively.

Although HPLC is considered to be one of the most effective methods for analyzing and detecting toxic substances in solutions, there are still many disadvantages as the speed of HPLC and its reliance on different polarities of compounds: two compounds with similar structure and polarities can exit the chromatography apparatus at the same time or nearly the same time [88]. Moreover, this technique requires a high cost of the instrument and cannot measure in situ samples.

c. Inductively coupled plasma mass spectrometry (ICP-MS)

ICP has been commercially available for almost 50 years and is widely used to measure heavy metals in a variety of kinds of solutions. It can be divided into two techniques, which are inductively coupled plasma–optical emission spectroscopy (ICP-OES) and inductively coupled plasma-mass spectrometry (ICP-MS) [89]. In principle, both techniques operate the same way but require different detectors. Between the two introduced ICP techniques, inductively Coupled Plasma Mass Spectrometry (ICP-MS) has been widely more used than the other because of its high sensitivity and specificity. Moreover, it is the most

reliable and effective method for multi-element determination [90–92]. ICP-MS is a method for identifying and analyzing trace multi-elemental and isotopic concentrations in liquid, solid, or gaseous samples [93]. **Figure 2.6** shows the essential instrument components of the ICP-MS.

The essential operation of ICP-MS begins with introducing a sample into the nebulizer, which converts the sample into a vapor. The sample has to be appropriately treated before introducing it into the machine. Then, the sample goes through the mixer before spraying to create a matrix effect. Finally, an ion detector converts the ions into an electrical signal multiplied and read by computer software [94].

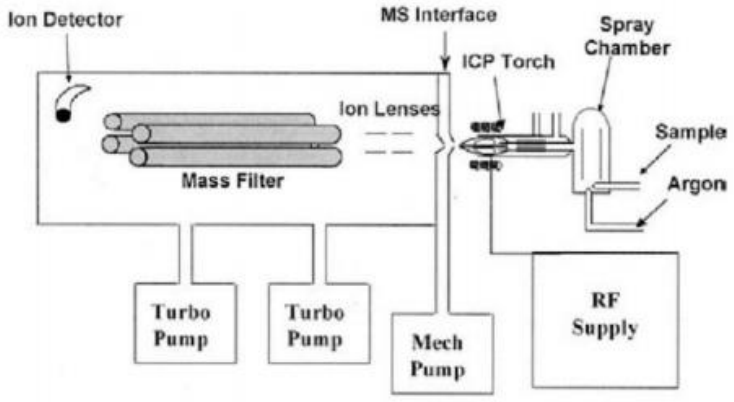

Figure 2.6 Basic instrument components of the ICP-MS [95]

Tanoshima *et al.* [96] have reported that the determination of Cr(VI) by IPC-MS takes only about 3 minutes and they were able to measure concentrations lower than ***0.2 µg/L***. It was also found that the detection limit for Cr(VI) was ***~0,008 µg/L***, which is below the draft Public Health Goal of ***5 µg/L*** proposed by the state of California [97]. The analysis of IPC-MS results [98–100] suggests that the ICP-MS method provides high-speed and accurate results with a small detection limit. Even though, this technique also contains drawbacks as high-cost consumption, not being easy to use, and requiring a high technical level.

d. Photometric method

The photometric method (also called colorimetric) for Cr(VI) determination is commonly used because it's easy to use and doesn't need high-cost analytical instruments. There are two different pathways to analyze the concentration of Cr(VI) in wastewater using colorimetric methods: indirect and direct measurements. In this thesis, we will use these techniques to measure the concentration of Cr(VI). In colorimetric method, the Beer-Lamberts law is applied to determine the element concentration. The basic of these techniques are presented below and the description of details will be presented in section **3.2.4**.

- **Indirect method**:

This method has been widely depicted in the literature [101–104]. In an acid medium, 1,5-diphenylcarbazide (DPC) reacts with Cr(VI) and a red-violet colored complex is produced. The absorption spectrum of this complex is at the wavelength of 540 nm.

For example, Zewdu *et al.* [61] reported that the concentration of hexavalent chromium in the discharged effluent of Bahir Dar tannery carried out by colorimetric method is 0.18 mg/L is above the permitted level of WHO guideline (***5 µg/L***). However, the solution should be prepared with acetone because the DPC is insoluble in water. Furthermore, the color reaction between DPC and Cr(VI) needs the participation of sulfuric acid or phosphatic acid to avoid interference.

- **Direct method:**

The concentrations is estimated by measuring the absorbance of the solution at a wavelength of 350 nm to 375 nm via the original color of Cr(VI) ions. Sanchez-Hachair *et al.* [105] have shown that high concentrations of Cr(VI) in the solution can be analyzed directly. Although this is a simple and effective method of detecting Cr(VI) in wastewater, there are certain limitations. Reports indicate that using the colorimetric method cannot analyze samples containing Cr(VI) content below ***3 µg/L*** [61,106,107]. Although this method has limitations in analyzing low concentrations of Cr(VI), this method has been used by most research groups within the laboratory scale because of its advantages.

e. Summary

The above methods show the ability to detect Cr(VI) in solution at relatively low concentrations, but they also do not avoid many disadvantages. **Table 2.3** summarizes the advantages and disadvantages of the techniques, and it also presents the limit of detection for each method.

As the main point of this thesis is based on the plasma discharge used to remove Cr(VI), next part, we will present an overview of these techniques.

Method	Advantages	Disadvantages	Limit of detection
Colorimetric using UV-vis	• Easy to use • Quick analysis ability • Not expensive	• Not stable • Long reaction time for color development • Not in situ measurement	3-10 µg/L only for Cr(VI) (depending on the cuvette length) [61]
Atomic absorption spectroscopy (AAS)	• High sample throughput • High precision	• Samples consumption • High cost • Not in situ • Requires high skill level	0.02 µg/L for Cr(III) 0.014 µg/L for Cr(VI) [108]
High-performance liquid chromatography (HPLC)	• High efficiency • Accurate and highly reproducible	• Time and samples consumptions • High cost • Not in situ • Requires high skill level	7.5 µg/L for Cr(III) 3.5 µg/L for Cr(VI) [83]
Inductively coupled plasma mass spectrometry (ICP-MS)	• Sensitivity • Multi-element detection • Fast detection • A large linear range	• High cost • Difficult for use • Not in situ	0.00443 µg/L for Cr(III) 0.0083 µg/L for Cr(VI) [99]

Table 2.3 The advantages, disadvantages, and limitations of various analytical techniques to the determination of chromium

2.2 Electric discharge in liquid

In this section, we present the differences in the configuration of plasma discharge in liquid and the properties of these discharges.

2.2.1 Plasma and electric discharge

Plasma is often referred to as the fourth state of matter in which a certain portion of particles in a gas is ionized [109–111]. Also, the density of electrons and ions are nearly equal, thus making plasma quasi-neutral. On earth, "natural plasmas" are not common; they are usually present only in the high atmosphere and in lightning. However, ground plasma can be generated artificially by several methods, such as flames, electrically heated furnaces, or mainly by **electric discharges** as glow discharge, corona discharge, dielectric barrier discharge, arc discharge, microwave discharge, and radiofrequency discharge [112,113]. Electric discharges involve different operating conditions (mainly controlled by the power supply and the pressure range), leading to different properties. Consequently, these plasmas are widely spread in multiple domains and used daily for high-tech industrial processes such as the microelectronic industry, surface treatment, nanoparticle synthesis, and many other fields [114–117].

Electric discharges can be classified into thermal or non-thermal plasma related to the energy levels of the electrons (T_e) and the plasma's heavy species (T_h).

Thermal plasma is in thermodynamic equilibrium. It is characterized by uniform and very high temperatures for electron and heavy particles in the plasma ($T_e = T_h$). Thermal plasma reaches or approaches the highest ionization degree (100 %) and has a high electron density: $10^{21} – 10^{26}$ m^{-3} [118–120]. The condition required to form hot plasma is that the working pressure should be sufficiently large, usually above 10^4 Pa. The high pressure facilitates a very large number of collisions between the elements, resulting in a quick redistribution of the energy back to the equilibrium state [121]. Current thermal plasma technology mainly consists of electric arc, radio frequency (RF) discharges, plasma torches, ultra-high-temperature plasma nuclear reaction, and discharge pulse plasma [120,122–124]. Thermal plasma is applied in a wide range of industries such as metallurgy, gas synthesis with plasma reforming, ceramic powder synthesis, plasma coating, physical vapor condensation, chemistry, and toxic removal. Nowadays, the thermal plasma will be used in many applications as plasma engines, in controlled thermonuclear fusion [122,124,125], but are limited in terms of energy efficiency due to high gas temperature and electrode related problems [116].

Non-thermal plasmas (NTP) are in thermal non-equilibrium, and the electron temperature is much higher than heavy particle temperature ($T_e >> T_h$). In NTP, the electron's temperature can reach 10^4 to 10^5 K (corresponding to the average electron energy of about 1-10 eV) [121]. They use to present a lower electron density than thermal plasma ($<10^{19}$ m^{-3}) and then a low ionization degree of about 10%. These

plasmas are rich in reactive chemical species and have a low gas temperature, making them widely used in multiple fields. The NTP technology has been applied, for example, in machining and surface treatment. Other economically important applications include micro-electric fabrication and technical preparation of plastic components used in liquid solvent paints [112,126]. In these current technologies, people mainly focus on three types of non-thermal plasma: low-pressure NTP, high-density low-pressure NTP and atmospheric pressure NTP. The most commonly used are low-pressure plasma techniques which include DC discharge (mostly at 1- 10 Pa), low-frequency AC discharge (usually using frequencies below 100 Hz), and high-frequency plasma (for example, RF high-frequency discharge plasma). For high-density low-pressure plasma, it is usually performed at very low pressure (2- 6 Pa), and higher ionization than conventional RF discharge, for example, plasma ERC (electron cyclotron resonance plasma) or microwave plasma (microwave plasma)[112,116,127].

In contrast with low-pressure plasma, atmospheric pressure NTP does not require a vacuum system. Conventional pressure plasma techniques include dielectric barrier electric discharge (DBD), corona discharge, plasma jet... In these plasmas, the energetic electrons can collide with background molecules (N_2, O_2, H_2O, etc.), producing secondary electrons, photons, ions, and radicals. Until now, NTP have been widely applied in many fields, including material science [128], space science and astronomy [129], electronic science [130], chemistry, chemical engineering [131], and environmental science [132–134]. More recently, the NTP have been found to have extremely high applications for environmental treatment. When reacting with NTP, the contaminant molecules are reduced or oxidized by strong reactive chemical species (*e.g.* radicals) and high-energy electrons.

As presented previously, plasma refers mainly to a gas environment. However, over the past few decades, there has been interest in electric discharge related to liquid due to extensively studied chemical, biotechnology, environmental, and medical applications.

This work mainly focuses on the applications of atmospheric NTP in liquid for the environmental field since this thesis deals with treatments of hexavalent chromium in liquid effluents.

We will now present the difference in the type of liquid plasma interactions. The details will be presented in the next section **a**.

a. Generalities on Plasma-Liquid Interactions (PLI)

Plasma–liquid interactions (PLI) represent a growing interdisciplinary area of research involving plasma science, fluid dynamics, heat and mass transfer, photolysis, multiphase chemistry, and aerosol science. In recent years, there is increasing interest in the non-thermal plasma discharges in liquids because of its potential applications for various biological, environmental, and medical technologies since they produce

highly reactive radicals (*e.g.*, ·OH) and molecule (*e.g.*, H_2O_2), the generation of strong UV emission, and the production of shockwaves [135–140].

For example, electric discharges have been developed as a non-chemical method for bio-fouling removal and contaminant abatement in water, potentially extending into a wide range of other water treatment applications [132,141]. In PLI systems, the operating pressures are in the range from very low values in ionic liquid to very high-pressure values in supercritical liquids [142], but most of the applications operate at atmospheric pressure.

Depending on the location of the NTP versus the liquid, discharges in liquids used to be classified into three categories [142]:

a) direct gaseous phase discharge (above liquid phase)

b) direct aqueous phase discharge (inside liquid phase)

c) multiphase discharge

b. Plasma discharge above the liquid phase

The electrode configuration of this PLI process is when the electric discharge is generated in the gas above a liquid surface and operated at atmospheric pressure (or higher). Plasma discharge above the liquid phase can be generated by various discharge geometries that correspond to various power supplies such as AC or DC. In this process, the DC power supply is the most commonly used. Plasma discharge above the liquid phase can be distinguished by four subgroups: corona and glow discharge, DBD (Dielectric barrier discharge), plasma jet, and arc discharge. Most studies are focused on corona, glow discharge, and plasma jet because they do not require complicated electrodes technology. The possible electrode configurations in these plasma processes are presented in **Figure 2.7** (a), (b), (c) with different geometries of high voltage electrodes used for corona and glow discharge. **Figure 2.7** (d) presents a type of plasma jet discharge above the liquid phase.

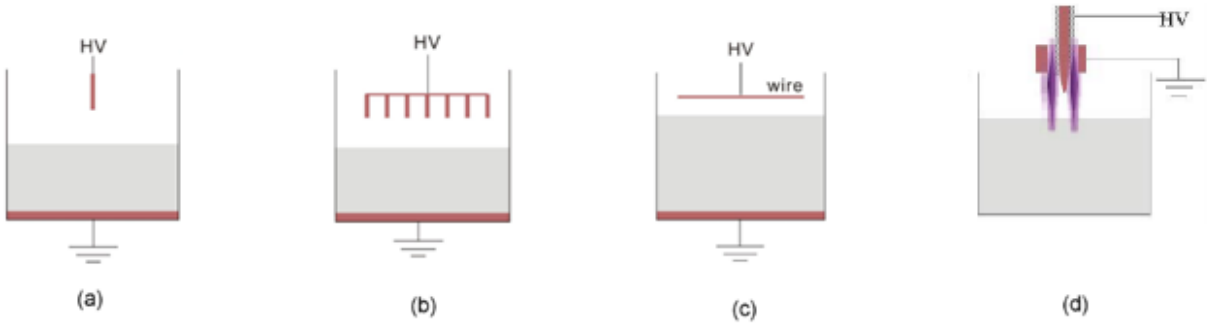

Figure 2.7 Types of discharge above the liquid phase: (a) pin-to-water, (b) multi-pin-to-water, (c) wire-to-water, (d) plasma jet [143]

The plasma produced in these configurations has a gas temperature close to room temperature (300-350 K) [143]. The densities of the chemically reactive species produced are high, for instance, concentrations of hydroxyl radical and oxygen atom are around 10^{19} m^{-3}- 10^{21} m^{-3} [144,145]. For the different kinds of plasma discharge above the liquid phase, the electric field intensity can be in the range of 1-100 kV/cm [146].

Low gas temperature and high density of chemical reactive species can be applied in biomedical and nano-synthesis applications. But since the plasma is generated above the liquid surface, an amount of plasma generated reactive species is wasted in the atmosphere, which reduces the efficiency for several applications.

c. Plasma discharges in the liquid phase

Direct discharge in liquid is a process in which the plasma is generated directly inside the bulk solution. In this configuration, a high voltage electrode is usually immersed in the liquid phase. The most commonly reported types of direct discharge are streamer or corona discharge. Various electrode geometries have been studied for the generation of plasma discharges in liquid. **Figure 2.8** shows some of the typical electrode configurations. For streamers, pin-to-pin electrodes (**Figure 2.8 (**a**)**) and pin-to-plate geometry (shown in **Figure 2.8 (**b**)**) have been the most commonly used configuration. Also, pin-to-plane geometry with multiple pins was used to generate a large volume corona discharge in water (**Figure** 2.8 (c)). Direct plasma discharge in the liquid has been generated by various power supply as DC, DC pulse, DC bipolar pulse, RF, or microwave power [143].

Discharges inside a liquid need a higher electric field than in gas because of the collisions of electrons with surrounding dense water molecules. Formation and propagation of filamentary discharge inside water need ca. 10^3 kV/cm of electric field intensity (a thousand times higher than in a gas) [146].

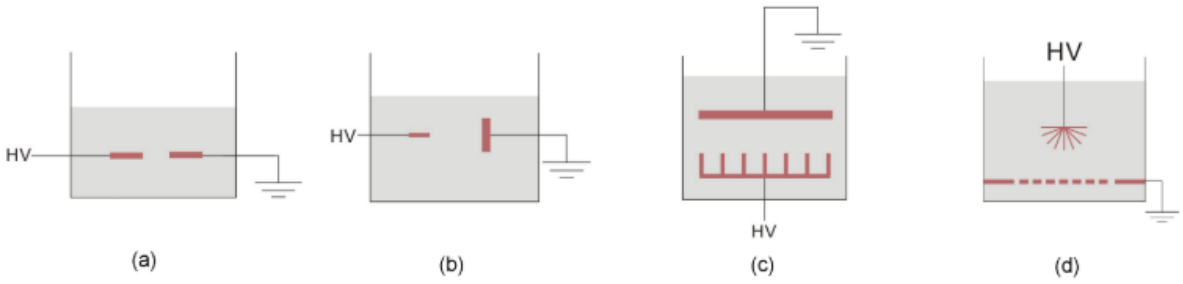

Figure 2.8 Types of plasma discharge inside liquid reactors: (a) pin-to-pin, (b) pin-to-plate, (c) multi-pin-to-plate, (d) brush-to-plate [143]

The main properties of direct aqueous discharges are: plasma generation time can be ns to μs depending on the power supply; the density of electrons is very high, which ranges from 10^{24} m^{-3} to 10^{26} m^{-3}; the electron temperature is about 1000-7000 K; the ionization degree of such discharge can be even up to 1;

the discharge current is in the amplitude of ampere and a large amount of reactive species are formed [141,142,147,148]. Generating plasma in complete liquid immersion creates a complex thermochemical system with two interfaces: plasma/gas and gas/liquid, as shown in **Figure 2.9**. Thus it leads to various temperatures and pressures in the different regions, especially involving the diffusion of the species after their formation.

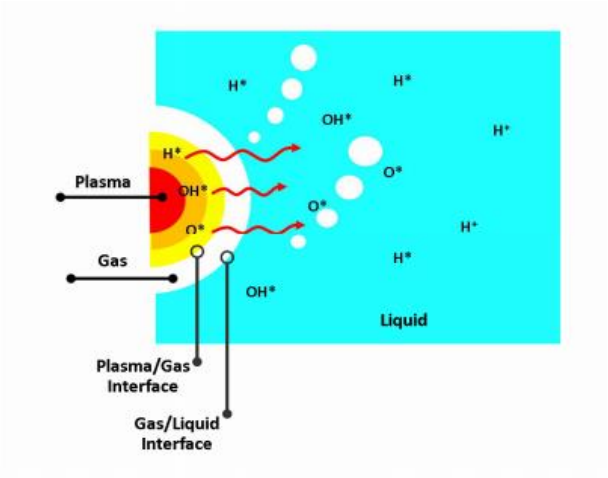

Figure 2.9 Schematic illustration of solution plasma and their chemical species [149]

Higher chemical reaction rates are expected in these processes due to the fact that complete immersion of the plasma in the liquid phase provides an increased contact of the plasma phase with the target species; thus, direct plasma discharge in liquid can become an attractive method in the field of wastewater treatment.

d. Plasma discharge in multi-phase system

Direct plasma discharge generally has low energy efficiency due to the difficulty of initiating the discharge inside the liquid phase. A lot of attention has been paid to enhance the efficiency of plasma discharge by applying bubble flow through the liquid [150]. Bubbling has the additional advantage of mixing the solution but the problem is a more complicated device (with a bubbling system). Moreover, discharge initiation in the gas phase minimizes electrode erosion, which lengthens the system's lifetime. **Figure 2.10** lists the common configurations of plasma sources selected for multiphase discharge.

For discharge in bubbles, a surface discharge is more inclined to be formed and propagates along with the interface of gas-liquid [150]. In such discharges, the temperature of electrons reaches 8 - 10 eV, and electrons' density can be up to 10^{22} m^{-3} [151]. Mass and thermal transfers are increased since most of the particles are produced close to the discharge surface.

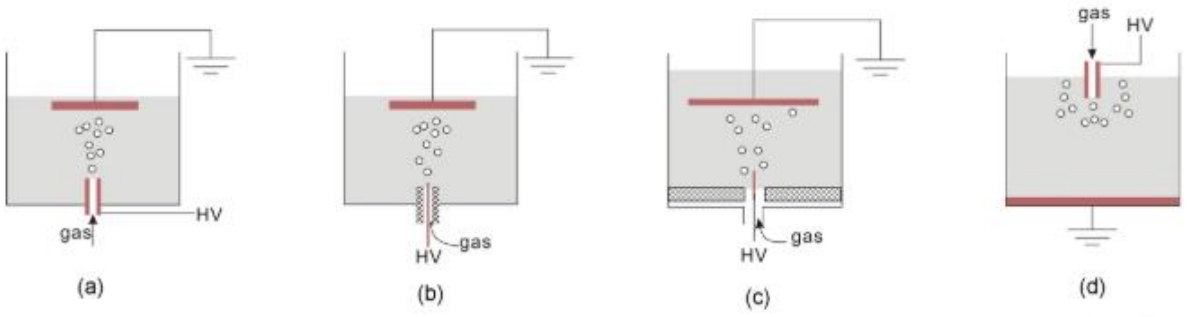

Figure 2.10 Types of bubble discharge reactors: (a) upward nozzle electrode-to-plate, (b) upward nozzle containing needle electrode-to-plate, (c) hole containing needle electrode-to-plate, (d) downward nozzle electrode-to-plate [143]

In this thesis, we focus on the **plasma discharge inside the liquid phase** (also called **direct PLI**) because of the high reactivity and the simplicity of the setup (no bubbling system). Due to their gas-liquid interfaces' physical and chemical properties, discharge plasmas in liquids have recently attracted much attention. Direct PLI allows all the formed reactive species to spread and immediately react. Due to this advantage, many applications have used plasma directly in the liquid phase, such as pollution elimination or sterilization. Direct PLI has been shown to be able to induce various reactions, including the degradation of contaminants and the synthesis of nanomaterials and polymers based on numerous physical and chemical processes [152–155].

2.2.2 Physical and chemical processes in direct PLI

The plasma-liquid interaction is a complicated physicochemical process. It includes diffusion and chemical reactions in the plasma channel at the gas-liquid interface and liquid phase as illustrated in **Figure 2.9**. The main feature of this interaction is the formation of various species, including both long-lived and short-lived reactive species [151]. In order to extend and optimize the utilization of discharge plasmas in liquids, an understanding of the physics and chemistry of discharge plasmas in liquids is required. Consequently, the following parts will present the physical processes observed generally in direct PLI, whereas the chemical processes analysis will be developed for aqueous solution, which is the main topic of this thesis.

a. Physical processes

A lot of researches have been conducted to better understand the mechanisms behind plasma discharge inside a liquid, but the research in this area is still challenging. We notice that the description of the physical mechanisms during direct PLI is very diverse and depends strongly on the intended use of that type of plasma. The physical processes strongly depend on the experimental conditions, which contain several parameters, including electrodes configuration, liquid nature, solutions conductivity, electric field,

and also configuration, liquid nature, solutions conductivity, electric field, and the applied voltage polarity.

The high electric field strength can usually be achieved by using needle electrodes with sharp tips (at least one), from which electric discharges directly in the liquid phase usually start. After that, discharges are generated as conductive and luminous structures in the liquid phase. Branches of such discharges are usually called streamers (in analogy with the discharges in gases). If the discharge does not reach the second electrode, it is called a partial discharge[147,156,157]. If the discharge reaches the opposite electrode, it makes a conductive channel between the two electrodes called a spark. If the current through the discharge is very high (above 1 kA), usually obtained for continuous discharge, it is usually called an arc discharge. The transition from partial discharge to spark discharge results in an electrical breakdown which involves voltage drop, high current, and strong emission. When an electric discharge takes place between two electrodes, it consumes a large part of the energy in forming a fully thermalized plasma channel. As a consequence, UV radiation is formed and emitted from the channel, and its expansion against the surrounding water generates intense shockwaves. For corona discharge in water, the shockwaves are weak or moderate, whereas they are generally very strong for a pulsed arc or spark.

The literature shows that two processes can explain the initiation of the discharge inside a liquid: directly in the liquid phase or through bubble generation [147,148,158–161]. According to the streamer theory, direct discharge in the liquid results from the avalanche multiplication of free charge carriers in the liquid. It forms the basis for a streamer or spark discharge in the liquid medium [160]. The second process is via bubble generation, by which the discharge inside water is initiated in gas cavities formed by heating up the liquid [162–164]. Most theoretical and experimental results support the second process based on the bubble theory because electrons are not sufficiently accelerated to ionize liquid molecules in dense media.

Most of the studies have been performed on discharge propagation mechanisms in a pin-to-plane electrode configuration [156,160,161,165]. This configuration has been used as a reference for understanding the processes that occur during the discharge of plasma directly in the liquid. As an example, positive streamers[a] commonly observed in different liquids show several different modes of propagation [156,166–168]. They can be distinguished into bush-like/primary streamers and filamentary/secondary streamers. In several experiments with positive streamers and pin-to-plane geometry, Lesaint and his co-workers [156,160,166,168,169] have investigated the appearance of bush-like and filamentary streamers that are shown in **Figure 2.11**. By modifying the sharpness and radius of the electrode's tip, they found that the formation of bush-like streamers mostly depend on the electrodes properties, while the propagation of filamentary streamers became independent with the tip radius and always occurred with the same voltage up to a

[a] By analogy with electric discharge in gas, the term “streamer” is commonly used in the literature to refer to discharge propagation in liquid.

critical radius. Above this critical radius, the initiation voltage increased proportionally with the radius of the electrode's needle. These results suggest the existence of a minimum filament radius for self-propagation. This radius depends on the nature of the liquid.

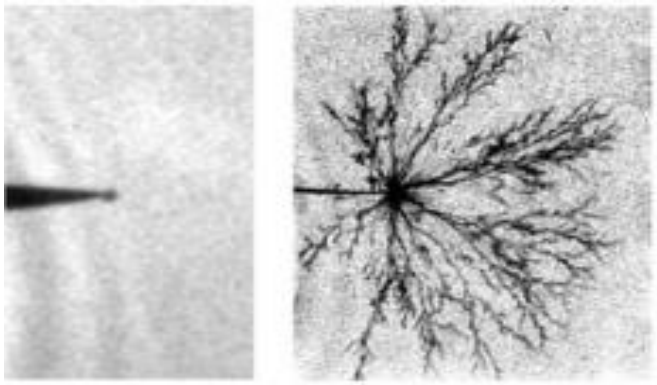

Figure 2.11 Images of typical streamers modes [169]

In order to study the propagation and structure of streamers in liquid dielectrics, Beroual *et al.* [170,171] reported that the negatively biased pin electrode discharges are also filamentary but the propagation mechanism is different, the fast filamentary discharges often happen for the positive polarity more than the negative polarity. The light emission, which is significantly less than that in positive polarity, starts almost immediately after applying the high voltage. It was also shown that breakdown conditions are completely different between positive and negative high voltage. In the case of positive polarity, the breakdown often occurs because of the easier propagation of the second positive mode.

Another example by Habib *et al.* [172] has shown that changing the electrical conductivity of the solution leads to a change in the physical properties of the discharge. It was shown that for the solution conductivity equal to 100 µS/cm, streamers show 6-8 main branchings and several sub-branches. While it was found that the number of streamer branchings was reduced to 2-5 for 500 µS/cm solution conductivity. In addition, a lot of vapor and bubbles are formed due to a high heat generated for 500 µS/cm solution conductivity with an increasing pulse number while fewer vapor has been observed for 100 µS/cm solution conductivity.

Another less common configuration is pin-to-pin discharge under the liquid. For example, this geometry has been used to synthesize nanoparticles using two different operation regimes called glow discharge and arc discharge by adjusting the applied voltage [173,174].

Recently, Rond *et al.* [175–177] have reported the analysis of pre-breakdown and breakdown phenomena for direct pin-to-pin discharge in liquid for conditions similar to those used in this work. They have also shown that bush-like and filamentary formation varies with changes on the applied voltage and conductivity of the solution, especially with the change in discharge initiation from either the anode or the

cathode. Moreover, they have reported that the same experimental conditions can involve different discharge modes, requiring a statistical approach [177] as it will be performed in this work.

In this thesis, we focus on studying the application of the pin-to-pin configuration for the formation of reactive species by the plasma discharge and Cr(VI) treatment. Detailed results will be described in the following chapters of the report.

b. Chemical processes in aqueous solution

As presented above, when the electric discharge is initiated between two electrodes immersed in an aqueous solution, the liquid around and/or between the two electrodes is vaporized and ionized, creating plasma. The high energy level produced by the discharge leads to the creation of active species.

The initial chemical reaction is the water dissociation in the core of the plasma[b]. The two major dissociated mechanisms by the electron impact dissociation (**Reaction 7**) and thermal dissociation (**Reaction 8**), are given as follows [131]:

$$H_2O + e^- \rightarrow OH\bullet + H\bullet + e^- \qquad \textbf{Reaction 7}$$

$$H_2O + H_2O \rightarrow H + OH + H_2O \qquad \textbf{Reaction 8}$$

The first ionization reaction of neutral water molecules follows the **Reaction 9** [178]:

$$H_2O + e^- \rightarrow 2e^- + H_2O^+ \qquad \textbf{Reaction 9}$$

After that water ions can react with water molecules to form hydroxyl radical [179]:

$$H_2O^+ + H_2O \rightarrow H_3O^+ + OH\bullet \qquad \textbf{Reaction 10}$$

The collisions of the electron with water molecules can also form excited water molecules [180]:

$$H_2O + e^- \rightarrow H_2O^* + e^- \qquad \textbf{Reaction 11}$$

The excited water molecules rapidly recover to their fundamental state by randomly reactions below: [181,182]:

$$H_2O^* + H_2O \rightarrow OH\bullet + H\bullet + H_2O \qquad \textbf{Reaction 12}$$

$$H_2O^* + H_2O \rightarrow O + H_2 + H_2O \qquad \textbf{Reaction 13}$$

$$H_2O^* + H_2O \rightarrow O + 2H\bullet + H_2O \qquad \textbf{Reaction 14}$$

Due to the expansion of the plasma volume, water molecules near the interface can be subjected to dissociation attachment by electron transfer [180,183]:

$$2H_2O + 2e^- \rightarrow 2(OH)^- + H_2 \qquad \textbf{Reaction 15}$$

$$H_2O + e^- \rightarrow H^- + OH \qquad \textbf{Reaction 16}$$

$$H_2O + e^- \rightarrow H_2 + O^- \qquad \textbf{Reaction 17}$$

In the liquid phase, reactions can also occur. Ultraviolet (UV) radiation from plasma discharges can lead to the photolysis of water to produce hydroxyl radicals [141,142]:

[b] Species in gas phase have no index whereas species in liquid phase are indicated with (aq) as $H_2O_{(aq)}$

$$H_2O_{(aq)} + h\nu \rightarrow H\bullet + OH\bullet \qquad \textbf{Reaction 18}$$

Photon can also lead to photoionization at the interface [184]:

$$H_2O_{(aq)} + h\nu \rightarrow H_2O^+ + e^-_{(aq)} \qquad \textbf{Reaction 19}$$

Highly energetic electrons, which are generated in the plasma phase, are injected into the water, which results in the generation of solvated electrons [185]:

$$e^- + H_2O_{(aq)} \rightarrow e^-_{(aq)} \qquad \textbf{Reaction 20}$$

Then the species (OH•, H•, e^-_{aq}) will diffuse in the liquid. As this diffusion proceeds, individual pairs may come close enough together to react with each other or with surrounding water [142,180,183,184,186].

$$H_{(aq)}\bullet + H\bullet_{(aq)} \rightarrow H_{2(aq)} \qquad \textbf{Reaction 21}$$

$$OH\bullet_{(aq)} + OH\bullet_{(aq)} \rightarrow H_2O_{2(aq)} \qquad \textbf{Reaction 22}$$

$$H\bullet_{(aq)} + OH\bullet_{(aq)} \rightarrow H_2O_{(aq)} \qquad \textbf{Reaction 23}$$

$$OH_{(aq)} + e^-_{(aq)} \rightarrow OH^-_{(aq)} \qquad \textbf{Reaction 24}$$

$$H_{(aq)}{}^+ + e^-_{(aq)} \rightarrow H\bullet_{(aq)} \qquad \textbf{Reaction 25}$$

$$2e^-_{(aq)} + 2H_2O_{(aq)} \rightarrow H_{2(aq)} + 2OH^-_{(aq)} \qquad \textbf{Reaction 26}$$

$$e^-_{(aq)} + H\bullet_{(aq)} + H_2O_{(aq)} \rightarrow H_{2(aq)} + OH^-_{(aq)} \qquad \textbf{Reaction 27}$$

$$e^-_{(aq)} + H_2O_{2(aq)} \rightarrow OH\bullet_{(aq)} + OH^-_{(aq)} \qquad \textbf{Reaction 28}$$

$$OH\bullet_{(aq)} + OH\bullet_{(aq)} \rightarrow H_2O_{(aq)} + O_{(aq)} \qquad \textbf{Reaction 29}$$

$$OH\bullet_{(aq)} + O_{(aq)} \rightarrow O_{2(aq)} + H\bullet_{(aq)} \qquad \textbf{Reaction 30}$$

The significance of the $e^-_{(aq)}$ consists in its ability to form superoxide radical ($O_2^{\bullet-}$), which could acts as an oxidizing or reducing agent depending on the conditions [180,183,187] :

$$O_{2(aq)} + e^-_{(aq)} \rightarrow O^{\bullet-}_{2(aq)} \qquad \textbf{Reaction 31}$$

Moreover, the oxygen radical anion can be formed from atomic hydrogen and molecular oxygen by [180,183,186,188]:

$$H\bullet_{(aq)} + O_{2(aq)} \rightarrow HO^{\bullet}_{2(aq)} \qquad \textbf{Reaction 32}$$

$$HO^{\bullet}_{2(aq)} \rightleftarrows H^+_{(aq)} + O^{\bullet-}_{2(aq)} \qquad \text{pKa} = 1{,}8*10^{10} \qquad \textbf{Reaction 33}$$

The primary way to hydrogen peroxide production is hydroxyl radical's recombination, as shown in reaction 22. However, hydrogen peroxide can be formed by the following reaction [141,142,189]:

$$HO^-_{2(aq)} + H^+_{(aq)} \rightarrow H_2O_{2(aq)} \qquad \textbf{Reaction 34}$$

UV radiation can catalyze other reactions in an aqueous solution as well. While hydrogen peroxide has a longer lifetime in water, photolysis of hydrogen peroxide can lead to the local production of hydroxyl radicals through this reaction[184]:

$$H_2O_{2(aq)} + h\nu \rightarrow 2OH\bullet_{(aq)} \qquad \textbf{Reaction 35}$$

In summary, it has been shown that electrical discharge under water initiates various and complex physical and chemical processes, and results in generating UV radiation, shock waves, molecular species (H_2, O_2, H_2O_2), ions (H^+ or H_3O^+, O^+, H^-, O^-, OH^-). Moreover, most importantly, reactive radicals (OH, O, H, HO_2) have an extensive application for environmental treatment. For example, the electrical discharge in water can be used to reduce the toxic hexavalent chromium in wastewater [190].

2.3 Chromium (VI) reduction in plasma discharge liquid systems

The generation of plasma-induced reactive species can promote the removal of Cr(VI) based on a reduction mechanism that transforms Cr(VI) into Cr(III). Several studies have shown that Cr(VI) can be reduced by using plasma discharge above or directly in the liquid phase [3–6,191–196]. Recently, most studies have been performed by using plasma discharge above the liquid phase, which is based on the ionization of the gas flow in contact with the liquid surface [5,191,194,195,197]. It was found that these processes involve a high reduction efficiency of Cr(VI), from 60 % to 100 %, depending on the plasma configuration. The different setup reports various power supply technologies (DC, AC, pulse…) with different energy efficiencies in the range of 1.5×10^{-6} to 6.6×10^{-3} g/kJ. It was shown that the reduction efficiencies also varied with the treatment time and initial concentration in the range of 60 % to 100 % for 7 to 25 minutes of treatment, and for an initial solution concentration ranging from 3 to 50 mg/L.

On the other hand, studies based on plasma discharge direct in the liquid have not paid much attention to Cr(VI) treatment. Only three works have been reported, mainly based on the glow discharge plasma configuration. In this part, a brief description summarizes the configuration of the experimental set up and the reduction efficiencies of these studies:

- Wang *et al.* [3] generated a glow discharge plasma in solution by a platinum wire as the anode in contact with the solution. The cathode made by a stainless-steel plate is immersed in the Cr(VI) solution of 50 mg/L. In this study, the plasma was ignited by a DC voltage of 500 V at a current of 100 mA. They reported a higher reduction ratio of about 97 % after 5 minutes of discharge with an energy efficiency of 4.9×10^{-4} g/kJ.
- Another study was reported by Jiang *et al.* [4]. They generated glow discharge plasma in the solution. They used a steel needle wire as the anode in contact with the solution, a graphite stick was used as the cathode and immersed in the solution. Plasma was produced by a DC voltage of 580 V and a current of 120 mA. In this study, the highest reduction rate of Cr(VI) (initial concentration of 31.2 mg/L) obtained after plasma treatment was around 96 % after 18 minutes with 6×10^{-5} g/kJ of energy efficiency.
- The last investigation of reduction using direct discharge plasma in liquid was presented by Harianti *et al.* [192]. They have used a glow discharge plasma in solution, the anode is a Tungsten wire in contact with the solution, and the cathode is a rod of stainless steel. They used an applied voltage of 500V DC. For a Cr(VI) initial concentration of 100 mg/L, the highest reduction rate after 30 minutes of discharge was 93 %, and the efficiency was 3.4×10^{-4} g/kJ.

Table 2.4 summarizes the experimental set up and the main results corresponding to the studies presented above. Whatever the plasma process used, most results indicate that the solution's Cr(VI) reduction is highly dependent on the initial parameters of the solution such as pH, chemical additives, etc., and strongly depends on the physical properties of the plasma as the injected energy.

Some of the chemical and physical process parameters that have been reported to significantly influence the treatment process will be discussed in the following sections based on previous studies.

Power supply	Geometry	Inter-electrode distance	Voltage	Current	Volume of reactor	Initial concentration	pH of solution	Time of process	Reduction efficiency	Energy Yield $G_{Cr(VI)}$/g/kJ	References
Plasma discharge above the liquid											
DC	Pin-to-plate	10 mm	-	40 mA	70 mL	10 mg/L	5.5	7 min	60%	1.5×10^{-4}	195
ns-pulsed	Pin-to-plate with gas supply	5 mm	9kV	-	20 mL	50 mg/L	2.5	15 min	70%	-	196
DC	Pin-to-tube with gas supply	5 mm	1.1-1.5 kV	35-40 mA	-	100 mg/L	-	-	50%	0.9×10^{-4}	197
AC	Plate-to-plate DBD type	3 mm	0.1 kV	1000 mA	100 mL	2.6 mg/L	7 3	21 min	70.7% 94%	1.5×10^{-6} * 1.9×10^{-6} *	193
DC	Pin-to-plate with gas supply	~3-5 mm	1.3 kV	40 mA	20 mL	40 mg/L	2	4 min	100%	0.64×10^{-4} *	6
High voltage transformers	Pin-to-plate with gas supply	6 mm	16 kV	-	50 mL	50 mg/L	2	5 min	40%	6.6×10^{-3} *	191
DC	Pin-to-plate with gas supply	2 mm	1 kV	40 mA	25 mL	40 mg/L	2	3 min	100%	1.4×10^{-4} *	5
Plasma discharge in the liquid											
DC	Pin-to-plate	-	0.6 kV	120 mA	150 mL	31.2 mg/L	2	18 min	96%	6×10^{-5} *	4
DC	Pin-to-plate	-	0.6 kV	936 mA	-	100 mg/L + 100ppm phenol	-	30 min	93.35%	3.4×10^{-4}	192
DC	Pin-to-plate	-	0.5 kV	100 mA	150 mL	50 mg/L 100 mg/L	2	5 min 15 min	97% <100%	4.9×10^{-4} * 3.3×10^{-4} *	3

Table 2.4 Application of non-thermal plasma for reduction of Cr(VI) (*these values are recalculated in this work using Equation 11)

2.3.1 Influence of the chemical parameters

The chemical parameters of the solution are one of the most important parameters which affect the removal efficiency of Cr(VI) when using the plasma discharge liquid interactions technique. The initial chemical parameters of the solution are not affected by the different plasma configurations, thus in this part, we report both studies of plasma discharge above and direct in the liquid phase.

a. Initial concentration of hexavalent chromium

The initial concentration of Cr(VI) has been shown to influence the efficiency rate during the process using plasma discharges. For example, Du *et al.* [5] have treated Cr(VI) for 5 minutes using argon micro-plasma discharge of 2 kV and 40 mA generated at the gas–solution interface. It was shown that an increase in the initial concentration of Cr(VI) from 20 mg/L to 100 mg/L resulted in a lower Cr(VI) reduction efficiency, which decreased from 100 % to 50 %, respectively.

Another study also performed plasma discharge above the liquid phase, in which a high voltage micro-plasma of 20 kV was generated during 25 minutes [191]. The plasma was sustained by an argon gas flowing through the inner electrode (stainless-steel rod) at 6 mm apart from the surface solution. The reduction of Cr(VI) was carried out at different initial concentrations: for 30 mg/L of Cr(VI), 99 % reduction efficiency was observed that decreased to 94 % and 90% for 40 mg/L and 50 mg/L of Cr(VI), respectively.

Furthermore, only one study, Wang *et al.* [3], has shown the effect of the initial concentration of Cr(VI) on the removal efficiency by using direct plasma discharge in solution (glow DC discharge of 500 V and 100 mA). Investigation of the effect of the initial concentration of Cr (VI) in reduction efficiency has been reported in a range from 100 mg / L to 1000 mg / L with an initial pH of 2. It was found that higher initial concentration resulted in lower Cr(VI) removal efficiency, but a higher amount of Cr(VI) removed. For example, with the initial Cr(VI) concentration of 50 mg/L, 97 % of Cr(VI) was removed within 5 min of treatment which corresponds to the amount of Cr(VI) removed of 7,28 mg. In comparison, with the initial Cr(VI) concentration of 1000 mg/L, about 15,3 % of Cr(VI) can be removed within the same treatment time, but the amount of Cr(VI) removed increased to 22,95 mg. They explain that as the initial concentration increases, more Cr(VI) species are available to react with the hydrogen atom produced in solution after plasma discharge.

Based on these results, it was shown that **the higher the initial concentration of Cr(VI), the lower the reduction efficiency** obtained by the non-thermal plasma method.

b. Initial pH

The effect of initial pH in the reduction of Cr(VI) by plasma direct discharge processes has been reported by Wang *et al.* [3]. As described previously, the plasma glow discharge in the liquid phase is obtained by a

Pt anode wire – stainless cathode plate configuration at 500 VDC – 100 mA. It was shown that the Cr(VI) reduction rate was higher in acidic conditions than in neutral or basic conditions. As an example, when the initial pH is 8.0, Cr(VI) can be reduced by 46 % within 10 minutes of process, while nearly 95 % of Cr(VI) can be removed with the initial pH is 2.0 within the same treatment time and for the same initial concentration of Cr(VI) of 100 mg/L.

A similar observation in the effect of the initial pH on the reduction of Cr(VI) by using glow discharge plasma in the liquid phase has been reported by Jiang *et al.* [4]. They have shown that nearly 95 % of Cr(VI) can be removed when the initial pH is 2.0 after 18 minutes of treatment, while only 39 % of Cr(VI) has been removed when the initial pH is 10.5.

The reduction of Cr(VI) under acidic conditions can be explained by the speciation of Cr(VI) (**Figure 2.2**). When the pH decreases to acidic medium, Cr(VI) tends to transform from CrO_4^{2-} into dichromate forms ($Cr_2O_7^{2-}$) and hydrogen chromate ($HCrO_4^-$) by the reactions below[3]:

$$CrO_4^{2-} + H^+ \rightleftarrows HCrO_4^- \qquad \textbf{Reaction 36}$$

$$2HCrO_4^- \rightleftarrows Cr_2O_7^{2-} + H_2O \qquad \textbf{Reaction 37}$$

It has been shown that it is easier to reduce $Cr_2O_7^{2-}$ than CrO_4^2 by reducing agents as H^o, based on the rate constants of **Reaction 38** and **Reaction 39** [3]:

$$Cr_2O_7^{2-} + 6H^o + 8H^+ \rightleftarrows 2Cr^{3+} + 7H_2O \qquad k = 2.0 \times 10^{10}\ M^{-1}\ s^{-1} \qquad \textbf{Reaction 38}$$

$$CrO_4^{2-} + 3H^o + 5H^+ \rightleftarrows Cr^{3+} + 4H_2O \qquad k = 8.2 \times 10^{9}\ M^{-1}\ s^{-1} \qquad \textbf{Reaction 39}$$

These results show the effect of the initial pH of the solution in reducing Cr (VI) by non-thermal plasma methods as **the removal efficiency increases due to the decrease in pH of the solution**. This is one of the important parameters that need to be paid attention to and studied for further application.

c. Effect of OH scavenger

As presented in **Reaction 8** and **Reaction 10** to **Reaction 18**, many hydroxyl radicals are produced in the solution. Hydroxyl radical is an oxidizing species, which can re-oxidize Cr(III) to Cr(VI) by the following the **Reaction 40** [191,198]:

$$3OH\bullet + Cr(III) \rightarrow Cr(VI) + 3OH^- \qquad \textbf{Reaction 40}$$

In addition, the hydroxyl radicals can react with hydrogen atoms to produce water, and so decrease the amount of H, which is one of the main reactive species that can reduce Cr(VI). The presence of OH radicals could lead to a decrease in the removal efficiency. In order to avoid the effect of hydroxyl radicals, many researchers have used organic solutes as OH scavengers (phenol or ethanol...) [3,5,6,196].

As an example, Z. Chen *et al*. [196] have reported the effect of ethanol on the reduction efficiency of Cr(VI) in solution by using argon plasma discharge above the liquid. The plasma is generated by using a nanosecond pulsed generator and the voltage applied was ± 9 kV. In this study, they have shown that 70%

of Cr(VI) can be reduced by the Ar plasma discharge with the addition of 1 ml ethanol in solution, while without ethanol, the reduction efficiency is only 10% with the same treatment time (15 minutes).

Moreover, from the above results, it was found that the addition of ethanol does not only promotes the Cr(VI) reduction by acting as a hydroxyl radical scavenger but also increases the production of H_2O_2 that seems to be responsible for the high reduction rate in low pH environment [3,6].

The explaination was given by Wang that, the addition of the hydroxyl scavenger transforms the hydroxyl radicals into organic radicals by reaction with organic solvents. In general, the organic radicals have a low reduction potentials (-1 to -2 V) and are therefore able to reduce Cr(VI) to lower oxidation states. It also inhibits the reoxidation of Cr(III) and converts the oxidizing species to reducing species[3].

These results showed that **adding ethanol** as an OH scavenger can increase **the reduction efficiency of Cr(VI)**.

d. Influence of hydrogen peroxide

Another interesting aspect of plasma discharges assisted Cr(VI) reduction is due to the formation of H_2O_2, which is capable of reducing Cr(VI) at low pH [191,199].

Hydrogen peroxide is not a chemical reagent present in the initial solution but is known to be a species produced by plasma discharge in several solutions. The advantages of H_2O_2 on the elimination of Cr(VI) by using non-thermal plasma discharge have been discussed by various researchers [3,191,196,199]. In particular, Chandana *et al*. [191] reported the effect of H_2O_2 at low pH on the reduction efficiency of Cr(VI) by using plasma discharge above the liquid phase. It was shown that even after switching off the plasma discharge, around 50 % conversion of Cr(VI) (with an initial concentration of 30 mg/L) was observed. They explained that at pH = 2, Cr(VI) standard reduction potential (+1.08 V) is higher than that of H_2O_2 (+0.56 V); hence H_2O_2 is a reducing agent for Cr(VI) via the **Reaction 41**[190,199]:

$$3H_2O_2 + Cr_2O_7^{2-} + 8H^+ \rightarrow 2Cr^{3+} + 3O_2 + 7H_2O \qquad \textbf{Reaction 41}$$

These results have shown that **forming H_2O_2 in an acidic environment** by plasma liquid interactions leads to an **increase in the removal efficiency** of Cr(VI).

The relation between H_2O_2 and Cr(VI) reduction will be detailed in **Chapter 7**.

2.3.2 Influence of physical parameters

In contrary to the influence of chemical parameters, the effects of physical parameters are very different for each plasma configuration such as plasma discharge above the liquid phase or direct discharge in a liquid phase. Thus, in this part, we mainly focus on the mechanisms of direct plasma discharge in the liquid phase for the reduction of Cr(VI). Indeed even though only a few studies have been done in this field, this configuration is the one used in our work.

The applied voltage is one of the most investigated physical plasma parameters that have been shown to influence the reduction process of Cr(VI). In the plasma discharge process, the increase of the applied voltage leads to an increase in the electric field and the injected energy (for a given electrode geometry). The influence of the applied voltage has been studied by [3,193] on the conversion efficiency of Cr(VI) to Cr(III) by using direct plasma discharge under solution.

Wang *et al.* [3] have used plasma glow discharge in solution generated by a platinum wire -stainless-steel plate configuration. They showed that, at 300 V, almost no Cr(VI) removal was observed after 15 minutes of treatment. The removal efficiency increased to 5% when the applied voltage was 400 V. The huge increase in removal rate increased to about 30 % when the applied voltage increased over 450 V and increased to 50 % at 500 V. They have suggested that glow plasma discharge was not fully grown when the voltage is lower than 400 V, and the number of reactive species produced in the solution was low, leading to a low Cr(VI) reduction rate.

Zhang *et al.* [193] have also reported that Cr(VI)'s removal efficiencies significantly increase as the input voltage increases. At an input voltage of 80 V, about 51 % of Cr(VI) was removed after 21 minutes of DBD plasma treatment, and approximately 80 %, 81 %, 83 %, and 84 % of Cr(VI) were degraded at input voltages of 90 V, 100 V, 110 V, and 120 V within the same treatment time, respectively. It was shown that increasing the applied voltage from 80 V to 90 V leads to a huge increase in Cr(VI) removal efficiency.

In general, the phenomena can be explained by the fact that when the applied voltage is decreased, the ignitions of the plasma are not strong enough, thus leading to a decrease in the formation of reactive species, which is the main agent that can reduce Cr(VI)[3].

These results show that **increasing the applied voltage** leads to an **increase in the reduction process of Cr(VI).** It is noted that most of these studies have been done using a DC power supply. Thus they work in the constant and low applied voltage, which is different from our configuration (with pulse power supply and the voltage is higher than 1 kV).

The relation between the applied voltage and Cr(VI) reduction will be discussed in **Chapter 6**

2.4 Conclusion

There are several oxidation (or valence) states of chromium, and each state has different chemical characteristics. The most common forms are trivalent chromium Cr(III) and hexavalent chromium Cr(VI). Trivalent chromium compounds can exist naturally occurring or be by-products of industry, and they are non-toxic, while hexavalent chromium compounds mostly result from industrial activity and represent a health hazard.

Besides, we have presented different analytical techniques that allow the determination of chromium VI compounds in solution, such as absorption spectroscopy. More complicated and precise methods include Atomic absorption spectroscopy (AAS), High-performance liquid chromatography (HPLC), or Inductively coupled plasma mass spectrometry (ICP-MS). However, various studies have shown the ease of use of UV-Vis absorption spectrometry, especially with 1,5-diphenylcarbazide.

Several methods can be applied to reduce Cr(VI) in the solution as ion exchange, adsorption, electrochemical, and precipitation methods, but the applicability and effectiveness of these approaches are limited by high costs, poor chemical distributions, and undesired side reactions in the solution. Not only that, but the electrochemical method also produces a second toxic waste such as Fe^{3+}, which pollutes the environment. In addition, the fact that Cr(VI) is not removed from the solution, but only changes its oxidation state, requires carefully evaluating the long-term stability of reduced products and possible re-oxidation mechanisms.

It is therefore of increasing interest to develop “green” techniques to remove Cr(VI). These would use less toxic and hazardous reagents and avoid producing the second pollution. In this regard, the Plasma-Liquid Interaction (PLI) process is proposed as a "green" technique to reduce Cr(VI) from wastewater. In PLI processes, a range of long- and short-lived reactive species (e.g. e_{aq}^- , H•, OH•, H_2O_2, etc.) is generated in the liquid phase, which reduces Cr(VI) to Cr(III). PLI processes are suitable for eliminating Cr(VI) without adding toxic chemicals and avoiding the production of the second pollution. Only three works using direct PLI have reported interesting results for Cr(VI), it is noted that they used DC power supply, unlike pulsed discharge in this work. The relation between the applied voltage and Cr(VI) reduction will be discussed in **Chapter 6.**

Chapter 3
Description of the experimental systems and applied methods

In this chapter, we present the techniques developed in the frame of this Ph.D. to remove and detect hexavalent chromium in solution. The technique used to reduce Cr(VI) is based on the generation of plasma discharges immersed in liquids. As presented in **Chapter 2**, only a few studies have been done on plasma discharge inside the liquid to reduce Cr(VI), then we are working on a new and fascinating field. Therefore, an essential part of this work is to develop an experimental setup for a plasma in-liquid (direct PLI) removal technique. The development of this removal process is managed to reduce Cr(VI) using a clean and isolated system. In this regard, a pair of electrodes completely isolated from the surrounding liquid media is developed as pin-to-pin electrodes.

This section also describes the method to collect and analyze data resulting from plasma liquid interactions.

In this section, the following items will be presented: the reactor system, the data acquisition and analysis, and finally, we will discuss the reproducibility of the experiments.

3.1 The experimental setup

3.1.1 Overall experimental configuration

A general schematic of the experimental setup is shown in **Figure 3.1**. It is dedicated to produce pulsed electrical discharges in liquid using a pin-to-pin configuration.

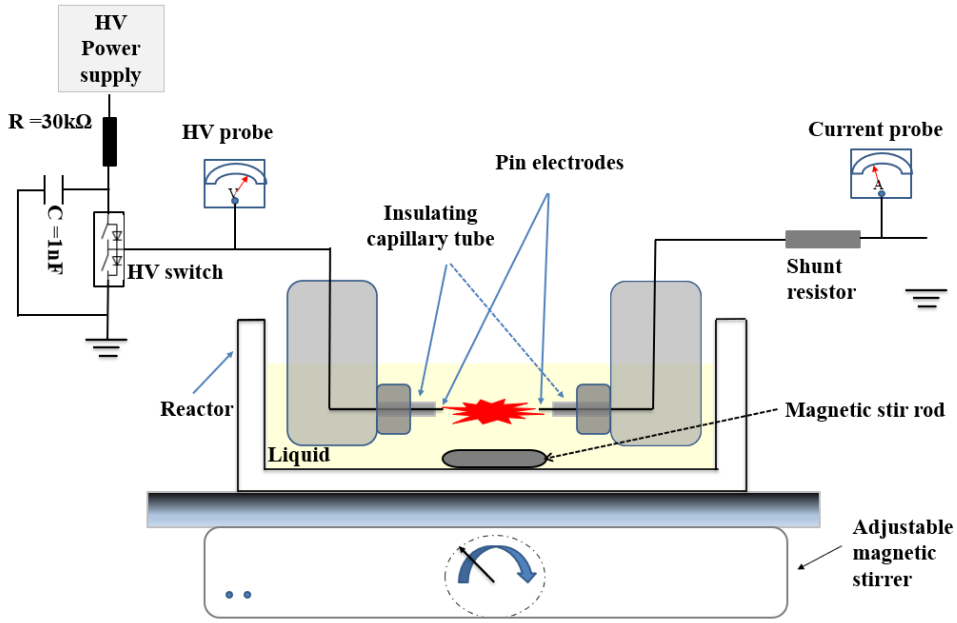

Figure 3.1 Schematic diagram of the experimental setup.

To generate the high voltage pulses, a low inductance capacitor (C = 1 nF) is charged by a 30 kV DC high voltage power supply (Ultravolt 30A24-P30), passing through a 30 kΩ resistor, which discharges through a fast-high voltage solid-state switch (Behlke HTS 301-03-GSM). The switching modules of the series Behlke HTS 301-03-GSM consist of two identical metal oxide semiconductor field-effect transistors (MOSFET), which form a half-bridge circuit, also called a push-pull circuit. The maximum electrical characteristics of this device are: Voltage 2×30 kV, Peak current 2×30 A; and the minimum output pulse width is 200 ns. Regardless of pulse width, frequency, and duty cycle, the device is precise in the timing of switches. The advantages of applying a Behlke HTS are the fast rise and fall times and short pulse durations [200]. The Behlke HV switch is powered by a stabilized 5 V DC power supply (ALR3003, ELC), and its control input (*i.e.* frequency and pulse duration) is performed using a pulse generator (TTI-TGP110).

In the process, one electrode is connected to the high voltage power supply, while the other one is connected to the ground. Regarding their electrical poles during the process, electrodes will be called anode and cathode, respectively. The two electrodes are immersed in a liquid contained by a reactor (more details in section **3.1.2**).

In order to maintain a homogeneous aqueous solution, a magnetic stirring bar at the bottom of the reactor is used to keep the solution well mixed.

In our experimental conditions, the positive high voltage pulse has a rise time equal to 30 ns. In this work, a variety of electrical parameters have been chosen for the study, as an example, the voltage range is between U = 2 kV and 12 kV, the pulse frequency is adjusted from f = 5 to 70 Hz, and the pulse duration is varied from Δt = 10 µs to 1 ms.

3.1.2 Reactor and electrodes

The pin-to-pin geometry of electrodes immersed in liquid has been used throughout this entire thesis (**Figure 3.1**). The metallic electrode components have been completely isolated from the surrounding liquid with electrically nonconductive plastic and capillary tubes. The length of the part of the two pin electrodes immersed in the liquid is measured with a microscope before and after the process for each experiment. Both electrodes are connected to a micrometer control system (XYZ) to adjust the positions of the electrodes, and so the distance between them (not shown in **Figure 3.1**).

It is worth noting that, depending on the experimental campaign, the reactor configuration and electrodes materials are changed relatively to water or Cr(VI) solution experiments. The specificities of the experimental setup are detailed below.

- ***In water*:**

In this study, pin electrodes of 100 µm diameter have been used. The length of the two pin electrodes protruding from the water is about 400 µm (±10 µm) for most of the studies. However, in a few experiments, we mention working with a 200 µm diameter, and the protruding length of the electrodes in water is about 0 ± 10 µm. The electrodes are set at 2 mm gap for all of the experiments in this study. Most of the experiments are performed using tungsten electrodes, but the use of platinum is also considered.

Experiments investigating H_2O_2 concentration during the discharge are performed in a cylinder glass reactor. In contrast, experiments dedicated to the variation of electrodes length involve a rectangular PVC reactor including two parallel silica windows for optical access.

The volume of the solution is 200 mL and 150 mL, corresponding to the two different reactors: cylinder glass and rectangular, respectively. For this campaign, the primary liquid is distilled water, and the conductivity of the solution is adjusted to σ = 200 µS/cm using sodium chloride (NaCl). We have verified that changing the shape and the volume of the vessel does not involve significant variations in the final results on either H_2O_2 or electrodes measurements (lower than the estimated uncertainties).

- ***In Cr(VI) solution:***

The electrode system consists of a symmetrical electrode pair of 100 or 200 µm in diameter platinum (Pt) wires of 99.99 % purity. The length of the pin electrode protruded from the insulator in the

solution ranges from 0 to 500 µm. The inter-electrode distance is adjusted from 0.5 to 5 mm. In this campaign, the treatment is carried out in two different reactors: a cylinder glass reactor (10 cm diameter) and a rectangular quartz vessel (100×50×50 mm). The volume of the solutions is kept the same at 100 mL for all of the experiments. A homemade cap is used to cover the reactor to prevent any toxic evaporation from the solution during treatment.

We choose to work with an initial concentration of Cr(VI) of about 50 mg/L (**stock solution**). This value is selected from reports of environmental pollution with Cr(VI) since it allows comparing the effectiveness of the treatment process with the common method, as presented in **Chapter 2**. The 50 mg/L Cr(VI) solution is prepared by dissolving 0,1414 g potassium dichromate ($K_2Cr_2O_7$) in distilled water, in a 1 L volumetric flask. Following a method given by the literature [201], the stock solution concentration is around 50 mg/L with a precision of 0.3 mg/L.

Moreover, in this work, we note that the treatment of Cr(VI) by the PLI is completed in an acidic medium because, as presented in **Chapter 2**, Cr(VI) is easier to reduce in an acidic environment. As a consequence, the **standard solution** corresponds to the mixture of the stock solution with sulfuric acid: 94 mL of 50.0 ± 0.3 mg/L Cr(VI) solution is mixed with 6 mL of acid H_2SO_4 0,1 M. Thus, the concentration of the standard Cr(VI) solution used at the beginning of the process is around 47.0 ± 0.3 mg/L.

The resulting properties of the standard solution are a conductivity equal to about σ = 4 mS/cm, and the pH = 2.3-2.4. It is noted that the value of conductivity and the pH of the standard solution is a consequence of mixing the stock solution with sulfuric acid.

3.2 Data collection and analysis

In this section, we present the techniques to collect and analyze the data of the experiment. We analyze the electrodes by microscopy and the discharge propagation by shadowgraphy. Moreover we note that the two main measurements performed during the campaigns are based on electrical and chemical analyses.

3.2.1 Electrode analysis

Microscopy measurements have been used to analyze the characteristic of the electrodes in the water solution during the PLI process.

- ***In situ* IDS imaging**

Both electrodes are imaged on a CCD Camera (IDS Imaging Development Systems) through a homemade microscope with a (×2)-magnification. A long working distance objective (Mitutoyo plan apochromatic, infinity corrected) is used to take into account the dimension of the reactor and is coupled to a tube lens with an f=200 mm focal length. This optical system allowed *in situ* and real-time measurement of the variation on the length of the electrodes during the plasma discharge (presented in **Figure 3.2**) with an accuracy of about 98 %.

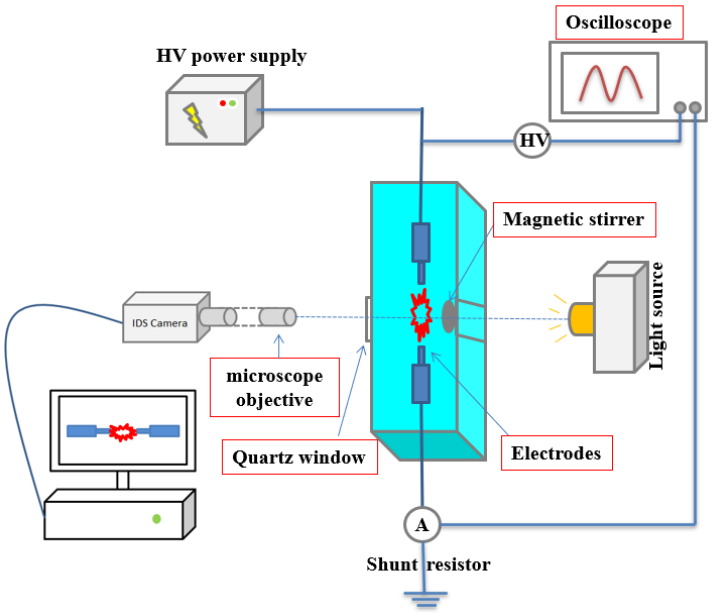

Figure 3.2 Schematic diagram of the optical diagnostics in water with IDS camera [202]

- ***Ex situ* material analysis**

Morphology of the electrodes after the discharge is studied ex situ by using Scanning Electron Microscopy (SEM). SEM is an electron microscopy technique in which a high-energy electron beam focused on the surface of a solid sample (as electrodes surface in this study) and scanned over a small surface area. The interaction between the electron beam and the surface atoms and molecules of a sample produces signals such as secondary electrons, backscattered electrons, and X-rays that provide information about the sample's topography, composition, conductivity, etc. Thus in SEM characterization, it requires the analysis sample need to be conductive [203].

In this work, a field emission gun (FEG)- SEM (Carl Zeiss, Supra VP40 FEG-SEM) is used to characterize the morphology of the electrodes in vacuum mode. It is noted that these measurements have been done under the guidance of Ovidiu Brinza (Department of measurement).

3.2.2 Shadowgraphy measurements

An shadowgraphy setup is used to study the discharge properties in a Cr(VI) solution (**Figure 3.3**). Regarding the optical diagnostics, a 1.5 W Ventus laser light source (532 nm) is focused by a condensing silicate lens system onto a slit (Ø = 100 um) and then brought to a parallel beam by a 300 mm focal lens and reflected by a mirror f=800 mm. After that, the light passes through a slit (Ø = 200 mm) and directly sight on the reactor. A 105 mm objective focuses the region of interest of the test cell (interelectrode gap) on the sensor of a high-speed camera (Photron SAS). Videos are recorded using an exposure time of 0.37 µs and a widescreen resolution of 128x80 pixels, allowing 372000 frames per second.

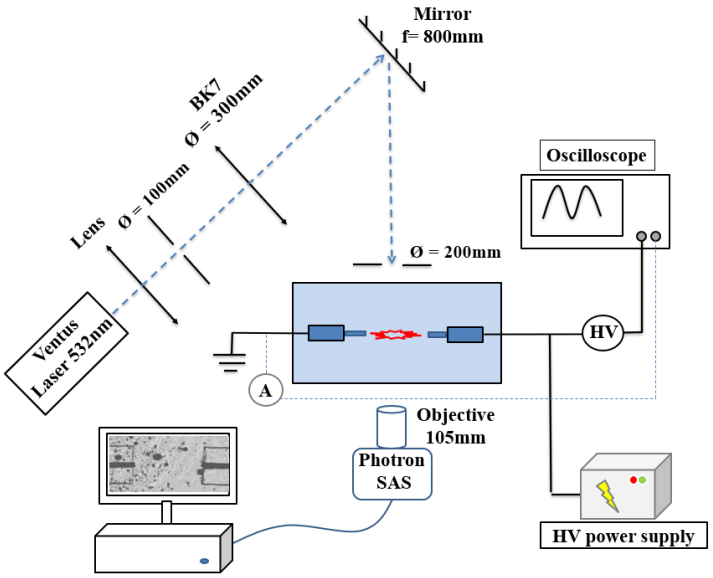

Figure 3.3 Schematic diagram of the optical diagnostics in Cr(VI)

In order to improve the time resolution, we make some changes in the settings of the image acquisition chain. The image is captured by the Andor istar 734 camera (replacing the Photron SAS camera) and the region of interest (the distance between the electrodes) is captured by a 105 mm objective and through a system consisting of three different objectives of 20 mm, 12 mm, and 36 mm. The delay time of the trigger is varied from 0.5 to 10 µs to scan the discharge propagation and the duration of the acquisition is 100 ns.

It is noted that this experimental campaign has been performed in collaboration with Hervé Rabat (GREMI) in the frame of the French Plasma Network actions (*IPMC – réseau Plasmas Froids*).

3.2.3 Electrical measurements

The anode is connected to an HV probe (LeCroy PMK 20 kV, 1000:1, 100 MHz), and the cathode is connected to a shunt current probe, as shown in **Figure 3.1** and **Figure 3.2**. For all the results of this chapter, the applied high voltage and discharge current are simultaneously recorded by an oscilloscope (HDO9104 - 1GHz, Teledyne LeCroy), recording the signal over 1 ms by using 1 MS leading to a time resolution of 1×10^{-9} s.

An example of the obtained signals is shown in **Figure 3.4**, and the analysis is developed in the next chapter.

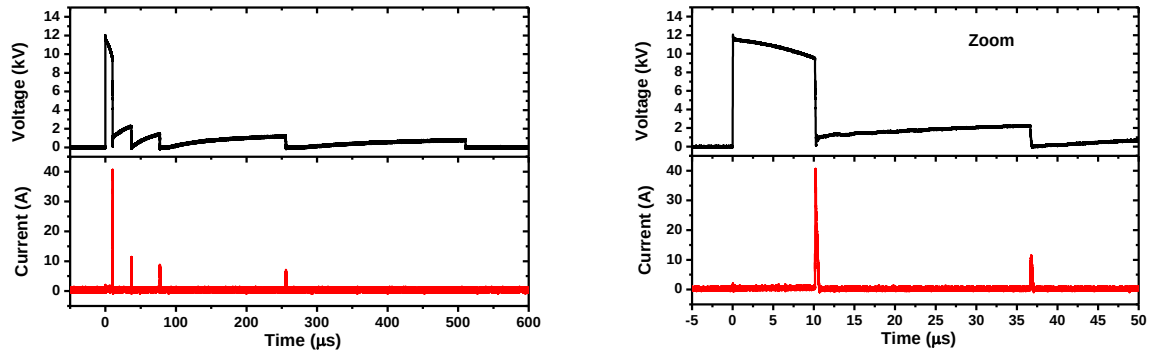

(a) (b)

Figure 3.4 (a) Voltage and current signals and (b) a zoom of a pin-to-pin discharge in Cr(VI) solution ([Cr(VI)]=47 mg/L; σ=4 mS/cm; pH=2.4) monitored for applied voltage of 10 kV, Δt = 500 µs and gap=2 mm.

The input energy of plasma discharges per pulse is determined using **Equation 1**. The injected energy (*J*) for one pulse $E_{/pulse}$ is determined by integrating the measured current and voltage values over the pulse duration.

$$E_{/\text{pulse}} = \int_{t_0}^{t_f} I \times U \, dt \qquad \textbf{Equation 1}$$

With U, I corresponding to measured voltage (V) and current (A), t_0 and t_f (s) are the time at the beginning and the end of pulse duration, respectively. As an example, the injected energy corresponding to the electrical signals of **Figure 3.4** is shown in **Figure 3.5**. The result will be discussed in **Chapter 4**.

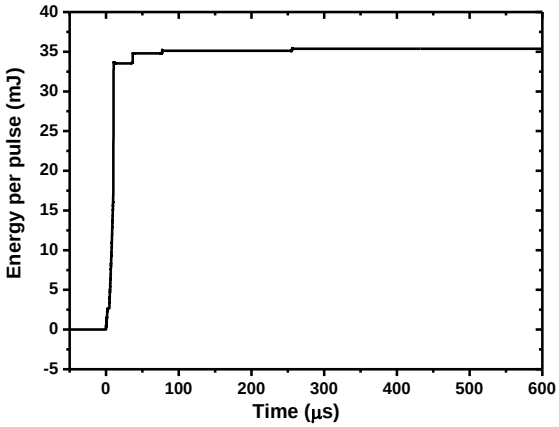

Figure 3.5 Energy per pulse of a pin-to-pin discharge in Cr(VI) solution ([Cr (VI)]=47 mg/L; σ=4 mS/cm; pH=2.4) monitored for applied voltage of 10 kV, Δt= 500µs and gap=2 mm

Using the Labview software, a homemade program has been developed by Nicolas Fagnon (Department of Design, Measurement, and Monitoring) to calculate the energy per pulse automatically during the experiment. This program also allows classifying the properties of the discharges between breakdown (BK) and no breakdown (NOBK). Because, as it will be presented in detail in **Chapter 4**, it is possible to monitor two different cases of discharge during the process. As a consequence, we note that in the case of mixing BK and NOBK, the average injected energy per pulse $\bar{E}_{/pulse}$ (mJ) is calculated by the **Equation 2**

$$\bar{E}_{/pulse} = [(\overline{E_{BK}} \times \%_{BK}) + (\overline{E_{NOBK}} \times \%_{NOBK})]/100 \qquad \textbf{Equation 2}$$

Where $\overline{E_{BK}}$ and $\overline{E_{NOBK}}$ are the average injected energies per pulse for discharge with and without breakdown respectively (in mJ): $\%_{BK}$ and $\%_{NOBK}$ are the distributions between breakdown and no breakdown (in %).

The total injected energy of the process E_{total} (J) is calculated by using **Equation 3**:

$$E_{total} = \bar{E}_{/pulse} \times f \times T_{total} \qquad \textbf{Equation 3}$$

Where f is the applied pulse frequency (Hz) and T_{total} is the total time of the process (s).

3.2.4 Chemical analysis

Ex situ measurements of conductivity (SensION+ EC71, HACH) and pH (SensION MM340, HACH) of the reactive media are conducted before and after the process. The temperature of the solution is also measured before and after by using an infrared non-contact thermometer with laser sighting (GM700I).

a. Colorimetric diagnostics

The concentration of various chemical compounds after discharges is determined by UV-vis spectrophotometry. The measurement is carried out by irradiating a sample with a light beam.

For quantitative measurements in UV-vis spectrophotometry, the Beer-Lamberts law is applied to determine the element concentration. Beer-Lamberts law states that the concentration c (mol/L) of an element is directly proportional to the absorbance (A) of the solution based on **Equation 4**:

$$A = \varepsilon c L \qquad \textbf{Equation 4}$$

Where L is the optical path length (cm), and ε is the molar absorption coefficient ($L/(mol.cm)$), which depends on the interaction between the element and the wavelength of the light source. Absorbance is related to transmittance (T) and is explained by the following **Equation 5**:

$$A = \log\frac{I_o}{I} = \log\frac{100}{T} \qquad \textbf{Equation 5}$$

Figure 3.6 shows an incident light source of intensity (I_0) irradiating and transmitting light intensity (I).

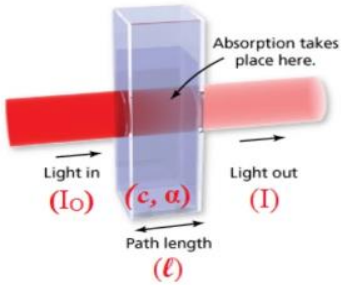

Figure 3.6. Illustration of a cuvette explaining the Beer-Lamberts law [204]

Because of the Beer-Lambert law principle, the increase of the optical path length allows better measurement sensitivity. This is why special attention will be paid to set up an optical cell to define an optical path length long enough to reach a low detection limit (*in situ* Cr(VI) measurements, **Annex 6.2**). This method is used to measure the concentration of Cr(VI) and H_2O_2, as presented in the following sections.

b. Concentration of Cr(VI)

In particular, for Chromium (VI), we use different ways to analyze the concentration by spectrophotometry. We use (i) ex situ technique with direct measurements and indirect measurements and (ii) *in situ* technique.

(i) *Ex situ* technique

For this technique, the absorbance is determined by UV-vis absorption spectroscopy consisting of a spectrometer (AvaSpec-2048 XL, Avantes) combined with a deuterium-halogen light source (AvaLight-DHC). The light beam travels through fiber optics cables and passes through a 1 cm light pathway sample (cuvette). The transmitted light beam reaches the spectrometer and is collimated by a mirror. A grating diffracts the collimated light which passes towards a second focusing mirror, and projects the spectrum onto a linear detector array. The software graphically visualizes the collected data as the amount of light absorbed or transmitted as a function of wavelength. The analysis is performed with an automatic integration mode (integration time: 13,97 ms, an average of 36 scans, and two smoothings), and the operating wavelengths range from 275-500 nm.

As presented in section **2.1.4**, there are two pathways to measure the concentration of Cr(VI) in solution using ex situ UV-visible spectrophotometry:

- The **direct measurement** is based on the original absorption of Cr(VI) ions, and it is able to measure the concentration of Cr(VI) above 1 mg/L at the wavelength of 350-375 nm.

  Experimental protocol: every 15 minutes during the treatment process, 2 mL of the treated solution is sampled, transferred into a 1 cm quartz cuvette, and placed in the sample holder of the spectrometer. The Avalight software performs the analysis at the wavelength of **350 nm**. For example, **Figure 3.7** shows the UV-vis absorption spectrum of Cr(VI) solution measured in the range of 275 - 600 nm.

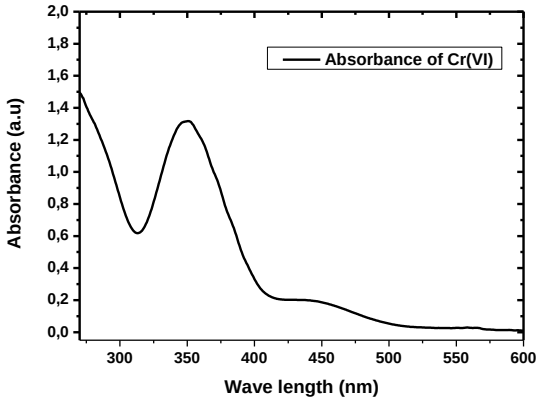

Figure 3.7 UV-vis absorption spectrum of Cr(VI) solution ([Cr(VI) = 40 mg/L)

- The **indirect measurement** is based on the addition of 1,5-diphenylcarbazide (DPC) to the studied liquid, which reacts with Cr(VI) but not with Cr(III), thus ensuring selectivity. The reaction between Cr(VI) and DPC in an acidic environment forms a colored complex with an absorption maximum at **540 nm**.

  Diphenylcarbazide solution is prepared by dissolving 250 mg of 1,5-diphenylcarbazide powder in 50 mL of acetone. All the powder is dissolved with the help of ultrasonication. The solution must be kept in a brown bottle to avoid the influence of light.

  Experimental protocol: Every 15 minutes during the treatment process, 2 mL of Cr(VI) solution is taken and transferred to a 1 cm quartz cuvette containing 0.2 mL of acidic H_2SO_4 (0.1 M) and 0.1 mL of DPC solution. Thus, after 10 minutes of mixing, the measure is carried out to obtain full color development. The Avalight software performs the analysis of the complex, as shown in **Figure 3.8**. We note that this method is mainly used to measure the Cr(VI) concentrations below 1 mg/L because of the intense color formation. In this work, we use this method to verify the concentration of Cr(VI) in the last 30 minutes of the treatment process.

It is worth noting that calibration curves with known concentrations of Cr(VI) are carried out to calculate the concentration for each method. The details of the calibration curve are presented in **annexes 3.1** and **3.2.** We also report that the calculation of uncertainties for the calibration curve is lesser than 1 %.

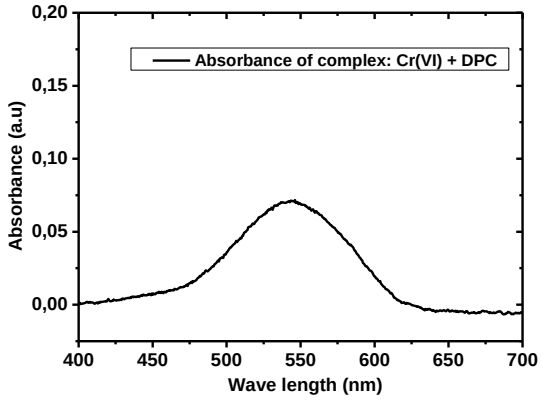

Figure 3.8 UV-vis absorption spectrum of the complex of Cr(VI) ([Cr(VI) = 0.01 mg/L) with DPC

(ii) *In situ* technique

Finally, we present a method that can accurately analyze Cr(VI) concentration by *in situ*, and real-time measurement during the process using UV-visible absorption. The advantage of this method is that there is no need to use any reagents, and above all, this method can accurately determine when Cr(VI) is completely reduced. The principle of this method is based on the changes in the transmitted

power of incoming light through the Cr(VI) solution during the process. **Figure 3.9** shows the experimental setup to measure the *in situ* concentration of Cr(VI) during the PLI process.

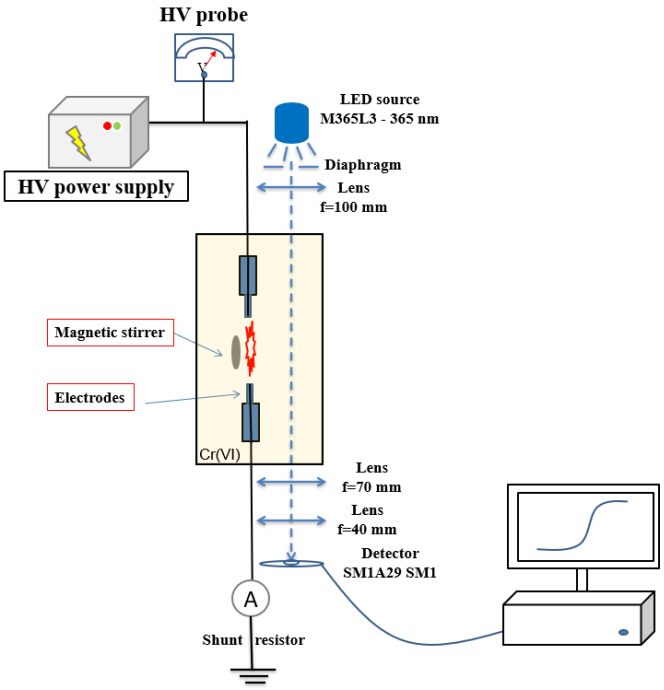

Figure 3.9 Schematic diagram of the experimental setup for direct *in situ* [Cr(VI)] measurement

A LED light source at 365 nm (M365L3 - 365 nm, 880 mW (Min) Mounted LED, 1000 mA) is collimated by a condensing lenses system and then focus by a 100 mm focal lens to pass through the reactor with the focus point mainly at the middle of the reactor. The remaining light is then refocused by a 70 mm and 40 mm lens on a photodiode power sensors detector (SM1A29 SM1), which is directly connected to a computer, thus recording the signal along the reduction process.

It is worth noting that a calibration curve with known concentrations of Cr(VI) is carried out to calculate the concentration. The details of the calibration curve are presented in **annex 3.3**. We also report that the calculation of uncertainties for the calibration curve is about 1 %, which is related to the standard deviation of several measurements for each concentration.

c. Concentration of hydrogen peroxide

The most stable and common oxidant that occurs after discharges is hydrogen peroxide (H_2O_2), and H_2O_2 plays an essential role in the disinfection of water. In particular, H_2O_2 affects the reduction process of Cr(VI), as presented in **Chapter 2**. Two methods are used to determine hydrogen peroxide production after the discharges in water and Cr(VI) solution.

- **Eisenberg method (in water):**

The well-known colorimetric method proposed by Eisenberg [205] is based on the analysis of the yellow-orange color present in a solution as a product of the reaction of hydrogen peroxide with titanyl sulfate. The reaction needs to occur in an acidic environment; thus, the yellow color produced

is due to the properties of peroxotitnylsulfonic acid. The reaction of H_2O_2 with the reagent takes place as follows by the reaction:

$$TiOSO_4 + H_2O_2 + H_2SO_4 \rightarrow TiO_2(SO_4)_2^{2-} + H_2O + 2H^+ \quad \textbf{Reaction 42}$$

The concentration of hydrogen peroxide is determined by measuring the absorbance at 410 nm of the product of a 2 mL sample with 1 mL of titanyl ions [205]. A calibration curve is constructed with the knowledge of H_2O_2 concentration using $TiOSO_4$. The details can be found in **annex 3.4** and **annex 3.5**. We note that the results of this study are presented with about 2 % of uncertainties, as calculated by the verification of the calibration curve and random error of preparation solution.
This method is used to measure the concentration of H_2O_2 in the water solution.

- **Christopher Andreas Vasko method (in Cr(VI)):**

Christopher Andreas Vasko's [206] method is based on measuring the absorption of the formed substance between H_2O_2 and NH_4VO_3 under acidic conditions by the reduction of vanadium(V) to vanadium(III) by H_2O_2. Accordingly, reduction of vanadium (V) leads to the formation of a red-orange peroxovanadium complex. The mixture of a 2 mL sample with 1 mL of NH_4VO_3 gives the maximum of absorbance at 440 nm [206–209]. The reaction between NH_4VO_3 and H_2O_2 is shown in the following reaction:

$$H_2O_2 + NH_4VO_3 + H_2SO_4 \rightarrow NH_4[VO(O_2)SO_4] + 2H_2O \quad \textbf{Reaction 43}$$

A detailed description of H_2O_2 measurements in water using this method is provided in **annex 3.6**.
We note that, in this work, Vasko's method is used to analyze the concentration of H_2O_2 formed after discharge in Cr(VI) solution. As presented in **Chapter 2**, the Cr(VI) solution has a yellow color and has an absorption peak at 350 nm; thus it leads to overlap of the signal for the Eisenberg method, which has absorption at 410 nm. To use Vasko's method, we perform a combination of three different calibration curves based on the absorptions at different wavelengths of Cr(VI) and the complex of NH_4VO_3 with H_2O_2. We have developed a specific method to measure simultaneously [H_2O_2] and [Cr(VI)], the detailed description is provided in **annex 3.7**. In this method, the results present an uncertainty under 15 %, calculated by the standard deviation of the multi calibration curves.

3.3 Reproducibility of the experiments

We note that the calculations in this section are applied to the error representation of Cr(VI) concentration through the treatment process. As presented in section **3.2.4**, the uncertainty regarding the measurement is less than 1 %. However, in section **3.2**, we showed that the discharge under liquid depends on the experimental conditions, thus leading to variation in the process. Due to this reason, it is necessary to verify the experiments' reproducibility to estimate the global uncertainties of the process. This section will present a formula for quantifying a measurement and its random error based on repeatedly measuring in the same way. Moreover, the formula is based on the calculation of the standard deviation.

3.3.1 Standard deviation

The standard deviation is the average amount of variability in the data set, and it indicates how far each value is from the mean on average. A high standard deviation means that values are generally far from the mean, while a low standard deviation indicates that values are close to the mean [210,211].
After collecting data from a sample, the standard deviation of the sample is used to make estimations or inferences about the population's standard deviation. The calculation of standard deviation is based on **Equation 6:**

$$s = \sqrt{\frac{\sum(X - \bar{x})^2}{n - 1}} \qquad \textbf{Equation 6}$$

With:

s = sample standard deviation

X = each value

$\bar{x}$ = sample mean

n = number of values in the sample

The formula's use of “n – 1” makes sense since using “n” would lead to a biased estimate that consistently underestimates variability. The standard deviation of the sample would tend to be lower than the true standard deviation of the population. Also, reducing the sample from n to n - 1 artificially increases the standard deviation and results in a conservative estimate of variability. The sample means $\bar{x}$ was calculated by dividing the sum of the value of all samples by the number of samples. By squaring the differences to the mean, the standard deviation more accurately reflects the uneven dispersion.

3.3.2 Estimation of uncertainty in repeated measurements

It is noted that we do several repeated measurements of concentration (for H_2O_2 and Cr(VI) experiments) in the function of time for the same experimental conditions. For each experimental condition, we calculate the standard deviation in order to choose the highest value as the uncertainty of all results.

For example, we discuss in this section the most repeated condition used for [Cr(VI)] measurements, with applied voltage U = 9 kV, the pulse duration Δt = 500 µs, the frequency f = 50 Hz, the gap between two pin electrodes is set at 2 mm. The electrodes are 200 µm diameter platinum wire, and the length of electrodes protruding in water are 0 ± 10 µm. The 100 mL working solution is prepared by mixing 94 mL of stock Cr(VI) 50 mg/L solution with 6 mL of sulfuric acid (H_2SO_4) 0.1 M. As a consequence, the conductivity of the working solution is equal to σ = 4 mS/cm, and the pH = 2,4. The duration of the treatment process is 2 hours. After every 15 minutes, 2 mL of solution is sampled, and to measure the absorbance is direct at 350 nm. The concentration is calculated by using the absorbance value compared with the calibration curve (presented in **annex 3.1**).

Figure 3.10 shows the concentration of Cr(VI) as a function of treatment time for 8 repeated experiments with the same conditions. Due to the discharge variations, the concentration of Cr(VI) has a variance for each experiment. **Figure 3.10** shows that the variations in Cr(VI) concentration mainly seem to occur between 30 and 75 minutes when we compare them individually. By calculating the standard deviation, we can more accurately evaluate discharge uncertainties in reducing Cr(VI).

Table 3.1 shows the experimental data and standard deviation value for each time sample. The final uncertainty for each time is calculated using the standard deviation divided by the mean and then multiplied by 100 to obtain the percentage. It is found that the highest uncertainty at 105 minutes of treatment time is about 20 %, and the percentage of uncertainty increases with increasing treatment time.

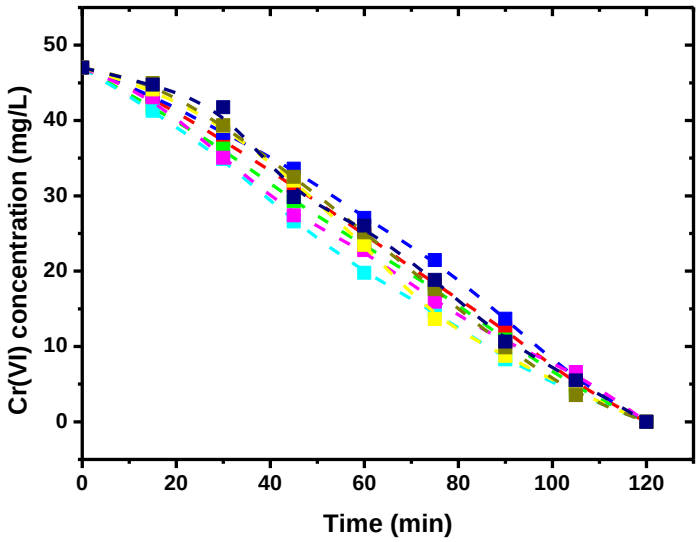

Figure 3.10 Concentration of Cr(VI) as a function of time with several repeated experiments. U = 9 kV, Δt = 500 µs, f =50 Hz, 2 mm gap, electrodes length = 0 ± 10 µm, (47 mg/L,σ=4 mS/cm,pH=2.4) .

We note that for other repeated experiment conditions, the results are similar to this condition. Being aware of the variability of the discharge characteristics due to the experimental setup, we estimate the global uncertainty for [Cr(VI)] measurements. We observe that this uncertainty depends on the Cr(VI) concentration. For example, the uncertainty increases from 3 % to 20 % when the concentration of Cr(VI) decreases from about 43 mg/L to 5 mg/L(**Table 3.1 and Figure 3.11**). Moreover, **Figure 3.11 shows** that the relation of [Cr(VI)] with uncertainty is almost linear. Thus we decide to define a function to estimate the uncertainty of [Cr(VI)] in relation to [Cr(VI)] (**Figure 3.11**). The uncertainty of Cr(VI) concentration is calculated by the **Equation 7**:

$$\Delta C = -0.403 \times C + 20.244 \qquad \textbf{Equation 7}$$

With:

ΔC is the uncertainty of [Cr(VI)]

C is the [Cr(VI)]

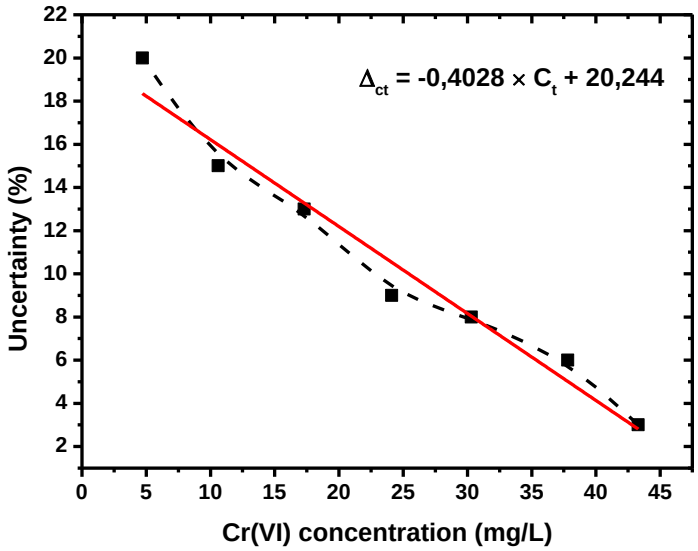

Figure 3.11 Realtion of [Cr(VI)] uncertainty as a function of concentration obtained by several repeated experiements. U = 9 kV, Δt = 500 µs, f =50 Hz, 2 mm gap, electrodes length = 0 ± 10 µm, (47 mg/L,σ=4 mS/cm,pH=2.4)

Using the same method, we calculate the uncertainties for measuring H_2O_2 concentration in water, as presented in **Table 3.2**. However, we do not observe a relationship between [H_2O_2] and the uncertainty, not like the Cr(VI) concentration as presented previously. Thus in the study regarding the measurement of H_2O_2 in the water, we chose to use the highest value of 15 % as an uncertainty for all concentrations.

We note that regarding the measurement of H_2O_2 in Cr(VI), we use a dedicated method to estimate the uncertainties, and the detail is discussed in **annex 3.4.**

Time (min)	Concentration of Cr(VI) mg/L								Average value (mg/L)	Standard deviation (mg/L)	Uncertainty (%)
0	47	47	47	47	47	47	47	47	47		
15	43,1	41,7	43,3	41,3	43,1	44,1	45,0	44,7	43,3	1,2	**3**
30	37,3	36,3	38,3	34,9	35,1	39,3	39,4	41,7	37,8	2,2	**6**
45	31,3	29,3	33,6	26,6	27,4	32,0	32,5	29,8	30,3	2,3	**8**
60	24,9	23,4	27,1	19,8	22,8	23,5	25,1	26,0	24,1	2,1	**9**
75	18,3	17,7	21,4	14,6	15,9	13,7	17,6	18,8	17,3	2,3	**13**
90	12,3	10,9	13,7	8,3	10,5	8,8	9,9	10,6	10,6	1,6	**15**
105	4,8	4,4	5,5	3,7	6,6	4,0	3,5	5,5	4,7	1,0	**20**
120	0,0	0,0	0,0	0,0	0,0	0,0	0,0	0,0	0,0	0,0	

Table 3.1 Standard deviation and uncertainty of repeated experiments for Cr(VI) experiments. U = 9 kV, ∆t = 500 µs, f =50 Hz, 2 mm gap, electrodes length = 0±10 µm, ([Cr(V)] = 47 mg/L,σ=4 mS/cm,pH=2.4)

Time (min)	Concentration of H_2O_2 (mM)			Average (mM)	Standard deviation (mM)	Uncertainty (%)
5	0,065	0,067	0,071	0,068	0,0031	4,5
10	0,195	0,228	0,207	0,210	0,0167	8,0
15	0,384	0,411	0,311	0,369	0,0517	**15,0**
20	0,514	0,541	0,436	0,497	0,0545	**11,0**
25	0,609	0,618	0,677	0,635	0,0369	5,8
30	0,784	0,808	0,846	0,813	0,0313	3,8

Table 3.2 Standard deviation and uncertainty of repeated experiments for [H_2O_2] measurement. U = 9 kV, ∆t = 500 µs, f =50 Hz, 2 mm gap, electrodes length = 400±30 µm, (in water, σ=200 σS/cm,pH=5.9)

3.4 Conclusion

The experimental setup presented in this chapter aims to reduce Cr(VI) using a technique based on generating plasma discharges in a liquid solution. The configuration is based on pin-to-pin immersed electrodes with a small diameter (100-200 µm). The power supply delivers microsecond pulses of a few kV by repetition of 50 Hz.

The various techniques used to characterize the electrodes were presented (IDS camera and SEM technique), and the sample preparation procedure is explained. The analysis of the process is performed using different diagnostics: shadowgraphy, electrical measurements, and chemical analysis based on photometric diagnostics.

In order to detect the lowest concentration of Cr(VI), we have developed an *in situ* experimental setup based on the absorption characteristics of Cr(VI) using a LED source at 365 nm. Two different methods used to measure the concentration of H_2O_2 in water and in Cr(VI) solution have been presented.

Finally, we have discussed the reproducibility of the experiment. The standard deviation calculation by repeated experiments has shown a maximum uncertainty of about 15 % for [H_2O_2] measurements. The uncertainties for [Cr(VI)] measurements have been determined by a function depending on [Cr(VI)] And we use a dedicated method to estimate the uncertainties of H_2O_2 in Cr(VI). These uncertainties are used as error bars for all results in the following chapters. A typical experimental procedure has been developed for the treatment of Cr(VI) and qualitative other products of plasma discharge underwater.

Chapter 4

Characterization of the discharge

This chapter presents the characterization of the discharge inside the liquid phase. This preliminary study aims to increase the understanding of plasma properties [175–177,202].

First, we present studies on plasma discharges in water at low conductivity, which is considered as a simple medium. Those results are related to the conditions used to study H_2O_2 production in water (chapter V). Then we present some comparisons with experiments performed in water at high conductivity. Therefore, we describe the different characteristics of discharge obtained in Cr(VI) solution with high conductivity, which represents the main topic of this project. We also study the influence of some parameters on the discharge characteristics, such as pulse mode (single or multi), the applied voltage, the gap between two electrodes, and finally the pulse duration.

As discussed in the previous chapter, the discharge characteristics strongly depend on the experimental conditions as the geometry, the power supply, or the solution. In the frame of this work, the same experimental setup (geometry and power supply) has been used, but two different solutions have been studied: water and chromium VI. We observe that the characteristics of these discharges present significant discrepancies. This section presents two different descriptions of electrical discharges: discharges in water and in Cr(VI) solution.

4.1 Single-pulse discharge in water

Keeping in mind that the study of discharge in water is not the focus of this thesis, most of the results presented below have been obtained by Rond *et al*., and more details are depicted in [175–177]. Few additional results obtained in the frame of this work are included.

4.1.1 Discharge descriptions using shadowgraphy

Considering all experimental results Rond *et al.* [175–177] have shown that three main different discharge cases in water have been identified and described. We mention that these studies have been performed with specific experimental conditions: single-pulse, low conductivity (100 µS/cm), electrodes gap equal to 2 mm, electrodes diameter 100 µm and length of about 400 µm. The interesting phenomena for each case are shown in **Figure 4.1**. It shows that the different cases could be observed for a unique set of experimental conditions**.**

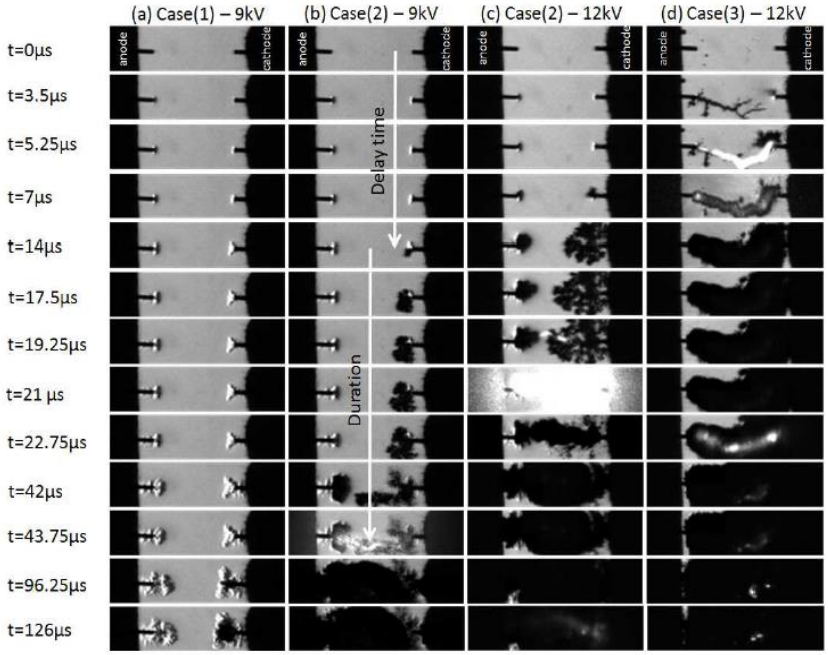

Figure 4.1 Time-resolved schlieren measurements of a pin-to-pin discharge obtained in water (σ=100 µS/cm) for 9 kV and 12 kV - the voltage pulse duration equals 1 ms, and the camera resolutions are 128x32 pixels and Δt=1.75 µs [175].

For cases 1 and 2, a bush-like structure propagates from the cathode to the anode, whereas case 3 shows a filamentary structure propagated from the anode to the cathode.

In case 1, at the beginning of the voltage pulse, a cone-shaped structure at the cathode and a spherical one at the anode are observed. Then, a bush-like channel forms at the cathode. These channels, containing excited gas (plasma) resulting from the vaporization and the excitation of the water, propagate slowly towards the anode but do not reach the electrode. This case is called partial electrical discharge [155].

In case 2, the plasma channels appear more rapidly at both electrodes, cathode and anode. Whereas the plasma phase at the anode expands more spherically and slowly, channels propagate from the cathode (to the anode) with a bushy structure. The propagation leads to the breakdown phenomena. A gas phase is formed and shows expansion/contraction cycles between the two electrodes It was also shown that several secondary emissions could be observed in the dark region during the post-breakdown period.

Regarding case 3, a fast filamentary structure appears and propagates from the anode to the cathode. Then a gas phase is formed and continues to expand in between the two electrodes. Secondary emissions have always been observed during the expansion of the gas region.

4.1.2 Electrical waveforms

Figure 4.2 shows the typical voltage and current waveforms obtained for one pulse with different cases (with different applied voltages of 9 kV and 12 kV). It is shown that by following the pulse, the rise time of the signals is about 30 ns.

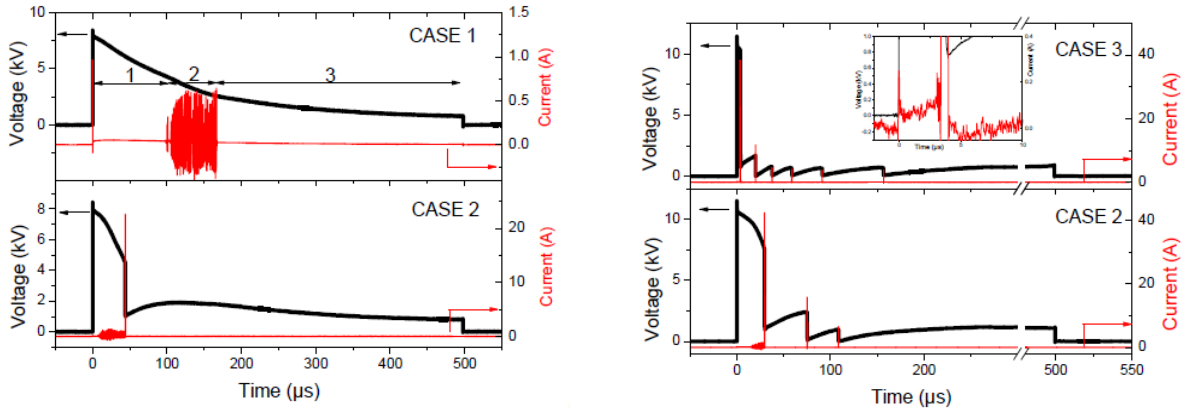

(a) (b)

Figure 4.2 Voltage and current signals of a single pin-to-pin discharge in water (σ=100µS/cm) monitored for applied voltages of 500 µs (a) 9 kV and (b) 12 kV [175]

It is shown that three distinct regions are identified for Case 1, as shown in **Figure 4.2**(a) with the numbering (1, 2, and 3). Region (1) shows the low variations in the electrical signals; the voltage decreases and the current reaches about one hundred milliamperes before slowly decreasing. For phase (2), after about 100 µs, the voltage signal shows a slope change, and a transient current showing rapid alternating positive and negative values is superimposed on the slowly varying current. Finally phase (3) shows that both the voltage and current signals slowly decrease. In this work, Rond *et al*[175] defined that the slowly varying current as of the RLC current and the alternating current as the transient current.

In case 2, the voltage signal drops faster from about 15 µs than in case 1, and the current waveform shows a high transient current as presented in **Figure 4.2**(a). Then, the capacitor is suddenly

discharged by breakdown phenomena characterized by a voltage drop, and a peak current of more than 20 A is obtained at the same time (about t = 50 µs). Subsequently, the capacitor recharges thanks to the long pulse duration, and the voltage slowly increases. After that, two different phenomena can be obtained: the voltage and current signal drop towards zero (**Figure 4.2**(a)), or one or more additional breakdown phenomena occur (2 additional breakdowns are shown in **Figure 4.2**(b)). It is noted that no transient current is recorded before the secondary peak currents.

In case 3 at 12 kV, no transient current occurs, only the RLC current during the precollapse (**Figure 4.2**(b)), and the breakdown occurs faster (< 5 µs) than in case 2 (about 50 µs). After the first breakdown, several successive breakdowns are obtained (5 additional breakdowns are shown in **Figure 4.2(**b).

For a given set of experimental conditions and for low conductivity (lower than 200 µS/cm), it is possible to observe these three different cases of discharge. These results will be taken into account in chapter V in order to analyze the production of H_2O_2 by the PLI process.

4.1.3 High conductivity results

A dedicated study also reports a statistical analysis of a single pin-to-pin discharge in water for a wide range of conductivities from 2 µS/cm to 1500 µS/cm and monitors the electrical parameters (breakdown voltage, current peak, breakdown duration) [177]. This work shows that the underwater discharge characteristics for high conductivity (1500 µS/cm) present only 2 different behaviors: a majority of case 1 previously described (without breakdown) and few percents of "double" case that involves breakdown due to discharges propagating simultaneously from the cathode (case 2) and anode (case 3) (**Figure 4.3**).

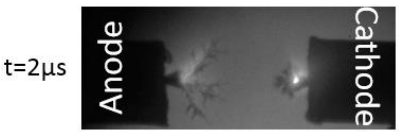

Figure 4.3 Schlieren images for double regime obtained for σ = 1500 µS/cm (U = 12 kV) (exposure time 1 µs)[177]

So it is known that the nature of the solution, especially the conductivity, has an effect on the discharge, and as a consequence, in the case of the standard Chromium VI solution used in this work that presents conductivity of about 4 mS/cm, it is possible to observe specific characteristics.The next part is dedicated to the analysis of discharge evolutions in the standard Cr(VI) solution.

4.2 Discharge in Cr(VI) solution

It is to mention that this study is not the main topic of this work, but it appears very useful to better analyze the effect of the plasma on the Cr(VI) reduction. In this study the volume of the working solution is 100 mL, with the initial concentration of Cr(VI) equal to 47 mg/L (details in **Chapter 3**). The initial pH of the solution is 2.4 and the initial conductivity of the solution is 4 mS/cm.

Taking into account a lot of experimental results, we highlight, using electrical measurements and shadowgraphy images, that only two different kinds of discharge are identified. This section analyzes the two different cases based on different properties of the electric waveforms and plasma propagation, and qualitative comparison of the results is done. At first sight, the main differences between these two cases are the presence or not of breakdown, as a consequence, they are called "NOBK" (for no breakdown) and "BK" (for breakdown). It is worth noting that, as in the case of discharge in water, the two different cases may be observed under a single set of experimental conditions. Consequently, a statistical study is performed for every experimental condition to determine the distribution between the two observed cases, and the results are reported below. For that, a LabVIEW program is used in real-time to identify a breakdown from the electrical signals automatically.

We remind that the shadowgraphy experimental campaign has been performed in collaboration with Hervé Rabat (GREMI) in the frame of the French Plasma Network actions (*IPMC – réseau Plasmas Froids*). The diagnostics used are the shadowgraphy technique (**Chapter 3**) and electrical measurements.

As an example, **Figure 4.4** shows the difference between Case NOBK and Case BK, obtained under the same experimental conditions for a single pulse. It can be seen that at the time t = 2.7 μs and 5.4 μs in case NOBK, only glowing plasma is observed at the two electrodes, then gas channels spread along the branches. On the other hand, in case BK from t = 2.7 μs, only small glowing plasma is observed at the tip of two electrodes. Then fastly at t = 5.4 μs the two electrodes are connected by a plasma channel (the emission is not shown in **Figure 4.4**).

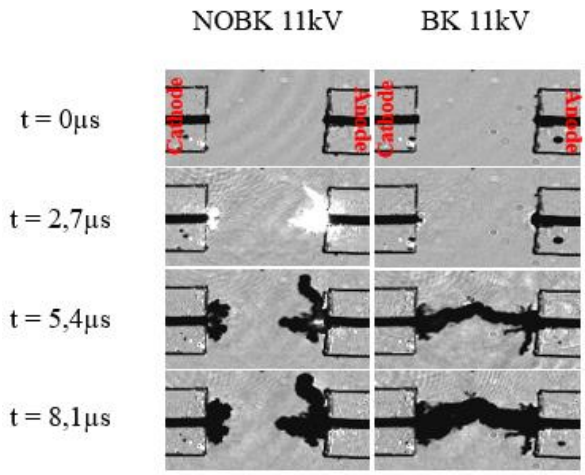

Figure 4.4 Examples of case NOBK and case BK of a pin-to-pin single discharge obtained in Cr(VI) solution (47 mg/L,σ=4 mS/cm,pH=2.4) for 11 kV, Δt=500 µs, gap = 2 mm, electrodes length = 0±10 µm, the camera resolutions are 128x80 pixels and Δt=2.7 µs.

The electrical measurements for a single-pulse have been performed using the Lecroy wj354a model, recording the signal over 1 ms by using 100 kpts, leading to a time resolution of 0,01 µs. The electrical signals corresponding to the experiments illustrated in **Figure 4.4** are given in **Figure 4.5**. It can be seen that **Figure 4.5** also confirms the different phenomena of voltage and current shape for case NOBK (no breakdown) and case BK (breakdown). For NOBK, due to the slowly decreasing voltage, the current increases to 4 A with two steps (shown in zoom). A significant part of the current mainly occurs during the first 10 µs and no transient current is observed. In contrast to the NOBK discharge in water, the voltage decreases faster to 2 kV, then decreases close to zero. Moreover, a different evolution of the signal appears on the electrical waveforms during the first 50 µs (**Figure** 4.5(a)), which looks like minor breakdowns showing small current peaks and voltage drops. These phenomena should be related to light emission. However, these light emissions are too weak to be observed due to the limitation of the equipment used in the shadowgraphy measurement.

In the case of BK, the voltage suddenly drops close to zero, then at the same time, the current fastly increases up to 30 A (at about t = 2,5 µs). From the electrical waveforms, we can see that the breakdown occurs very early in the range of t = 2.5 to 2.7 µs; however, due to the limitation and delay of the camera, we do not obtain an image of the luminous plasma channel at t = 2,7 µs (as shown in **Figure 4.4**). After the first breakdown, several additional breakdown phenomena occur (**Figure 4.5** shows two other breakdown phenomena at about 40 and 110 µs).

It is noted that, in case of discharge in Cr(VI) solution with σ=4 mS/cm, we do not observe the transient current for NOBK and BK cases.

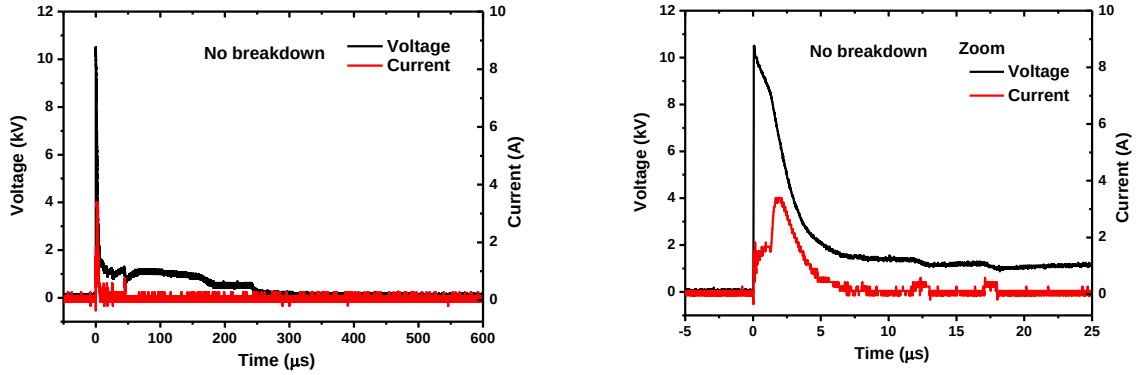

(a)

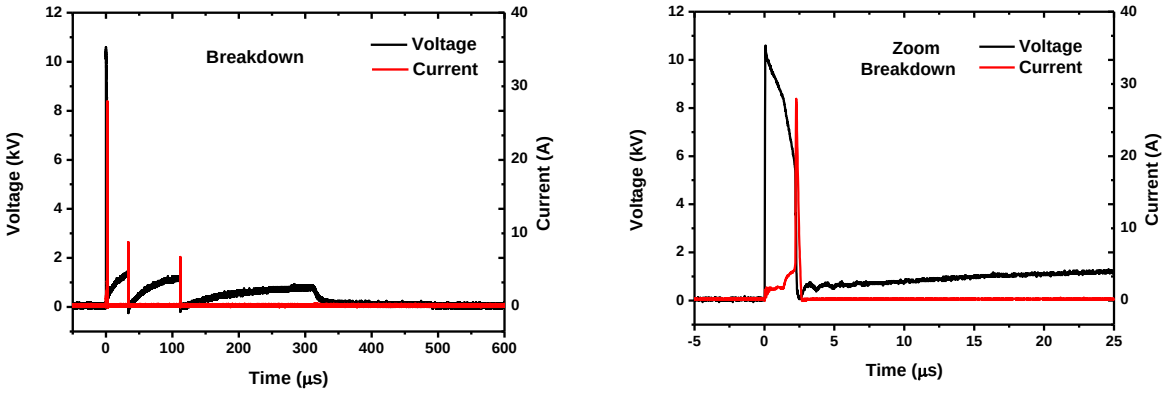

(b)

Figure 4.5 Voltage and current signals for (a) case 1 NOBK and a zoomand (b) case 2 BK and a zoom of a pin-to-pin single discharge obtained in Cr(VI) solution (47 mg/L,σ=4 mS/cm,pH=2.4) for 11 kV, Δt=500 µs, gap = 2 mm, electrodes length = 0±10 µm

Unfortunately, the Photron fast camera does not provide the time resolution to observe the fast propagation of the discharge for BK case. We change the setup to perform fast imaging, and especially the detector to an Andor camera to increase the time resolution, as shown in **Chapter 3**. We can capture a single image with a low time resolution with this setup. For example, **Figure 4.6** shows images for different acquisition times of three BK experiments. **Figure 4.6** shows that the glow at both electrodes appears as soon as t = 1 µs and is more significant at the anode than the cathode. Then filamentary structure initiates and propagates mainly from the anode toward the cathode (at t = 1,5 µs). At t = 1.7 µs, the filamentary connects the two electrodes.

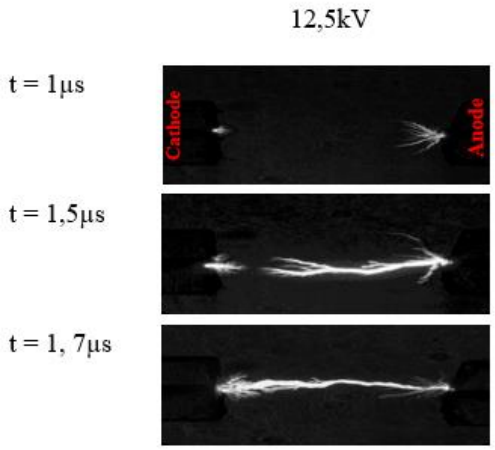

Figure 4.6 Pin-to-pin single discharges obtained in Cr(VI) solution (47 mg/L,σ=4 mS/cm,pH=2.4) for BK experiments (U=12,5 kV) with three successive imaging measurements. V = 100 mL, gap = 2 mm, electrodes length = 0±10 µm.

These results prove that the discharge characteristics in Cr(VI) (4 mS/cm) are very similar to those observed in water for 1,5 mS/cm. We obtain two different regimes: without breakdown (case 1) and with breakdown combining filament propagation from the anode simultaneously with a bush from the cathode (double case).

In order to better understand the discharge phenomena in Cr(VI), we study the effects of some experimental parameters, which are described in detail below. It is noted that for these studies, the immersed length of the two electrodes is always kept the same at 0 µm, the frequency is f = 50 Hz, the conductivity σ=4 mS/cm, the pH = 2,4 and the camera resolutions are 128x80 pixels with Δt=2.7 µs.

4.2.1 Effect of multi-pulse

It is noted that the previous discussions of discharge in water and Cr(VI) have been done with the single pulse mode. However, due to the scope of this thesis work on the reduction of Cr(VI), we proceed to work with the multi-pulse mode. Therefore, it is interesting to compare the differences in the character of the discharge for two different discharge modes: Single pulse and multi-pulse.

Figure 4.7 illustrates the differences in the discharge phenomena of multi-pulse and single-pulse cases for NOBK and BK with the same voltage of 11 kV. First, we can observe that multi-pulse discharge generates more bubbles than a single pulse for both cases. These microbubbles result from the gas phase created from the previous discharge (shown in **Figure 4.4**). In the case of multipulse, the gas phase existing between the electrodes does not have time to be dissolved between two pulses (Δt=0 ms). Details of bubbles dynamic are described in the following sections. The influence of microbubbles on the discharge dynamics has been reported in literature [163,165,214,215]. In the case of a discharge with the presence of microbubbles, it has been assumed that the bubbles, which can be driven near or attached to the electrodes, then facilitate the propagation of the plasma channel inside bubbles since the gas phase requires smaller electric fields than the liquid phase. Another possibility is

that the electric field is increased by creating cusps at the contact point between two bubbles when many bubbles are present between the two electrodes[214,216]. However, better analytical methods need to be investigated to understand these processes and evaluate the bubbles' stable or repeatable distribution.

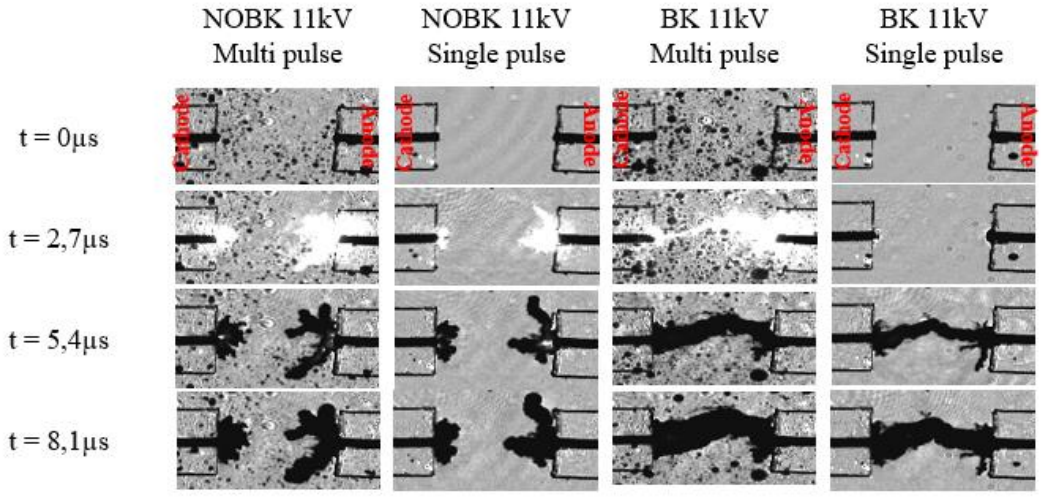

Figure 4.7 Time-resolved shadowgraphy measurements of multi-pulse and single-pulse with NOBK and BK of a pin-to-pin discharge obtained in Cr(VI) solution (47 mg/L, σ=4 mS/cm,pH=2.4) for 11 kV , V = 100 mL, Δt = 500 µs, gap = 2 mm, electrodes length = 0±10 µm, f = 50 Hz for multi-pulse

For both NOBK and BK discharge, we perceive a similar discharge behavior for single and multi-pulse:

- In the case of NOBK:

At t = 2,7 µs, luminous plasma can be observed at both electrodes for both discharge modes, then gas channels spread along the branches (at t = 5,4 µs to 8,1 µs) as shown in **Figure 4.7.**

- In the case of BK:

We note that at t = 2,7 µs, the two electrodes are very rapidly connected by an intense luminous plasma channel for the multi-pulse mode, while at the same time, for the single-pulse mode, it is only a faint appearance of the glow plasma at the electrode tips. The presence of microbubbles may explain this phenomenon. However, it is not easy to compare only by shadowgraphy measurements (as presented previously in **section 4.2**) due to equipment limitations. Then at t = 5,4 µs, we obtain the gas channel for both discharge modes, and this channel continues to expand in between the two electrodes as presented at t = 8,1 µs.

The electrical signals corresponding to the experiments shown in **Figure 4.7** are presented in **Figure** 4.8. It is noted that **Figure 4.8** shows some differences in the electrical shape for two discharge modes in both cases of NOBK and BK.

We note that the electrical measurements for a multi-pulse in this section have been performed with a time resolution of 0.5 µs (using the Lecroy wj354a model, recording the signal over 50 ms by using 100 kpts) while the single pulse is recorded using a time resolution of 0,001 µs.

We also note that the electrical waveforms presented in this section are only used to illustrate the phenomena depicted by the shadowgraphy images. For all detailed studies performed in this work, we use the signal with high time resolution (1×10^{-9} s), for example, to calculate the energy, as presented in **Chapter 3.** Moreover, electrical signals with different time resolutions are given in **Annex 4**.

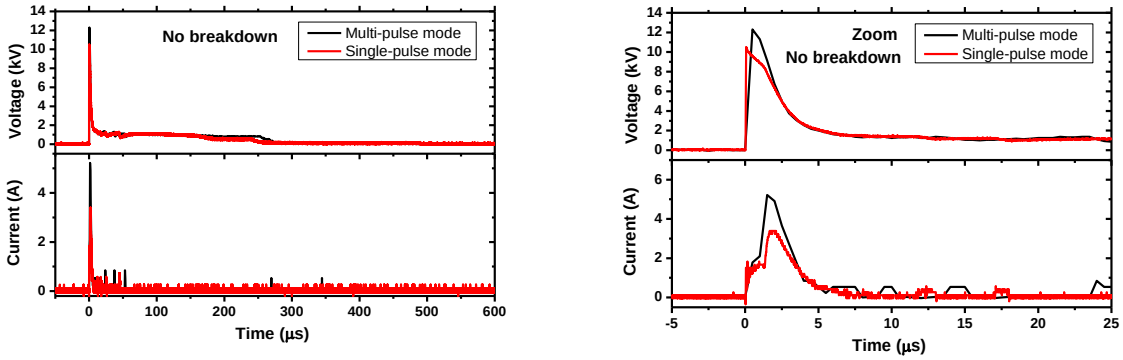

(a)

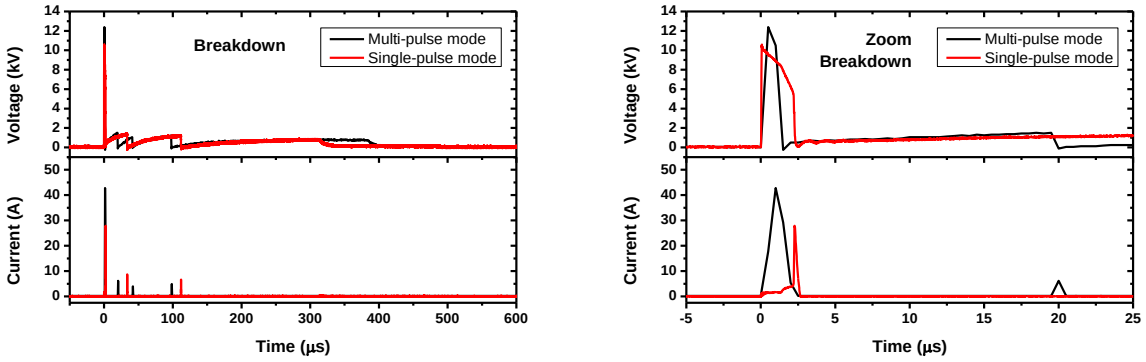

(b)

Figure 4.8 Voltage and current signals for (a) case 1 NOBK and a zoom, (b) case 2 BK and a zoom for multi-pulse and single-pulse modes, of a pin-to-pin discharge obtained in Cr(VI) solution (47 mg/L,σ=4 mS/cm,pH=2.4) for 11 kV, V = 100 mL, Δt = 500 µs, gap = 2 mm, electrodes length = 0±10 µm, f = 50 Hz for multi-pulse

Rigorously, we cannot compare the rising time of the voltage signal as it looks different in **Figure 4.8** because of the low time resolution for the multi-pulse mode. However, despite the different time resolutions, we validate the difference in the maximum voltage and current peaks obtained for the two modes, multi-pulse signals being higher than single-pulse signals. The difference in the electrical waveform between single and multi pulses may be due to the circuit's overdamped and the capacitor's discharge [217,218]. In the case of BK, **Figure 4.8**(b) shows a difference in the breakdown duration for the two different modes, which is not only due to the reproducibility of the experiment. For the multi-pulse, the breakdown always occurs earlier than for the single-pulse. The second or third breakdown's time duration also appears earlier in multi-pulse than in the single-pulse mode.

Finally, we also observe that changing the discharge mode leads to a change in the number of BK/NOBK, which is one of the significant parameters for the treatment process. Multi-pulse involves

a higher number of BK cases than a single-pulse. For example, at 11 kV, a single pulse involves very few BK (not accurately measured), whereas multi-pulse reports about 25 % of BK. This result can be related to the fact that the multi-pulse mode involves more bubbles and certainly a more disturbed liquid by convective effects.

From these results, we conclude that the discharge propagation phenomena are similar for both single and multi-pulse modes. Regarding the electrical signals, the general shape is also the same, but we obtain for multi-pulse the overdamp of voltage and current and a higher BK/NOBK ratio. Moreover, in the case of BK, the breakdown duration is faster in multi-pulse mode than in single-pulse mode (as confirmed from **Figure 4.7** and **Figure 4.8**).

For the following studies, we only work in the multi-pulse mode because it is the experimental condition for Cr(VI) reduction.

4.2.2 Effect of applied voltage

The applied voltage is one of the essential parameters that influence the process of plasma formation. This part presents the characteristics of the two regimes (NOBK and BK) for different applied voltages. The voltage is changed from 7 kV to 11 kV. We observe the two regimes with the voltages 9 kV, 10 kV, and 11 kV, and it could be noted that for 7 kV, the number of breakdowns is deficient (about 1 %); thus we can consider that for 7 kV we only have case NOBK. The increase of the applied voltage leads to a change in the number of no breakdowns and breakdowns, as shown in **Table 4.1**. The number of breakdowns increases from 15 % to 25 % for 9 kV to 11 kV, respectively.

Applied Voltage (kV)	7	9	10	11
Number of BK / NOBK (%)	1 / 99	15 / 85	24 / 76	25 / 75

Table 4.1 Distribution of cases BK / NOBK according to the applied voltage of multi-pulse pin-to-pin discharges obtained in Cr(VI) solution (47 mg/L,σ=4 mS/cm,pH=2.4) Δt=500 µs, gap = 2 mm, electrodes length = 0±10 µm, f = 50 Hz.

a. In the case of No breakdown

Figure 4.9 shows the time-resolved shadowgraphy measurements of a pin-to-pin discharge obtained in Cr(VI) solution (σ=4 mS/cm) for 7, 9, 10, and 11 kV, respectively. The figure only reports the significant times of the measurements.

In general, a luminous plasma is formed at both electrodes and can be observed very early (at t = 2.7 µs). After that, bubbles form, grow and collapse at both electrodes from t = 5.4 µs to t = 280.8 µs. In **Figure 4.9** red stars indicate the images representing the maximum radius of these bubbles. It is noted that the resulting glow seems to be stronger at the anode than at the cathode. Because the luminescence is stronger at the anode than at the cathode, the size of the bubble is more significant at the anode than at the cathode. At the cathode, the maximum size of the bubbles is

reached earlier and then collapses more rapidly than at the anode. We will comment on this only in general terms since the dynamics of the bubbles are not the primary goal of this study.

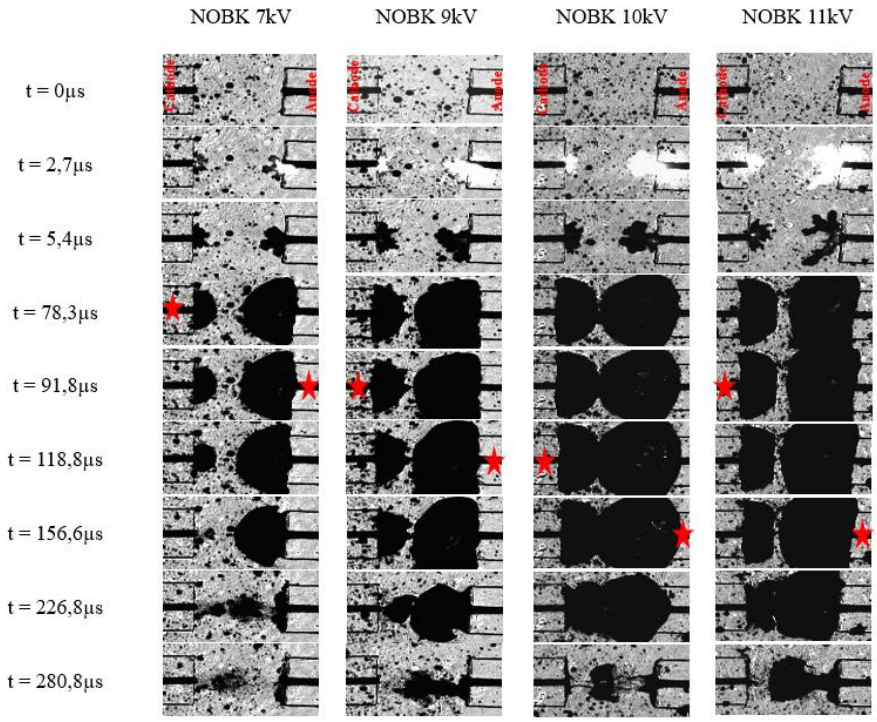

Figure 4.9 Time-resolved shadowgraphy measurements of a pin-to-pin discharge obtained in Cr(VI) solution (47 mg/L,σ=4 mS/cm,pH=2.4) for 7, 9, 10 and 11 kV, V = 100 mL, Δt = 500 µs, gap = 2 mm, electrodes length = 0±10 µm, f = 50 Hz and the camera resolutions are 128x80 pixels and Δt=2.7 µs. The red star presents the maximum size of the bubbles.

It can be observed quite well that at 2.7 µs the glow at the electrodes becomes more intense with increasing voltage. At 7 kV, for example, the glow at the anode and cathode is weaker than at 11 kV. It is also observed that the size of the bubble increases gradually with increasing voltage at both electrodes. In addition, it is found that the dynamics of bubbles at both electrodes are different at different voltages. For example, at 7 kV, t = 78.3 µs can be considered as the time of the maximum size of the bubble at the cathode and at t = 91.8 µs as the maximum size of the bubble at the anode. However, at 9 kV, the maximum is found at t = 91.8 µs and t = 118.8 µs for the cathode and anode, respectively. It is difficult to precisely determine when the bubbles reach their maximum size because the process is very fast and equipment has limited resolution. Moreover, for high voltage, it is more difficult to analyze the maximum size of the bubble since the contact between the bubbles (*e.g.* @ 78.3 µs for 10 kV) stops the horizontal propagation to the benefit of vertical growth.

The bubble's deflation is also found to occur earlier at 7 kV than in the other cases. The total collapse of the bubble at both electrodes is found at t = 226.8 µs for 7 kV, while for the other applied voltages, it occurrs at t = 280.8 µs.

Interestingly, at 10 kV from t = 78.3 µs to t = 226.8 µs, the bubbles at the anode and cathode are connected, but no breakdown occurs. This phenomenon is also observed at 9 kV and 11 kV, but the

results are not shown in **Figure 4.9**. This result proves that the gas phases developing from the electrodes are not ionized. The growth of the bubble does not correspond to discharge propagation but to a gas bubble's expansion due to a fast local energy injection (glow).

Figure 4.10 shows the typical waveforms of the voltage and current monitored for cases of NOBK for different applied voltages. There is no difference in the voltage waveform compared with the ones previously discussed. This is in agreement with the results of discharge in water with high electrical conductivity, as described in [176]. Obviously, we observe that the maximum voltage increases with the applied voltage.

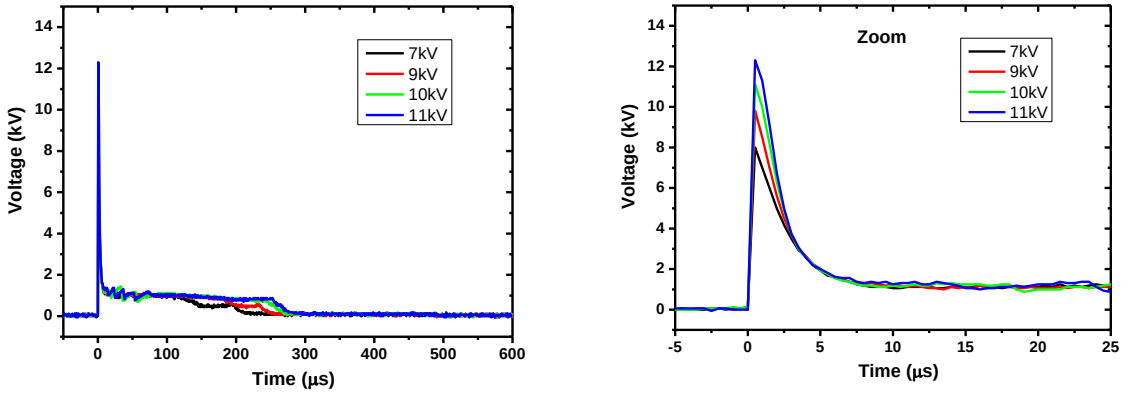

(a)

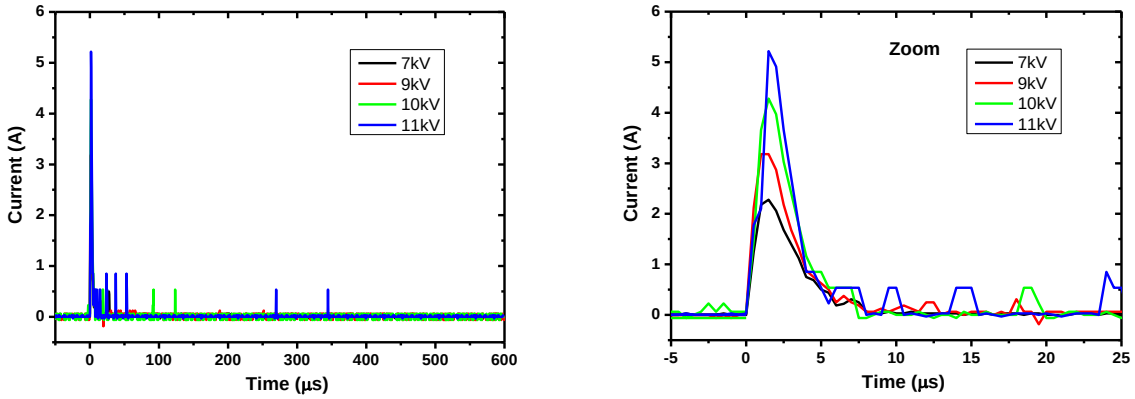

(b)

Figure 4.10 (a) Voltage and (b) current signals of a pin-to-pin discharge for case NOBK in Cr(VI) solution (47 mg/L,σ=4 mS/cm,pH=2.4) for 7, 9, 10, and 11 kV. V = 100 mL, Δt = 500 µs, gap = 2 mm, electrodes length = 0±10 µm, f = 50 Hz. (See annex 4.2.2 (a) for the signals with high time resolution)

It can be seen that the maximum current peak (at t ~ 2.5 µs) regularly increases with the applied voltage, from 2 A at 7 kV to 5 A at 11 kV, which is consistent with the increase of the emission intensity reported previously. The secondary current peaks also appear higher as the voltage increases (presented in part **4.2**). In case of NOBK, the shape of voltage and current generally do not differ much due to the change of the applied voltage, but the maximum intensities do.

b. In the case of Breakdown

Figure 4.11 shows the time-resolved shadowgraphy measurements for case BK of a pin-to-pin discharge obtained in Cr(VI) solution (σ=4 mS/cm) for 9, 10, and 11 kV. In contrast to case NOBK, plasma glow is not clearly visible at the two electrodes before the breakdown (more rapid). At the very beginning (observed at t=2.7 us for 10 and 11 kV) an intense emission is produced due to the connection of the filaments between the two electrodes. Several secondary breakdowns occur (observed in **Figure 4.11** @ 21.6 µs and 43.2 µs for 11 kV and 35.1 µs for 9 kV), and the channel expands spherically. In this case, the maximum expansion of the plasma channels is very difficult to determine because the bubble grows out of the frame. However, we roughly estimate that the maximums are reached almost at around t = 110 µs whatever the applied voltage. In the case of breakdown in Cr(VI) solution, the phenomena that occur are similar to the breakdown in water.

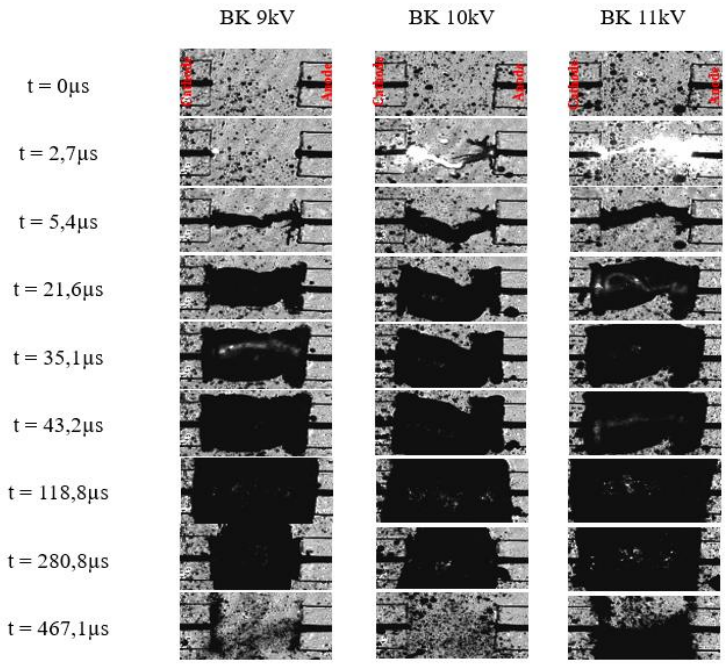

Figure 4.11 Time-resolved ombroscopy measurements of a pin-to-pin discharge obtained in Cr(VI) solution (47 mg/L,σ=4 mS/cm,pH=2.4) for 7, 9, 10 and 11 kV respectively, V = 100 mL, Δt = 500 µs, gap = 2 mm, electrodes length = 0±10 µm, f = 50 Hz and the camera resolutions are 128x80 pixels and Δt=2.7 µs.

Figure 4.12 shows the voltage and the current signals of case BK for 9, 10, and 11 kV discharge in Cr(VI) solution (σ=4 mS/cm). In the case of BK, the breakdown phenomenon occurs around 2 or 3 µs just after the beginning of the pulse. In general, the voltage drops to a value below 1 kV at the first breakdown. It seems that all the breakdowns in Cr(VI) always occur between 10 µs and 100 µs (for Δt=500µs), then the voltage slowly increases again to about 1 kV and goes to zero after 350 µs.

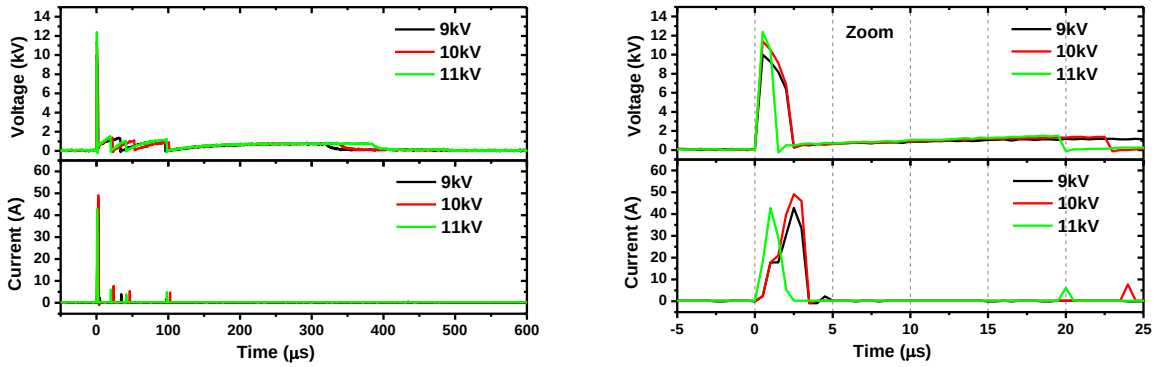

(a) (b)

Figure 4.12 (a) Voltage and current signals and (b) a zoom of a pin-to-pin discharge in Cr(VI) solution (47 mg/L,σ=4 mS/cm,pH=2.4) for 9, 10, and 11 kV, V = 100 mL, Δt = 500 µs, gap = 2 mm, electrodes length = 0±10 µm, f = 50 Hz. (See annex 4.2.2 (b) for signals with high time resolution)

The low resolution of both the electrical signals (±0.5µs) and the shadowgraphy measurements (±2,7 µs) leads to a difference in the time of breakdown visualization between the voltage waveforms and shadowgraphy measurements. Consequently, the following analyses present only qualitative comments and order of magnitude. The electrical signals show that increasing the applied voltage slightly increases the current peak and leads to a faster breakdown.

It could be concluded that the applied voltage slightly influences the plasma discharge properties and the number of breakdowns. To increase the applied voltage results in increasing the current and the number of case BK.

4.2.3 Effect of the interelectrode gap

In the context of this thesis, the distance between the two electrodes is one of the parameters to study since a change in the distance leads to a change in discharge characteristics (due to a change in the electric field). The gaps of 2 and 5 mm have been chosen in this work. It is noted that there is no breakdown for the 5 mm gap at a high applied voltage of 11 kV; thus, in this part, we only compare case NOBK for the 2 and 5 mm gaps.

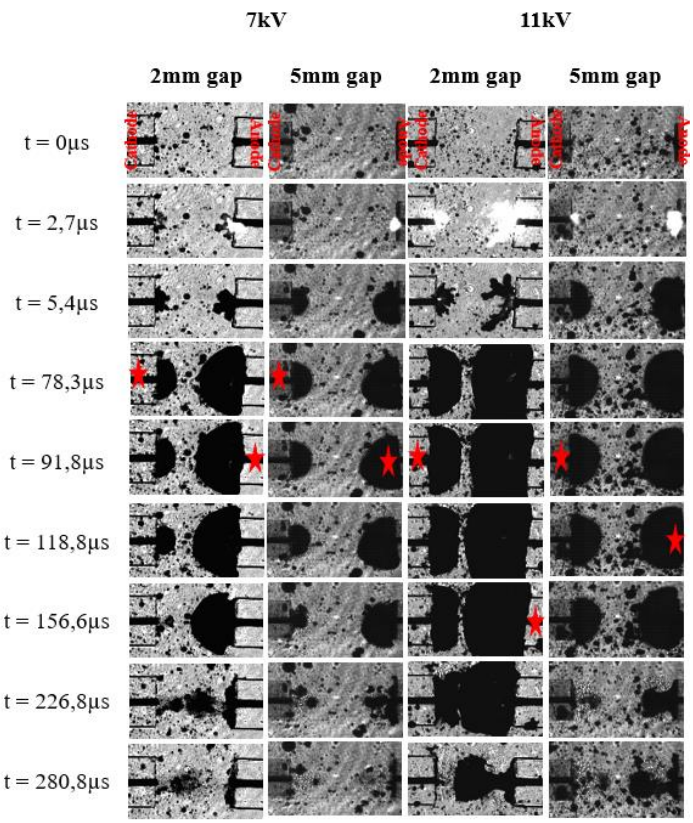

Figure 4.13 The time-resolved shadowgraphy measurements of a pin-to-pin discharge obtained in Cr(VI) solution (47 mg/L,σ=4 mS/cm,pH=2.4) for 7 kV and 11 kV and 2 different gaps V = 100 mL, Δt = 500 µs, electrodes length = 0±10 µm, f = 50 Hz.

Figure 4.13 shows the discharge phenomena for 2 and 5 mm gaps, obtained by shadowgraphy measurements. The experiments are performed for different applied voltages, but only images for 7 and 11 kV are shown in **Figure 4.13** to illustrate the results. In this study, we adjust the distance of the lens and camera with the reactor to obtain the best spatial resolution. Therefore, the electrode size imaged for studies with a 5 mm gap is smaller than for the 2 mm gap.

On the one hand, we can conclude that some of the characteristics already discussed previously are observed for both gaps, as:

- At t = 2.7 µs, plasma glows are observed at both electrodes
- The bubble's size at the cathode is always smaller than at the anode, and the bubble at the cathode always collapses faster than at the anode.
- The bubble size increases as the voltage gradually increases from 7 kV to 11 kV for both gaps.
- The gap does not seem to have a significant influence on the maximum bubble size.

On the other hand, changing the gap involves some differences in the discharge characteristics:

- The glow at the beginning is more important for 2 mm and the discharge propagation presents more branches than for 5 mm thus, it leads to the difference in the bubbles dynamics for different gaps obtained for 11 kV. For example, at t = 226.8 µs, the bubble seems to collapse totally for a 5 mm gap, while at the same time, for a 2 mm gap, the bubble still appears at both electrodes.

- For the 5 mm gap, due to the considerable electrode distance, there is no connection between the bubbles as presented in 2 mm.

The voltage and current signals of different voltages for the 2 and 5 mm gaps are shown in **Figure 4.14**. On the one hand, we obtain a similar shape of electrical signals for the different gaps with the same applied voltage. We can conclude that the interelectrode gap does not influence the time evolution of the signals. However, we observe that the value of the peak current changes with the gap on the current waveforms. The maximum current for 5 mm is generally lower by about 20 % than the maximum measured for 2 mm.

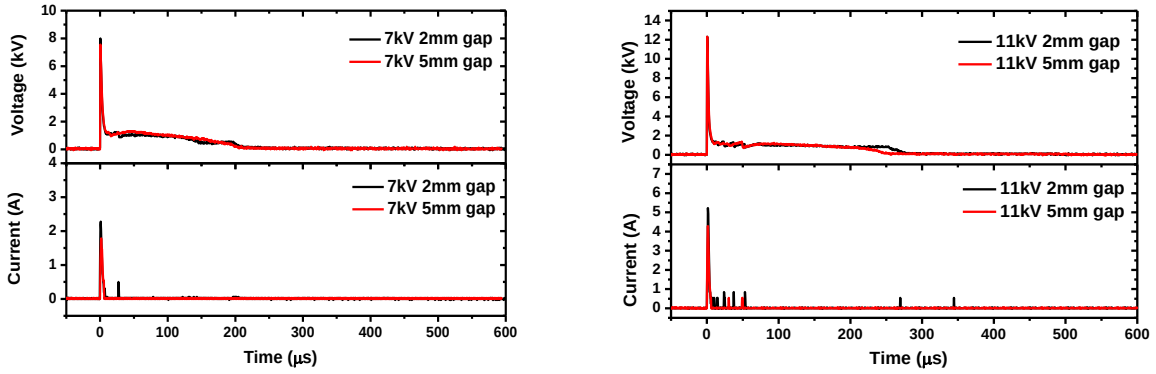

(a) (b)

Figure 4.14 Voltage and current signals of a pin to pin discharge in Cr(VI) solution (47 mg/L,σ=4 mS/cm,pH=2.4) for (a) 7 kV and (b) 11 kV with gap of 2 and 5 mm, V = 100 mL, Δt = 500 µs, electrodes length = 0±10 µm, f = 50 Hz. (See annex 4.2.3 for signals with high time resolution)

It could be concluded that changing the gap from 2 to 5 mm does not significantly influence the bubble dynamics and electrical waveforms. However, we show that increasing the gap results in a less intense glow at the beginning and a lower maximum current (charge injection). These results are consistent with the fact that increasing the gap causes the decrease of the electric field.

Finally, the effect of the last parameter, the pulse duration, is presented in the next section.

4.2.4 Effect of pulse duration

The pulse duration has been reported to have some physical effects, such as the intense electric field at the tip of the electrode[219]. In this section, we present only basic estimations of the influence of the pulse width on the plasma formation and, in particular, on the dynamics of the bubbles formed after the discharge. We present the effect of pulse duration on the two different cases: case NOBK (for 9 kV, gap of 5 mm) and case BK (for 11 kV and gap of 2 mm). The pulse width ranges from 10 µs to 500 µs.

a. In the Case of NOBK:

The time-resolved discharge measurements for the different pulse durations in case NOBK are presented in **Figure 4.15**. In general, we obtain for all pulse durations similar phenomena as previously discussed for case NOBK. For a given pulse duration, the glow plasma is observed at both electrodes at t = 2,7 µs. Then, the bubble grows and reaches its maximum, for a given electrode, at the same time for the different pulse durations As presented in **Figure 4.15**, whatever the pulse duration, the maximum size of a bubble is always around t = 91.8 µs at the cathode and at t = 118.8 µs at the anode. Based on this phenomenon, we can guess that bubbles' growth dynamics is mainly due to the dissipation of energy injected into the solution before t=10 µs, during the glow discharge.

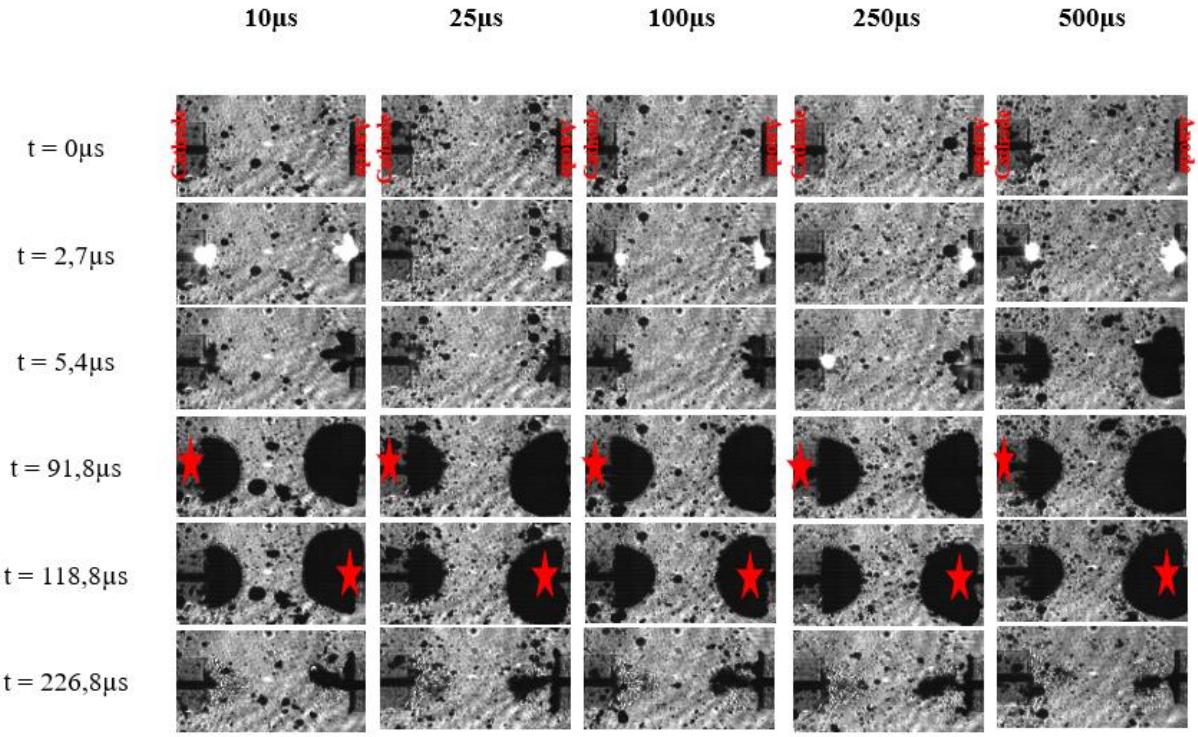

Figure 4.15 The time-resolved shadowgraphy measurements of a pin-to-pin discharge obtained in Cr(VI) solution (47 mg/L,σ=4 mS/cm,pH=2.4) for different pulse durations with U = 9 kV V = 100 mL, gap = 5 mm, electrodes length = 0±10 µm, f = 50 Hz. Red stars identify the maximum radius.

Figure 4.16 presents the electrical signals and zooms for case NOBK with different pulse durations in Cr(VI) solution. There are almost no significant differences in the voltage and current waveforms with varying the pulse width (except the end of the pulse).

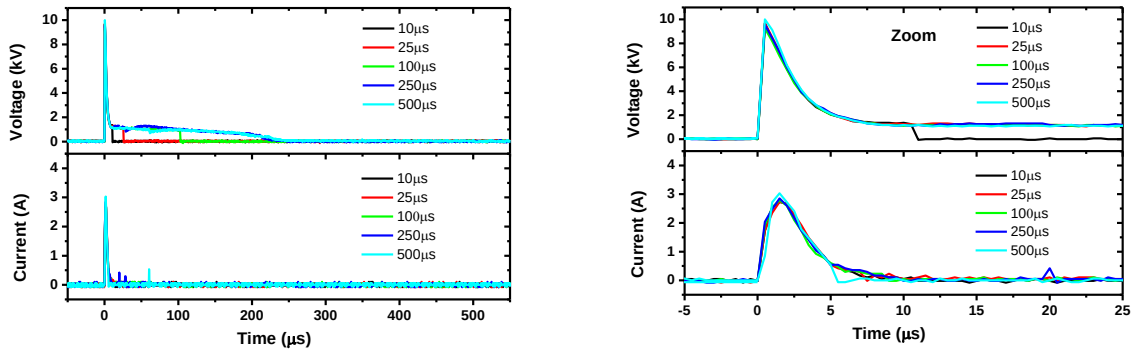

(a) (b)

Figure 4.16 (a) Voltage and current signals and (b) a zoom of 9 kV discharge in Cr(VI) solution (47 mg/L,σ=4 mS/cm,pH=2.4) for different pulse durations with U = 9 kV, V = 100 mL, gap = 5 mm, electrodes length = 0±10 µm, f = 50 Hz. (See annex 4.2.4 (a) for signals with high time resolution)

b. In the Case of BK

In order to study the effect of the pulse width for the breakdown case, we adjusted the applied voltage to 11 kV and the gap to 2 mm. As for case NOBK, no significant modifications are observed on the discharge propagation. For all tested pulse widths, a filamentary structure propagates to connect the two electrodes very fastly as observed at t = 2,7 µs (**Figure 4.17**). The light emission is very intense when a plasma channel connects the two electrodes (not shown for the case of 10 µs pulse width in **Figure 4.17**). Then the plasma channels expand spherically. Also, the maximum size of the channel coincided whatever the pulse duration at around t = 118,8 µs. After reaching the maximum, the bubble decreases and implodes.

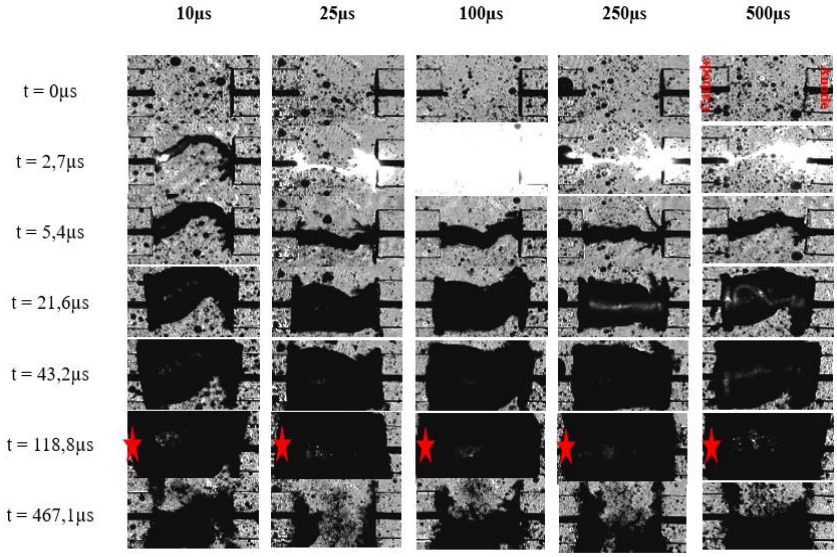

Figure 4.17 The time-resolved shadowgraphy measurements of a pin-to-pin discharge obtained in Cr(VI) solution (47 mg/L,σ=4 mS/cm,pH=2.4) for different pulse duration with U = 11 kV V = 100 mL, gap = 2 mm, electrodes length = 0±10 µm, f = 50 Hz. Red stars show the maximum radius

The voltage and current waveforms of discharge with different applied pulse durations are presented in **Figure 4.18**. The signals are very similar. Because the breakdown appears very fast (before 10 µs), this leads the voltage drops faster than in the case of NOBK. As already discussed, we obtain a variation on the maximum peak of current (**Figure 4.18**(b)) because the random distribution of intensity of the current for multi-pulse mode depends on the capacitor's charge and discharge (remaining charge stored in the reservoir capacitor after discharge) [217] and maybe also because of the memory effect of residual charge in the solution[220]. However, there is almost no significant difference in the current shape with varying pulse width. The decrease in the pulse duration leads to a decrease in the number of additional breakdown phenomena. For example, with a pulse width of 10 µs there is only one breakdown, while there are 2 when the pulse width is increased to 25 µs and 4 when the pulse width is 500 µs.

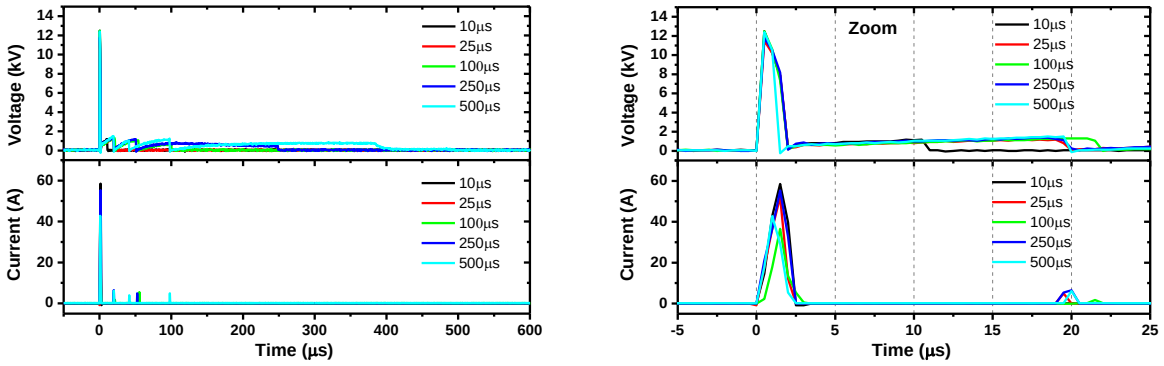

(a) (b)

Figure 4.18 (a) Voltage and current signals and (b) a zoom of 11 kV discharge in Cr(VI) solution (47 mg/L,σ=4 mS/cm,pH=2.4) for different pulse duration. V = 100 mL, gap = 2 mm, electrodes length = 0±10 µm, f = 50 Hz

It could be concluded that whatever the discharge case (with a breakdown or without breakdown), the changing of the pulse width gives similar characteristics of the discharge. The only main difference is the presence or not of secondary breakdowns.

Different results regarding the influence of pulse durations on discharge in the liquid have been reported in the literature. For example, Yang *et al*[221]. have shown that the propagation velocity of discharges is constant with a pulse width shorter than 1 µs whereas, for longer pulses, the discharge velocity decreases with increasing pulse width.

As the results show that the discharges characteristic strongly depends on the experimental conditions, in the next chapter, we will study the influence of these parameters on the H_2O_2 production and the reduction efficiency of Cr(VI).

4.3 Conclusion

This chapter refers to the discharge characteristics measurements by shadowgraphy and electrical measurements for both water and Cr(VI) solutions.

It has been reported that pin-to-pin discharge in water with low conductivity propagates in three cases, possibly obtained by a unique set of experimental conditions [175]. Another result shows that the character of discharge is different when the conductivity is higher. In this condition, only two cases are reported, one without breakdown and the other one with breakdown, called mixed regime since it involves initiation phenomena at both cathode and anode.

In a similar way to the discharge characteristics in water with high conductivity, we found that when discharging in Cr(VI) with high conductivity, only two different cases occur, namely NOBK (without breakdown) and BK (with breakdown). For the BK discharge, we observe on the electrical signals that the first breakdown occurs after 2-3 µs and we confirm that the initiation comes from the two electrodes and the propagation of the filament mainly occurs from the anode to the cathode.

Regarding the variations between the single and multi-pulse modes, we reported similar behaviors on the discharge propagation phenomena and the general shape of the electrical signals; but the multi-pulse mode involves more bubbles, a faster breakdown, the overdamp of voltage and current and a higher BK/NOBK ratio.

It is found that the applied voltage is one of the most critical parameters, which has a much more significant influence on the discharge characteristics, including the change in the current and in the number of BK and NOBK.

Regardless of the distance 2 and 5 mm, the characteristics of case NOBK are similar considering the bubble dynamics and electrical waveforms. However, we showed that increasing the gap results in a less intense glow at the beginning and a lower maximum current (charge injection). The applied pulse width does not significantly influence the discharge characteristics, for both no breakdown or breakdown cases. The only main difference is the presence or not of secondary breakdowns.

Now that we have described the characteristics of the discharge for the experimental conditions used for water and Cr(VI) experiments, the next chapters will be dedicated to the application of PLI for H_2O_2 production and Cr(VI) reduction. The influence of pulse duration on the formation of H_2O_2 and the reduction of Cr(VI) in the next chapter will show a significant variation, event as shown in this chapter, the discharge characteristics for BK or NOBK are almost the same for a given pulse duration.

Chapter 5

Preliminary studies: discharges in water

As presented in **Chapter 2**, many active species are generated by the plasma-liquid interaction (PLI), for example, hydrogen peroxide (H_2O_2), hydroxyl radical (OH), solvated electron (e_{aq}^-) and other radicals or molecular species [186,222–225]. It is generally considered that active species generated by PLI are the key to remove pollutants. Among these, H_2O_2 is in great demand for the treatment of polluted water because it is a powerful oxidizing agent due to the specific property of its oxygen-oxygen single bond [226]. Moreover, the influence of H_2O_2 has been discussed in the reduction of Cr(VI) in an acidic medium [190,191,199], as reported in **Chapter 2**. Finally, H_2O_2 is a long-lived species that is easy to monitor. Therefore, the study of the formation of H_2O_2 after an electrical discharge is a significant step in understanding the reaction processes involved in the formation of species and molecules.

Before working in a complex Cr(VI) solution (chapter VI), we present in this chapter a preliminary analysis of discharges in water and the consequences in H_2O_2 production. This chapter reports the measurement of H_2O_2 concentration by two different methods as presented in **Chapter 3** after underwater discharges using pin-to-pin configuration. First, we present the comparison of these two methods to measure the formation of H_2O_2 in water after electrical discharge. Then, a series of experiments are performed for different discharge cases in water, as presented in **Chapter 3**, by changing the applied voltage, pulse frequency, and pulse duration to determine the hydrogen peroxide production. We also report the effect of different electrode parameters such as: materials (Tungsten and Platinum) and diameter on hydrogen peroxide production. Finally we present measurement performed for different electrolytes and conductivities to introduce conditions close to those of Cr(VI) solution (**Chapter 6**).

This experimental campaign also highlights the effect of the discharge on electrodes lifetime. In order to have a global approach of the process, it is of great interest to complete the chemical analysis with the study of the electrode erosion. The final section presents a study of the electrode erosion by the pulsed electrical discharge in water according to the material and the case of the discharge.

5.1 Comparison of methods for measuring H_2O_2.

As presented in **Chapter 3**, two different methods can measure the concentration of H_2O_2 formation after discharge in water: Eisenberg method by using $TiOSO_4$ as a reagent and Christopher Andreas Vasko method by using NH_4VO_3. We note that the Vasko method is introduced with the purpose of measuring H_2O_2 concentration in Cr(VI) solution. However, before working with Cr(VI) solution, we evaluate this method in water to compare the results with the Eisenberg method for our experimental conditions.

The experiments are carried out using the same experimental conditions: tungsten electrodes (Ø = 100 µm), the length of both electrodes about 400 ± 100 µm; electrodes gap = 2 mm; applied voltage = 6 kV; Δt = 500 µs; f =50 Hz. The process is carried out for 30 minutes. The measurements are performed using two protocols:

- Eisenberg method: The concentration of hydrogen peroxide is determined every 5 minutes by measuring the absorbance at 410 nm of the product of 2 mL sample with 1 mL of titanyl ions giving a yellow-colored complex (see **Chapter 3**).
- Vakso's method: The concentration of hydrogen peroxide is determined every 5 minutes by measuring the absorbance at 440 nm of the product of 2 mL sample with 1 mL of 0.06 M NH_4VO_3 solution giving a yellow-colored complex (see **Chapter 3**).

The absorbance measurement is performed after 15 min of mixing to have full-color development. Hydrogen peroxide concentrations are obtained from the measured absorbance compared with the established calibration curve (**Annex 3.5** and **3.6**).

Figure 5.1 shows the concentration of H_2O_2 produced by the plasma discharge measured by the two different methods: Eisenberg's method ($TiOSO_4$) in black curve and Vasko's method (NH_4VO_3) in the green curve for 6 kV. The two curves have a similar trend, and the concentration of H_2O_2 production is also detected after 10 minutes for the NH_4VO_3 method, which is similar to the $TiOSO_4$ method. The final concentrations of H_2O_2 equal 0.28 mM and 0.3 mM for NH_4VO_3 and $TiOSO_4$ methods, respectively. The energy yield calculated for the NH4VO3 method is 8.3×10^{-4} g/kJ compared with 9.2×10^{-4} g/kJ for the $TiOSO_4$ method.

Consequently, we confirm that the two methods have similar results and positively point out the experiment's reproducibility. This leads to the validation of the use of NH_4VO_3 to measure H_2O_2 formation by electrical discharge in water.

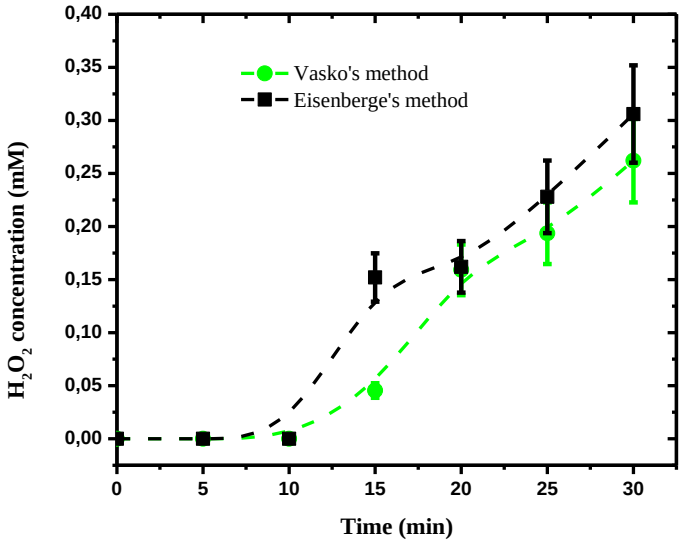

Figure 5.1 H_2O_2 concentration as a function of time measurement by two different methods using NH_4VO_3 (Vasko's method) and $TiOSO_4$ (Eisenberg's method). V=200 mL, f=50 Hz, Δt=500 µs, 2 mm of gap, Voltage = 6 kV, σ=200 µS/cm. Uncertainty of H_2O_2 concentration is 15 %

We would like to point out that before measuring the H_2O_2 concentration in the Cr(VI) solution (**Chapter 6**), we perform additional parametric studies on the H_2O_2 production in water. For example, we study the effect of the applied voltage, pulse frequency and pulse duration. We also change the electrode parameters (electrodes length, diameter) and the conductivity of the solution (4 mS/cm obtained by adding NaCl or H_2SO_4 0.1 M). These experimental conditions have been chosen because they allow better understanding the effect of discharge characteristics on H_2O_2 production. Also, few parameters are similar to those performed with Cr(VI). We note that few studies have been done using Eisenberg's method, and few studies have been done using Vasko's method. The details are presented in the following section.

5.2 Effect of applied voltage on H_2O_2 production

The discharge is performed in water for V = 200 mL, f = 50 Hz, Δt = 500 µs, 2 mm of the gap, and σ = 200 µS/cm adjusted by NaCl. The electrodes used are tungsten wire Ø = 100 µm. The length of both pin electrodes protruding from the capillary tube in water is about 400 µm (± 100 µm).

As presented in **Chapter 4**, we obtain three different discharge cases in water with a low solution conductivity [175]. To better understand the effect of discharges on the production of H_2O_2 in water with low solution conductivity, we present the effects of three different discharge cases on the production of H_2O_2 by changing the applied voltage. Three different voltages 4, 6, and 9 kV, have been applied in order to obtain cases 1, 2, and 3, respectively, as discussed in **Chapter 3**. Before presenting the results on the H_2O_2 measurement, we first present the electrical characteristics of the discharge in water.

We keep in mind that the discharge is performed under multi-pulse mode for all of the studies in this chapter.

5.2.1 Electrical characteristics of the discharge

It is noted that the experiment is performed at room temperature, and the temperature of the solution has been measured before and after the process. An increase in the solution temperature at the end of the discharge is observed. However, this increase does not exceed 10°C, and the solution reaches a maximum of 30°C after the 30 minutes process.

Figure 5.2(a) shows the typical voltage and current waveforms obtained for one pulse with different applied voltages (4, 6, and 9 kV). Detailed analysis of the waveforms can be obtained in [175] and **Chapter 4**. The value of the applied voltage has been determined to obtain the three cases of discharge mentioned previously with f = 50 Hz [175,177]. Indeed, even if the cases can occur randomly for given initial conditions, it is possible to identify a set of experimental conditions that make a case dominant. Accordingly, a majority of cases 1 (NOBK), cases 2 (BK-cathode), and cases 3 (BK-anode) of the discharge corresponds to applied voltages of 4 kV, 6 kV, and 9 kV, respectively. **Figure 5.2**(a) also confirms that the electrical waveform of the three cases is similar to the results obtained in [175]. It is noted that the terms (case 1, case 2, and case 3) are only used to describe the three different discharge cases obtained in water with the conductivity σ = 200 µS/cm in this section.

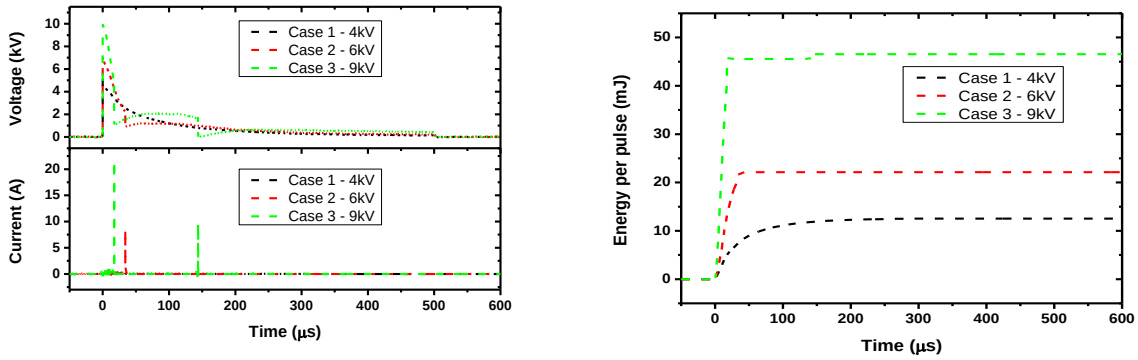

(a) (b)

Figure 5.2 Typical electrical waveforms of pin-to-pin discharge generated in water V = 200 mL, f = 50 Hz, Δt = 500 µs, 2 mm of gap, and σ = 200 µS/cm); (a) Voltage and Current signals and (b) Time evolution of the energy per pulse [202]

In addition to analyze the different discharge cases, electrical signals are used to estimate the energy delivered to the discharge (**Chapter 4**). The energy per pulse results from the time integration of the current and voltage product (**Figure 5.2**(b)). We observe that most of the energy is deposited in the liquid during the first 50 µs of the discharge. Since the variations of the waveforms from pulse to pulse are lower than 10 %, we determine the average energy per pulse by considering the average of all the waveforms measured (every 5 minutes) during the experiment. As an example for the experimental conditions reported in **Figure 5.2**, the average energy per pulse delivered for case 1 is about 12 mJ, case 2 is 25 mJ, and case 3 is 46 mJ (reported in **Table 5.1**). We also determine the total energy of the process by integrating the average energy per pulse over the experiment's total duration considering the pulse generator's frequency (as presented in **Chapter 3**). Considering the same example, we obtain total energy equal to 1.08 kJ for case 1, 2.25 kJ for case 2, and 4.14 kJ for case 3 (**Table 5.1**).

	Case 1	Case 2	Case 3
Energy per pulse (mJ)	12	25	46
Total energy for 30 min (kJ) - *(kWh)*	1.08 - (3×10^{-4})	2.25 – (6.25×10^{-4})	4.14 - (11.5×10^{-4})

Table 5.1 Average energy per pulse and total injected energy after 30 minutes for three different cases of pin-to-pin discharge generated in water. V = 200 mL, f = 50 Hz, Δt = 500 µs, 2 mm of gap, and σ = 200 µS/cm

5.2.2 H_2O_2 measurements

We note that these measurements have been done by using the Eisenberg method. The time evolution of H_2O_2 production is obtained by sampling 2 mL of the solution every 5 min (**Figure 5.3** (a)). After 30 min of discharge, the concentration of H_2O_2 remains very low in case 1 (< 0.1 mM); it reaches 0.3 mM in case 2; whereas the value is the highest one in case 3 with almost 0.8 mM. Moreover, the

detection time of H_2O_2 production changes with the case since H_2O_2 is detected after 30 min in case 1, after 15 min in case 2, and from 5 min in case 3. Once H_2O_2 is detected, its concentration increases almost linearly with time. It is noted that the error bar of 15 % is obtained by calculating the standard deviation (as presented in **Chapter 3**).

The global production rate has been estimated for each case and reported in **Table 5.2**. The production rate (g/h) is calculated by **Equation 8**:

$$\text{Production rate} = \frac{d[H2O2]}{dt} \times V \times M \qquad \textbf{Equation 8}$$

$\frac{d[H2O2]}{dt}$ is the concentration of H_2O_2 by time (mol/(L.h)), V is the volume of the solution (L), and M is the molar mass of H_2O_2 (g/mol).

Values from about 10^{-3} g/h (case 1) to 10^{-2} g/h (case 3) are obtained and are about one order of magnitude lower than those reported in Locke *et al.* [222]. This difference may be due to the lower energy used in this work, as detailed previously.

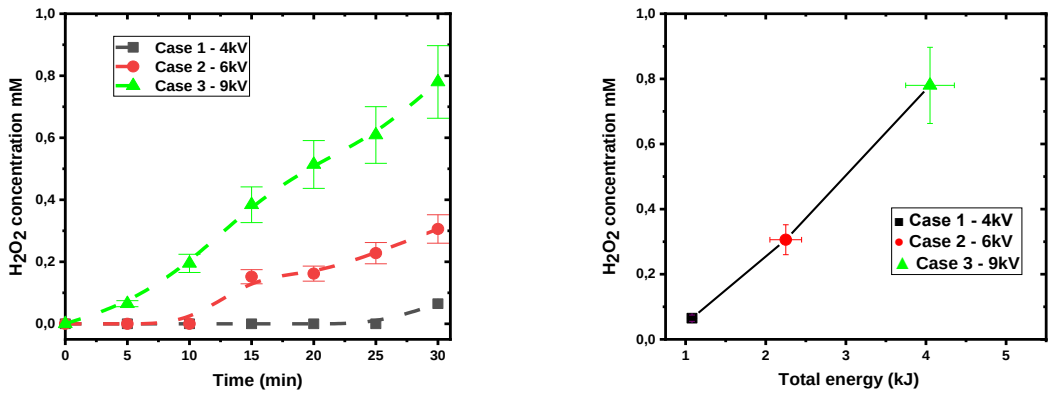

(a) (b)

Figure 5.3 Hydrogen peroxide concentration for three different cases (applied voltages). (a) Concentration of H_2O_2 as a function of time. (b) Final concentration of H_2O_2 as a function of total injected energy (measured after 30 min) (V = 200 mL, f = 50 Hz, Δt = 500 µs, 2 mm of gap, σ = 200 µS/cm). Uncertainties of [H_2O_2] and energy are 15 % and 10%, respectively

The formation of hydrogen peroxide by pulsed corona discharge in deionized water used to be represented by the global reaction [189,227–229]:

$$6H_2O \rightarrow 2H_2O_2 + 4H_2 + O_2 \qquad \textbf{Reaction 44}$$

Reaction 44 is assumed to be directly initiated by the discharge, zero-order (considering that the water concentration remains constant) [228] and dominating the other reactions [227].

Measurements of [H_2O_2] corresponding to case 3 show a linear increase concerning the time, which could be expressed as: $\frac{\Delta[H_2O_2]}{\Delta t} = k_1$, k_1 is then the rate constant of **Reaction 44**, $\Delta[H_2O_2]$ is the change in peroxide concentration (mol/L), Δt is the change in time (s). This equation shows that **Reaction 44** dominates the H_2O_2 production. Consequently, the rate constant k_1 can be estimated

from the slope of the plot, equal to about k_1^{case3} = 4.7×10^{-7} M/s for case 3. This model is not perfectly adapted to describe H_2O_2 production for case 1 and case 2 because of the presence of an ignition delay. Nevertheless, using the same approach for case 2 (from 10 min), the estimation of the rate constant k_1^{case2} provides 2.3×10^{-7} M/s, which is two times lower than case 3. The differences between the ignition delay and the estimated rate constant according to the cases suggest that the chemical processes strongly depend on the discharge regime or injected energy.

The values of these rate constants are in good agreement with measurements obtained for needle-to-plate configurations [227,228,230,231]. Using this configuration, the authors have reported up to [H_2O_2] = 2 mM after 30 min, but these performances have been obtained using very high energy (about 40 times higher than this work) [230]. For the same duration, Potocky *et al.*[232] have reported H_2O_2 concentrations equal to 1.8 mM in unbridged conditions (similar to case 1) and equal to 2.7 mM in bridged conditions (similar to case 2 or case 3). These values have been obtained using a needle-to-needle geometry with low energy (10 mJ/pulse) but for higher solution conductivities (at least 500 µS/cm) and higher electrode diameter (1 mm).

As reported in **Figure 5.2**(b) and **Table 5.1**, the energy delivered to the discharge depends on the case. **Figure 5.3**(b) presents the H_2O_2 concentration measured after 30 minutes of discharge according to the total energy injected during the experiment. The highest the total energy, the highest the H_2O_2 concentration, and the relationship is quite linear with a coefficient of about 0.19 mM/kJ. This coefficient can be interpreted as the H_2O_2 formation efficiency.

We also calculate the energy yield (g/kJ) in order to compare with other works by **Equation 9**:

$$Energy\ yield = \frac{Production\ rate}{Total\ injected\ energy} \times t \qquad \textbf{Equation 9}$$

With the production rate in *g/h*; the total energy in *kJ,* and t the duration of the process in *h*

The calculations of the corresponding energy yield for each case are reported in **Table 5.2**.

	Case 1	Case 2	Case 3
Production rate (g/h)	9 ×10^{-4}	4 ×10^{-3}	10^{-2}
Energy yield (g/(kJ)	4.1 ×10^{-4}	9.2 ×10^{-4}	1.3 ×10^{-3}

Table 5.2. Hydrogen peroxide production rate and energy yields for three different cases after 30 minutes of pin-to-pin discharge generated in water. V = 200 mL, f = 50 Hz, Δt = 500 µs, 2 mm of gap, and σ = 200 µS/cm

We obtain energy yields from 4.1×10^{-4} g/kJ (case 1) to 1.3×10^{-3} g/kJ (case 3), which are close to the values reported in Locke *et al.* [189].

Table 5.3 shows the pH and the conductivity of the solution before and after plasma discharge for the three different cases (applied voltages). It is noted that the experiment with 4 and 6 kV does not show considerable variations in solution pH and conductivity. In comparison, the one with 9 kV presents a decrease in pH (about 14 %) and an increase in conductivity (about 5 %) after the discharge. This

variation of conductivity and pH may be due to an increase in the amount of ions and species present in the solution, which occurs due to water dissociation by plasma electrical discharges [186,186,223,233].

Applied voltage	pH		Conductivity (µS/cm)	
	Initial	Final	Initial	Final
Case 1 – 4 kV	5.8	5.8	205	208
Case 2 – 6 kV	5.9	5.6	207	210
Case 3 – 9 kV	5.9	**5.2**	202	**222**

Table 5.3 Initial and final solution parameters obtained from ex situ pH and conductivity measurements for three different cases after 30 minutes of pin-to-pin discharge generated in water. V = 200 mL, f = 50 Hz, Δt = 500 µs, 2 mm of gap, and σ = 200 µS/cm.

Considering these results, two different parameters are responsible for the increase in H_2O_2 production: the increase of the energy and the change of the discharge case. In order to discriminate the influence of these two parameters on H_2O_2 production, the variation of the frequency and the pulse width are also inspected.

5.3 Effect of the pulse frequency on the H_2O_2 production

As previously, the discharge is performed in water for V = 200 mL, Δt = 500 µs, 2 mm of the gap, and σ = 200 µS/cm adjusted by NaCl. The electrodes used are tungsten wire Ø = 100 µm. The length of both pin electrodes protruding from the capillary tube in water is about 400 µm (± 100 µm). This section uses the Eisenberg method to measure the H_2O_2 concentration.

In order to study the influence of both the total energy and the discharge case on H_2O_2 production independently, we perform experiments by decreasing the pulse frequency. This study focuses only on case 2 and case 3 experiments since H_2O_2 production is very low for case 1. It is to notice that changing the pulse frequency influences the total energy consumption and discharge characteristics. Indeed whereas only case 2 is observed for 50 Hz-6kV and 25 Hz-6kV, a mix of case 1 and case 2 appears for 5 Hz-6kV. In order to isolate the influence of the total energy only, we have to adjust the applied voltage to ensure that only case 2 is present at 5 Hz, which involves the increase of the voltage to U = 8 kV and then leads to the additional condition 5Hz-8kV. There is no significant modification in the electrical waveforms for case 2 and case 3 with changing the pulse frequency, the details are present in **annex 5.1**.

Figure 5.4 shows that, for a given case (either for case 2 or case 3), the increase of the energy involves the increase of [H_2O_2].

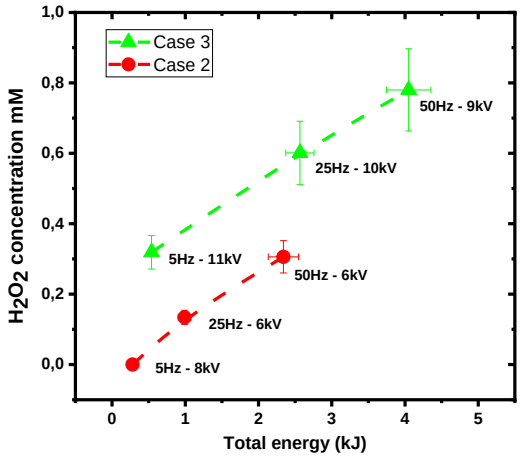

Figure 5.4 H_2O_2 concentration according to the total energy for 2 different cases of pin-to-pin discharge generated in water (V = 200 mL, Δt = 500 µs, 2 mm of gap, σ = 200 µS/cm) – couples "frequency-applied voltage" are reported. Uncertainties of [H_2O_2] and energy are 15 % and 10%, respectively

The evolution is almost linear, with a coefficient equal to about 0.12 mM/kJ for both cases. This value is lower than those estimated from **Figure 5.3**(b) (0.19 mM/kJ), which includes the influence of both the total injected energy and the discharge case. It confirms that both parameters exercise comparable influence on H_2O_2 production. This result is also observable directly in **Figure 5.4**, which shows that for the same total injected energy, the concentration of H_2O_2 in case 3 is more significant than that in

case 2. For example, at 2.5 kJ, case 3 conditions (25 Hz-10 kV) produce twice more H_2O_2 than case 2 conditions (50 Hz-6 kV).

These results are in good agreement with the rate constants estimated previously, which have shown that k_1^{case2} is 2 times lower than k_1^{case3}. These results confirm that chemical processes involved in the discharge mechanisms strongly depend on the discharge regime (case). They are consistent with Locke *et al.* [189], which suggest that the power is not the only parameter determining H_2O_2 production.

It is noted that we also obtain a more significant change in the pH and conductivity in case 3 than in case 2, whatever the applied frequency and the total energy as presented in **Table 5.4**. Moreover, for a given case, the changes are more important when the total energy increases. For example, the pH of the solution decreased from 10 to 14 % after 30 min observed at 5 Hz-11 kV (0.54 kJ) and 50 Hz-9 kV (4.14 kJ), respectively.

Frequency - Voltage	Case	Total energy (kJ)	pH		Conductivity (µS/cm)	
			Initial	Final	Initial	Final
5 Hz-8kV	2	0.24	5.9	5.8	205	205
25 Hz-6kV	2	0.90	5.9	5.7	205	207
50 Hz-6kV	2	2.25	5.9	5.6	207	210
5 Hz-11kV	3	0.54	5.9	5.4	204	210
25 Hz-10kV	3	2.57	5.9	5.2	208	217
50 Hz-9kV	3	4.14	5.9	5.2	202	222

Table 5.4 Initial and final solution parameters obtained from ex situ pH and conductivity measurements for case 2 and case 3 with different applied frequencies after 30 minutes of pin-to-pin discharge generated in water. V = 200 mL, Δt = 500 µs, 2 mm of gap, and σ = 200 µS/cm

The pulse duration is the following parameter that we will focus on studying the influence on the formation of H_2O_2.

5.4 Effect of pulse duration on the H_2O_2 production

As previously, the discharge is performed in water for V = 200 mL, f = 50 Hz, 2 mm of the gap, and σ = 200 µS/cm adjusted by NaCl. The electrodes used are tungsten wire Ø = 100 µm. The length of both pin electrodes protruding from the capillary tube in water is about 400 µm (± 100 µm). This section uses the Eisenberg method to measure the H_2O_2 concentration. In order to analyze the effect of the discharge kinetics on the H_2O_2 production, the length of the pulse duration is changed from 50 to 500 µs. There is no significant modification in the electrical waveforms for case 2 and case 3 with changing the pulse duration, the details are presented in **annex 5.2**.

Figure 5.5 presents the concentration of H_2O_2 measured for case 2 (6 kV) and case 3 (9 kV) for different pulse durations. [H_2O_2] increases with the pulse duration. We have previously shown (**Figure 5.4**) that the influence of the injected energy is similar for both cases, but the influence of the pulse duration is different on H_2O_2 production according to the case. For case 2, from 50 to 500 µs, the concentration of H_2O_2 increases by 100 % (from 0.15 to 0.3 mM), but by only 10 % for case 3 (from 0.72 to 0.78 mM) (**Figure 5.5**). This result shows that the chemical kinetics initiated by the discharge is very different for case 2 and case 3. In particular, experiments at 50 µs give information on what happens during the pre-breakdown and the breakdown (that occurs around 25 µs), whereas experiments performed at 100 and 500 µs also include post breakdown. We observe that for case 3, most of the H_2O_2 production is performed during the pre-breakdown and breakdown since the increase of [H_2O_2] is low with the pulse duration.

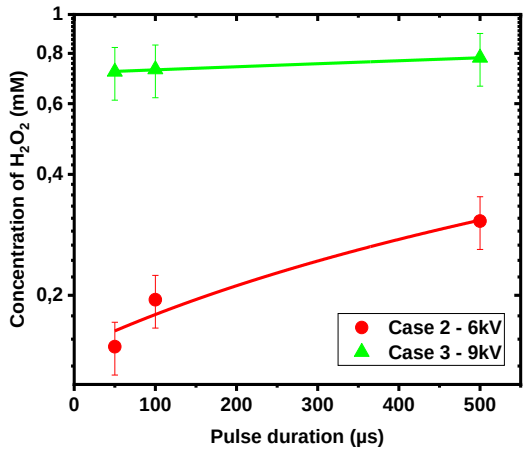

Figure 5.5 H_2O_2 production measured for different pulse durations (Δt =50, 100, 500 µs) and reported for 2 different cases of pin-to-pin discharge generated in water. V = 200 mL, f = 50 Hz, 2 mm of gap, σ= 200 µS/cm, Time of process 30 min. Uncertainty of [H_2O_2] is 15 %

To increase the pulse duration from 50 to 500 µs means increasing the post-breakdown duration. H_2O_2 production is much more efficient during this phase for case 2 than for case 3. H_2O_2 production seems to be mainly driven by the initial stage of the discharge in case 3, whereas the tail of the discharge also has a significant influence for case 2. These results confirm that the chemical processes induced by the discharge are very different according to the regime.

Table 5.5 shows the change of pH and conductivity of the solution before and after for case 2 and case 3 with different applied pulse durations. We find that in case 2 and case 3, after 30 minutes of discharge, there is no appreciable change in the pH and conductivity of the solution with the pulse width.

Applied pulse duration	Case	pH		Conductivity (µS/cm)	
		Initial	Final	Initial	Final
50 µs - 6kV	2	5.9	5.8	205	205
100 µs - 6kV	2	5.8	5.7	205	207
500 µs - 6kV	2	5.9	5.6	207	210
50 µs - 9kV	3	5.7	5.3	205	226
100 µs - 9kV	3	5.9	5.2	206	227
500 µs - 9kV	3	5.9	5.2	202	222

Table 5.5 Initial and final solution parameters obtained from ex situ pH and conductivity measurements for cases 2 and 3 with different applied pulse duration after 30 minutes of pin-to-pin discharge generated in water. V = 200 mL, f = 50 Hz, 2 mm of gap, and σ = 200 µS/cm.

In the next section, we present the influence of different electrode parameters on the formation of H_2O_2.

5.5 Effect of Electrode Parameters on H_2O_2 Formation

The discharge is performed in water for V = 200 mL, f = 50 Hz, Δt = 500 µs, 2 mm of the gap, and σ = 200 µS/cm adjusted by NaCl.

We have shown that case 3 is more efficient than case 2 for H_2O_2 production. Even if energy cost and chemical efficiency are important parameters of the process, its durability is also essential. The weak point of such a process is the lifetime of the electrodes. The erosion phenomena are very different according to the physical and chemical mechanisms occurring during the discharge and electrode material's nature [234].

Before studying the erosion processes, we propose investigating the influence of the electrodes material and size on the H_2O_2 production for our experimental conditions. This study also aims to have a first look at the chemical analysis before working with the same electrode geometry on Cr(VI) solution.

5.5.1 Effect of different electrode materials on H_2O_2 formation

We note that this section uses the Eisenberg method to measure the H_2O_2 concentration. Two different materials are reported in this part: Tungsten (W) and Platinum (Pt). First, it should be noted that changing the electrode material has no effect on the electrical waveform, and the energy delivered is similar for three cases regardless of the material of electrodes, as shown in **annex 5.3**.

Figure 5.6 shows H_2O_2 concentration obtained using electrodes in tungsten (dotted curve), in platinum (solid curve), and a combination of platinum for the anode and tungsten for the cathode (dash and dot curve). It is noted that the combination of material has been tested since it shows very interesting result regarding the erosion process (as discussed in section **5.7**).

The measurements are performed for three different applied voltages and during 30 min of discharge, except for experiments using platinum electrodes at 6 kV and 9 kV (solid blue curve) because of the total erosion of the cathode (GND) after 10 min.

For case 1 and case 2, the electrode material has no influence on the total energy consumed after 30 min of discharge, as already observed by Holzer *et al.* [231]. For case 3, we observe that the total energy injected during the experiment is about 20 % higher for Pt–W electrodes than for W–W electrodes (using the same applied voltage and same duration).

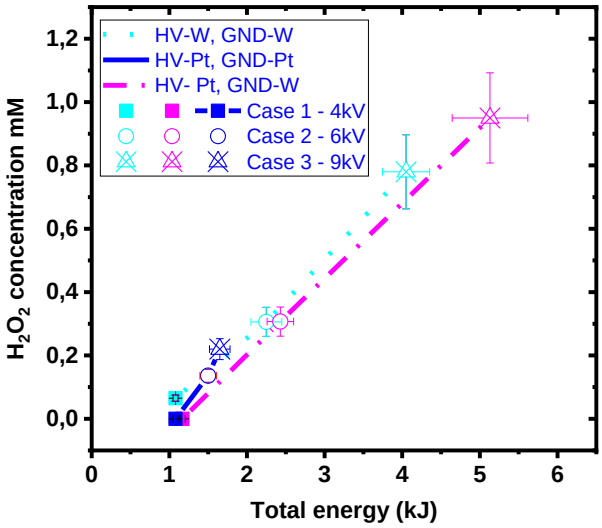

Figure 5.6 The effect of electrode material on the production of H_2O_2 by pin-to-pin discharge generated in water (V = 200 mL, f = 50 Hz, Δt = 500 µs, 2 mm of gap, σ = 200 µS/cm). HV means anode, and GND is for the cathode. Duration is 30 min except for Platinum 6 and 9 kV (10 min). Uncertainty on [H_2O_2] is 15 %

On the whole range of reported energy, the influence of the electrode material on the H_2O_2 production is low. At very low energy (1.08 kJ), H_2O_2 is not detected either with Pt-electrodes or Pt-W electrodes, whereas a low concentration is measured with W-electrodes ([H_2O_2] = 0.065 mM). For medium energy (~ 2 kJ), the concentrations of H_2O_2 are similar whatever the electrode material (~ 0.25 mM). Finally, at high energy (4–5 kJ), the concentration of H_2O_2 generated after using the combination of two different materials for the electrodes is similar to the production obtained with W-electrodes (for given energy). This result is consistent with [231,232], which have reported no influence of the electrode material on the initial H_2O_2 formation rates. However, it has been shown that after several tens of minutes of discharge, tungsten particles dissolved into the bulk solution via the erosion of the electrodes leading to H_2O_2 decomposition by catalysis reactions [231,235]. Moreover, it has been shown that hydrogen peroxide concentration can be affected when Pt is used (depending on the pH) [236]. Therefore, in addition to limiting the process, the erosion of electrodes by electrical discharge in water can modify the chemical activity in the solution. Even if such catalytic effect has not been observed in our conditions, the erosion of tungsten and platinum electrodes will be investigated in detail in the section **5.7**.

Table 5.6 shows the variation in the pH and conductivity of solution after 30 minutes of the process for three different cases with the combination in the material of electrodes (HV-Pt and GND-W) and no combination electrodes (only W). The condition of platinum electrodes is not reported because of their total erosion after 10 min. It is noted that the changes in the pH solutions after 30 minutes of discharge are not significant for case 1 - 4 kV when changing the electrodes material. However, we obtain a variation of about 7 % in the pH at the end of the process for 6 and 9 kV due to the change of electrodes material (as shown in **Table 5.6**), the final pH is higher for W-electrodes than for Pt-W

electrodes. For example, at 6 kV, the final pH value is 5.2 for the discharge with the combination of electrodes (HV-Pt, GND-W), while it is 5.6 only for the discharge by tungsten electrodes.

On the other hand, we do not obtain much difference in conductivity according to the electrode material at the end of the process. For example, at 4 kV, the conductivity value after 30 minutes of discharge is 207 µS/cm in the case of a mixture of electrode materials (HV -Pt, GND-W) compared to 208 µS/cm in case of no combination (HV -W, GND-W). This result is also found for 6 kV and 9 kV, as presented in **Table 5.6**.

Applied voltage	Electrodes material	pH		Conductivity (µS/cm)	
		Initial	Final	Initial	Final
4kV – case 1	HV-Pt . GND-W	5.8	5.8	206	207
4kV – case 1	HV-W . GND-W	5.8	5.8	205	208
6kV – case 2	HV-Pt . GND-W	5.8	5.2	204	208
6kV – case 2	HV-W . GND-W	5.9	5.6	207	210
9kV – case 3	HV-Pt . GND-W	5.9	4.9	207	225
9kV – case 3	HV-W . GND-W	5.9	5.2	202	222

Table 5.6 Initial and final solution parameters obtained from ex situ pH and conductivity measurements for 4,6 and 9 kV after 30 minutes of pin-to-pin discharge generated in water. V = 200 mL, f = 50 Hz, 2 mm of gap, and σ = 200 µS/cm, HV-Pt and GND-W (HV means anode and GND is for cathode)

In the next section, we present the measurement of H_2O_2 formation in water using different electrode diameters and lengths.

5.5.2 Effect of different electrode diameters and lengths on H_2O_2 production

This section uses the Vasko's method to measure the H_2O_2 concentration. Since platinum electrodes (Ø = 200 µm, lengths = 0 ± 10 µm) are used for Cr(VI) reduction experiments, we measure the concentration of H_2O_2 produced in water after plasma discharge with platinum electrodes of 200 µm diameter with the length of two electrodes = 0 ± 10 µm. We compare these measurements with the previous experiment (section 5.2.2) performed with tungsten electrodes with the diameter of 100 µm, and the length of two electrodes = 400 ± 100 µm Since the concentration of H_2O_2 formation in case 1 is very low at 4 kV (and it is not used for working in Cr(VI) solution), we use only two different applied voltages, 6 kV and 9 kV, in this study.

We obtain a similar evolution of the electrical signals and energy per pulse, regardless of the length and size of the electrodes (as presented in **annex 5.4**). We can conclude that the change of electrodes materials (Pt, W), the size (100 µm or 200 µm), and the length (l = 400 ± 100 µm or l = 0 ± 50 µm) does not have any significant influence on the electrical signal and energy injected into the solution.

Consequently, due to the similar physical properties of the discharge and the injected energy, we expect no significant change in the H_2O_2 production by changing the electrode parameters.

Figure 5.7 compares [H_2O_2] as a function of time using different electrode parameters. It is noted that the solid line shows the concentration of H_2O_2 formation when using W electrodes Ø = 100 µm (as shown in 5.2.2), and the dashed line shows the concentration of H_2O_2 formation when using Pt electrodes Ø = 200 µm. The production of H_2O_2 after 30 minutes is similar in both experiments. For example, the H_2O_2 concentration reaches about 0.32 mM after 30 minutes with an applied voltage of 6 kV, regardless of the type of electrodes (the blue lines in **Figure 5.7**). It is found that H_2O_2 can be detected earlier for (HV-0-Pt, GND-0-Pt) (at 10 minutes) than for (HV-400-W, GND-400-W) (at 15 minutes) in the case of 6 kV. The H_2O_2 concentration in the first 15 minutes is higher at 9 kV (HV-0-Pt, GND-0-Pt) than at (HV-400-W, GND-400-W). However, after 15 minutes, the concentration of H_2O_2 is similar. At 9 kV, the H_2O_2 concentration after 30 minutes using Pt and W electrodes is 0.68 mM and 0.78 mM, respectively.

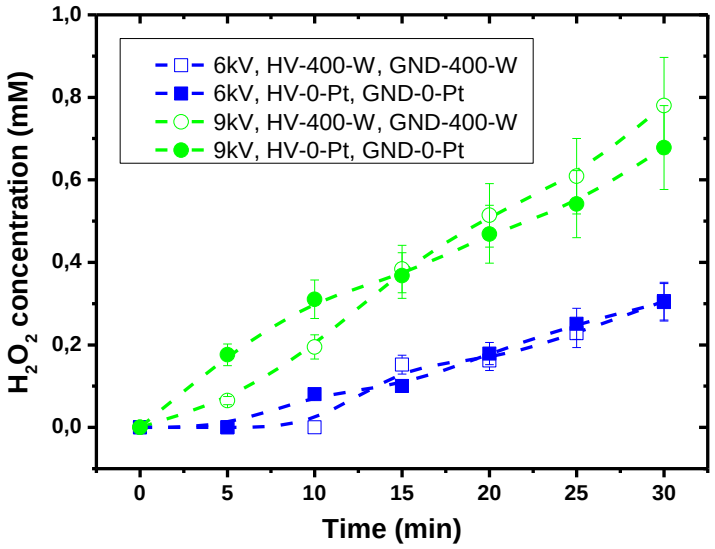

Figure 5.7 Hydrogen peroxide concentration for different applied voltages (6 and 9 kV) with different electrodes (lengths and diameter) after 30 minutes of pin-to-pin discharge generated in water. V = 200 mL, f = 50 Hz, Δt = 500 µs, 2 mm gap σ = 200 µS/cm, Ø = 100 µm for W electrodes with the length = 400 µm, Ø = 200 µm for Pt electrodes with the length = 0 µm). Uncertainty of [H_2O_2] (15 %)

As a conclusion, the change of electrodes parameters does not have a significant influence on H_2O_2 production during the whole duration of the experiment (30 minutes).

The variations in pH and conductivity are shown in **Table 5.7** for two applied voltages. The experiment at 6 kV does not show high variation in the pH and conductivity of the solution by changing the nature of the electrodes. However, the experiment at 9 kV shows a variation in pH and conductivity of the solution after discharge. For the condition of platinum electrodes, the decrease of the pH at the end of the process is more significant than in the case of tungsten electrodes.

Moreover, the increase in conductivity is more significant when platinum electrodes are used than in the case of tungsten electrodes.

Applied voltage	Electrodes material	pH		Conductivity (µS/cm)	
		Initial	Final	Initial	Final
6 kV	HV-0-Pt, GND-0-Pt	5.9	5.5	205	212
6 kV	HV-400-W, GND-400-W	5.9	5.6	207	210
9 kV	HV-0-Pt, GND-0-Pt	5.7	**4.7**	202	**235**
9 kV	HV-400-W, GND-400-W	5.9	**5.2**	202	**222**

Table 5.7 Initial and final solution parameters obtained from ex situ pH and conductivity measurements for 6 and 9 kV after 30 minutes of pin-to-pin discharge generated in water. V = 200 mL, f = 50 Hz, 2 mm of gap, and σ = 200 µS/cm Δt = 500 µs, Ø = 100 µm for W with the length = 400 µm ,Ø = 200 µm for Pt electrodes with the length = 0 µm (HV means anode and GND is for cathode)

From these results, we can conclude that the type of electrodes (regardless of their size, length, and materials) does not significantly influence the physical properties of the discharge and the formation of H_2O_2. However, it has some influence on the chemical properties of the solution for case 3.

In the next section, we present the effect of the solution conductivity on the production of H_2O_2 after the electrical discharge.

5.6 Effect of the electrolytes on the production of H_2O_2

In this test, the experimental conditions used are: Pt electrodes Ø = 200 µm; 2 mm of electrodes gap; the length of two electrodes was 0 ± 10 µm, Δt = 500 µs; f =50 Hz, U=9 kV.

As described in detail in **Chapter 4** and [176,177], the discharge characteristics change for different conductivities, which can lead to different production of H_2O_2 after discharge. To illustrate this point, we analyze the concentration of H_2O_2 formed in a solution with high conductivity σ = 4 mS/cm. We note that the conductivity of the Cr(VI) solution used for the reduction is 4 mS/cm, obtained from the addition of 0.1 M sulfuric acid. The volume of the solution is 100 mL which is the same as the experimental condition for Cr(VI) reduction.

For this study, two different water solutions with the same conductivity of σ = 4 mS/cm are performed. The first solution is prepared using NaCl to adjust the conductivity up to 4 mS/cm. The second solution is obtained by mixing 6 mL H_2SO_4 0.1 M with 94 mL of distilled water. It is noted that we have differences in the initial pH for two different solutions (**Table 5.8**). The experiment in the H_2SO_4 solution is performed in a strongly acidic medium (pH = 2.4), while the NaCl solution is a weakly acidic medium (pH = 5.7).

In this section, we briefly present both the effect of the electrolyte nature and the effect of the solution conductivity.

Table 5.8 shows that increasing the initial conductivity (with NaCl) results, after 30 min of discharges, in a lower variation of the final pH and conductivity of the solution. Indeed, the pH does not change for 4 mS/cm, whereas it decreases of about 17 % for 200 µS/cm (from 5.7 to 4.7); and the increase of the conductivity is more significant (5%, from 4.01 to 4.2 µS/cm) when the discharge is performed at high conductivity than at low conductivity (15 %, from 202 to 235 µS/cm).

Electrolytes	pH		Conductivity	
	Initial	Final	Initial	Final
(a) NaCl	5.7	4.7	202 µS/cm	235 µS/cm
(b) NaCl	5.7	5.7	4.01 mS/cm	4.2 mS/cm
(c) H_2SO_4	2.4	2.4	4.15 mS/cm	4.01 mS/cm

Table 5.8 Initial and final solution parameters obtained from ex situ pH and conductivity measurements according to the electrolytes. The final values are obtained after 30 minutes of pin-to-pin discharge generated in water. (a) V = 200 mL σ = 200 µS/cm , (b) and (c) V = 100 mL and σ = 4 mS/cm. f = 50 Hz, 2 mm of gap, U = 9 kV , Δt = 500 µs

Moreover, we observe that the pH of the solution does not vary by changing the nature of the electrolyte, while the conductivity of the solution changes, increasing in the case of NaCl (from 4.01 to 4.2 µS/cm) and decreasing in the case of H_2SO_4 (from 4.15 to 4.01 µS/cm).

Figure 5.8 shows the distribution of energy per pulse obtained by the discharge using different solutions. The data is recorded using a lab-made program (as presented in **Chapter 3**). In this case, the energy per pulse is recorded every 5 s.

As already evoked in **Chapter 4**, the variation of the **conductivity** changes the physics of the discharge and also the distribution of breakdown and no breakdown. It is noted that the distribution of BK/NOBK is 97/3 for 200 µS/cm whereas it is 3/97 for 4 mS/cm (with NaCl). The electrical waveforms are modified by the conductivity of the solution (as discussed in [176]), so the injected energy is also changed. **Figure 5.8** also presents the energy for BK and NOBK. We obtain similar energies per pulse for NOBK (about 55 mJ for 200 µS/cm and 57 mJ for 4 mS/cm) but more different values for BK since for 200 µS/cm the total ịnected energy is equal to 41 mJ whereas for 4 mS/cm it is equal to 36 mJ. But because of the very low percentage of BK for discharge at 4 mS/cm, it is not easy to conclude that. Moreover, due to the very different BK/NOBK distribution, the total injected energy is also very different (**Equation 3** in **Chapter 3**), being equal to 3.9 kJ for 200 µS/cm and 5.1 kJ for 4 mS/cm (**Table 5.9**).

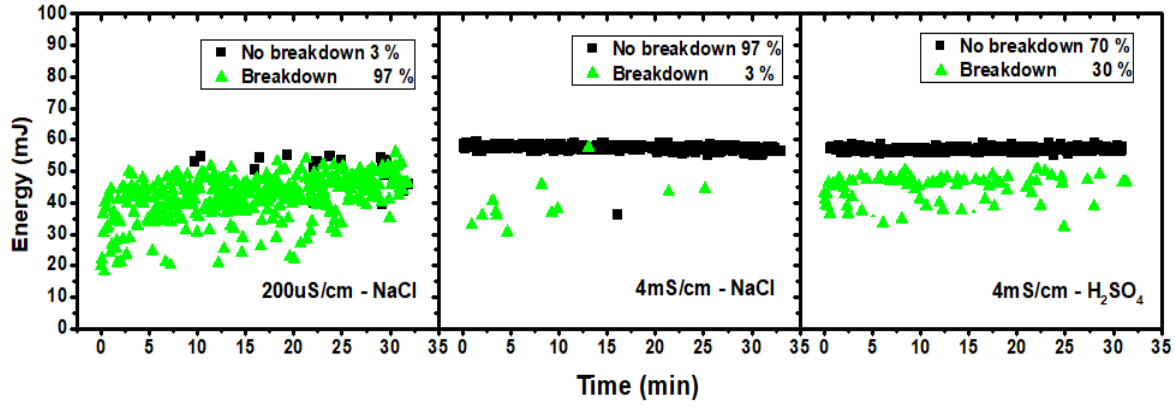

Figure 5.8 Distribution of energy per pulse of pin-to-pin discharge generated in water at 9 kV for different conductivities and electrolytes, V = 100 mL - σ = 200 µS/cm adjusted by NaCl, V = 200 mL - σ = 4 mS/cm adjusted by NaCl and H_2SO_4 0.1 M. f = 50 Hz, 2 mm of gap, Δt = 500 µs, HV-0-Pt and GND-0-Pt, Ø = 200 µm

Moreover, it is noted that the distribution of BK/NOBK depends on the **electrolyte** since it is 3/97 for the discharge in NaCl solution whereas it is 30/70 when discharge is performed in H_2SO_4 solution. Due to the low percentage of BK with NaCl solution, it is difficult to compare the electrical signals of BK discharge for different electrolytes. The electrical signals of NOBK are similar for the discharge for the two electrolytes (**annex 5.5**). **Figure 5.8** also presents the energy for NOBK and BK, and we obtain a similar energy per pulse for NOBK (57 mJ) for both electrolytes. But we obtained different values for BK since for discharge in NaCl the energy is equal to 36 mJ whereas for the discharge in H_2SO_4 it is equal to 43 mJ. Thus, the injected energy measured for BK may depend on the electrolyte, but because of the very low percentage of BK for discharge in NaCl, it is not easy to conclude that.

Moreover, due to the different BK/NOBK distribution, the total injected energy is slightly different, being equal to 5.1 kJ for NaCl and 4.8 kJ for H_2SO_4 (**Table 5.9**).

Alteri *et al.*[237] have studied the effect of the different electrolytes on the discharge characteristics. Although the configuration is not the same in our case, they have found that the discharges are more favorable in a solution with H_2SO_4 as an electrolyte. This result is in agreement with our observations.

Conductivity	Average Energy per pulse BK / NOBK (mJ)	BK / NO BK (%)	Total injected energy (kJ)	$[H_2O_2]$ (mM)	Energy yield (g/kJ)
(a) 200 µS/cm NaCl	41/55	98/2	3.9	0.68	12.5×10^{-4}
(b) 4 mS/cm NaCl	36/57	3/97	5.1	0.54	7.2×10^{-4}
(c) 4 mS/cm H_2SO_4	43/57	30/70	4.8	0.60	8.5×10^{-4}

Table 5.9 Effect of the conductivity on H_2O_2 production of pin-to-pin discharge generated in water at 9 kV after 30 minutes, f = 50 Hz, 2 mm of gap, Δt = 500 µs, HV-0-Pt and GND-0-Pt, Ø = 200 µm (a) σ = 200 µS/cm adjust by NaCl, V= 200 mL (b) σ = 4 mS/cm adjust by NaCl, V = 100 mL (b) and (c) σ = 4 mS/cm adjust by H_2SO_4 0.1 M, V= 100 mL, HV means anode and GND is for cathode)

Table 5.9 also shows the effect of the solution conductivity and electrolyte on H_2O_2 production measured after 30 minutes of PLI. We note that the experimental conditions between low and high conductivities are not exactly the same (the volume of the solution). However, we have already shown that the concentration of H_2O_2 formation does not depend on the volume of the reactor (as presented in **Chapter 3**). Thus it is interesting to compare the influence of the conductivity in the formation of H_2O_2 after 30 minutes of the discharge.

As a result, the concentration of H_2O_2 formation after 30 minutes with the low conductivity solution is 0.68 mM, higher than 0.54 mM for the high conductivity solution, as presented in **Table 5.9.** Moreover, the energy yield decreases from 12.5×10^{-4} g/kJ to 7.2×10^{-4} g/kJ when the conductivity increases from 200 µS/cm to 4 mS/cm. The variations can be explained due to the effect of the number of BK/NOBK, as we concluded in section **5.3**. We remind that changing the number of BK/NOBK leads to a change in the injected energy.

Figure 5.9 shows the concentration of H_2O_2 as a function of time for two different electrolytes. After 30 minutes, the concentration of H_2O_2 reaches about 0.54 mM with the solution using NaCl and 0.6 mM with the solution using H_2SO_4. The nature of the electrolyte does not have a significant influence on the H_2O_2 production.

We also calculate the energy yield for these two experiments. We logically obtain similar values equal to 7×10^{-4} g/kJ for the case discharge in NaCl solution and 8.3×10^{-4} g/kJ for the experiment performed in H_2SO_4 since both the injected energy and the H_2O_2 production are similar.

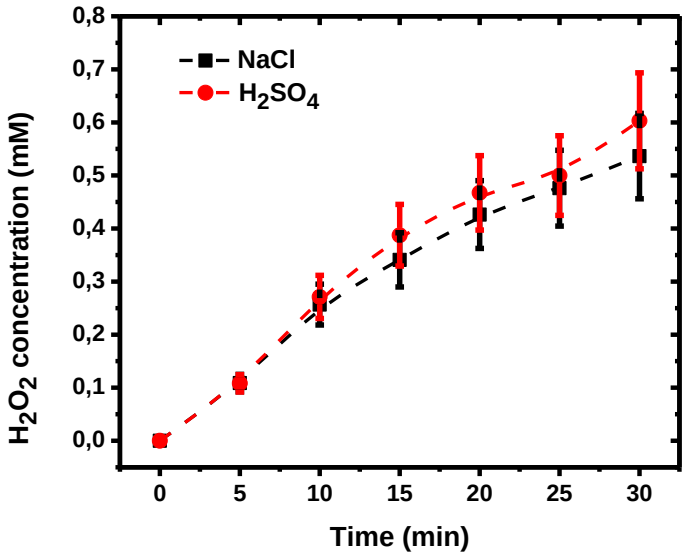

Figure 5.9 Time evolution of H_2O_2 concentration for two different electrolyte solutions. The red curve presents the results of the solution with H_2SO_4, and the black curve for the solution with NaCl. V=100 mL, f = 50 Hz, Δt = 500 µs, 2 mm of gap, Voltage = 9 kV, σ = 4 mS/cm). HV-0-Pt and GND-0-Pt, Ø = 200 µm (HV means anode, and GND is for cathode). Uncertainty of H_2O_2 concentrations is 15 %

In conclusion, we do not observe a significant influence on H_2O_2 formation for two electrolyte compositions. However, in the same electrolyte solution (as NaCl), the H_2O_2 formation is higher when the discharge is performed in low solution conductivity (200 µS/cm**)** than in the high solution conductivity (4 mS/cm)

As presented in **5.5**, the weak point of this process is the lifetime of the electrodes. In the next section, we present the study on the erosion of the electrodes by using some methods presented in **Chapter 3**.

5.7 Erosion of Electrodes

This additional work aims to analyze both the lifetime of the process and the surface mechanisms processes by considering the damage of the electrodes. This section presents the study of the erosion of the electrodes. The measurements of electrodes lengths have been done *in situ* by using of IDS camera. Analysis of the electrodes surface has been performed ex situ by SEM analysis (as presented in **Chapter 3**).

The discharge is performed in water for V = 150 mL, f = 50 Hz, Δt = 500 µs, 2 mm of the gap, and σ = 200 µS/cm adjusted by NaCl. The electrodes used are tungsten wire Ø = 100 µm. The length of both pin electrodes protruding from the capillary tube in water is about 400 µm (± 100 µm).

5.7.1 In situ length measurements

The erosion of the electrodes is estimated from the decrease of the length of the protruding part with time. *In situ* measurements have been performed every 5 minutes using an IDS camera (**Chapter 3**). Even though the measurements have shown that the erosion is all around the electrodes, the variation of the length is a good indicator to describe the erosion process.

Figure 5.10 shows the time evolution of the normalized length of positive (HV) and ground (GND) electrodes for experiments performed with either W or Pt at three different applied voltages (*i.e.* different energies per pulse, which involve different cases). Obviously, the erosion of both materials (tungsten and platinum) increases with the discharge time. However, the erosion of electrodes strongly depends on the material, the case, and the energy per discharge:

- It is to notice that for **case 1** (*e.g.* discharge in cathode regime without breakdown), the erosion of both electrodes is not significant for both materials (decrease lower than 10 %), except for W-anode, which shows a fast decrease (85 %) after 10 minutes of discharge.
- The variation of the length of the electrodes for **case 2** (*e.g.* discharge in cathode regime with breakdown) is significant for W-anode (55 %) and Pt-cathode (85 %) but negligible for W-cathode (15 %) and Pt-anode (5 %).
- The variation of the length of the electrodes for **case 3** is about 95% for W-anode, 30% for Pt-anode, 50% for W-cathode and 100% Pt-cathode.

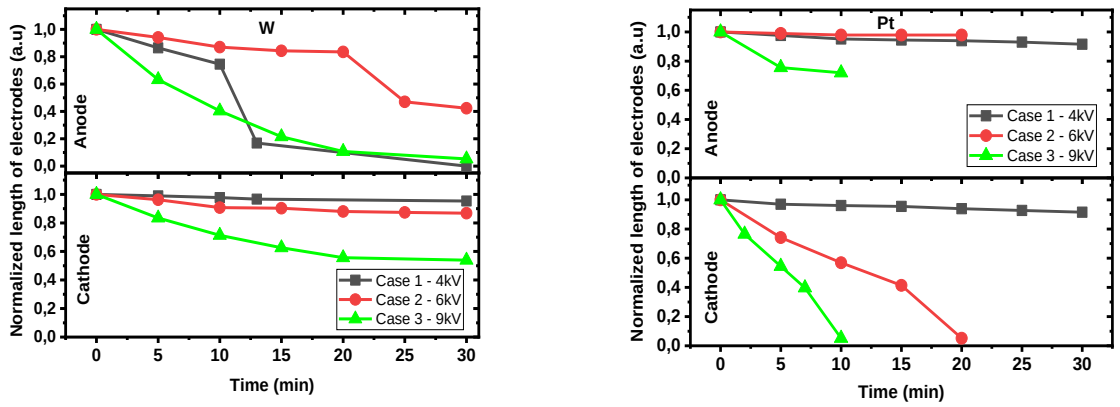

(a) (b)

Figure 5.10 Variation of normalized length of anode and cathode electrodes as a function of time, (a) tungsten electrodes, (b) platinum electrodes (V = 150 mL, f = 50 Hz, Δt = 500 µs, 2 mm of gap, σ = 200 µS/cm). Uncertainty of equipment is not discernable (2 %)

Regarding breakdown conditions, the erosion of both electrodes is always more important for case 3 (initiation of the discharge from the anode) than for case 2 (from the cathode), which is expected since the energy per pulse is higher in case 3 than in case 2 (**Figure 5.2**(b)).In contrast, Potocký *et al.*[232] have shown that the erosion rate for an unbridged discharge was lower than for a bridged discharge with W electrodes.

Nevertheless, several processes might be considered when dealing with electrode discharge-induced erosion, as presented in other works [232,234,238,239]. One of these processes concerns electrochemical reactions that may occur at the surface of the electrodes.

In the case of **tungsten electrodes**, the anodic oxidation of W to WO_3 [240], followed by the oxide dissolution into tungstate ions, WO_4^{2-} [241], is to be considered:

$$W + 3H_2O \rightarrow WO_3 + 6H^+ + 4e^- \qquad \textbf{Reaction 45}$$

$$WO_3 + H_2O \rightarrow WO_4^{2-} + 2H^+ \qquad \textbf{Reaction 46}$$

This mechanism could explain the W-anode length decrease presented in **Figure 5.10**(a), whereas no significant change is observed for the cathode.

A significant length variation is only observed at the cathode for the **platinum electrodes**. We might take into account the possible cathodic reactions taking place during the process, one of these being oxygen reduction:

$$O_2 + 2H_2O + 4e^- \rightarrow 4OH^- \qquad \textbf{Reaction 47}$$

In addition, the presence of chloride ions might have a role in the erosion of Pt electrodes [242] according to the reactions:

$$Pt + 4Cl^- \rightarrow [PtCl_4]^{2-} + 2e^- \qquad \textbf{Reaction 48}$$

$$Pt + 6Cl^- \rightarrow [PtCl_6]^{2-} + 4e^- \qquad \textbf{Reaction 49}$$

Thus, cathodic reduction of oxygen added to easier oxidation of Pt electrodes in the presence of chloride ions could explain the significant length change observed at the Pt-cathode.

Furthermore, for **W electrodes** (**Figure 5.10(**a**)**), erosion is more important at the anode than at the cathode, showing respective variations of 55 %/15 % for case 2 and 90 %/45 % for case 3. This result is consistent with experiments performed in plate-to-plate configuration [238]. Liu *et al.* [238] suggested that a larger amount of mass is lost from the anode since the arc develops from the anode. This phenomenon can only explain case 3 results since for case 2, and the discharge is initiated from the cathode. In contrast, for **platinum electrodes** (**Figure 5.10**(b)), erosion is less intense at the anode than at the cathode, showing respective variations of 5 %/85 % for case 2 and 30 %/90 % for case 3. These results justify experiments performed with a combination of material using platinum for the anode and tungsten for the cathode. This configuration gives the best result in terms of electrodes erosion. We point out that the evolution of the electrodes showed similar behavior to **Figure 5.10**(a) for cathode and **Figure 5.10**(b) for anode (the results are not shown).

The decreases in the length are almost linear for all the conditions presented in **Figure 5.10**, except for the tungsten anode electrode in case 1 (as already reported). In case 2, a fast decrease occurs after 20 minutes of discharge. These results will be discussed in the next section. A lot of different physical and chemical mechanisms can explain the different behaviors reported for the erosion of the electrodes. In order to better understand, we have performed additional analysis of the electrodes surface.

5.7.2 SEM analysis

The morphology of the electrodes exposed to the discharge is studied with Scanning Electron Microscopy (SEM). **Figure 5.11** and **Figure 5.12** show the SEM images of anode and cathode for W and Pt electrodes after few minutes of plasma discharge in water. The duration of the plasma discharge (from 5 to 15 min) has been adapted to the erosion rate observed for each condition (**Figure 5.10**). It is noted that **Figure 5.12** shows the SEM images focused on the tip with orientation and higher magnification than in **Figure 5.11**. These images confirm the results shown in **Figure 5.10**.

The initial shapes of the electrodes are sharp and they became rounded after discharge exposure, except for HV-Pt, GND-W and more slightly for GND-Pt used in case 1 (**Figure 5.11**(a)); as well as for HV-Pt and GND-W used in case 2 (**Figure 5.11**(b)), conditions for which the erosion process is not significant.

The results show the diversity of the surface states according to the polarity and the materials, which confirms that many physical and chemical processes take action on electrodes erosion during pulse discharges in water [234,238,239].

We remind that **case 1** corresponds to cathode initiation of the discharge, which does not span the electrode's gap. Based on previous studies [232,238,239], we can state that for case 1, the dominant process

that causes the electrode erosion is electrochemistry involving anodic electrodissolution (anodic oxidation + electrolyte dissolution). Indeed, the erosion process is only significant for the HV-W electrode, which presents a lower standard potential than platinum (E^0=-0.119 V < E^0=1.2 V) (also presented in **Figure 5.12**(a)). It has been suggested that electrolysis is most predominant before the formation of the conductive channel in the water, but when electrons arrive at the anode, they inhibit the anodic electrodissolution [239].

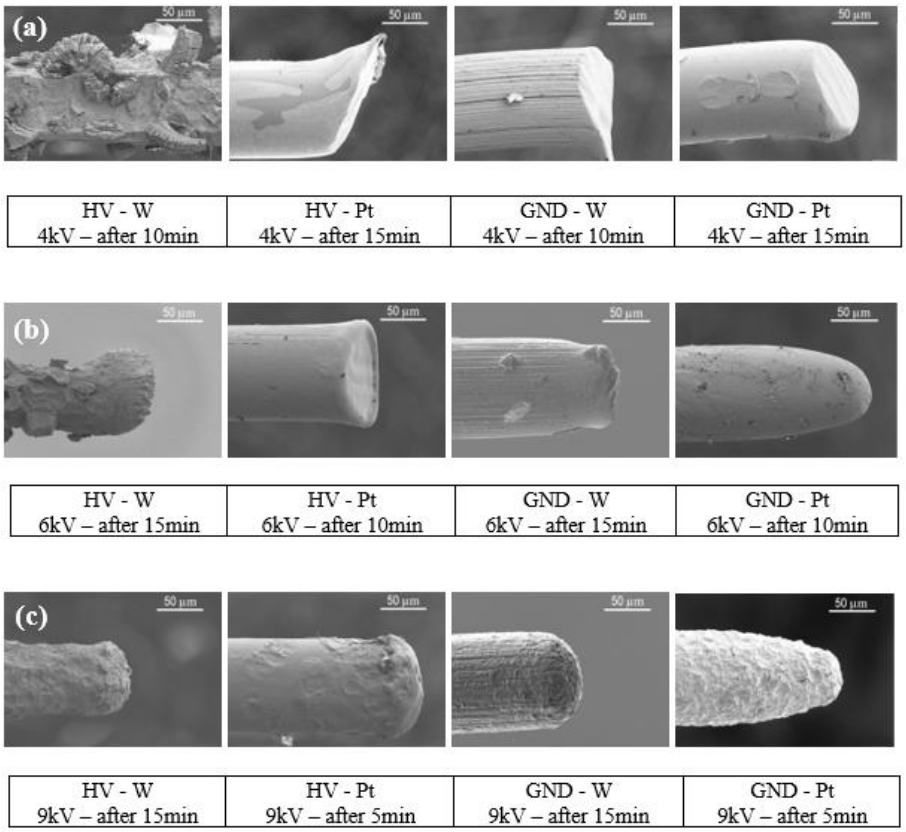

Figure 5.11 SEM images of the eroded tip of tungsten and platinum electrodes after the electrical discharge obtained for (a) case 1 (4 kV), (b) case 2 (6 kV) and (c) case 3 (9 kV), anode and cathode are shown on left and right respectively (V = 150 mL, f = 50 Hz, Δt = 500 µs, 2 mm of gap, and σ = 200 µS/cm) with a ×500 magnification

As a consequence, we observe that for **case 2** (cathode initiation with breakdown), the body of HV-W also shows typical patterns for the electrochemical oxidation process (**Figure 5.11**(b)), *i.e.* the surface is not smooth anymore, whereas the tip of the electrode (**Figure 5.12**(b)), which receives a high electron bombardment through the conductive channel, shows mainly protrusions. On the contrary, the HV-Pt electrode presents a smooth surface. Thermal processes are primarily responsible for erosion due to melting (evaporation can also be considered) followed by condensation. The differences observed on the surface roughness can be explained by the physical properties of tungsten and platinum. Tungsten has much higher thermal conductivity than platinum (164 W/(mK) > 72 W/(mK), leading to a faster solidification of the tungsten surface after melting. As a result, the

molten tungsten part quickly solidifies to produce a thorny structure on the tip of the electrode surface, while a slower solidification of platinum leads to a smoother electrode surface [231,235,239]. Both ground electrodes also show patterns characteristic of thermal processes, but we also report spherical cavities due to ions bombardment.

For **case 3** (**Figure 5.11**(c) and **Figure 5.12**(c)), the energy per pulse is higher, so the electrochemical and bombardment processes are no more significant in comparison to the thermal effect. Surface patterns of the electrodes are quite similar to those observed for case 2, except for GND-Pt, which shows a smooth crater like surface with no more cavities. It is to notice that cracks have been observed on W-electrodes, which can be explained by the fact that at high temperatures, tungsten recrystallizes and becomes brittle [243] (**Figure 5.12**(c)), whereas platinum is known to be fragile. This property can explain the break of the electrode tip reported for HV-W in case 1 and case 2 after 10 and 20 minutes of discharge, respectively.

Finally, we can conclude that the electrodes' erosion depends on the nature of the electrodes, the cases of discharge, and the polarity of the electrodes. We also obtain very different erosion phenomena mechanisms related to electrochemistry, sputtering, evaporation, and melting.

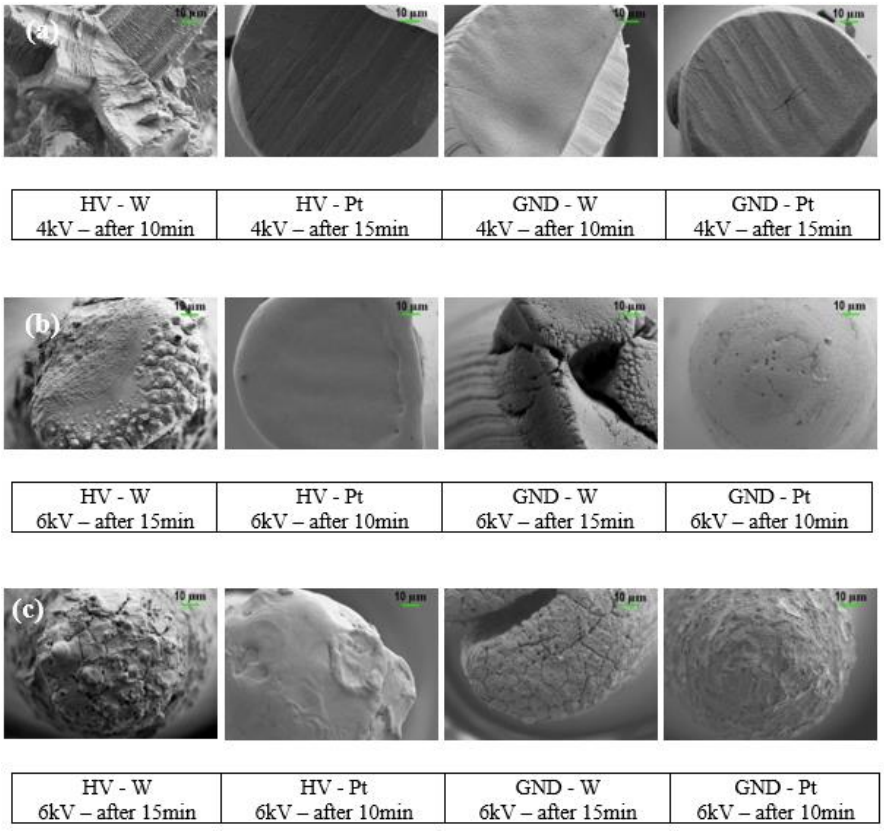

Figure 5.12 SEM images of the eroded tip of tungsten and platinum electrodes after the electrical discharge obtained for (a) case 1 (4 kV), (b) case 2 (6 kV) and (c) case 3 (9 kV), anode and cathode are shown on left and right respectively (V = 150 mL, f = 50 Hz, Δt = 500 µs, 2 mm of gap, and σ = 200 µS/cm) with a ×1000 magnification

5.8 Conclusion

We studied the formation of hydrogen peroxide in water by pin-to-pin microsecond pulsed discharge and measured its concentration using two different methods. First of all, we would like to conclude that the two measurement methods give similar results on the concentration of H_2O_2 formation in the same experimental condition.

We have estimated the concentrations of H_2O_2 for the three different discharge modes of operation for solution of 200 µS/cm: lower than 0,1 mM in case 1 (cathode regime – no breakdown), reaches 0.3 mM for case 2 (cathode regime – breakdown), and 0.8 mM for case 3 (anode regime – breakdown). Besides different mechanisms, the cases also consume different total energies (estimated over 30 minutes of the process): case 1 – 1.1 kJ, case 2 – 2.25 kJ, and case 3 – 4.14 kJ. So we can estimate the energy yield of the process, which is equal to 4.1×10^{-4} g/kJ for case 1, 9.2×10^{-4} g/kJ for case 2, and its 1.3×10^{-3} g/kJ for case 3. We report that the concentration of H_2O_2 changes with both the cases and the energy, the influence of these two parameters being in the same order of magnitude. On the one hand, we have reported that the hydrogen peroxide concentration increases linearly with the total energy. On the other hand, we have shown that for a given energy case 3 produces more H_2O_2 than case 2. Moreover, we have highlighted that the post-discharge plays an important role in case 2 whereas it does not significantly affect the concentration of H_2O_2 in case 3. These results confirm that the two discharge regimes (cathode and anode), which involve very different initiation and propagation mechanisms, lead to different chemical activities.

Moreover, we have demonstrated that the production of H_2O_2 does not depend on the nature of the electrode by comparing tungsten and platinum, the length, and the different size of electrodes. We also noted that the concentration of H_2O_2 does not depend on the electrolyte as NaCl or H_2SO_4 with the same conductivity (4 mS/cm). However, changing the conductivity from 200 µS/cm to 4 mS/cm (adjusted by NaCl) led to a decrease in the concentration of H_2O_2 from 0.68 mM to 0.54 mM. Finally, regarding the strong erosion occurring during the process, we have performed experiments with a combination using W-cathode and Pt-anode that allows improving the process lifetime.

Time evolution of the electrodes' length and SEM images provide new and complementary results in order to study the erosion processes according to the discharge cases, the material, and the polarity of the electrodes. We suggest that for case 1, the dominant process of electrode erosion is electrochemistry (anodic oxidation followed by electrolyte dissolution) which is only significant at the anode. For case 2 and case 3, this process is no more effective, but thermal processes are dominant in the erosion process.

This work contributes to a better understanding of pin-to-pin micro-pulsed discharge in water. H_2O_2 measurements together with the erosion study highlight very different mechanisms involved in the discharge according to the case. Studying H_2O_2 concentration is the first step to studying the complex chemical activities in the solution after plasma discharge. Then this preliminary study is of great interest before working on the Cr(VI) reduction process.

Chapter 6

Reduction of Cr(VI) by PLI

Nowadays, the world has a problem with water pollution [244]. One of the main problems is the presence of heavy metals such as hexavalent chromium. These pollutants originate from the wastewater systems of many industrial facilities[9,14,21] (also presented in **Chapter 2**). Due to pollution and lack of fresh water, the permissible pollutant levels are becoming more stringent. Therefore, there is a need to develop more efficient remediation strategies capable of removing heavy metals from contaminated water even at very low concentrations. From a literature review, some existing methods exist. However, these methods also have disadvantages, as outlined in **Chapter 2**. Therefore, the Plasma Liquid Interaction (PLI) process is used to reduce Cr(VI) contaminants in water as a green and promising technique. The first experiments performed in the frame of this work have rapidly shown, as suggested by the literature, that PLI can reduce significantly Cr(VI) in solution.

As presented previously (**Chapter 2**, **Figure 2.2**) and in agreement with the work of Kachoosangi *et al.*[245], for the initial concentration of Cr(VI) equal to 47 mg/L, and pH =2.4, hydrogen chromate ($HCrO_4^-$), dichromate ($Cr_2O_7^{2-}$), and chromate (CrO_4^{2-}) are the major initial forms of Cr(VI) in our experimental conditions. Moreover, by performing a rough calculation using the software Visual Minteq[246], we confirm these results with as order of magnitude of the following concentrations:

Species	Concentration (mol/L)
$HCrO_4^-$	8.52×10^{-4}
$Cr_2O_7^{-2}$	2.81×10^{-5}
H_2CrO_4 (aq)	2.02×10^{-6}
CrO_4^{-2}	7.82×10^{-8}

Table 6.1 Concentration of Cr(VI) species in the initial solution. Estimated by Visual Minteq[246] software with the initial concentration of Cr(VI) = 47 mg/L (9×10^{-4} mol/L), pH = 2.4.

These species can be reduced in different ways, involving short lived species as solvated electrons (e_{aq}^-) or H^o radical due to the reaction below[3,247]:

$Cr_2O_7^{2-} + 14H^+ + 6e_{aq}^- \rightarrow 2Cr^{3+} + 7H_2O$ $k = 3 \times 10^{10}$ (L mol^{-1} s^{-1}) **Reaction 50**

$HCrO_4^- + 7H^+ + 3e_{aq}^- \rightarrow Cr^{3+} + 4H_2O$ $k = 3 \times 10^{10}$ (L mol^{-1} s^{-1}) **Reaction 51**

$Cr_2O_7^{2-} + 6H^0 + 8H^+ \rightarrow 2Cr^{3+} + 7H_2O$ $k = 2.3 \times 10^{10}$ (L mol^{-1} s^{-1}) **Reaction 52**

$HCrO_4^- + 3H^0 + 4H^+ \rightarrow Cr^{3+} + 4H_2O$ **Reaction 53**

$CrO_4^{2-} + 3H^0 + 5H^+ \rightarrow Cr^{3+} + 4H_2O$ **Reaction 54**

Moreover, Cr(VI) can also be reduced by long-lived species such as H_2O_2. Several studies have been performed on the reduction of Cr(VI) by H_2O_2 in an acidic environment [3,4,190,199,248], as reported in **Chapter 2**. They have shown that in an acidic environment, Cr(VI) can be slowly reduced to Cr(III) by the H_2O_2 produced in PLI by the reactions below[3,199]:

$Cr_2O_7^{2-} + 4H_2O_2 + 2H^+ \rightarrow 2CrO_5 + 5H_2O$ $\quad k = 10^3$ (L mol^{-1} s^{-1}) **Reaction 55**

$2CrO_5 + 6H^+ \rightarrow 2Cr^{3+} + 2H_2O + H_2O_2 + 3O_2$ **Reaction 56**

$2HCrO_4^- + 3H_2O_2 + 8H^+ \rightarrow 2Cr^{3+} + 3O_2 + 8H_2O$ **Reaction 57**

The main purpose of **Chapter 6** is to perform parametric studies on the reduction of Cr(VI) with a focus on the physical parameters of the process in order to optimize and to better understand the reduction. We first present the studies on the influence of electrode configuration on the reduction of Cr(VI). The studies mainly concern the length and diameter of the platinum electrodes. From the analysis of these effects, we determine the most suitable electrode configuration for the treatment of Cr(VI) based on the reduction efficiency and durability of the electrodes. Furthermore, this geometry is chosen for all the studies after.

Then we study the influence of several physical parameters on the reduction of Cr(VI): on the one hand, the applied voltage, the gap between the two electrodes, and the pulse frequency that all involve a change in the injected energy, and on the other hand the pulse duration.

Two parameters are of great interest to reach these objectives because they allow performing comparisons between different experimental conditions. The first one is η (%) the **removal efficiency** of Cr(VI) that is calculated following by **Equation 10**:

$$\eta = \frac{C_0 - C_t}{C_0} \times 100\% \qquad \textbf{Equation 10}$$

where C_0 is the initial concentration of the reactant (g/L); C_t is the concentration of the reactant after a certain reaction time period t (g/L).

The second one is Y (g/kJ), the **energy yield** of the Cr(VI) degradation that is calculated by **Equation 11** [249]:

$$Y(g/kJ) = \frac{C_0 \times V \times \frac{1}{100} \times \eta}{E_{total}} \qquad \textbf{Equation 11}$$

With C_0 is the initial concentration of the solution (g/L), V is the volume of the solution (L), η the removal efficiency (%), E_{total} is the total injected energy (kJ). The energy yield can be converted from g/kJ to g/kWh in order to compare with other works of the literature if necessary (**Chapter 2**).

6.1 Study of electrode geometry (length & diameter)

We note that electrodes geometry is studied to consider the best electrodes pin-to-pin configuration to reduce the Cr(VI) solution. The lengths of both platinum electrodes that are used are 0±10 µm (the electrodes do not show off the capillary), 100±30 µm and 400±30 µm, noted HV-0-GND-0, HV-GND-100, and HV-GND-400 respectively. The electrodes length is measured ex situ by color 3D Laser Microspcoe (VK-9710K) before and after the PLI process. The used diameters are Ø = 100 µm and 200 µm. The experiments are carried out using the same experimental conditions: electrodes gap = 2 mm; applied voltage = 9 kV; Δt = 500 µs; f =50 Hz. The volume of the working solution is 100 mL, with the initial concentration of Cr(VI) equal to 47 mg/L (details in **Chapter 3**). The initial pH of the solution is about 2.3, and the initial conductivity of the solution is 4 mS/cm. The process is carried out for 120 minutes. The [Cr(VI)] measurement is performed every 15 minutes by sampling 2 mL of solution (see **Chapter 3**). The Cr(VI) concentrations are obtained from the measured absorbance of the solution at 350 nm (**Annex 3.1**).

6.1.1 Effect of electrode parameters on Cr(VI) reduction

Representing the time evolution of [Cr(VI)] during PLI, **Figure 6.1** shows the effect of the electrodes length on Cr(VI) reduction for different electrode diameters ((a) 100 µm and (b) 200 µm).

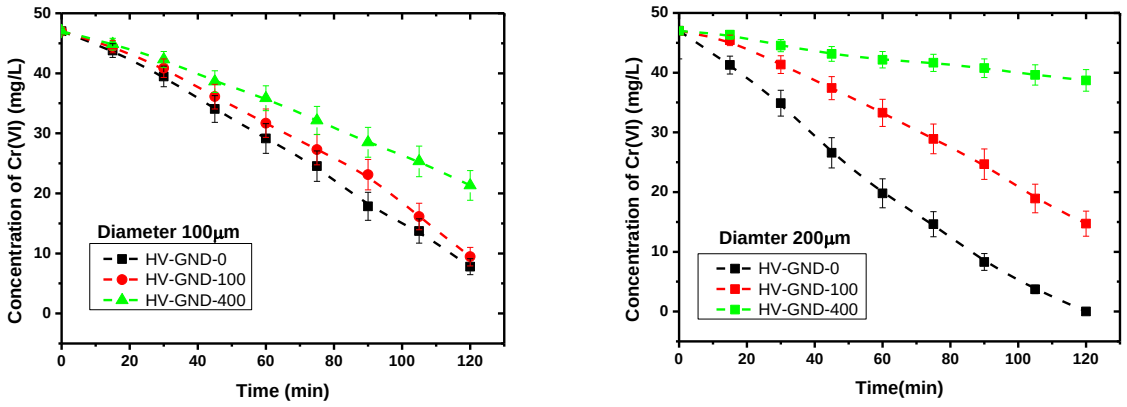

(a) (b)

Figure 6.1 Concentration of Cr(VI) as a function of time for different electrodes lengths (0, 100, 400 µm) and for two diameters (a) Ø = 100 µm and (b) Ø = 200 µm. Cr(VI) solution (47 mg/L,σ=4 mS/cm,pH=2.3), V = 100 mL , U = 9 kV, f = 50 Hz, Δt = 500 µs, gap = 2 mm.

First, it is noted that we obtain a linear behavior in the decrease of [Cr(VI)] with time for all of the conditions, for the given length and diameter of the electrodes. We have a significant effect on the length and diameter of the electrodes on the [Cr(VI)]. For both diameters, it is observed that the shortest the length, the lowest the final concentrations. This result can be discussed regarding the reduction efficiency of Cr(VI) (**Equation 10**).

Table 6.2 shows the reduction efficiency after 120 minutes of the discharge for the different electrodes lengths and diameters. It is observed that the reduction efficiency increases with decreasing the length of the electrodes for a given diameter. For a diameter of 100 µm, the reduction efficiency decreases from 85 % to 80 % and 55 % when the length of the electrodes increases from 0 to 100 and 400 µm, respectively; and for a diameter of 200 µm, the reduction rate decreases from 100 % to 70 % and 16 % when the length of the electrodes increases from 0 to 100 and 400 µm, respectively.

Length(µm) / Diameter(µm)	**HV-GND-0**	**HV-GND-100**	**HV-GND-400**
Ø = 100 µm	85 %	80 %	55 %
Ø = 200 µm	100 %	70 %	16 %

Table 6.2 Reduction efficiency after 120 minutes for the discharge with different electrodes lengths and diameters. Cr(VI) solution (47 mg/L, σ=4 mS/cm, pH=2.3), V = 100 mL , U = 9 kV, f = 50 Hz, Δt = 500 µs, gap = 2 mm.

From **Figure 6.1** and **Table 6.2**, we also note that the influence of the diameter depends on the length of the electrodes:

- For the condition HV-GND-0: the reduction of Cr(VI) with the Ø = 200 µm (100 %) is better than for the Ø = 100 µm (85 %).
- For the condition HV-GND-100: On the opposite, the reduction of Cr(VI) is slightly better for the low diameter. The reduction rate is 70 % for the discharge with the Ø = 200 µm in comparison with 80 % for the discharge with the Ø = 100 µm.
- For the condition HV-GND-400, we obtain a considerable difference in the reduction efficiency for the different diameters. The reduction of Cr(VI) is only 16 % when the discharge is performed with the Ø = 200 µm, while it is 55 % for the discharge with the Ø = 100 µm.

We can conclude that the surface of the electrodes in contact with the solution has an influence on the reduction process. Based on the study of Ceccato *et al.* [243], the surface of the electrodes can be important for the discharge initiation. This surface presents some oxide layer due to the heating by the passing current that introduces defects modifying the initial conditions of the discharge. These variations can also be related to variations in the electrical signals and then into the injected energy or the number of BK.

6.1.2 Effect of electrode parameters on the distribution of BK/NOBK

The different kinds of discharge obtained (BK and NOBK as defined in **section 4.2**) are monitored during the duration of the experiments (as presented in **Figure 6.2** for HV-GND-0), as well as the injected energy per pulse (discussed in **section 6.1.3**). Indeed we expect that this information are helpful to better understand the chemical processes [175,202].

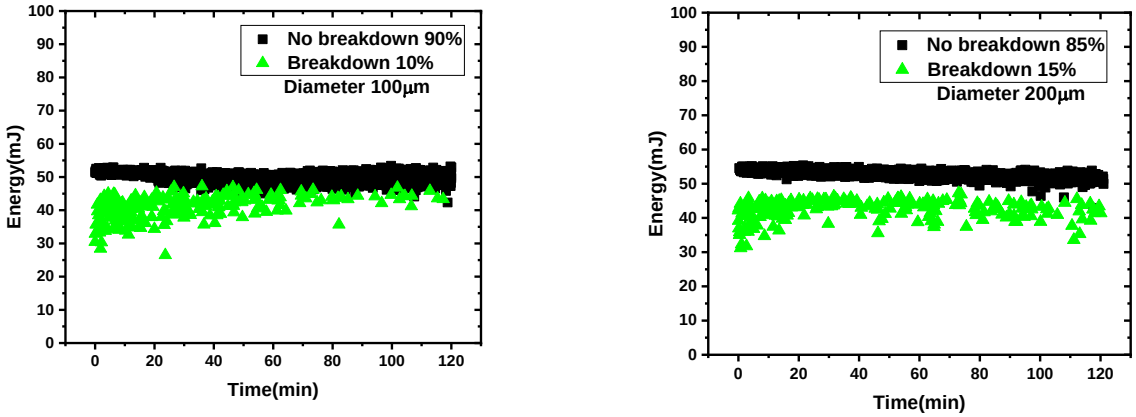

(a) (b)

Figure 6.2 Time evolution of injected energy per pulse for the HV-0, GND-0, (a) Ø = 100 µm and (b) Ø = 200 µm. Cr(VI) solution (47 mg/L,σ=4 mS/cm,pH=2.3), V = 100 mL , U = 9 kV, f = 50 Hz, Δt = 500 µs, gap = 2 mm.

The average distribution of BK and NOBK during one experiment is estimated, and the ratio is calculated for all the conditions (**Table 6.3**). We observe that the variation of BK/NOBK is low. Especially for the diameter of 100 µm, the BK/NOBK ratio is 10/90 when discharge is performed with HV-GND-0; this value decreases to 6/94 and 4/96 when the discharge is performed with HV-GND-100, and HV-GND-400, respectively. In comparison, we obtain more significant variations in the number of BK/NOBK with a diameter of 200 µm. The ratio of 15/95 for the BK/NOBK is obtained when the discharge is carried out with HV-GND-0, while it is 9/91 and 0/100 when the electrodes' length is increased to 100 and 400 µm, respectively.

We can generalize the results by writing that the lower the length, the higher the number of BK. This can be explained by the higher electric field or the lower heating surface process in favor of discharge [161,243].

Length(µm) / Diameter(µm)	**HV-GND-0**	**HV-GND-100**	**HV-GND-400**
Ø = 100 µm	10 / 90	6 / 94	4 / 96
Ø = 200 µm	15 / 85	9 / 91	- / 100

Table 6.3 Ratio of BK/ NOBK after 120 minutes for the discharge with different lengths and diameters of the electrodes. Cr(VI) solution (47 mg/L,σ=4 mS/cm,pH=2.3). V = 100 mL , U = 9 kV, f = 50 Hz, Δt = 500 µs, gap = 2 mm

A relation between **Table 6.2** and **Table 6.3** would suggest that the highest number of breakdowns give the best reduction. However, this conclusion is not reasonable due to the change of many parameters. The influence of the BK will be discussed explicitly in **section 6.2**.

Figure 6.2 also shows the BK/NOBK distribution along with the experiments, and we observe that the BK/NOBK distribution changes with time: the number of BK decreases during the process. This variation does not depend on the electrode diameter. For example, for HV-GND-0 with a diameter of

100 µm, we obtain a value of 40 % of BK during the first 20 minutes, while it decreases to 2 % in the last 20 minutes. In comparison, for HV-GND-0 with a diameter of 200 µm, we obtain 38 % of BK during the first 20 minutes, and it decreases to 10 % in the last 20 minutes. The variation in the number of BK/NOBK and the energy of BK discharge could be explained by the modification of the length of the electrodes that decrease due to the erosion process [202].

Observations performed at the end of the experiments show that for a diameter of 100 µm, the electrodes are much more damaged (eroded) than 200 µm (as shown in **Table 6.4**).

Length(µm) / Diameter(µm)	**HV-GND-100**	**HV-GND-400**
Ø = 100 µm	100 / 100	100 / 100
Ø = 200 µm	10 / 100	1 / 1

Table 6.4 Part of the electrodes HV/GND eroded after 120 minutes (in %) for the discharge with different lengths and diameters of the electrodes. Cr(VI) solution (47 mg/L,σ=4 mS/cm,pH=2.3), V = 100 mL , U = 9 kV, f = 50 Hz, Δt = 500 µs, gap = 2 mm

For example, for HV-GND-400, both electrodes totally disappear (100% of erosion) for Ø = 100 µm, whereas the erosion is low (1%) for Ø = 200 µm. When the electrodes are eroded, the interelectrode gap increases, and thus, the electric field decreases that involving less breakdown phenomena. Considering the Cr(VI) reduction, this erosion of electrodes seems insignificant since we do not observe a change in the time evolution: **Figure 6.1** shows that the behavior is linear all along the process for all conditions.

6.1.3 Effect of electrode parameters on the injected energy

The injected energy per pulse is estimated by $\int U.I.dt$ as detailed in **Chapter 2**, and it is monitored during the duration of the experiments (as presented in **Figure 6.2**).

We remind that the injected energy depends on the breakdown phenomena (the energy per pulse is about 20 % lower for BK than those of NOBK). As an example, **Figure 6.2** shows the measurements performed for the condition of HV-GND-0. As for BK/NOBK distribution, we observe that the energy per pulse changes slightly with time due to the electrode erosion (more details in **section 6.2.2**).

The average injected energy per pulse equals about 40 mJ for BK and 50 mJ for NOBK, for both diameters. It is noted that these energies per pulse for BK and NOBK are similar for all the conditions (diameters and lengths). Then this parameter is not responsible for the variation of the Cr(VI) reduction efficiency.

For all conditions, we calculate the total injected energy (**Equation 3 in Chapter 3**) using the energy per pulse and the distribution BK/NOBK (**Table 6.3**). We obtain the total injected energy between 17.6 and 19.8 kJ after 120 minutes, as shown in **Table 6.5**.

	Length / Diameter	**HV-GND-0**	**HV-GND-100**	**HV-GND-400**
Average injected energy per pulse BK / NOBK (mJ)	**Ø = 100 µm**	42/52	41/52	41/52
Total energy (kJ)		18.4 kJ	18.5 kJ	18.7 kJ
Average injected energy per pulse BK / NOBK (mJ)	**Ø = 200 µm**	42/54	42/54	0/55
Total energy (kJ)		18.8 kJ	19.1 kJ	19.8 kJ

Table 6.5 The total injected enery after 120 minutes for the discharge with different lengths and diameters of the electrodes. Cr(VI) solution (47 mg/L,σ=4 mS/cm,pH=2.3). V = 100 mL, U = 9 kV, f = 50 Hz, Δt = 500 µs, gap = 2 mm

We obtain that the variation of the total energy with the difference in length and diameter is low, about 7 %. This variation can be explained by either the uncertainty or the variation in the number of BK/NOBK. As previously, the variation of the total injected energy does not explain the variation of the reduction efficiency. This result is confirmed by the energy yield that changes with the length and the diameter of the electrodes (**Table 6.6**). As presented previously, the surfaces of the electrodes present some oxide layer due to the heating. Thus these results confirm that a part of the energy is lost (by Joule effect) and not directly used for Cr(VI) reduction since the energy yield decreases when the surface increases.

Considering the energy yield (**Table 6.6**), HV-GND-0 with 200 µm diameter of the electrode is the best configuration, giving the highest energy yield value (2.5×10^{-4} g/kJ). This configuration appears to be the most interesting one.

Length(µm) / Diameter(µm)	**HV-GND-0**	**HV-GND-100**	**HV-GND-400**
Ø = 100 µm	2.2×10^{-4}	2.1×10^{-4}	1.4×10^{-4}
Ø = 200 µm	2.5×10^{-4}	1.7×10^{-4}	0.38×10^{-4}

Table 6.6 Energy yield in g/kJ after 120 minutes for the discharge with different lengths and diameters of the electrodes. Cr(VI) solution (47 mg/L,σ=4 mS/cm,pH=2.3), V = 100 mL , U = 9 kV, f = 50 Hz, Δt = 500 µs, gap = 2 mm

6.1.4 Effect of electrode parameters on the chemical properties

All these variations have an influence on the chemical properties of the solution. **Table 6.7** shows the variation of the pH and conductivity of solution after 120 minutes of the process for different lengths and diameters of the electrodes. It is noted that a slight variation of the pH solution is observed at the end of the process according to the length and diameter of the electrodes $(pH_{ini} \approx 2.3 \; and \; pH_{fin} \approx 2.4)$. We also obtain a significant change in conductivity according to the lengths and diameters of the electrodes. The decrease in conductivity is more evident when the discharge is performed with a short length of electrodes for a given diameter:

- For the Ø = 100 µm: a decrease in conductivity of about 22 % after 120 minutes is obtained for the discharge with HV-GND-0 and HV-GND-100 (from 4.02 and 4.05 mS/cm to 3.15 and 3.16 mS/cm, respectively). In comparison, the decrease is only about 13 % (from 4.02 to 3.49 mS/cm) when the discharge is performed with a length of the electrode of 400 µm.
- For the Ø = 200 µm: a decrease in conductivity of about 24 % after 120 minutes for the discharge with HV-GND-0 (from 4.02 to 3.08 mS/cm), while it is 19 % with the discharge of HV-GND-100 and only 6% when the length of the electrodes increases to 400 µm.

It is also interesting to compare variations in the conductivity for the same length with different diameters of the electrode. We note that there is no huge influence of the diameter on the conductivity variation. For example, the decrease in the conductivity when discharging with HV-GND-0 at a diameter of 200 µm is 24 % compared to 22 % when discharging with a diameter of 100 µm.
The explanation for the variation of pH and conductivity are discussed in part **6.2.1.**

Diameter	Length	pH		Conductivity (mS/cm)	
		Initial	Final	Initial	Final
Ø = 100 µm	HV-GND-0	2.3	2.4	4.02	3.15
	HV-GND-100	2.4	2.4	4.05	3.16
	HV-GND-400	2.3	2.5	4.02	3.49
Ø = 200 µm	HV-GND-0	2.3	2.4	4.02	3.08
	HV-GND-100	2.3	2.4	4.03	3.26
	HV-GND-400	2.3	2.4	4.02	3.77

Table 6.7 Initial and final (after 120 minutes) solution parameters obtained from ex situ pH and conductivity measurements for 9 kV with different lengths and diameters. Cr(VI) solution (47 mg/L,σ=4 mS/cm,pH=2.3), V = 100 mL, f = 50 Hz, Δt = 500 µs, gap = 2 mm

6.1.5 Conclusion

In conclusion, the length and diameter of the electrodes have a significant influence on the reduction of Cr(VI) by PLI.

We observe the evolution of the discharge characteristics with time (BK/NOBK and BK energy), but the Cr(VI) reduction looks linear with time. Thus, we can first conclude that these evolutions do not directly influence the reduction of Cr(VI) by PLI.

Due to the highest efficiency and stability of the electrodes, we would like to conclude that **the geometry HV-GND-0 with a diameter of 200 µm is the best condition for the reduction of Cr(VI)** by PLI. Consequently, this geometry is used for all the following works of this chapter, and this experimental condition can be considered a reference (**Table 6.8**).

Reduction efficiency	Total injected energy (kJ)	BK/NO BK (%)	Energy yield (g/kJ)	pH		Conductivity (mS/cm)	
				Initial	Final	Initial	Final
100%	18.8	15/85	2.5×10^{-4}	2.3	2.4	4.02	3.08

Table 6.8 Characteristics of the experiments Ø = 200 µm - HV-0 - GND-0 after 120 minutes Cr(VI) solution (47 mg/L,σ=4 mS/cm,pH=2.3), V = 100 mL , U = 9 kV, f = 50 Hz, Δt = 500 µs, gap = 2 mm

Now that we have identified the best electrode parameters, we aim to optimize the PLI process by changing other experimental parameters. The following section presents the influence of injected energy on Cr(VI) reduction by changing the applied voltage, the gap between two electrodes, and the applied frequency.

6.2 Influence of injected energy

Injected energy is one of the most important parameters when evaluating the efficiency of the reduction process. In this section, several parameters have been changed to study the effect of the injected energy on the reduction of Cr(VI) by PLI. The first parameter is the applied voltage; after that, we present the effect of the gap between two electrodes and finally, the applied frequency effect.
The conditions used for this section are: the length of both platinum electrodes equal to HV-GND-0 with a diameter of 200 µm; Δt = 500 µs. The volume of the working solution is 100 mL, with the initial concentration of Cr(VI) equal to 47 mg/L (**Chapter 3**). The initial pH of the solution is about 2.3, and the conductivity of the solution is about 4 mS/cm. The measurement is performed every 15 minutes by sampling 2 mL of solution (see **Chapter 3**). The Cr(VI) concentrations are obtained from the measured absorbance of the solution at 350 nm (**annex 3.1**).

6.2.1 Effect of the applied voltage

Changing the applied voltage is one parameter that directly affects the injected energy. This section presents the effect of voltage for two different electrode gaps, which are 2 mm and 5 mm. By changing the gap, we are able to study the effect of two different discharge regimes, BK and NOBK, as presented in **Chapter 4**.

a. Influence of the applied voltage on Cr(VI) reduction for 2 mm gap

In this section, the applied voltage is changed from 2 kV to 12 kV. The discharge is performed with the frequency = 50 Hz. **Figure 6.3** shows the variations of the Cr(VI) concentration with the treatment time. We note that for 2 kV, no discharge is observed, only an electrochemical effect occurs, and there is no change in the concentration of Cr(VI) after 120 minutes. So it is not interesting to include this result in the discussion later.
We obtain that for all conditions, the **Cr(VI) reduction** follows a linear tendency, and increasing the applied voltage leads to an increase in the reduction efficiency (**Figure 6.3**). After 120 minutes for 7 kV, we obtain only about 54 % of the reduction of Cr(V), while at an applied voltage of 9 kV, it is possible to reduce 100 % of Cr(VI) **(Table 6.9**). In comparison, at 10 kV, a total Cr(VI) reduction is achieved after 105 minutes, and at 11 kV, the total reduction of Cr(VI) is obtained after 90 minutes and becomes faster at 70 minutes when the applied voltage increases to 12 kV.

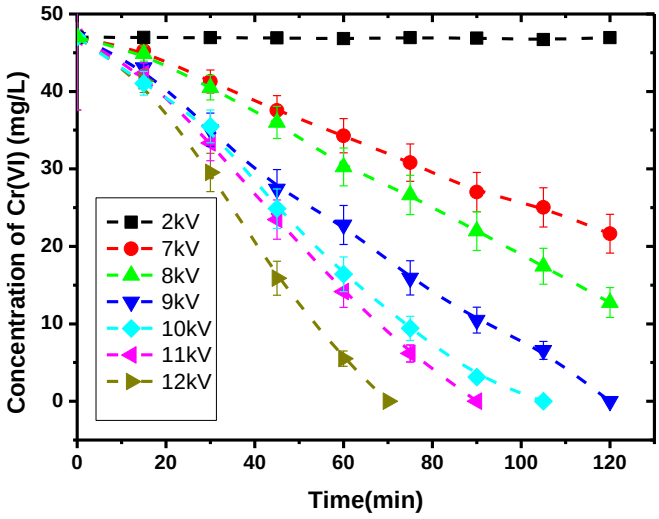

Figure 6.3 Concentration of Cr(VI) as a function of time of a pin-to-pin discharge obtained in Cr(VI) solution (47 mg/L,σ=4 mS/cm,pH=2.3) for 2, 7, 9, 10, 11 and 12 kV, V = 100 mL, Δt = 500 µs, gap = 2 mm, electrodes length = 0±10 µm, f = 50 Hz.

As shown previously, we monitor the energy per pulse and the nature of the discharge (BK or NOBK) for all the experiments (**Figure 6.4**).

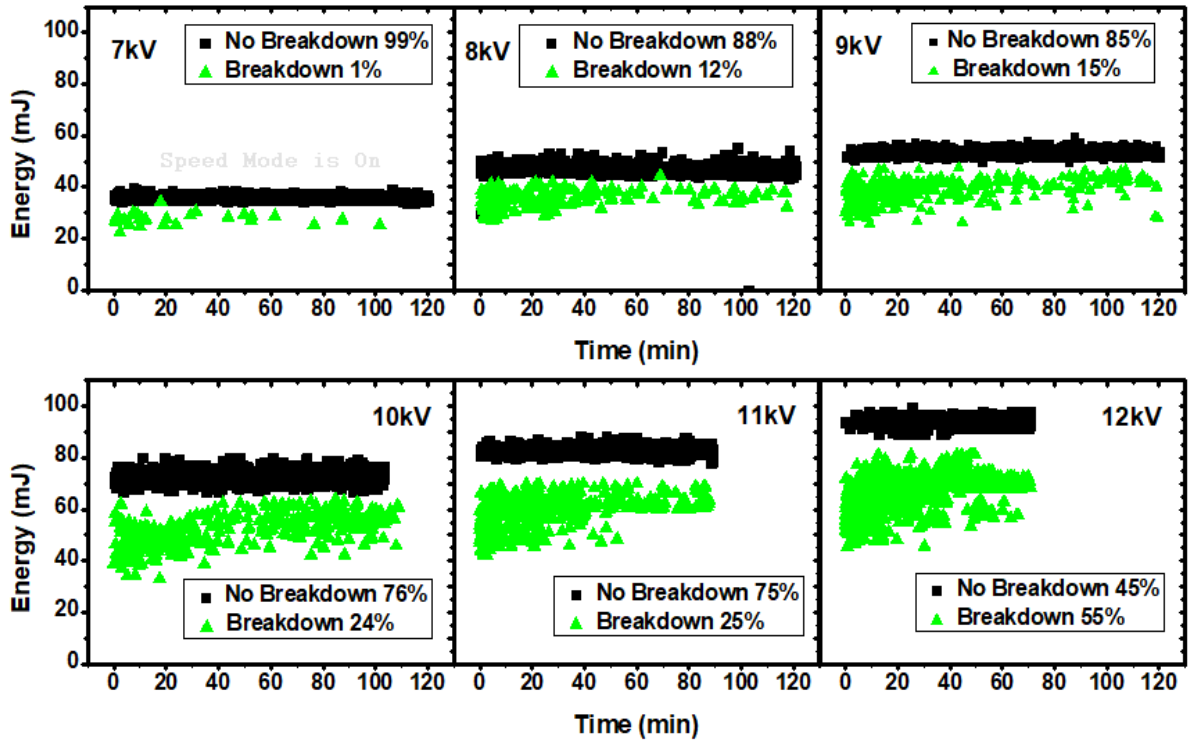

Figure 6.4 Time evolution of the injected energy per pulse for the different applied voltage from 7 kV to 12 kV. Cr(VI) solution (47 mg/L,σ=4 mS/cm,pH=2.3), V = 100 mL, Δt = 500 µs, gap = 2 mm, electrodes length = 0±10 µm, f = 50 Hz

We observe that the increase of the applied voltage changes the **number of breakdowns** during the experiment: only 1 % of BK is obtained for the discharge at 7 kV, and it is increased to about 55 % for the discharge at 12 kV (**Figure 6.4 and reported in Table 6.9)**. This result is to be expected because increasing the applied voltage leads to an increase in the electric field at the tip of the electrodes. The increase of the applied voltage is also reported to increase the propagation velocity of the filamentary structure [175,243]. As expected, since the injected energy per pulse depends on the applied voltage (**Equation 2** of **Chapter 3**), it increases with the applied voltage for both BK and NOBK discharges, as shown in **Figure 6.4**. For example, the average energies per pulse for BK/ NOBK at 9 kV is about 38/53 mJ, while these values are 66/95 mJ when the discharge is performed at 12 kV (**Table 6.9** and **Figure 6.4**).

We also note that the standard deviation of the energy per pulse for NOBK discharge is below 10 % for a given applied voltage. However, the standard deviation of the energy per pulse for BK discharge increases with increasing the applied voltage. For example, the variation in energy per pulse for discharge at 9 kV is about 30 %, while at 12 kV, it is 45 %. This variation can be explained by the influence of the applied voltage on the breakdown duration[175,176]. For high conductivity, a low applied voltage involves mainly a long breakdown duration, whereas a high applied voltage can involve faster breakdown phenomena. Considering the random nature of the breakdown, this leads to a higher variation in the energy per pulse that is calculated by using $\int U.I.dt$.

Applied voltage (kV)	**2 kV**	**7 kV**	**8 kV**	**9 kV**	**10 kV**	**11 kV**	**12 kV**
Reduction efficiency	0 %	54 %	73 %	100 %	100 %	100 %	100 %
Number of BK/NOBK (%)	0 / 100	1 / 99	12 / 88	15 / 85	24 / 76	25 / 75	55 / 45
Average injected energy per pulse BK / NOBK (mJ)	- / 3.4	28 / 36	36 / 47	42 / 54	51 / 73	59 / 83	66 / 95
Total injected Energy (kJ)	1.2	13	16.7	18.8	21.3*,1	20.7*,2	16.7*,3
Energy yield (g/kJ)	0	2.0×10^{-4}	2.1×10^{-4}	2.5×10^{-4}	2.2×10^{-4}	2.3×10^{-4}	2.8×10^{-4}

Table 6.9 Influence of applied voltage on Cr(VI) reduction efficiency and the discharge characteristics. Cr(VI) solution (47 mg/L,σ=4 mS/cm,pH=2.3), V = 100 mL, Δt = 500 µs, gap = 2 mm, electrodes length = 0±10 µm, f = 50 Hz. * these values are calculated with different durations (1:105 min, 2:90 min, and 3: 70 min)

It is noted that increasing the applied voltage leads to an increase in the **total injected energy**, when considering the same duration (from 7 to 9 kV). However, when all the results are considered, the total injected energy changes non-monotonously (**Table 6.9**) since it increases from 13 kJ at 7 kV up

to 21.3 kJ at 10kV and then decreases to 16.7 kJ when the discharge is performed at 12 kV. This is due to the difference in the process duration, for example, we obtain the total reduction of Cr(VI) after 70 minutes for discharge at 12 kV.

It is noted that the duration related to the total reduction of Cr(VI) depends on the sampling rate that is equal to 15 minutes. Consequently, the total duration can be overestimated, as the total injected energy necessary to completely reduce the Cr(VI). As an example, the trend of the curve obtained for 10 kV (**Figure 6.3**) suggests that the total reduction is obtained before 105 minutes. Then in order to better evaluate the process, it is necessary to identify the exact duration for the complete reduction of Cr(VI). For that, a new experimental approach is proposed and discussed in **annex 6.3** [c].

We obtain that the applied voltages of 8 kV and 12 kV result in a similar total injected energy of 16.7 kJ whereas the results of reduction efficiency are different (73 % compared with 100 %, respectively), so the energy yield is one of the interesting parameters necessary to evaluate the reduction efficiency.

We calculate the **energy yield** for each condition, as shown in **Table 6.9**. We obtain an increase in the energy yield from 2.0×10^{-4} g/kJ to 2.5×10^{-4} g/kJ when the applied voltage increases from 7 kV to 9 kV. Then, from 9 to 11 kV, the energy yield is quite constant (around 2.4×10^{-4} g/kJ). This result can be explained by the uncertainty on the total injected energy (total duration), as discussed previously. Finally, we obtain the highest value of energy yield (2.8×10^{-4} g/kJ) when discharging at 12 kV. This variation at 12 kV can be explained by the fact that even if the injected energy per pulse is higher than at 10 and 11 kV, the duration of the process is much faster, as we have shown before. This reduces the total injected energy, which is an important parameter for calculating the energy yield. The variation of the energy yield with the applied voltage shows that the injected energy is not the only parameter that has an influence on the Cr(VI) reduction.

Table 6.10 shows the **pH and the conductivity** of the solution before and after plasma discharge for the different applied voltages.

At the end of the process, we observe a slight change in the pH from 2.3 to 2.4 for the almost applied voltage. This increase can be explained by the consumption of hydronium ions to reduce Cr(VI), as presented by **reactions 50-57**. This hypothesis can also be obtained from the studies of Wang *et al*[3]. and they have shown that the pH of the solution increase from 2 to 2.2 at the end of the process when the discharge is performed in Cr(VI) solution.

On the other hand, we obtain a significant change in the **solution conductivity** at the end of the process regarding the increase in the input voltage. The conductivity decreases more with increasing

[c] *This in situ technique, also based on absorption spectroscopy, is of great interest to reduce the uncertainties of the measurements. The obtained results are of great interest but they are not included in this chapter since the technique has been developed at the end of this work.*

the applied voltage, and the variation is not linear. For example, we obtain a decrease of about 10 % (from 4.01 mS/cm to 3.57 mS/cm) at the end of the process with 7 kV, while it decreases of about 23 % (from 4.01 mS/cm to 3.08 mS/cm) for 9 kV and about 25 % (from 4.01 mS/cm to 2.98 mS/cm) with the applied voltage of 12 kV. As discussed previously, the hydronium ions are consumed to reduce Cr(VI) to Cr(III) can be because during the treatment process. Moreover, the mobility of Cr(III) ions is much lower than hydronium ions, which leads to decreased conductivity of the solution[3]. However, in our conditions as presented previously (**Table 6.10),** we note that the pH before and after the process are not shown a huge variation, thus meaning that the hydronium ions are more or less constant. Thus the hypothesis of Wang and Chandana are not enough to explain our phenomena. The increase of the applied voltage significantly changes the composition of the solution, leading to an increase in the production rate of reactive species [189,202,227,228,231] such as H_2O_2, OH^-, O_2. Thomas *et al.* [250] have reported that increasing the concentration of H_2O_2 in an acidic medium (such as H_2SO_4) leads to a decrease in the conductivity of the solution.

Therefore, we have determined that these phenomena are exciting and should be elucidated by analyzing the species that form in Cr(VI) solution, such as H_2O_2, and it will be discussed in **Chapter 7**.

Another possibility to explain the decrease in conductivity is due to the reaction of Cr(III) with sulfate ions (SO_4^{2-}). Fogel *et al*[251]. have reported that Cr(III) can react with sulfate ions in an acidic environment to form a kind of Cr(III)-sulfate. Moreover, in our conditions, the dominant ionic species are Cr(VI), H^+, and SO_4^{2-}; thus, Cr(III) produced by the reduction of Cr(VI) and sulfate ion can react together after the reduction. We have also noticed blue-black precipitates appearing at the bottom of the reactor after the treatment, which is one characteristic of Cr(III)-sulfate. However, this hypothesis requires further analysis, such as the EDX method, to better identify the complex precipitates characteristics.

We first note that the more reduction of Cr(VI) leads to more decrease of the conductivity, as presented in **Table 6.9** and **Table 6.10**

Applied voltage	pH		Conductivity (mS/cm)	
	Initial	Final	Initial	Final
2 kV	2.3	2.4	4.08	4.01
7 kV	2.3	2.4	4.01	3.57
8 kV	2.4	2.4	4.01	3.43
9 kV	2.3	2.4	4.01	3.08
10 kV	2.4	2.4	4.01	3.03
11 kV	2.3	2.4	4.01	3.01
12 kV	2.3	2.4	4.01	2.98

Table 6.10 Initial and final solution parameters obtained from ex situ pH and conductivity measurements for the different applied voltages. Cr(VI) solution (47 mg/L,σ=4 mS/cm, pH = 2.3-2.4),. V = 100 mL, ∆t = 500 µs, gap = 2 mm, electrodes length = 0±10 µm, f = 50 Hz

In summary, increasing the applied voltage increases the reduction efficiency of Cr(VI), the energy per pulse, and the number of BK. Moreover, increasing the applied voltage leads to more decrease the conductivity of the solution. As already observed in **Chapter 5** regarding the production of H_2O_2 in water, the chemical activity induced by PLI involves intricate and interdependent phenomena. All these results show that the reduction of Cr(VI) does not only depend on the total energy injected in the solution by the discharge, and the breakdown phenomena may also play an important role.

From **Table 6.9** and **Figure 6.3**, we can conclude that 9 kV and 12 kV are the best applied voltages to reduce Cr(VI) by PLI based on the successful reduction time and energy consumption. However, observations performed at the end of the experiments highlight that the increase of the applied voltage also damages the electrodes. Thus, **an input voltage of 9 kV is the most suitable condition**, fulfilling both criteria: complete reduction of Cr(VI) and reduced damage of material.

Nevertheless, as described previously, increasing the applied voltage leads to increasing both energy injected and the number of BK. So it is not possible to discriminate the cause of the reduction efficiency increase between the energy per pulse and the number of breakdowns. That is why we define a condition for which we can manage the number of (no) breakdowns to only study the influence of injected energy. As presented in **Chapter 3**, we do not observe any BK when increasing the gap between two electrodes to 5 mm. Thus, the next section presents the influence of applied voltage on Cr(VI) reduction performed with the 5 mm gap between the two electrodes.

b. Influence of the applied voltage on Cr(VI) reduction for 5 mm gap

We remind that this section is performed in the case of only NOBK discharge, and the voltage is changed from 7 kV to 10 kV. We note that the applied voltages of 11 and 12 kV are not attractive because of the electrodes' damage and the limitation of the equipment. The discharge is performed with the frequency = 50 Hz.

We observe in Figure 6.5, as for the gap of 2 mm, a linear time evolution of [Cr(VI)] and that the reduction increases when the applied voltage increases. As a consequence, the reduction rate also increases, from 50% for 7 kV to 100% for 10 kV.

It is noted that the injected energy per pulse also increases with the increase of the applied voltage, from 40 mJ for 7 kV to 71 mJ for 10 kV (**Figure 6.6**). As a consequence, we can conclude that the reduction rate increases from 50 % to 100 % when the average injected energy per pulse increases from 40 to 71 mJ (corresponding with the increase of the applied voltage from 7 kV to 10 kV), as shown in **Table 6.11**. These experiments confirm that the reduction of Cr(VI) is the best when the energy per pulse is the highest.

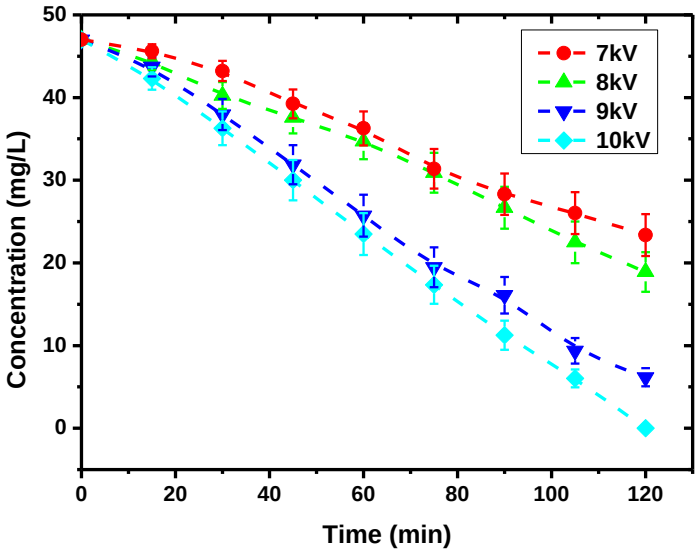

Figure 6.5 Concentration of Cr(VI) as a function of time of a pin-to-pin discharge obtained in Cr(VI) solution (47mg/L, σ=4 mS/cm,pH=2.4) for 7, 8, 9, and 10 kV respectively, V = 100 mL,Δt = 500 µs, gap = 2 mm, electrodes length = 0±10 µm, f = 50 Hz.

We note that the increase of the applied voltage from 7 to 10 kV also corresponds to the increase of the total injected energy: from 14.4 to 25.5 kJ (**Table 6.11**). We obtain the increase in the energy yield from 1.6×10^{-4} to 2×10^{-4} g/kJ when the applied voltage increases from 7 to 9 kV. However, when the voltage increases to 10 kV, the energy yield slightly decreases to 1.8×10^{-4} g/kJ. This decrease is due to an increase in the injected energy of about 23% from 56 mJ to 71 mJ, while the difference in the reduction efficiency is only 13 % for the same 120 minutes. This result has to be analyzed with caution considering the uncertainty on the total injected energy (duration of the total reduction).

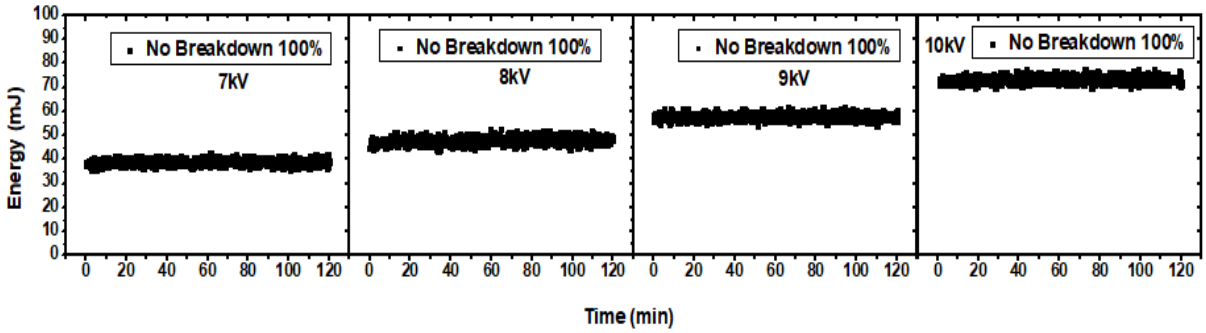

Figure 6.6 Time evolution of the injected energy per pulse for the different applied voltages from 7 kV to 10 kV. Cr(VI) solution (47 mg/L,σ=4 mS/cm,pH=2.3-2.4), V = 100 mL, Δt = 500 µs, gap = 5 mm, electrodes length = 0±10 µm, f = 50 Hz

As already noted for 2 mm, the variation of the energy yield shows that the Cr(VI) reduction does not only depend on the total injected energy. As expected, we can highlight that the total injected energy is not the only parameter that influences the reduction rate. The increase of the applied voltage involves other physical and chemical mechanisms that play a role in Cr(VI) reduction.

Applied voltage (kV)	**7kV**	**8kV**	**9kV**	**10kV**
Reduction efficiency	50%	60%	87%	100%
Average energy per pulse (mJ)	40	46	56	71
Total Energy (kJ)	14.4	16.6	20.2	25.5
Energy yield (g/kJ)	1.6×10^{-4}	1.7×10^{-4}	2×10^{-4}	1.8×10^{-4}

Table 6.11 Influence of applied voltage on Cr(VI) reduction efficiency and the discharge characteristic after 120 minutes. Cr(VI) solution (47 mg/L,σ=4 mS/cm,pH=2.4), V = 100 mL, Δt = 500 µs, gap = 5 mm, electrodes length = 0±10 µm, f = 50 Hz

Table 6.12 shows the **pH and the conductivity** of the solution before and after plasma discharge for the different applied voltages with 5 mm of the gap. We do not observe a significant change in the pH for a given applied voltage. Similar to the results presented in **section a,** we also obtain the change in conductivity at the end of the process, and the final conductivity decreases more when the applied voltage (the reduction efficiency) is increased. For example, the decrease is about 6 % (from 4.06 to 3.83 mS/cm) for the discharge at 7 kV, while it is about 13 % (from 4.05 to 3.52 mS/cm) when the discharge is performed at 10 kV.

Applied voltage	pH		Conductivity (mS/cm)	
	Initial	Final	Initial	Final
7 kV	2.4	2.4	4.06	3.83
8 kV	2.4	2.4	4.05	3.76
9 kV	2.4	2.4	4.05	3.57
10 kV	2.4	2.4	4.05	3.52

Table 6.12 Initial and final solution parameters obtained from ex situ pH and conductivity measurements for the different applied voltages. Cr(VI) solution (47 mg/L,σ=4 mS/cm,pH=2.4) V = 100 mL, f = 50 Hz, Δt = 500 µs, for 5 mm of gap.

c. Conclusion

In summary, we note that the applied voltage has an effect on the reduction rate: the highest the applied voltage, the highest the reduction efficiency. For both gaps we observe that the increase of the reduction efficiency is related to the increase of the injected energy per pulse. The decrease of the conductivity can be explained by the production of H_2O_2 and the consumption of Cr(III) ions and sulfate ions.

However, increasing the injected energy by increasing the applied voltage leads to changes in the discharge characteristics, especially at 2 mm gap with the increase in the number of breakdowns. It is not very easy to distinguish the influence of each effect because they are interconnected.

Finally, we can conclude that the highest applied voltage is not the best condition regarding the electrode's lifetime and energy yield**. Indeed 9 kV provides the suitable condition, including the high energy yield and a long lifetimes of the electrodes for both gaps** (2.5×10^{-4}g/kJ and 2×10^{-4}g/kJ for 2 and 5 mm gap, respectively).

We also perceive that the gap plays a role in the Cr(VI) reduction through this study. We remembered that a change in the gap results in a change in the electric field, leading to variation in the breakdown properties. Therefore, in the next section, we study especially the effect of the gap on the reduction of Cr(VI) by keeping the same applied voltage of 9 kV.

6.2.2 Influence of the gap

As presented in section 6.2.1, the applied voltage from 10 to 12 kV is not the best condition for reducing Cr(VI) due to the low energy yield, unlike 9 kV. Thus in this section, an applied voltage of 9 kV is used for all conditions, and the discharge is performed with frequency = 50 Hz.

To study the influence of the gap, we decrease the gap from 5 mm to 0.5 mm. **Figure 6.7** shows the time evolution of Cr(VI) concentration for the different gaps. We obtain almost linear behavior of the reduction for a given gap, and the reduction efficiency increases when the gap decreases. For example, Cr(VI) is completely reduced after 90 minutes with a gap of 0.5 mm, and the duration

increases to 110 minutes[d] when the gap is increased to 1 and 1.5 mm. In comparison, when discharging with a 5 mm gap, only 87 % of Cr(VI) is reduced after 120 minutes.

We identify three groups based on the reduction efficiency (from **Figure 6.7** and **Table 6.13**): 5 mm, 1-2 mm, and 0.5 mm. The total reduction time is different for these three groups, so we compare the reduction efficiency after 90 minutes. It is noted that 5 mm is the worst condition with a 66 % reduction rate, then 1, 1.5, and 2 mm gives about the same result of 80-83 %, and for the discharge at 0.5 mm is 100 %.

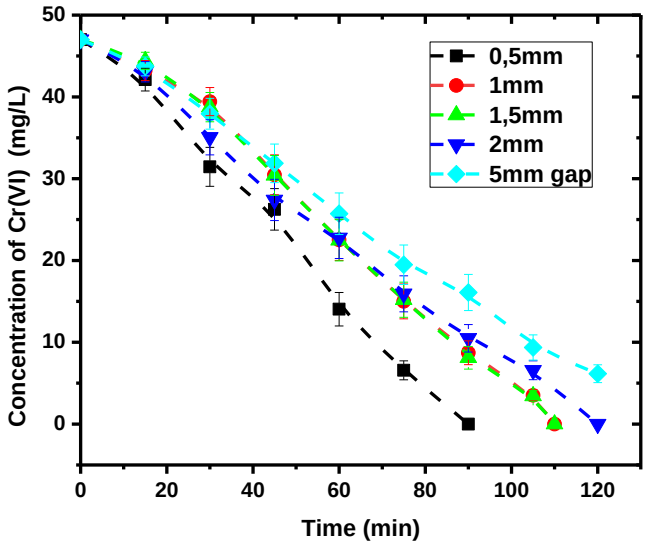

Figure 6.7 Concentration of Cr(VI) as a function of time of a pin-to-pin discharge obtained in Cr(VI) solution (σ=4 mS/cm) for differents gaps, U= 9 kV, Cr(VI) solution (47 mg/L,σ=4 mS/cm,pH=2.4), V = 100 mL, Δt = 500 µs, electrodes length = 0±10 µm, f = 50 Hz. The uncertainty of [Cr(VI)] is 20 %. It is noted that last values for 1 and 1.5 mm are given for 110 min.

As shown in **Figure 6.8** and **Table 6.13**, the increase of the gap from 0.5 to 5 mm leads to a decrease in the **number of BK**, from 80 to 0 %. As discussed previously, the increase of the electric field favors the breakdown conditions. We obtain that the average energy per pulse for NOBK is relatively constant, around 50-55 mJ whatever the gap; while for BK condition, the average energy per pulse slightly increases when the gap increases, from 33 mJ at 0.5 mm to about 40 mJ for 1.5 mm. This is due to different standard deviations and also different time evolution of the energy. For the discharge at 0.5 and 1 mm, we only obtain BK discharge during the first 20 minutes. Also, in these two conditions, we obtain a significant increase of energy per pulse for BK from about 5 mJ to 35-40 mJ. These variations can be explained because of the high initial electrical field. First, this latter involves a fast erosion of the electrodes, so the gap increases significantly (relatively to the small initial value), resulting in the variation of the electric field, so the injected energy is increased. Moreover, as already

[d] Note that for 1 and 1.5 mm the protocol has changed for the last sampling, the sampling has been done at 110 min instead of 120 min

discussed, the high initial electric field involves fast breakdowns, and a short breakdown duration leads to a low injected energy. However, it is interesting to notice that despite the variation in the injected energy during the 30 first minutes for gaps equal to 0.5 and 1 mm, we do not observe a different trend in the time evolution of the Cr(VI) reduction in **Figure 6.7**.

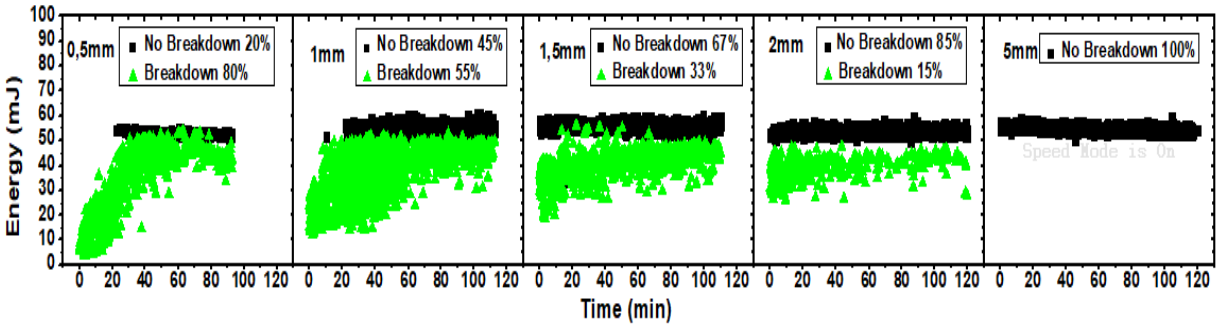

Figure 6.8 Time evolution of the injected energy per pulse for the different gaps from 0.5 mm to 5 mm. U= 9 kV, Cr(VI) solution (47 mg/L,σ=4 mS/cm,pH=2.4), V = 100 mL, Δt = 500 µs, electrodes length = 0±10 µm, f = 50 Hz.

We also obtained an increase in the **total injected energy** by increasing the gap (as presented in **Table 6.13**). For example, the total injected energy slightly increases from 9.9 kJ to 13 and 15 kJ when the discharge is performed at 0.5, 1.5, and 5 mm gaps, respectively. These increases in total injected energy are not able to explain the difference in reduction rate since the highest reduction efficiency is obtained for the lowest total injected energy. As an example, we obtain the energy yield equal to 4.7×10^{-4} g/kJ for 0.5 mm and only 2.1×10^{-4} for 5 mm. For these conditions, the number of BK/NOBK cannot explain the variations of the reduction efficiency because we obtain similar values (80%) for 1, 1.5, and 2 mm despite very different numbers of BK/NOBK (from 65/35 to 16/84). So we conclude that the variations **of the reduction efficiency are due to many additional effects including the injected energy and the number of BK**.

Gap (mm)	0.5 mm	1 mm	1.5 mm	2 mm	5 mm
Reduction efficiency at 90 minutes	100%	83%	83%	80%	66%
Number of BK/NOBK (%)	80 / 20	65/35	36/63	16/84	0 / 100
Energy per pulse BK / NOBK (mJ)	33 / 51	37 / 54	40 / 54	42 / 54	- / 56
Total Energy (kJ) at 90 minutes	9.9	11.6	13.1	14.1	15.1
Energy yield (g/kJ) at 90 minutes	4.7×10^{-4}	3.4×10^{-4}	3.0×10^{-4}	2.7×10^{-4}	2.1×10^{-4}

Table 6.13 Influence of the gap on Cr(VI) reduction efficiency and the discharge characteristic after 90 minutes. U= 9 kV, Cr(VI) solution (47 mg/L,σ=4 mS/cm,pH=2.4), V = 100 mL, Δt = 500 µ, electrodes length = 0±10 µm, f = 50 Hz

We observe a slight change in the **pH**, but we can see that this change is not a huge variation for a given applied voltage, as shown in **Table 6.14**. We show that the decrease in **conductivity** is more significant when the gap decreases (*i.e.* the reduction efficiency increases). For example, the decrease is 27 % (from 4.03 to 2.94 mS/cm) when the discharge occurs at a gap of 0.5 mm, while at gaps of 1/1.5/2. and 5 mm, the decrease is about 25 % and 12 %, respectively. The explaination is presented previously in section **6.2.1.**

Applied gap (mm)	pH		Conductivity (mS/cm)	
	Initial	Final	Initial	Final
0.5	2.3	2.4	4.03	2.94
1	2.4	2.4	4.05	3.02
1.5	2.4	2.4	4.05	3.03
2	2.3	2.4	4.02	3.08
5	2.4	2.4	4.05	3.57

Table 6.14 Initial and final solution parameters obtained from ex situ pH and conductivity measurements for the different gaps. Cr(VI) solution (47 mg/L,σ=4 mS/cm,pH=2.4), U = 9 kV, V = 100 mL, f = 50 Hz, Δt = 500 µs.

In conclusion, we confirm that the reduction efficiency increases when the gap between two electrodes decreases. The decrease of the gap leads to an increase in the number of BK but also leads to a decrease in the injected energy. Finally, based on the energy yield, we confirmed that a gap of 0.5 mm is the best condition to reduce Cr(VI) by PLI, but the damages of the electrodes are significant; thus, we decide that 2 mm is a good compromise.

Reminding the results obtained from **section 6.2.1** (the highest the injected energy, the highest the reduction efficiency), it is still a challenge to distinguish if the reduction of Cr(VI) is mostly due to BK or the injected energy since the change of applied voltage or gap also includes the energy and BK variation.

In the next section, we present the study on the influence of pulse frequency in reducing Cr(VI) by PLI. Thus, this study aims to better understand the influence of both energy and BK on reducing Cr(VI).

6.2.3 Effect of pulse frequency

Several studies have reported the influence of pulse frequency on the discharge characteristics in water and on the chemical activity[252–255]. They found that changing the applied pulse frequency leads to changing the injected energy due to the different pulse repetition rates. However, there is no report on the effect of pulse frequency on Cr(VI) reduction. Because of equipment limitations, we only change the pulse frequency from 10 Hz to 70 Hz for discharge at 8 kV[e].

We note that to obtain the same total number of pulses, a decrease in pulse frequency has to be compensated by increasing the time of the process. As a consequence, the duration of the experiment is 105 minutes with 70 Hz, 120 minutes with 50 Hz, 300 minutes with 25 Hz, and 540 minutes with 10 Hz (**Figure 6.9**(a)). We obtain a linear behavior in the reduction of Cr(VI) with time. Obviously, we observe a variation in the slope for each condition. For example, the complete reduction of Cr(VI) is obtained after 105 minutes when the discharge is performed at 70 Hz, while it is only 64 % when the discharge is performed at 10 Hz, even after 540 minutes. We note that it is not interesting to study time evolution because the frequency changes. Therefore, the number of pulses is a suitable parameter to compare the influence of the applied pulse frequency on the reduction efficiency.

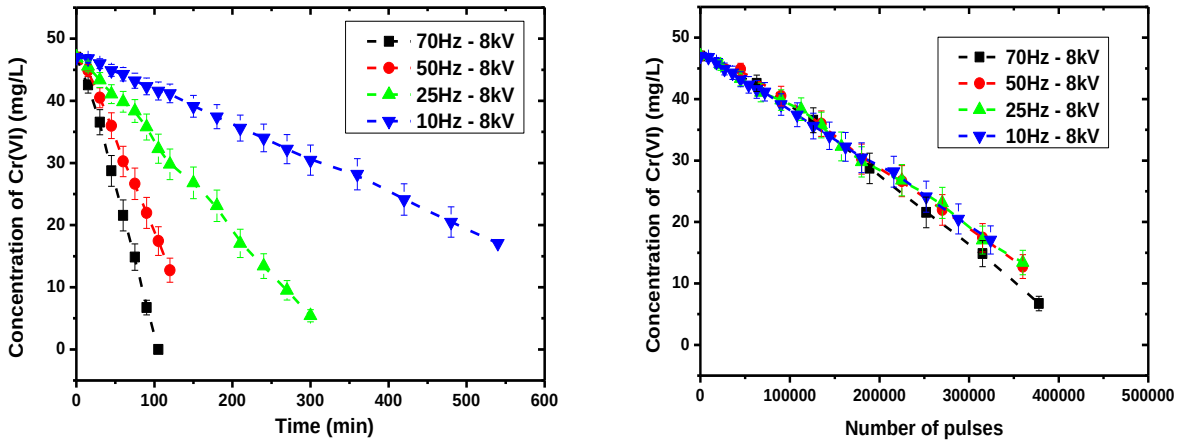

(a) (b)

Figure 6.9 Concentration of Cr(VI) as a function of time (a) and pulse number (b) of a pin-to-pin discharge obtained in Cr(VI) solution (47 mg/L,σ=4 mS/cm,pH=2.4) for different pulse frequencies, U = 8 kV, V = 100 mL, Δt = 500 µs, gap = 2 mm, electrodes length = 0±10 µm.

[e] We also perform experiments from 10 Hz to 50 Hz for discharge at 9 kV, the results are presented in **annex 6.1**

Figure 6.9(b) shows the reduction of Cr(VI) in dependence on the number of pulses for different frequencies at the same applied voltage of 8 kV. We obtain a linear behavior on Cr(VI) reduction, and Cr(VI) reduction is similar for all applied pulse frequencies. It is noted that the experiment at 10 Hz stops at the number of the pulse of 324000, so we compare the discharge characteristics and reduction efficiency during only a reduced number of pulses equal to 315 000 for 25, 50 and 70 Hz and 324 000 for 10 Hz (**Table 6.15**).

As shown in **Figure 6.10** and **Table 6.15**, the increase of pulse frequency leads to an increase in the **number of BK**. For example, the number of BK is only 1 % for the discharge at 10 Hz, while it is increased to 15 % when the pulse frequency increases to 70 Hz. We remind that in our configuration, the expansion of a gas phase following the plasma ignition is observed (as presented in **Chapter 4**). So the increase of the frequency results in the increase of gas-phase production. From the literature (as presented in **Chapter 2**), it is known that the discharge is easy to create in the gas phase than in the liquid phase. This hypothesis also can be obtained by Ruma *et al*. [255]. They have found that increasing the pulse frequency leads to creating a discharge inside the spheroidal gas bubble with plasma discharge underwater by a pin-to-plate configuration. Unlike previously, these experiments do not show any significant influence of the number of BK/NOBK on the Cr(VI) reduction.

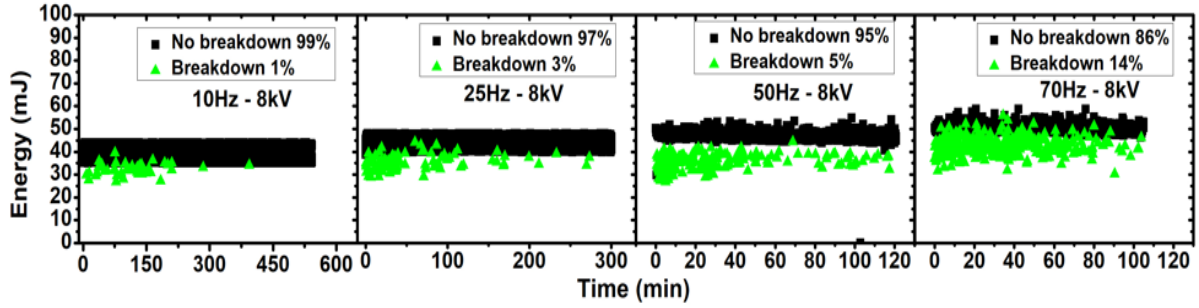

Figure 6.10 Time evolution of the injected energy per pulse for the different frequencies from 10 Hz to 70 Hz. U= 8 kV, (47 mg/L,σ=4 mS/cm,pH=2.4), V = 100 mL, Δt = 500 µs, electrodes length = 0±10 µm, gap = 2 mm. The different times correspond to the same number of pulses equal to 324000 for 10 Hz and 315000 for 25, 50 and 70 Hz.

We also find that the average **energy per pulse** of BK/NOBK increases slightly with the increase of the applied pulse frequency. The increase from 32/40 to 42/51 mJ of BK/NOBK energy is obtained when the pulse frequency increases from 10 Hz to 70 Hz. We observe an increase of the total injected energy from 13.1 to 15.5 kJ, with an increase in pulse frequency from 10 to 70 Hz, respectively. It is noted that we obtain a different effect as compared with the literature [253–255]. They have shown that the injected energy is almost similar for a given applied pulse frequency.

The increase of the pulse frequency from 10 to 70 Hz involves a low decrease of the energy yield from 2.3×10^{-4} to 2.1×10^{-4} g/kJ. Despite the increase of the injected energy and the increase of the ratio BK/NOBK, we obtain the same order of magnitude for the energy yield when the number of pulses is

the same. Therefore, we can conclude that the reduction efficiency and the energy yield strongly depend on the number of pulses.

Pulse frequencies (Hz)	**10 Hz**	**25 Hz**	**50 Hz**	**70 Hz**
Reduction efficiency	64 %	64 %	64 %	68 %
Number of BK/NOBK	1 / 99	3/ 97	5 / 95	14 / 86
Energy per pulse BK / noBK (mJ)	32 / 40	35 / 44	36 / 47	42 / 51
Total Injected Energy (kJ)	13.1	13.5	14.5	15.5
Energy yield (g/kJ)	2.3×10^{-4}	2.2×10^{-4}	2.1×10^{-4}	2.1×10^{-4}

Table 6.15 Influence of applied pulse frequencies on Cr(VI) reduction efficiency and the discharge characteristic. U= 8 kV, (47 mg/L,σ=4 mS/cm,pH=2.4), V = 100 mL, Δt = 500 µs, electrodes length = 0±10 µm, gap = 2 mm, number of pulses of 315 000 (except for 10 Hz that is 324 000).

Annex 6.1 shows the **pH and the conductivity** of the solution before and after plasma discharge for the different pulse frequencies for the applied voltage of 8 kV. It is not easy to draw an accurate conclusion because the time of the process and the number of pulses are very different for each experiment, especially for the conductivity.

The experiments with 9 kV (**annex 6.1**) are performed with the same total duration of 120 minutes, so the comparison of the final conductivity is meaningful to highlight the effect of the number of pulses. As shown in **annex 6.1**, the conductivity of the solution decreases more when the number of pulses is increased. For example, when discharging at 10 Hz (a pulse number of 75 000), we obtain a decrease of only 4 % (from 4.07 to 3.89 mS/cm), while when discharging at 50 Hz (a pulse number of 360 000), we obtain a decrease of 23 % (from 4.01 to 3.08 mS/cm). So it confirms that the increase of the number of pulses involves a lower conductivity and that this lower conductivity is related to a higher Cr(VI) reduction. Moreover, results from both studies (8 and 9 kV) show that we do not observe any significant change in the final pH values for an increase in the pulse frequency of plasma discharge.

In summary, we note no influence of pulse frequency on the Cr(VI) reduction for the same pulse number. Despite the different characteristics of the discharge (BK/NOBK, energy) with the frequency, the energy yield is similar for a given number of pulses. The evolution of the final conductivity with the reduction rate is similar to the previous observations.

It is also noted that the results show that nothing seems to occur between two pulses. As presented in **Chapter 4** by shadowgraphy, the gas channel disappear during the end of the pulse (at about 500 µs), and the shorter period is about 14 ms between two pulses (at 70 Hz) is too long, thus all the reactive species created by the discharge in the bubble have diffused during the pulse, which means that there is nothing happen during the off-time between two pulses.

However, we have to keep in mind that this study is conducted in a small pulse frequency range (only from 10 Hz to 70 Hz). Therefore, it is not sufficient to make a precise statement about the influence of pulse frequency on the reduction of Cr(VI) by PLI. However, to obtain the same number of pulses by reducing the frequency, the duration of the process must be considerably prolonged (540 minutes for 10 Hz and 300 minutes for 25 Hz with discharge at 8 kV, but this is still not enough to achieve a complete reduction of Cr(VI)). Thus we can conclude that it is not interesting to work at low frequency.

It seems that there is a considerable difference between discharge with and without breakdown. So the nature and the dynamics of the discharge are essential. Thus in the next section, we present the study of the influence of the pulse width of the discharge on the reduction of Cr(VI).

6.3 Effect of pulse duration

We propose to analyze the discharge's time effect on the Cr(VI) reduction by changing the pulse duration. This study aims to highlight the kinetics of the discharge. We also plan to study the effect of the breakdown. However, the problem is that the breakdown duration is very short (2-3 µs) and not reproducible (as observed in electrical signals, **Chapter 4**). In this section, the pulse width changes from 10 µs to 1 ms, the experiments are carried out for 2 mm and 5 mm gaps with the same applied voltage of 9 kV. The results are presented for both gaps, and then the results are compared and analyzed.

The conditions used for this section are: the length of both platinum electrodes is HV-0-GND-0 with a diameter of 200 µm. The volume of the working solution is 100 mL, with the initial concentration of Cr(VI) equal to 47 mg/L. The initial pH of the solution is 2.4, and the initial conductivity of the solution is about 4 mS/cm. The measurements are performed every 15 minutes by sampling 2 mL of solution and scanning it at 350 nm by UV-visible absorption spectroscopy (**annex 3.1**).

6.3.1 Influence of the pulse duration on Cr(VI) reduction for 2 mm gap

Figure 6.11 shows the time evolution of Cr(VI) concentration for different applied pulse durations. For all conditions, the Cr(VI) reduction follows a linear behavior, and we obtain an increase in the reduction when the pulse duration is increased. For example, the reduction efficiency increases from 39 % to 83 % and up to 100 % when the applied pulse duration is increased from 10 µs to 100 and 500 µs, respectively (reported in **Table 6.17**). It is noted that the increase in the pulse duration up to 1 ms is not showing any difference in the reduction rate as compared with 500 µs. We also observed a similar behavior during the first 30 minutes for all applied pulse durations.

Figure 6.12 shows that the number of BK is similar, about 15 % for the pulse duration of 100 µs, 250 µs, 500 µs, and 1 ms. The number of BK decreases to 5 % and 3 % when the pulse duration decreases to 25 µs and 10 µs, respectively, and most of the BK distribution is during the first 30 minutes of the process. As presented in **Table 6.16**, we can observe that the BK discharge distribution is similar (equal to about 20 %) for all pulse durations during the first 30 minutes. Thus it can explain that during the first 30 minutes, we obtain the same behavior on the reduction efficiency, as presented previously.

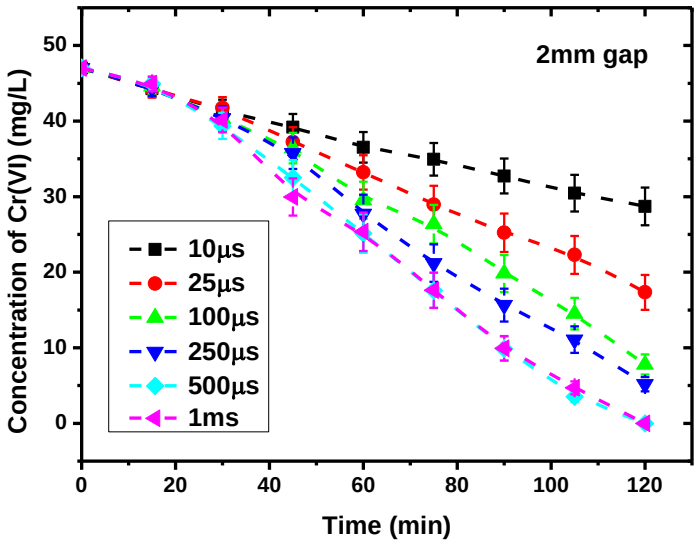

Figure 6.11 Concentration of Cr(VI) as a function of time of a pin-to-pin discharge obtained in Cr(VI) solution (47 mg/L,σ=4 mS/cm,pH=2.4) for different pulse durations, U = 9 kV, V = 100 mL, gap = 2 mm, electrodes length = 0±10 µm, f = 50 Hz.

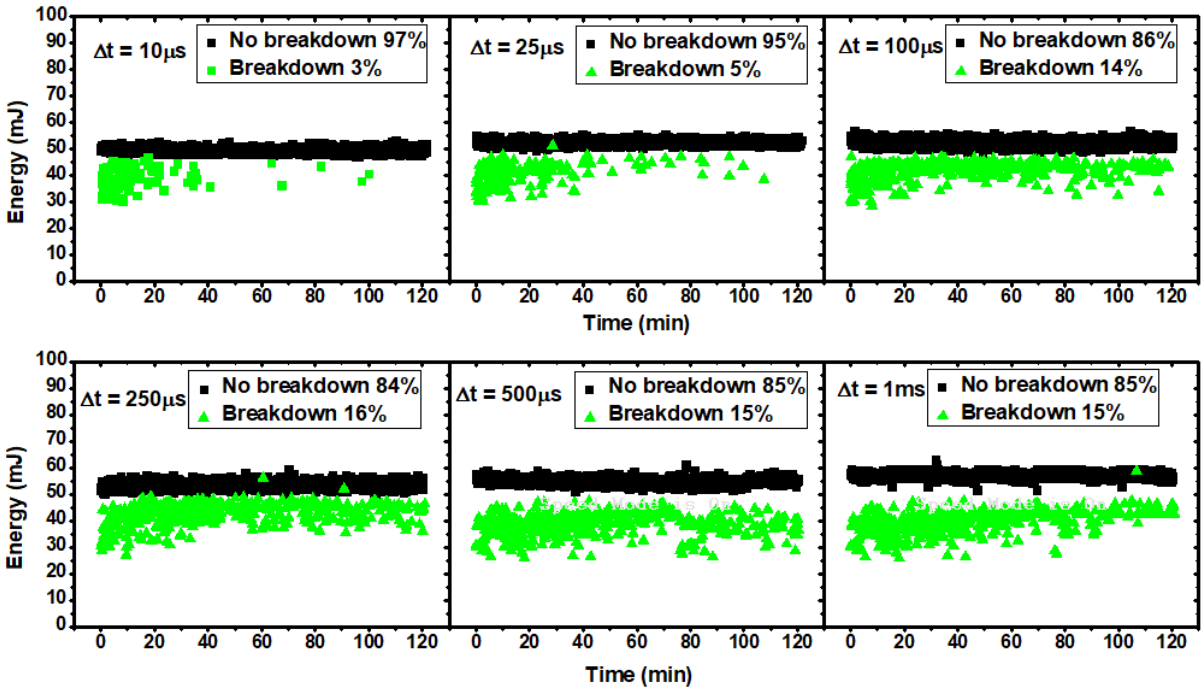

Figure 6.12 Time evolution of the injected energy per pulse for the different pulse duration from 10 µs to 1 ms. U = 9 kV, Cr(VI) solution (47 mg/L,σ=4 mS/cm, pH=2.4) V = 100 mL, Δt = 500 µs, gap = 2 mm, electrodes length = 0±10 µm.

After 30 minutes, the Cr(VI) reduction is very different for each pulse duration. The corresponding ratio BK/NOBK decreases to a maximum 2 % for 10 and 25 µs and to about 15 % for higher pulse durations (**Table 6.16**). These variations can be explained due to the increase of breakdown strength

with the decreasing of pulse widths, as shown in the literature[221,256]. This leads to the number of BK decrease with a decrease of the pulse width. However, these results show that the Cr(VI) reduction variation is not only related to the breakdowns.

Pulse duration	**10 µs**	**25 µs**	**100 µs**	**250 µs**	**500 µs**	**1 ms**
Number of BK/NOBK (%) on 0- 30 minutes	14/86	17/83	19/81	21/79	21 /79	21 / 79
Number of BK/NOBK (%) on 30-120 min	1/99	2/98	11/89	14/86	16/84	16/84

Table 6.16 The distribution of BK/NOBK during first 30 minutes of time of a pin-to-pin discharge obtained in Cr(VI) solution (47 mg/L, σ=4 mS/cm, pH=2.4) for different pulse durations, U = 9 kV, V = 100 mL, gap= 2 mm, electrodes length =0±10 µm, f = 50 Hz

We also observe a considerable difference in the reduction efficiency between 10, 25 µs, and 100 µs. The reduction efficiency increases from 39 % to 63 % and to 83%, respectively (**Table 6.17**). For higher pulse duration, the observed variation is lower.

We obtain similar **energy per pulse** for BK and NOBK, about 38-41 mJ for BK and 50-54 mJ for NOBK. As a consequence, the total injected energy does not increase significantly (lower than 10 %) with the pulse duration, despite the different values of BK/NOBK.

However, the variation in reduction efficiency results in different **energy yields**. We note that the energy yield increases from 1×10^{-4} g/kJ to 2.5×10^{-4} g/kJ when the duration of the applied pulse is increased from 10 µs to 500 µs. It confirms that the increase of the pulse duration up to 500 µs involves a significant increase of Cr(VI) reduction efficiency and energy yield.

Pulse duration	**10 µs**	**25 µs**	**100 µs**	**250 µs**	**500 µs**	**1 ms**
Reduction efficiency after 120 minutes	39 %	63 %	83 %	89 %	100 %	100 %
Number of BK/NOBK (%)	3 / 97	5 / 95	14 / 86	16 / 84	15 / 85	15 / 85
Energy per pulse BK / noBK (mJ)	39 / 50	41 / 52	41 / 54	41 / 54	42 / 54	42 / 54
Total Energy (kJ)	17.9	18.5	18.8	18.7	18.8	18.8
Energy yield (g/kJ)	1.0×10^{-4}	1.6×10^{-4}	2.1×10^{-4}	2.2×10^{-4}	2.5×10^{-4}	2.5×10^{-4}

Table 6.17 Influence of pulse duration on Cr(VI) reduction efficiency and the discharge characteristics. U = 9 kV, Cr(VI) solution (47 mg/L, σ=4 mS/cm, pH=2.4), V = 100 mL, Δt = 500 µs, gap = 2 mm, electrodes length = 0±10 µm, f = 50 Hz.

As shown in **Table 6.18**, there is no change in the **pH** values for an increase in the pulse duration of the discharge. A decrease between the initial and final solution **conductivities** is observed for all pulse durations. Moreover, this decrease is more significant when the applied pulse duration increases. For example, we observe a decrease of about 10 % (from 4.06 to 3.7 mS/cm) for the pulse discharge at 10 µs. In comparison, we obtain a decrease of about 24 % (from 4.06 to 3.08 mS/cm) when the applied pulsed duration increases to 500 µs. However, no considerable variations in the conductivity of the solution are observed at the end of the process, with pulse duration from 100 µs to 1 ms, conditions giving similar energy yield.

Pulse width	pH		Conductivity (mS/cm)	
	Initial	Final	Initial	Final
10 µs	2.4	2.4	4.06	3.70
25 µs	2.4	2.4	4.06	3.40
100 µs	2.4	2.4	4.06	3.10
250 µs	2.4	2.4	4.06	3.09
500 µs	2.3	2.4	4.06	3.08
1 ms	2.4	2.4	4.06	3.07

Table 6.18 Initial and final solution parameters obtained from ex situ pH and conductivity measurements for the different pulse duration after 120 minutes. Cr(VI) solution (47 mg/L, σ=4 mS/cm, pH=2.4) U = 9 kV, V = 100 mL, f = 50 Hz, gap = 2 mm, electrodes length = 0±10 µm

In **summary**, the reduction efficiency and the energy yield increase significantly with the increased applied pulse duration from 10 to 100 µs and then more slightly up to 500 µs. This effect is observed from 30 minutes after the beginning of the process since the [Cr(VI)] evolution is similar for all pulse durations during the 30 first minutes. We distinguish two different groups regarding the discharge characteristics. From 100 µs to 1 ms, there is almost no change in the number of BK and energy per pulse and final conductivity. For 10 and 25 µs we report lower BK/NOBK and variation in the energy and final conductivity.

Therefore, further studies are required to understand the effect of pulse width on reducing Cr(VI) (especially the influence of BK). Thus in the next part, we try to clarify the effect of BK on reducing Cr(VI) using PLI by increasing the electrode gap at 5 mm.

6.3.2 Influence of the pulse duration on Cr(VI) reduction for 5 mm gap

Same as previously with 2 mm gap, the change of pulse duration is from 10 µs to 1 ms, and discharge occurs at 9 kV but for 5 mm of the gap. As shown in **Figure 6.13**, we obtain a linear behavior on the time evolution of [Cr(VI)]. We also observe that the reduction efficiency of Cr(VI) increases with the increase of the applied pulse duration. During the first 15 minutes, the reduction of Cr(VI) is quite similar for all pulse durations (considering uncertainties), and then the time evolution changes according to the pulse duration, showing very similar behavior for 10 and 25 µs, for 100 and 250 µs, and for 500 µs and 1 ms.

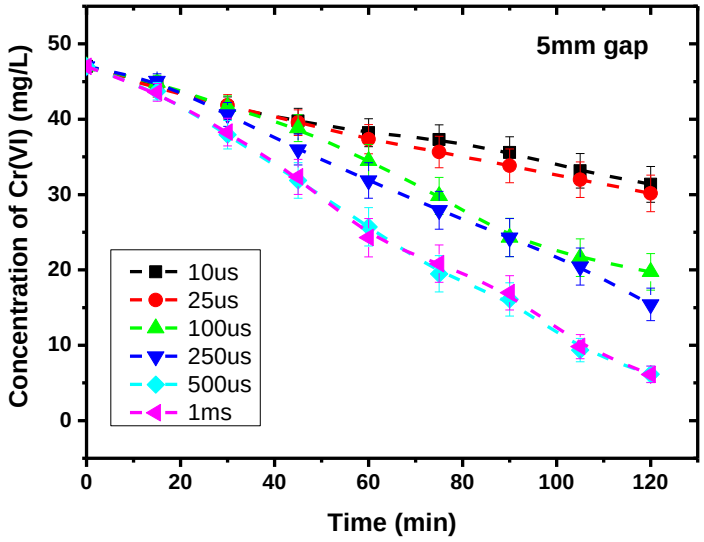

Figure 6.13 Concentration of Cr(VI) as a function of time of a pin-to-pin discharge obtained in Cr(VI) solution (47 mg/L, σ=4 mS/cm, pH=2.3) for different pulse durations, U = 9 kV, V = 100 mL, gap = 5 mm, electrodes length = 0±10 µm, f = 50 Hz.

On the contrary, we observe similar values of the **injected energy** per pulse for all pulse durations, and the value is slightly increased from 51 mJ to 57 mJ when the pulse width increased from 10 µs to 1 ms, as shown in **Figure 6.14** and **Table 6.19**. This is in agreement with the electrical signals reported in **Chapter 5,** which shows that the current is almost zero after 5 µs.

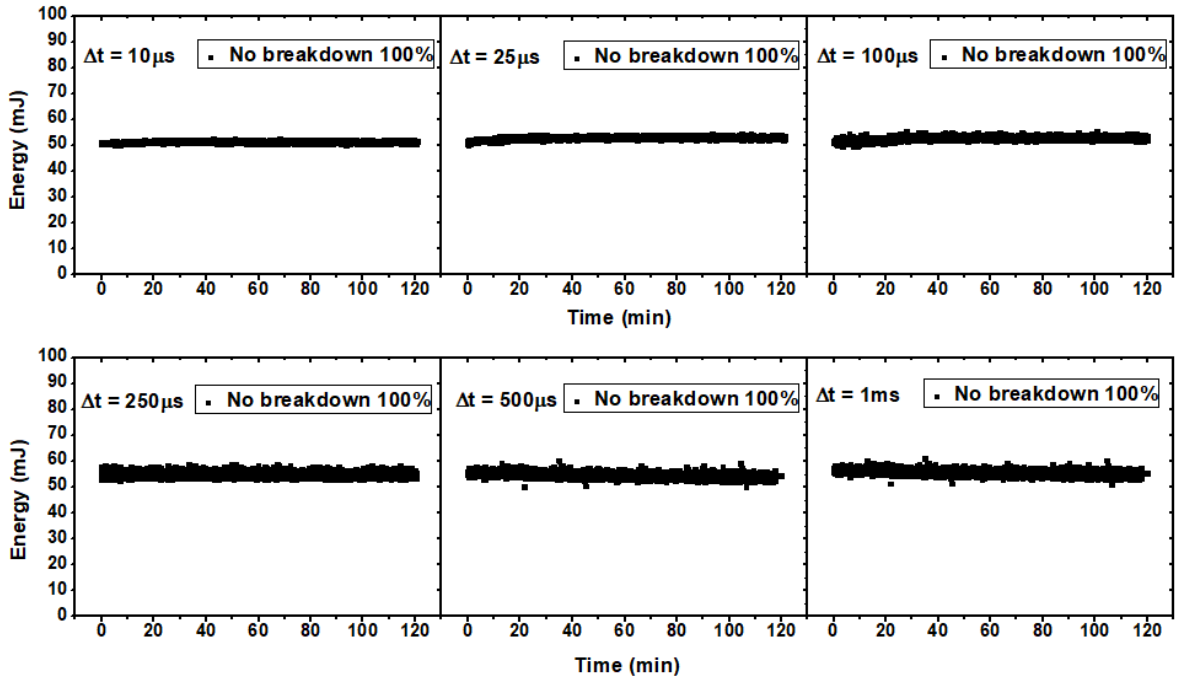

Figure 6.14 Time evolution of the injected energy per pulse for the different pulse durations from 10 µs to 1 ms. U = 9 kV, Cr(VI) solution (47 mg/L, σ=4 mS/cm, pH=2.3), V = 100 mL, Δt = 500 µs, gap = 5 mm, electrodes length = 0±10 µm, f = 50 Hz.

Consequently, **Table 6.19** points out that the total injected energy is also slightly increased (in the range of 18.4-20.5 kJ) with an increase of pulse width. This agreement is also found in the reports of Kawano *et al.*[257] and Tamaribuchi *et al.*[258]. Although the plasma configurations (corona discharge or discharge inside bubble in water) are not the same as our configuration, they also show that the input energy increases with increasing of the pulse width. However, it is reported that the efficiency of organic dye degradation is higher when the pulse width is shorter. In comparison with our results, we found that the reduction efficiency of Cr(VI) increases with increasing pulse width. However, it is noted that in the work of Kawano[257] and Tamaribuchi[258], the change in pulse width is much smaller than our (in the range of 0.05 µs to 1.2 µs compared with 10 µs to 1 ms in this work). As a summary, we identify three groups based on the results in **Table 6.19**:

- The first group (10 - 25 µs) gives similar results on 34-36 % reduction efficiency. We also obtained the same order of magnitude on the total injected energy of about 18.4-18.7 kJ and the energy yield of about 0.9×10^{-4} g/kJ.
- The second group (100 – 250 µs) presents an increase in reduction efficiency to about 60 %. **Table 6.19** also shows the similar value of the total injected energy (about 19 kJ) and the energy yield (1.5×10^{-4} g/kJ) for this group.
- The final group (500 µs - 1 ms) shows the highest reduction rate of 87 % and the energy yield of 2×10^{-4} g/kJ, and the total energy of 20 kJ

We note that the increase of the injected energy results in a better reduction. However, the evolution due to the pulse duration (corresponds with three groups) cannot be explained only by this effect.

Pulse duration	**10 µs**	**25 µs**	**100 µs**	**250 µs**	**500 µs**	**1 ms**
Reduction efficiency after 120 minutes	34 %	36 %	58 %	67 %	87 %	87 %
Number of BK/noBK	- / 100	- / 100	- / 100	- / 100	- / 100	- / 100
Energy per pulse BK / noBK (mJ)	- / 51	- / 52	- / 53	- / 54	- / 56	- / 57
Total Energy (kJ)	18.4	18.7	19.1	19.4	20.2	20.5
Energy yield (g/kJ)	0.9×10^{-4}	0.9×10^{-4}	1.4×10^{-4}	1.6×10^{-4}	2×10^{-4}	2×10^{-4}

Table 6.19 Influence of pulse duration on Cr(VI) reduction efficiency and the discharge characteristic after 120 minutes. Cr(VI) solution (47 mg/L, σ=4 mS/cm, pH=2.3), U = 9 kV, V = 100 mL, gap =5 mm, electrodes length = 0±10 µm, f = 50 Hz

We observe a slight change in the final **pH** values from 2.3 to 2.4 according to the pulse duration (**Table 6.20**). We also obtain a significant decrease in the solution conductivity when the pulse duration increases. For example, the final solution conductivity decreases about 5 % (from 4.08 to 3.85 mS/cm) with 10 µs. In comparison, the decrease of the final conductivity is about 13 % (from 4.01 to 3.57 mS/cm) when the discharge is performed at the pulse duration of 500 µs.

Pulse width	pH		Conductivity (mS/cm)	
	Initial	Final	Initial	Final
10 µs	2.3	2.4	4.08	3.85
25 µs	2.3	2.4	4.1	3.71
100 µs	2.3	2.4	4.03	3.69
250 µs	2.3	2.4	4.06	3.66
500 µs	2.4	2.4	4.01	3.57
1 ms	2.3	2.4	4.07	3.54

Table 6.20 Initial and final solution parameters obtained from ex situ pH and conductivity measurements for the different pulse duration after 120 minutes. Cr(VI) solution (47 mg/L, σ=4 mS/cm, pH=2.3) U = 9 kV, V = 100 mL, f = 50 Hz, gap = 5 mm, electrodes length = 0±10 µm.

We first conclude that in the case of the 5 mm gap, when the applied pulse duration increases, it slightly increases the injected energy and significantly increases the reduction efficiency and the energy yield. No easy relationship between these parameters can be established.

6.3.3 Comparison and analysis of the results

In sections **6.3.1** (2 mm) and **6.3.2** (5 mm gap), we show that the increase in the Cr(VI) reduction may be related to the increase of the injected energy, which is due to the increase of the pulse duration. However, we also highlight that it is not the only parameter that affects the reduction efficiency, and we note that it is not easy to understand the phenomena.

Figure 6.15 shows the energy yield as a function of pulse duration for the discharge at 2 and 5 mm gaps. We confirm that increasing the pulse duration for both conditions leads to an increase in the energy yield.

The log scale of **Figure 6.15**(b) shows that, for both gaps, the evolution can be divided into two successive steps. The discharges (for both BK and NOBK) exist during about the first 2-3 µs of the process (**Chapter 4**). They generate reactive species, which can diffuse into solution and be responsible for Cr(VI) reduction. Despite the short duration of the discharge, its effect is significant on Cr(VI) reduction and does not depend on the gap ($\approx 10^{-4}$ g/kJ for 10 µs).

Then, the kinetics of the mechanisms depends on the gap: the change into the energy yield evolution appears at 10 µs for 2 mm, and it is shifted to 25 µs for 5 mm. We have already discussed that changing the gap modifies the discharge characteristics. Some differences between experiments performed at 2 and 5 mm gaps have been previously identified and may be discussed to explain the difference in Cr(VI) reduction.

The variation could be due to the presence or not of breakdown. The BK discharge generates a strong emission (resulting from the formation of excited species as H(n=3), H(n=4), OH [212]), a shock wave, reactive species that play a role in Cr(VI) reduction. To discuss about the effect of the only BK, it is useful to analyze the result obtained for a short pulse duration (at 10 µs) since the breakdown occurs at about 2-3 µs. We observe that for 10 µs the reduction efficiency is similar for 2 mm (BK) and 5 mm (NOBK), so the BK phenomena do not appear to be directly responsible for the Cr(VI) reduction.

Here we distinguish the effect of the discharge (plasma) and the breakdown. We have shown that the discharge (BK and NOBK) directly affects Cr(VI) reduction, whereas the breakdown has not a direct effect.

The breakdown occurs before 10 µs, so they do not directly explain the difference observed between 10 and 25 µs when the gap is changed from 2 to 5 mm. However, the indirect effect may happen due to complex chemistry. BK and NOBK discharge do not produce the same reactive species in the same thermodynamic conditions, so the kinetics is not the same. So we can suggest that reactive long-lived species (such as H_2O_2) are produced faster for 2 mm than for 5 mm gap. This production involves a second mechanism for Cr(VI) reduction.

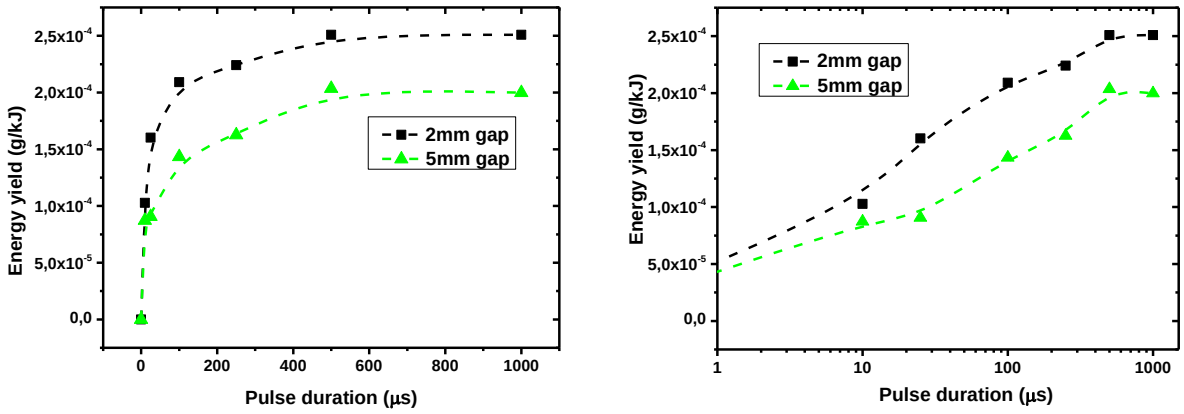

Figure 6.15 Energy yield versus pulse duration (a) and log scale (b) for 2 and 5 mm gap of a pin-to-pin discharge obtained in Cr(VI) solution (47 mg/L, σ=4 mS/cm, pH=2.4) U = 9 kV, V = 100 mL, f = 50 Hz, electrodes length = 0±10 µm.

After the plasma discharge, we still observe the reduction of Cr(VI) since the energy yield continues to increase with the pulse duration. This second step occurs during the post-breakdown phase, which mainly involves forming long-lived species such as H_2O_2. Despite different discharge durations, the post-breakdown kinetics seems to be similar for both gaps since the evolution of the energy yield is comparable.

This result can also be confirmed by comparing the evolution of the conductivities (**Figure 6.16**). We observe that the conductivity decreases when the pulse duration increases for both gaps with similar two-step mechanisms. The first step occurs on the range [0-25] µs for 5 mm gap and on [0-100] µs for 2 mm gap. The shift of about 0.5 mS/cm in the conductivity is related to chemical activity occurring between 25 and 100 µs.

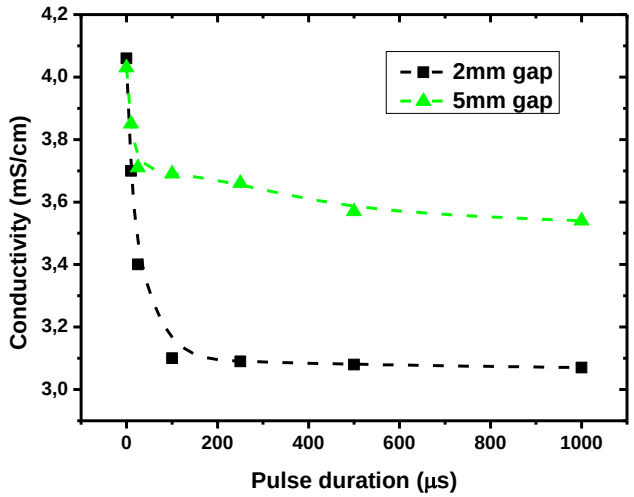

Figure 6.16 Final solution conductivity versus pulse duration for 2 and 5 mm gap of a pin-to-pin discharge obtained in Cr(VI) solution (47 mg/L, σ=4 mS/cm, pH=2.4) U = 9 kV, V = 100 mL, f = 50 Hz, electrodes length = 0±10 µm

In order to better understand these complex and intricated phenomena, more chemical analyses are necessary. For these reasons, H_2O_2 generation are discussed in **Chapter 7**.

6.4 Comparison of the energy yield with the literature

As a summary, we report in this work that we are able to reduce 100% of Cr(VI) in solution by PLI. This result has been obtained for different experimental conditions (applied voltage, gap, pulse duration), providing an energy yield from 1.8 to 4.7×10^{-4} g/kJ. The best experimental condition considering energy yield and electrode erosion (9 kV, 2 mm gap) corresponds to an energy yield of 2.5×10^{-4} g/kJ. **Table 6.21** shows the comparison of the reduction efficiency and energy yield for the Cr(VI) reduction between this work and other configurations using the PLI method in the literature. The two types of PLI shown in **Table 6.21**, are discharge above the liquid and discharge within the liquid. As reported in **Chapter 2**, most of the works use **discharges above the liquid**. For example, the best result has been published by Chandana *et al*. [191], which showed that the energy yield is about 6.6×10^{-3} g/kJ when the discharge is performed in 50 mL of Cr(VI) 50 mg/L. However, this work did not successfully reduce Cr(VI) since they reported only a 40% reduction. This is a problem because it is known that Cr(VI) may be toxic even at very low concentration[9,12,21]. Moreover, to reach these high values of energy yield, they need to use additional materials such as argon gas.

In comparison with the **discharge in liquid**, Wang *et al*.[3] have reported that the energy yield is about 5×10^{-4} g/kJ when a glow discharge in liquid is performed in 150 mL of Cr(VI) solution (50 mg/L). It is the only discharge in the liquid process that has nearly succeeded in totally reducing Cr(VI), but not totally, which is a problem as previsouly discussed. Moreover, a cooling system is required because in this configuration the plasma formation leads to raise the solution's temperature involving the evaporation of the solution.

Then we obtain a similar energy yield of 4.7×10^{-4} g/kJ compared with the study of Wang *et al*.[3] but we succed to completely remove of Cr(VI) in solution. We remind that in our configuration, the discharge is performed by using of pin-to-pin configuration with the applied voltage of 9 kV and the inter-electrodes gap of 0.5 mm. However, as we presented previously, this configuration damages the capillary and the electrodes; thus, it is not an economic study. The other electrode geometry in our work, with an inter-electrode gap of 2 mm, shows a lower energy yield of 2.5×10^{-4} g/kJ.

In **summary**, we would like to conclude that our plasma configurations give good results on the energy yield evaluation and allows the total Cr(VI) reduction. We obtain a similar value of energy yield compared with the same type of plasma discharging directly into the solution. Plasma discharges above liquid present the highest energy values, but most of these configurations require high power consumption and other additional materials, such as the gas supply, and do not successfully reduce Cr(VI) in solution. Therefore, our configuration offers promise techniques for water and wastewater treatment, especially for the treatment of Cr(VI) contamination.

Power supply	Geometry	Inter-electrode distance	Voltage	Current	Volume of reactor	Initial concentration	pH of solution	Time of process	Reduction efficiency	Energy Yield $G_{Cr(VI)}$/g/kJ	References
Plasma discharge above the liquid											
DC	Pin-to-plate	10 mm	-	40 mA	70 mL	10 mg/L	5.5	7 min	60%	1.5×10^{-4}	[195]
ns-pulsed	Pin-to-plate with gas supply	5 mm	9kV	-	20 mL	50 mg/L	2.5	15 min	70%	-	[196]
DC	Pin-to-tube with gas supply	5 mm	1.1-1.5 kV	35-40 mA	-	100 mg/L	-	-	50%	0.9×10^{-4}	[197]
AC	Plate-to-plate DBD type	3 mm	0.1 kV	1000 mA	100 mL	2.6 mg/L	7 3	21 min	70.7% 94%	1.5×10^{-6} * 1.9×10^{-6} *	[193]
DC	Pin-to-plate with gas supply	~3-5 mm	1.3 kV	40 mA	20 mL	40 mg/L	2	4 min	100%	0.64×10^{-4} *	[6]
High voltage transformers	Pin-to-plate with gas supply	6 mm	16 kV	-	50 mL	50 mg/L	2	5 min	40%	6.6×10^{-3} *	[191]
DC	Pin-to-plate with gas supply	2 mm	1 kV	40 mA	25 mL	40 mg/L	2	3 min	100%	1.4×10^{-4} *	[5]
Plasma discharge in the liquid											
DC	Pin-to-plate	-	0.6 kV	120 mA	150 mL	31.2 mg/L	2	18 min	96%	6×10^{-5} *	[4]
DC	Pin-to-plate	-	0.6 kV	936 mA	-	100 mg/L mix with phenol	-	30 min	93.35%	3.4×10^{-4}	[192]
DC	Pin-to-plate	-	0.5 kV	100 mA	150 mL	50 mg/L 100 mg/L	2	5 min 15 min	97% <100%	4.9×10^{-4} * 3.3 x 10^{-4} *	[3]
Pulse DC	Pin-to-pin	2 mm 0.5 mm	9 kV	Peak 40 A	100 mL	47 mg/L	2.4	120 min 90 min	100 % 100 %	2.5×10^{-4} 4.7×10^{-4}	This work

Table 6.21 Energy efficiency for Cr(VI) reduction using the non-thermal plasma method (*these values are recalculated by using Equation 11)

6.5 Conclusion

The first objective of this work regarding the reduction of Cr(VI) using pin-to-pin microsecond pulsed discharge has been successfully reached.

In studying the reduction of Cr(VI) by the PLI process, we first study the electrode geometry (length and diameter) to optimize the best configuration. For the first study on the electrode geometry, both platinum electrodes' length is changed by HV-GND-0 µm, HV-GND-100 µm, and HV-GND-400 µm with the diameter is Ø = 100 µm and 200 µm. This study showed that the reduction efficiency of Cr(VI) increases as the length of the electrode decreases. We observed a linear behavior in the decrease of Cr(VI) for a given length and diameter of the electrodes. For the same length of the electrodes HV-GND -100 µm and HV-GND -400 µm, the reduction rate is higher when the discharge is performed at a diameter of Ø = 100 µm than at a diameter of Ø = 200 µm. However, for a length of HV-GND -0 µm, the discharge with a diameter of Ø = 200 µm gives a 100 % reduction of Cr(VI), while for the discharge with a diameter of Ø = 100 µm, it is only 85 %. We noted that increasing the length of the electrodes also decreases the number of BK, thus leading to an increase in the total injected energy. We estimate the energy yield of the process, which is the highest value of 2.6×10^{-4} (g/kJ) obtained for the case of HV-GND-0 µm with a diameter of Ø = 200 µm. So we can conclude that the discharge with **HV-GND-0 µm and Ø = 200 µm is the best configuration** to study the reduction of Cr(VI) by PLI process, and this electrode geometry is used along all of the studies in this thesis.

Then we study the **influence of some physical parameters** that have an influence on the reduction of Cr(VI). These parameters concern: applied voltage, inter-electrode gap, applied pulse frequency, and pulse duration. The first parameter focuses on the influence of the applied voltage from 2 to 12 kV. We study the influence of the **applied voltage** with two different gaps between two electrodes: 2 mm and 5 mm. In general, the reduction efficiency of Cr(VI) with an increase of the applied voltage. For discharges at 2 mm, an increase in the applied voltage leads to a simultaneous increase in the injected energy and the number of BK. The time to completely remove Cr(VI) also decreased with increasing voltage, from 120 minutes for the discharge at 9 kV to 70 minutes when the applied voltage increased to 12 kV. However, the reduction of Cr(VI) is related to both parameters: the injected energy and the amount of BK. Therefore, studies with 5 mm are required to highlight the influence of BK and input energy. For discharge at a gap of 5 mm without BK discharge, increasing the applied voltage only increases the injected energy and thus increases the reduction efficiency of Cr(VI). Considering these results, we can first conclude that Cr(VI) reduction increases as the input energy increases. On the other hand, comparing the effect of Cr(VI) reduction with the same applied voltage or input energy for 2 mm and 5 mm, we found that discharge at 2 mm in the presence of BK consistently achieves higher efficiency than at 5 mm, where NOBK discharge is obtained. Thus, we concluded that the process should be accomplished in the presence of BK to achieve the high efficiency of Cr(VI)

treatment. However, we pointed out that this is not an economically viable solution at the applied voltages of 11-12 kV due to the high energy consumption and especially the destruction of materials such as electrodes and capillaries.

The second parameter that was investigated is the **inter-electrode distance** from 0.5 mm to 5 mm for a fixed applied voltage of 9 kV. We found that the complete reduction of Cr(VI) occurs more rapidly when the inter-electrode distance is decreased. For example, the time required to reduce 100 % Cr(VI) is 120 minutes for the discharge at 2 mm, while it is only 90 minutes for the discharge at 0.5 mm. Reducing the electrode gap leads to an increase in the electric field at the tip of the electrode, resulting in a faster reduction of Cr(VI).

The third parameter, the influence of **pulse frequency** was determined. Due to the limitations of the equipment, the change of applied pulse frequency is only from 10 Hz to 70 Hz. This study showed that the reduction of Cr(VI) is similar with the same number of the pulse. However, to obtain the same number of pulses, the decrease in pulse frequency must be compensated by an increase in discharge time. This leads to time consuming, for example, with the discharge of 10 Hz – 8 kV, it required 540 minutes to reach the same pulse number at 315000 as at 70 Hz – 8 kV, but the Cr(VI) reduction efficiency is less than 100 %. Therefore, we conclude that low frequency (<50 Hz) is not suitable for use in Cr(VI) treatment in this work. We also noted that there is no effect of the off time between two pulses on the reduction of Cr(VI)

As the final parameter, the influence of **pulse duration** from 10 µs to 1 ms for a fixed applied voltage of 9 kV was investigated. We also studied the influence of the pulse duration for different gaps between two electrodes: 2 mm and 5 mm. In general, we obtained that Cr(VI) reduction is increased with increased pulse duration. However, changing the pulse width within each condition of the electrode gap presents a huge difference in Cr(VI) reduction even though the injected energy is almost the same. This presents a new challenge for future investigations to better understand the influence of the post-discharge phase on the plasma generations and, in particular, the reduction of Cr(VI) by the PLI process.

We noted that the **pH** of the solution increased slightly at the end of the process, but this increase is not a huge variation for a given condition. The increase of pH can be explained due to the consumption of hydronium ions to reduce Cr(VI). We also observed a decrease in the solution **conductivity** after the process, and this decrease is more significant when the reduction efficiency is increased. It can be explained due to the consumption of some ions such as hydronium, Cr(III), and sulfate. However, further analysis is required to demonstrate this hypothesis clearly.

The Cr(VI) reduction results show a difference at different physical parameters. However, the change in physical parameters also leads to a change in chemical properties in the solution during discharge. Therefore, it is interesting to analyze the influence of some physical parameters on the formation of active species by PLI in Cr(VI). As presented in **Chapter 2**, H_2O_2 is a species that affects the reduction efficiency due to the reducing properties in acidic medium, and moreover, H_2O_2 is a long-

lived species, so quite easy to monitor. This study may help us to understand the reduction process better.

In the next chapter, we will present the effects of some physical parameters such as applied voltage and pulse width on the production of H_2O_2 in Cr(VI) solution. The measurement of H_2O_2 is performed by using the Vaska method, as described in **Chapter 3.**

Chapter 7
H_2O_2 formation in Cr(VI) solution

This chapter focuses on studying the influence of input voltage and pulse width on the formation of H_2O_2 in Cr(VI) solution. The aim is to identify the relationship between the variations of both [H_2O_2] and [Cr(VI)] in order to better understand the mechanisms responsible for Cr(VI) reduction.

The electric discharge initiates the generation of reactive oxidizing or reducing species such as H, OH, H_2O_2, e_{aq}^-. These species can diffuse in the liquid phase and induce oxidation-reduction reactions with dissolved elements[186,222–225], as for the reduction of dissolved Cr(VI). However, it is not easy to distinguish which species are most effective in reducing the Cr(VI). Moreover, the formation of these species depends on the conditions such as conductivity, pH, electrolyte[222,228,259].

As noted in **Chapter 6**, short-lived species can reduce Cr(VI) as aqueous electrons and H radical. Moreover, Cr(VI) can also be reduced by long-lived species such as H_2O_2 by the reactions below[3,199]:

$$Cr_2O_7^{2-} + 4H_2O_2 + 2H^+ \rightarrow 2CrO_5 + 5H_2O \qquad \textbf{Reaction 55}$$

$$2CrO_5 + 6H^+ \rightarrow 2Cr^{3+} + 2H_2O + H_2O_2 + 3O_2 \qquad \textbf{Reaction 56}$$

$$2HCrO_4^- + 3H_2O_2 + 8H^+ \rightarrow 2Cr^{3+} + 3O_2 + 8H_2O \qquad \textbf{Reaction 57}$$

Although H_2O_2 and Cr(VI) reactions are quite slow and require an acidic medium, H_2O_2 is very interesting to monitor since it is one of the major products formed in solution by PLI and a long lived species. Therefore, to better understand the reaction process, the study of the formation of H_2O_2 after an electrical discharge is a significant step.

This chapter presents the study of the H_2O_2 formation in Cr(VI) solution. The concentration of H_2O_2 is measured by Vasko's method, as presented in **Chapter 3** and **Chapter 4**. We note that this method is able to measure both concentrations of Cr(VI) and H_2O_2 simultaneously. The measurements are performed every 15 minutes by mixing 2 mL of the solution with 1 mL of 0.06 M NH_4VO_3. The H_2O_2 and Cr(VI) concentrations are calculated by comparing the absorbance of the solution with various calibration curves (as described in **annex 3.6**).

In order to validate the method for our experimental conditions, we compare the measurements of Cr(VI) concentration using Vasko's method with the results given by the ex situ direct method (**Chapter 6**). The highest deviation is about 15 %, which is acceptable (below the maximum uncertainty of [Cr(VI)] equal to 20%), the method is then validated. The details of the comparison can be found in **annex 7**.

7.1 Influence of the applied voltage

We change the applied voltage from 7 to 10 kV. The conditions used for this section are classical: the length of both platinum electrodes is HV-GND-0 with a diameter of 200 µm; Δt = 500 µs, f =50 Hz. The volume of the working solution is 100 mL, with the initial concentration of Cr(VI) equal to 47 mg/L (**Chapter 3**). The initial pH of the solution is 2.4, and the initial conductivity of the solution is about 4 mS/cm. We also perform the experiments for two different gaps (2 mm and 5 mm) to highlight the influence of the discharge properties on the production of H_2O_2 in Cr(VI) solution. We note that in this chapter, we first present the measurement results on [H_2O_2] for different conditions, then after the comparison and analysis are presented.

7.1.1 Influence of the applied voltage on H_2O_2 production for 2 mm gap

The concentrations of H_2O_2 and Cr(VI) are simultaneously monitored as a function of time. **Figure** 7.1 shows the time evolution of the concentrations obtained for three different applied voltages (7, 9, 10 kV). We obtain a relatively linear increase with time for the concentration of H_2O_2. More precisely, the evolution is almost linear for 9 and 10 kV, but for 7 kV, we first observe a plateau around 0.05 mM until 45 minutes before an almost linear increase of the [H_2O_2] concentration.

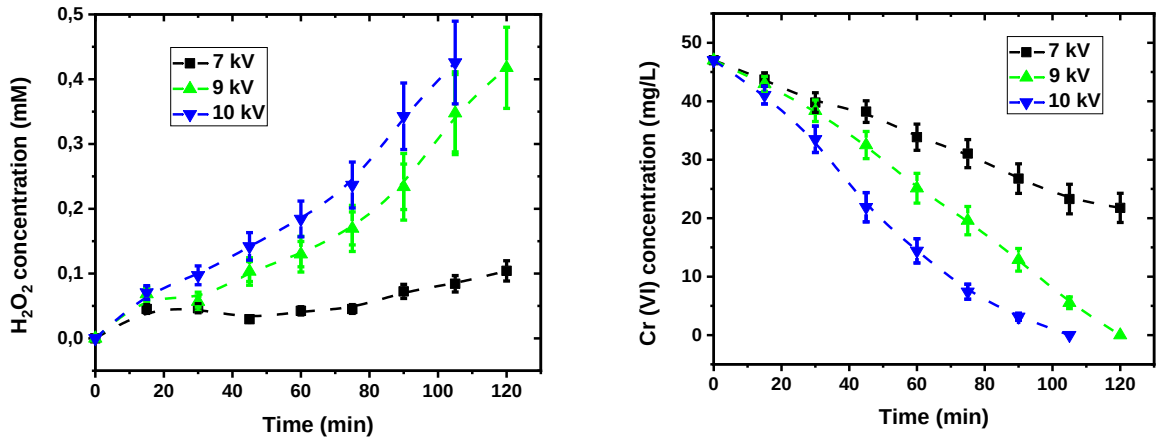

(a) (b)

Figure 7.1 The concentration of (a) H_2O_2 and (b) Cr(VI) as a function of time of a pin-to-pin discharge obtained in Cr(VI) solution (47 mg/L, σ = 4 mS/cm, pH = 2.4) for 7, 9, and 10 kV, V = 100 mL, Δt = 500 µs, gap = 2 mm, electrodes length = 0±10 µm, f = 50 Hz. The uncertainty of [H_2O_2] is 15 %.

Since the total time of the process is not the same, we compare the variations after 105 minutes instead of 120 minutes. The concentration of H_2O_2 is very low with the applied voltage of 7 kV (0.08 mM); it reached 0.35 mM when the voltage increased to 9 kV, and the value is the highest one (0.43 mM) when the discharge is performed at 10 kV. We can see that Cr(VI) concentration decreases when H_2O_2 increases and that efficient reduction of Cr(VI) is related to higher production of H_2O_2. However, at the moment, we cannot indicate a direct relation between [H_2O_2] increase and [Cr(VI)]

decrease; thus, here, we only present the observation results. For example, in the case of 7 kV, it is reported that the concentration of Cr(VI) decreases very slowly after 120 minutes, along with a very slow increase in [H_2O_2]. Whereas at 10 kV, the concentration of Cr(VI) decreases faster, and the concentration of H_2O_2 also increases faster. We note that [Cr(VI)] evolution is almost linear all along the process (no plateau effect). Finally, we can conclude that increasing the applied voltage leads to both effects simultaneously, *i.e.* an increase in the reduction of Cr(VI) and an increase in the H_2O_2 production.

In Section **5.6** of **Chapter 5**, we showed that the concentration of H_2O_2 produced in water at 9 kV (for the same experimental conditions and solution conductivity) is 0.6 mM after only 30 minutes. This value is much higher than 0.05 mM reported in this study after 30 minutes with the same applied voltage of 9 kV. This result is also found in the descriptions of Jiang *et al.*[4] obtained for pin-to-plate configuration. The authors have reported a concentration of H_2O_2 in water up to 7.2 mM after 18 minutes. However, these values decrease to 4.01 mM when the discharge is performed in Cr(VI).

In a first approach, we can assume that 0.55 mM of H_2O_2 has been used to reduce Cr(VI) from 47 to 40 mg/L (about 0.13 mM). This result is in agreement with [199] which showed "*practically that an excess of at least 10 times the [Cr(VI)] of H_2O_2 is required for effective reduction of aqueous Cr(VI)*".

In a second approach, due to the excess of H_2O_2 consumption compared to the stoichiometry of **Reaction 55** and **Reaction 57** involving $Cr_2O_7^{2-}$, $HCrO_4^-$ and H_2O_2, we can assume that H_2O_2 generated in the Cr(VI) solution is also related to many other processes. As an example, this process can be either the consumption of H_2O_2 by other reactions (*e.g.*, $H_2O_2 + 2H^+ + 2e \rightarrow 2H_2O$)[199] or the consumption of OH radical (which is the main species to produce H_2O_2 as presented in **Chapter 2**).

OH can be consumed to oxidize the low states of chromium into higher states[190,198] by the reactions[3]:

$Cr(III) + OH^o \rightarrow Cr(IV) + OH^-$ $\quad k = 3.8 \times 10^5\ M^{-1}s^{-1}$ **Reaction 58**

$Cr(V) + OH^o \rightarrow Cr(VI) + OH^-$ $\quad k = 1.5 \times 10^9\ M^{-1}s^{-1}$ **Reaction 59**

However, these oxidation reactions are mainly found in the pH of the solution above 7, as reported in the literature [3,4,190,198,260], which is not our case (pH of 2.4). Bokare *et al.*[260] have shown that the oxidation potential of Cr(VI) increases with the decrease of the solution pH; thus, the oxidation process of low states of chromium via hydroxyl radical is less important under an acidic medium.

By using pin-to-plate discharge configuration, Jiang *et al*[4]. also reported that the consumption of hydroxyl radical could occur because of the reaction with solvated electrons (e_{aq}^-.) by the following reaction:

$e_{aq}^- + OH^o \rightarrow OH^-$ $\quad k = 3 \times 10^{10}\ M^{-1}s^{-1}$ **Reaction 60**

As the rate constant of the reaction e_{aq}^- and OH^o ($3\times10^{10}\ M^{-1}s^{-1}$) is much higher than Cr(III) and OH^o ($3.8\times10^5\ M^{-1}s^{-1}$) and the linear evolution of Cr(VI) with time, as seen in **Figure 7.1** (b), we would

conclude that the oxidation process is not dominant under our conditions. Thus the hydroxyl radical is mainly consumed by the reaction with other species such as solvated electrons or recombination in the solution to produce H_2O_2, as presented in section **2.2.2**.

Table 7.1 shows the influence of the applied voltage on the production rate and the energy yield of H_2O_2 after 105 minutes. It is noted that the production rate increased from 2.7×10^{-4} g/h to 15×10^{-4} g/h when the applied voltage increased from 7 kV to 10 kV. We also obtained an increase of the energy yield from 2.4×10^{-5} g/kJ to 7.3×10^{-5} g/kJ with an increase of applied voltage from 7 kV to 9 kV. However, the energy yield is similar when the applied voltage increases from 9 kV to 10 kV since the total injected energy and the H_2O_2 concentration increase proportionally.

Applied voltage	**7 kV**	**9 kV**	**10 kV**
[H_2O_2] (mM) after 105 minutes	0.08	0.35	0.43
Number of BK/NOBK	1 / 99	15 / 85	25 / 75
Energy per pulse BK / NOBK (mJ)	28 / 36	42 / 54	51 / 73
Total Energy (kJ)	11.3	16.4	21.3
Production rate (g/h)	2.7×10^{-4}	12×10^{-4}	15×10^{-4}
Energy yield (g/kJ)	2.4×10^{-5}	7.3×10^{-5}	6.9×10^{-5}

Table 7.1 Influence of applied voltage on the formation of H_2O_2 by pin-to-pin discharge in Cr(VI) solution (47 mg/L, σ = 4 mS/cm, pH = 2.4) after 105 minutes. V = 100 mL, Δt = 500 µs, gap = 2 mm, electrodes length = 0±10 µm, f = 50 Hz

In the next section, we present the change of H_2O_2 concentration when the electrode gap is increased to 5 mm. From this, we can have further conclusions about the influence of the applied voltage on the reduction process of Cr(VI) based on the formation of H_2O_2.

7.1.2 Influence of the applied voltage on H_2O_2 production for 5 mm gap

We reported in **Chapter 5** that the concentration of H_2O_2 formed in water solution (low conductivity) without BK discharge is lower than in the case of BK discharge. In this section, we aim to study if we observe any change in H_2O_2 production without BK, *i.e.* when the gap is increased to 5 mm in Cr(VI) solution (high conductivity).

Figure 7.2 shows the time variation of Cr(VI) and H_2O_2 concentrations for different applied voltages at a 5 mm gap. We obtain different time evolutions in the formation of H_2O_2 during the treatment time according to the applied voltage. For all the studied applied voltages, [H_2O_2] shows the same evolution up to 45 min, but then some changes appear. For low values of the applied voltage (7 and 8 kV), [H_2O_2] remains constant (0.06 mM) from 15 minutes to the end of the process; for 9 kV, [H_2O_2] remains constant (0.08 mM) from 15 min to 90 min and then increases slightly, and finally for 10 kV, [H_2O_2] remains constant (0.06 mM) from 15 min to 45 min and then increases significantly.

Despite very different behaviors on [H_2O_2], we still observe a linear decrease of [Cr(VI)] (**Figure** 7.2(b)). It is noted that Cr(VI) is ongoing reduced for low voltages, whereas [H_2O_2] is constant at the beginning of the process (as also observed in section **7.1.1**)

The final concentration of H_2O_2 globally increases with an increase in applied voltage. For example, the final H_2O_2 concentration increases from 0.06 mM to 0.3 mM (after 120 minutes) when the applied voltage is increased from 7 kV to 10 kV. However, we find that the H_2O_2 production is similar ([H_2O_2] is about 0.06 mM after 120 minutes) when the applied voltage is increased from 7 to 8 kV.

Unlike 2 mm, the relationship between the reduction of Cr(VI) and the production of H_2O_2 is not clearly observed. The comparison is developed in **section 7.1.3**.

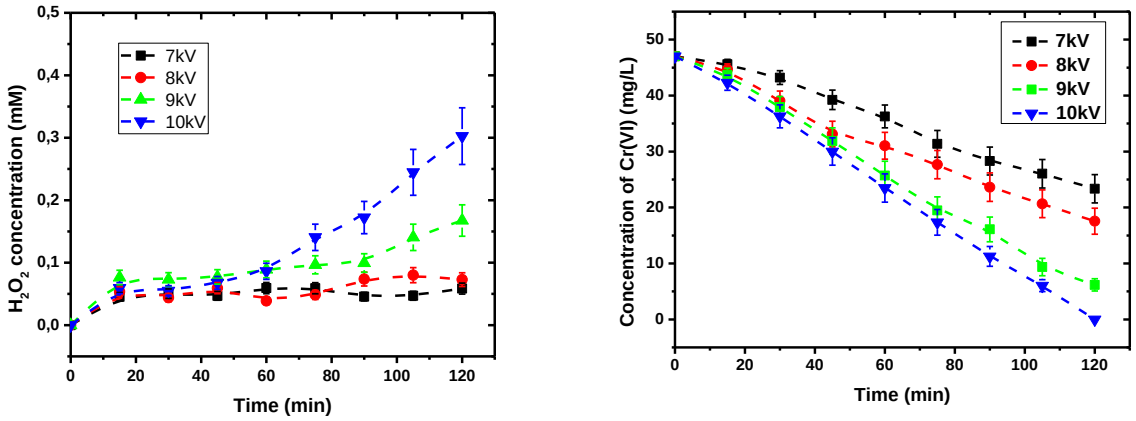

(a) (b)

Figure 7.2 The concentrations of (a) H_2O_2 and (b) Cr(VI) as a function of time of a pin-to-pin discharge obtained in Cr(VI) solution (47 mg/L, σ = 4 mS/cm, pH = 2.4) for 7, 8, 9, and 10 kV, respectively, V = 100 mL, Δt = 500 µs, gap = 5 mm, electrodes length = 0±10 µm, f = 50 Hz. The uncertainty of [H_2O_2] is 15 %.

Table 7.2 shows the influence of applied voltage on the production rate and energy yield of H_2O_2 with the discharge at a 5 mm gap. It is noted that increasing the total injected energy leads to an increase in the formation of H_2O_2 and the production rate. For example, we observe an increase in the total injected energy from 14.4 kJ to 25.6 kJ, while at the same time, the H_2O_2 concentration increases from 0.06 mM to 0.3 mM. This increase leads to an increase in the production rate from 2.1×10^{-4} g/h to 11×10^{-4} g/h.

We find that the variation in the total energy injected also leads to a change in the value of the energy yield. As we can summarize in **Table 7.2**, the total injected energy increases by about 43 % from 14.4 kJ to 25.6 kJ with the increase of applied voltage from 7 to 10 kV. Due to the increase of injected energy and [H_2O_2], we obtain an increase in the energy yield from 1.4×10^{-5} to 4×10^{-5} g/kJ, respectively.

Applied voltage	7 kV	8kV	9 kV	10 kV
[H_2O_2] (mM)	0.06	0.07	0.17	0.3
Number of BK/NOBK	0 / 100	0 / 100	0 / 100	0 / 100
Energy per pulse BK / NOBK (mJ)	0 / 40	0 / 46	0 / 56	0 / 71
Total Energy (kJ)	14.4	16.6	20.2	25.6
Production rate (g/h)	2.1×10^{-4}	2.4×10^{-4}	5.8×10^{-4}	1.1×10^{-3}
Energy yield (g/kJ)	1.4×10^{-5}	1.4×10^{-5}	2.9×10^{-5}	4×10^{-5}

Table 7.2 Influence of applied voltage on the formation of H_2O_2 by pin-to-pin discharge in Cr(VI) solution (47 mg/L, σ = 4 mS/cm, pH = 2.4) after 120 minutes. for 7, 8, 9, and 10 kV, respectively, V = 100 mL, Δt = 500 µs, gap = 5 mm, electrodes length = 0±10 µm, f = 50 Hz.

In this case, we can confirm that an increase in the input energy leads to an increase in the formation of H_2O_2, which is also presented in **Chapter 4** for pure water (low conductivity). But the increase of the energy yield involves that the total injected energy is not the only parameter that contributes to H_2O_2 production.

7.1.3 Comparison and analysis

Finally, we present a summary to illustrate the relationship of H_2O_2 formation with Cr(VI) reduction during the PLI process.

Figure 7.3 shows the relation of [Cr(VI)] with the [H_2O_2] for different applied voltages and for 2 and 5 mm gaps (measurements performed at 15, 45, 90, and 120 minutes). We show that the highest formation of [H_2O_2], the best reduction of [Cr(VI)]. We note a good agreement with the literature [4,5,248] that the reduction of Cr(VI) in an acidic environment increases when the concentration of H_2O_2 increases.

We also note that the relationship between [Cr(VI)] and [H_2O_2] is not linear. For example, Cr(VI) concentration decreases from 47 mg/L to about 20 mg/L despite very low H_2O_2 concentrations (less than 0.1 mM) for all conditions. In particular, for 7 kV half of the Cr(VI) is reduced after 120 minutes for both gaps, but the concentration of [H_2O_2] is equal to about 0.1 mM for 2 mm and 0.05 mM for 5 mm. Moreover, we can observe that [Cr(VI)] is completely removed when [H_2O_2] is about 0.3 mM at 10 kV and 5 mm gap, while in the case of 2 mm, the complete removal of Cr(VI) is achieved when [H_2O_2] is about 0.42 mM. These phenomena can be explained by the fact that H_2O_2 is not the only species involved in the reduction of Cr(VI).

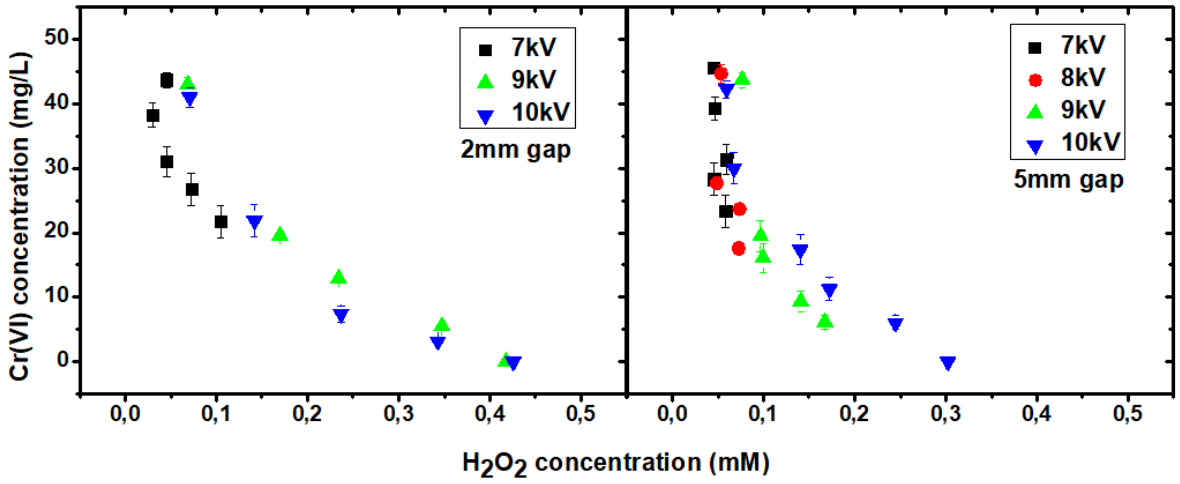

Figure 7.3 Concentration of Cr(VI) as a function of [H_2O_2] for different applied voltages and gaps by pin-to-pin discharge in Cr(VI) solution (47 mg/L, σ = 4 mS/cm, pH = 2.4). V = 100 mL, Δt = 500 µs, electrodes length = 0±10 µm, f = 50 Hz - measurements performed at 15, 45, 90 and 120 minutes

As presented in **Chapter 6**, the pulse duration is one of the parameters that have an influence on the reduction efficiency of Cr(VI), thus it is interesting to study the effect of the pulse width on the formation of H_2O_2 in Cr(VI) solution.

7.2 Influence of applied pulse duration

In this section, the applied pulse duration is varied, as presented in **section 6.3** of **Chapter 6**, from 10 µs to 1 ms, and we also study the effect for two different gaps of 2 mm and 5 mm. The same applied voltage of 9 kV is used for this study. The conditions used for this section are classical: the length of both platinum electrodes is HV-GND-0 with a diameter of 200 µm, f =50 Hz. The volume of the working solution is 100 mL, with the initial concentration of Cr(VI) being 47 mg/L (**Chapter 3**). The initial pH of the solution is 2.4, and the initial conductivity of the solution is about 4 mS/cm.

7.2.1 Influence of the pulse duration on H_2O_2 production for 2 mm gap

Figure 7.4 shows the effect of the pulse duration on the reduction of Cr(VI) and the production of H_2O_2 after 120 minutes of discharge at 9 kV and 2 mm gap. As we can see from **Figure 7.4**(a), the formation of H_2O_2 in case of short pulse duration (10 µs and 25 µs) is very low (<0.05 mM). We obtain a very different time evolution in the concentration of H_2O_2 during the treatment time when the pulse width increases from 100 µs to 1 ms. We observe three different groups on the concentration of H_2O_2, and their related values are given in **Table 7.3**:

- Group 1 (10-25 µs): The concentration is constant all along the process, we obtain a very low final concentration of H_2O_2 (<0.05 mM). The value of the production rate is 1.4×10^{-4} g/h, and the energy yield is 0.3×10^{-1} g/kJ.
- Group 2 (100-250 µs): The concentration is constant (0.06 mM) until 60 minutes, and then it increases linearly. The final concentration of H_2O_2 increases to 0.14 mM for the second group. The value of production rate is 4.8×10^{-4} g/h, and the energy yield is about 0.90×10^{-1} g/kJ.
- Group 3 (500 µs-1 ms): The concentration can be considered constant until 30 minutes (0.08 mM), and then it increases. This group presents the highest concentration of H_2O_2, about 0.42 mM. The value of production rate is 14×10^{-4} g/h, and the energy yield is about 2.7×10^{-1} g/kJ.

As previously, the relationship between [H_2O_2] and [Cr(VI)] is not obvious, except that the highest [H_2O_2] corresponds with the lowest [Cr(VI)]. We have previously discussed in **Chapter 6** that the concentration of Cr(VI) is similar until 30 minutes for all pulse durations. On the contrary, we observe that [H_2O_2] is very different during the first 30 minutes according to the pulse duration. Moreover, for groups 2 and 3 (100-250 µs and 0.5-1 ms), similar H_2O_2 concentrations are related to similar Cr(VI) concentrations; but for group 1 (10-25 µs), we obtain similar values for [H_2O_2] and different Cr(VI) reduction process.

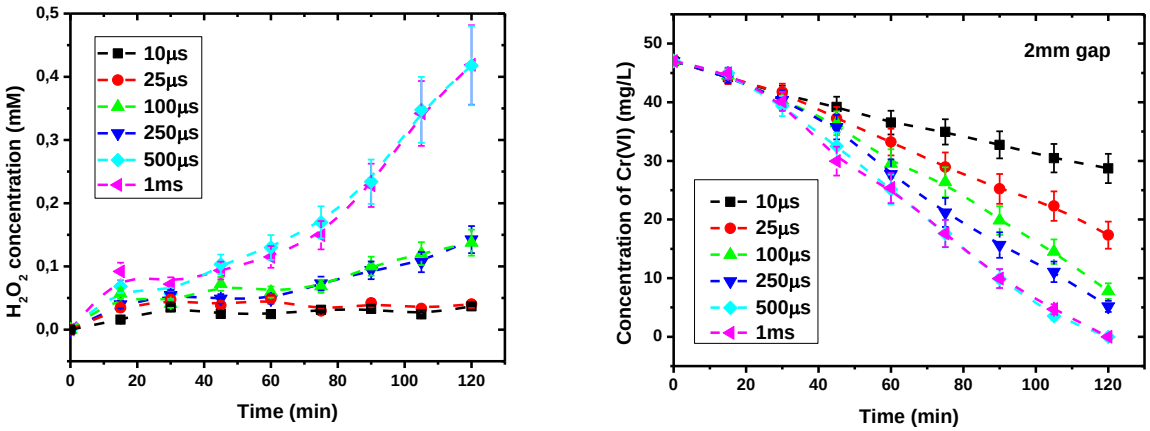

(a) (b)

Figure 7.4 The concentrations of (a) H_2O_2 and (b) Cr(VI) as a function of time of a pin-to-pin discharge obtained in Cr(VI) solution (47 mg/L, σ = 4 mS/cm, pH = 2.4) for different pulse durations after 120 minutes. U = 9 kV, V = 100 mL, gap = 2 mm, electrodes length = 0±10 µm, f = 50 Hz. The uncertainty of [H_2O_2] is 15 %,.

Table 7.3 summarizes the influence of duration on the formation of H_2O_2 in Cr(VI) by discharge at 9 kV.

Pulse duration	**Group 1**		**Group 2**		**Group 3**	
	10 µs	**25** µs	**100** µs	**250** µs	**500** µs	**1 ms**
[H_2O_2] (mM)	0.04	0.04	0.14	0.14	0.42	0.42
Number of BK/noBK	3 / 97	5 / 95	14 / 86	16 / 84	15 /85	15 / 85
Energy per pulse BK / noBK (mJ)	39 / 50	41 / 52	41 / 54	41 / 54	42 / 54	42 / 54
Total Energy (kJ)	18	18.6	18.2	18.7	18.8	18.8
Production rate (g/h)	1.4×10^{-4}	1.4×10^{-4}	4.8×10^{-4}	4.8×10^{-4}	14×10^{-4}	14×10^{-4}
Energy yield (g/kJ)	0.3×10^{-1}	0.3×10^{-1}	0.9×10^{-1}	0.9×10^{-1}	2.7×10^{-1}	2.7×10^{-1}

Table 7.3 Influence of pulse duration on the formation of H_2O_2 by pin-to-pin discharge in Cr(VI) solution (47 mg/L, σ = 4 mS/cm, pH = 2.4) after 120 minutes. U = 9 kV, V = 100 mL, gap = 2 mm, electrodes length = 0±10 µm, f = 50 Hz.

Considering these results, we can conclude that the concentration of H_2O_2 increases with the increase of pulse duration, and the duration from 250 µs to 500 µs reports the highest production of H_2O_2 in Cr(VI) solution. Moreover, the relationship between [H_2O_2] and [Cr(VI)] is not direct.

The following section investigates the influence of pulse duration on H_2O_2 formation for 5 mm gap.

7.2.2 Influence of the pulse duration on H_2O_2 production for 5 mm gap

Figure 7.5 shows the effect of the pulse duration on the reduction of Cr(VI) and the production of H_2O_2 after 120 minutes of discharge at 9 kV and 5 mm gap. As previously, the H_2O_2 production highlights three different groups (**Figure 7.5** (a)), we can obtain that the formation of H_2O_2 is almost zero for the discharge at the pulse durations of 10 µs and 25 µs; the final concentration increases to about 0.1 mM when the pulse width increases to 100 µs and 200 µs; we obtain the increase of H_2O_2 to 0.16 mM with the increase of pulse duration to 500 µs and 1 ms.

These results seem to show a relationship between [H_2O_2] and [Cr(VI)]. However, we cannot develop an argument to explain well these relationships. Indeed we observe the same three groups in **Figure 7.5**(b) that were obtained for 2 mm gap. The results also show that when [H_2O_2] increases, [Cr(VI)] decreases.

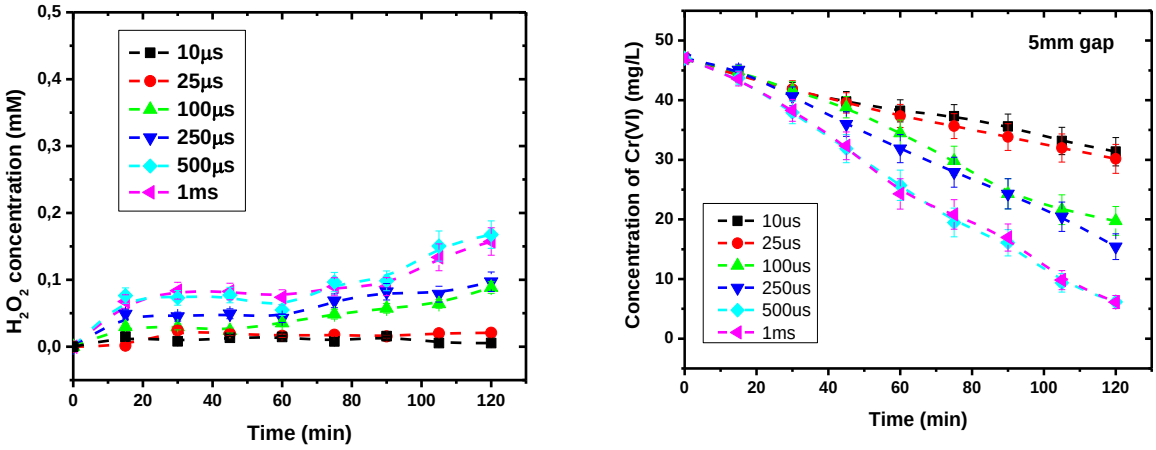

(a) (b)

Figure 7.5 The concentration of (a) H_2O_2 and (b) Cr(VI) as a function of time of a pin-to-pin discharge obtained in Cr(VI) solution (47 mg/L, σ = 4 mS/cm, pH = 2.4) for different pulse durations after 120 minutes. U = 9 kV, V = 100 mL, gap = 5 mm, electrodes length = 0±10 µm, f = 50 Hz. The uncertainties of [Cr(VI)] and [H_2O_2] are 20 % and 15 %, respectively

Table 7.4 shows the influence of pulse duration on the formation of H_2O_2 for the discharge at 9 kV and 5 mm of the gap. We obtain the same order of magnitude on the production rate and energy yield for each group. For example, the production rate is about 3.2×10^{-4} g/h for group 2 and 5.6×10^{-4} g/h for group 3, corresponding with the energy yield of about 1.7×10^{-5} g/kJ and 2.8×10^{-5} g/kJ, respectively.

Pulse duration	Group 1		Group 2		Group 3	
	10 μs	**25** μs	**100** μs	**250** μs	**500** μs	**1 ms**
[H_2O_2] (mM)	0.01	0.02	0.09	0.1	0.17	0.16
Number of BK/NOBK	0 / 100	0 / 100	0 / 100	0 / 100	0 / 100	0 / 100
Energy per pulse BK / NOBK (mJ)	- / 51	- / 52	- / 53	- / 54	- / 56	- / 56
Total Energy (kJ)	18.4	18.7	19.1	19.4	20.2	20.2
Production rate (g/h)	0.34×10^{-4}	0.7×10^{-4}	3.1×10^{-4}	3.4×10^{-4}	5.8×10^{-4}	5.5×10^{-4}
Energy yield (g/kJ)	0.2×10^{-5}	0.4×10^{-5}	1.6×10^{-5}	1.8×10^{-5}	2.9×10^{-5}	2.7×10^{-5}

Table 7.4 Influence of pulse duration on the formation of H2O2 by pin-to-pin discharge in Cr(VI) solution (47 mg/L, σ = 4 mS/cm, pH = 2.4) after 120 minutes. U = 9 kV, V = 100 mL, gap = 5 mm, electrodes length = 0±10 μm, f = 50 Hz

In the next part, we present the comparison and analysis of the influence of pulse duration in the formation of H_2O_2 in Cr(VI) solution and the relationship between [H_2O_2] and reduction of Cr(VI).

7.2.3 Comparison and analysis

We present a comparison to illustrate the effect of pulse duration on the formation of H_2O_2 for 2 mm and 5 mm gaps. **Figure 7.6** shows the final concentration of H_2O_2 as a function of pulse duration for the discharge at 2 and 5 mm gaps. We confirm that increasing the pulse duration for both conditions leads to an increase in H_2O_2 production.

As for Cr(VI) reduction, these variations seem to be not directly related to modifications of discharge characteristics. Indeed we have shown in **Chapter 4** (from electrical signals and shadowgraphy measurements) that changing the pulse width gives similar characteristics of the discharge whatever the discharge case (for BK and NOBK).

We observe two different behaviors according to the gap. In the case of 5 mm gap, the concentration of H_2O_2 increases slowly from near zero up to 0.16 mM due to the increase of pulse duration from 10 μs to 1 ms. Whereas in the case of discharge at a 2 mm gap, the concentration of H_2O_2 increases with three different stages, as shown in **Figure 7.6**. In particular, we obtain a significant change in the H_2O_2 concentration when the pulse duration increases from 250 μs to 500 μs. However, we note that this hypothesis requires further investigation due to the different plasma types (the configuration and properties of the discharge) and pulse durations. As for Cr(VI) reduction, we observe that 2 mm gap is more efficient for H_2O_2 production than 5 mm (**Chapter 6**, **Figure 15**). But unlike the evolution of Cr(VI), we do not observe a different behavior at 25 μs between 2 and 5 mm, the main differences occur at 100 μs and 500 μs.

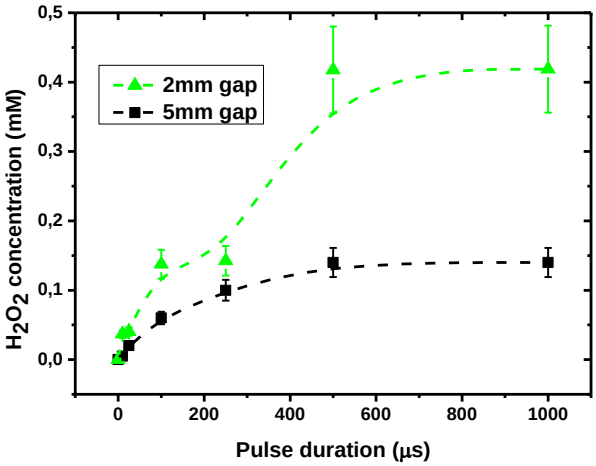

Figure 7.6 Concentration of H_2O_2 versus pulse duration for 2 and 5 mm gap of a pin-to-pin discharge obtained in Cr(VI) solution (47 mg/L, σ = 4 mS/cm, pH = 2.4) after 120 minutes. U = 9 kV, V = 100 mL, electrodes length = 0±10 µm, f = 50 Hz. The uncertainties of [H_2O_2] is 15 %

In order to analyze the relationship between both species, **Figure 7.7** shows the Cr(VI) concentration according to [H_2O_2] for different pulse durations for 2 and 5 mm gaps (measurements performed at 15, 45, 90 and 120 min are reported).

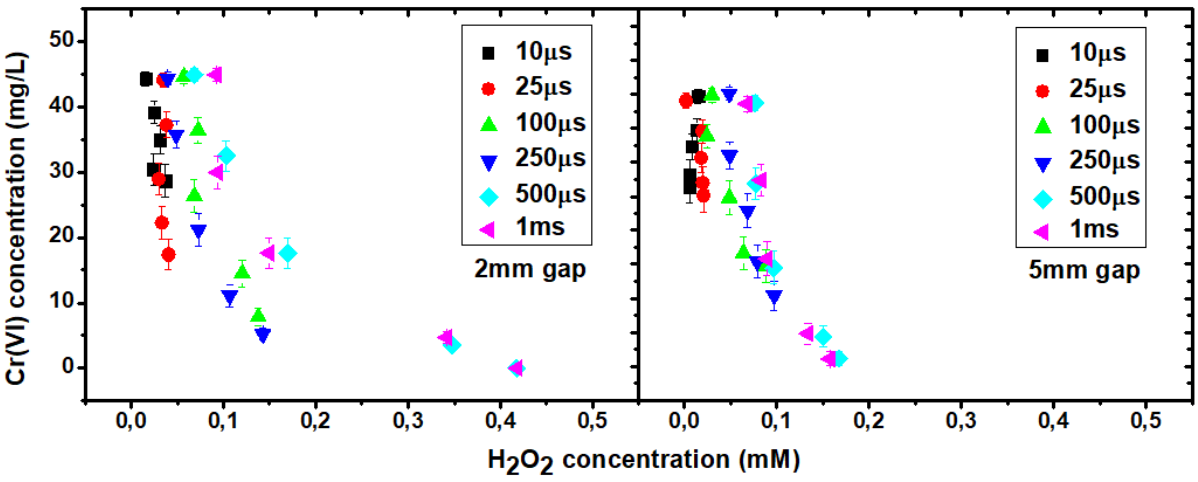

Figure 7.7 Cr(VI) concentration as a function of H_2O_2 formation by pin-to-pin discharge in Cr(VI) solution (47 mg/L, σ = 4 mS/cm, pH = 2.4) for different pulse durations and gaps. U = 9 kV, V = 100 mL, electrodes length = 0±10 µm, f = 50 Hz - measurements performed at 15, 45, 90 and 120 minutes are reported

Surprisingly, the results are similar to the results in section **7.1.3**, suggesting that decreasing the pulse duration involves similar effects on the chemistry as decreasing the applied voltage. We obtain the highest formation of [H_2O_2], the best reduction of [Cr(VI)]. However, we also note that the

relationship between [Cr(VI)] and [H_2O_2] is not linear for a given condition. For example, Cr(VI) concentrations decrease from 47 mg/L to about 20 mg/L despite very low H_2O_2 formation concentrations of less than 0.1 mM for all conditions. On the other hand, for 5 mm gap, we can observe that [Cr(VI)] is decreased about 87 % when [H_2O_2] is about 0.15 mM (at the pulse duration of 500 µs and 1 ms), while in the case of 2 mm, the complete removal of Cr(VI) is achieved when [H_2O_2] is about 0.42 mM.

The effect of pulse duration on the chemical activity of a solution for discharge in liquid has been reported in the literature. The results strongly depend on the nature of the solution and the pollutant. For example, Kawano *et al*[257]. have shown that, in their conditions, the energy efficiency for decolorization of an organic dye by pulsed discharge increased with decreasing the pulse width (from 1200 to 10 ns).

7.3 Conclusion

We have measured the concentration of H_2O_2 and Cr(VI) simultaneously by using NH_4VO_3 as a reagent during the PLI process for different experimental conditions.

This study was performed to better understand the reduction process of Cr(VI)by electrical discharge. The analytical method is based on measuring the absorbance at 440 nm of the complex formed by the reaction of H_2O_2 and NH_4VO_3. Using this method, we successfully measured the concentration of Cr(VI) and H_2O_2 simultaneously during the treatment process. We also study the influence of some physical parameters such as applied voltage and pulse duration on the formation of H_2O_2 in Cr(VI) solution. In general, we observe that when the Cr(VI) concentration is reduced more, the H_2O_2 concentration is produced more. We also show that for the same experimental conditions, $[H_2O_2]$ measured in Cr(VI) solution is about ten times lower than in water solution.

The first parameter varied in this work is the voltage that is changed from 7 to 10 kV for different inter-electrodes gaps (2 mm and 5 mm). The concentration of H_2O_2 is increased with an increase in the applied voltage. We also obtained that the concentration of H_2O_2 is higher when the discharge is performed at 2 mm than at 5 mm gaps.

The second parameter concerns the influence of the pulse duration from 10 µs to 1 ms at a fixed applied voltage of 9 kV for different inter-electrodes gaps of 2 mm and 5 mm. In general, we observed that the concentration of H_2O_2 is increased with an increase of pulse duration for a given gap. In addition, we obtained three different groups based on H_2O_2 production: the first group corresponds to the pulse width of 10 µs and 20 µs with the lowest production concentration of H_2O_2. The second group shows the increase in the concentration formation at a pulse duration of 100 µs and 250 µs, and the last group shows the highest value of H_2O_2 concentration when the pulse duration increases to 500 µs and 1 ms. Due to the very low production of H_2O_2 for the discharge at the pulse duration of 10 µs and 25 µs, it is proved that Cr(VI) can be reduced by the other species produced by the PLI method as the solvated electron or H^0 radical.

The comparison of the experiments suggests that the variation of pulse duration and applied voltage involves a similar global effect on the solution chemistry during 120 minutes regarding both the production of H_2O_2 and the Cr(VI) reduction.

Even though H_2O_2 is not the main factor leading to the reduction of Cr(VI) in the plasma process, however, studying the formation of H_2O_2 in the Cr(VI) solution still contributes to better understanding the reduction process of Cr(VI) by the PLI method.

Chapter 8
Conclusion & perspectives

The main objective of this thesis is to develop and optimize a plasma liquid immersion (PLI) process with a focus on the reduction of Cr(VI). However, this project is also multidisciplinary, so it involves very different subjects. For example:

- Chemical measurement such as H_2O_2, OH, Cr(VI) concentration to understand the discharge properties and reduction process.
- A lot of optical diagnostics such as Uv-vis absorption spectroscopy, Ombroscopy, diode absorption spectroscopy
- The plasma physics process includes the discharge characteristics, electrical measurements, and the electrode's erosion.

As presented previously, the experimental setup is based on pin-to-pin immersed electrodes with small diameters (100-200 µm). Based on this experimental setup, several studies were performed.

8.1 Characterization of the discharge

This work presents the characterization of pin-to-pin discharge in aqueous liquids using electrical and shadowngraphy measurements. Two solutions were considered: water (with NaCl or H_2SO_4) and Cr(VI) aqueous solution (47 mg/L, pH=2.4, σ=4 mS/cm). By comparing the electrical signal, the injected energy, and the discharge characteristics, it is shown that **the conductivity and the nature of the electrolyte involve changes but not the presence of Cr(VI).**

The conductivity has an influence on the structure of the discharge. For low conductivity (water, 200 µS/cm), three different types of discharge have been identified: case 1 (cathode regime – no breakdown), case 2 (cathode regime – breakdown), and case 3 (anode regime – breakdown). Whereas for discharge with high conductivity (water and Cr(VI), at 4 mS/cm), we found that there are only two different cases: NOBK (without breakdown) and BK (with breakdown). In the case of BK, the filament propagate mainly from the anode to the cathode.

The comparison between the number of discharges with and without shows that both the conductivity and the electrolyte have an effect, but a similar distribution of BK/NOBK (30/70) is obtained with and without Cr(VI).

A more dedicated study has been performed on **Cr(VI) solution**. It has been seen that the applied voltage is one of the most critical parameters that have a much more significant effect on the

discharge characteristics, including the change in the current and in the number of BK and NOBK. Increasing the gap leads to a less intense glow at the electrodes and a lower maximum current (charge injection). Finally, the applied pulse width has no significant effect on the discharge characteristics, both for the cases without and with breakdown. The only significant difference is the presence or absence of a secondary breakdown.

8.1.1 Pulse plasma discharge in water

This work contributes to a better understanding of pin-to-pin micro-pulsed discharge in water. Two complementary approaches are present: chemical analyses with H_2O_2 production after the discharge and the discharge mechanisms due to the electrode erosion.

8.1.2 H_2O_2 production

The study of H_2O_2 concentration is the first step to investigate the complex chemical activities in the solution after plasma discharge. The generation of hydrogen peroxide in water by pin-to-pin microsecond pulsed discharge has been investigated by using colorimetric methods based on the reaction of H_2O_2 with titanyl ions and NH_4VO_3. The study shows that hydrogen peroxide production by the discharge depends mainly on the input energy, the case of the discharge (propagation from cathode or anode), and the solution conductivity. The hydrogen peroxide concentration increases linearly with the input energy and also increases between case 1, case 2, and case 3. However, the concentration of H_2O_2 decreases with the increase of solution conductivity. We estimated the energy yield of H_2O_2 production, and **the maximum value of 1.3×10^{-3} g/kJ** was obtained for case 3 (anode regime – breakdown) at 200 µS/cm.

The study of the electrode properties shows that the concentration of H_2O_2 formation does not depend on the electrodes' material, length, and diameter.

8.1.3 Electrode erosion

It is reported that the erosion processes are strongly dependent on the discharge characteristics, electrode material, and electrodes' polarity. In case 1, the dominant process of electrode erosion is electrochemistry (anodic oxidation followed by electrolyte dissolution), which is significant only at the anode. In cases 2 and 3, this process is no more effective, but thermal processes dominate the erosion process.

The H_2O_2 measurements and the erosion study highlight very different mechanisms involved in the discharge depending on the case.

8.2 Pulse plasma discharge in Cr(VI) solution

The working Cr(VI) solution is composed of 50 mg/L Cr(VI) with the H_2SO_4 0.1 M and no further addition of chemical compounds. Thus the initial concentration of the Cr(VI) working solution is 47 mg/L with conductivity is about $\sigma = 4$ mS/cm and pH = 2.4.

8.2.1 Reduction of Cr(VI)

From the first study of the electrode geometry, we showed that the electrodes configuration of HV-GND-0 µm (length) and Ø = 200 µm with the use of platinum material is the best configuration to study the reduction of Cr(VI) by PLI process, and this electrode geometry is used along with this thesis.

Then our study mainly focused on the physical parameters for the reduction Cr(VI) process and included the following parameters: applied voltage, the inter-electrode distance, pulse frequency, and pulse duration. From this parametrical study, it was shown that:

- **The reduction efficiency of Cr(VI) increases with an increase of the applied voltage from 2 to 12 kV for 2 mm gaps and from 7 kV to 10 kV for 5 mm gaps**. At the same applied voltage, the reduction efficiency of Cr(VI) is higher at 2 mm than at 5 mm, which is due to the presence of BK. Thus the process should be accomplished in the presence of BK to achieve the high efficiency of Cr(VI) treatment. **At an applied voltage of 12 kV with a gap of 2 mm, Cr(VI) is completely degraded more rapidly after 70 minutes**. However, this condition is not an excellent economic point of view due to the high energy consumption and especially the destruction of materials such as electrodes and capillaries.
- **The complete reduction of Cr(VI) occurs more rapidly when the inter-electrode distance is decreased from 5 mm to 0.5 mm**. Complete Cr(VI) reduction occurs more rapidly when the interelectrode gap is reduced from 5 mm to 0.5 mm. However, reducing the electrode gap also leads to faster damage of capillary and electrode erosion.
- Investigation of the effect of pulse frequency on the reduction efficiency of Cr(VI) is not possible over a wide range due to equipment limitations. The change in applied pulse frequency is only from 10 to 70 Hz for the applied voltage of 8 kV and from 10 to 50 Hz for 9 kV. **The reduction of Cr(VI) is similar for the same number of pulses**, but the decrease in pulse frequency must be compensated by an increase in discharge time over several hours. **Therefore, the low frequency (< 50Hz) is not suitable for the treatment process in our work**.

  As the final parameter, the results show that the Cr(VI) reduction is increased with increasing the pulse duration from 10 µs to 1 ms for both 2 and 5 mm gaps, although the injected energy is almost the same. **This presents a new challenge for future studies to**

better understand the post-discharge phase's influence on the reduction of Cr(VI) by the PLI process.

- **We have shown that the presence of breakdowns favors the Cr(VI) reduction, but it seems that the effect of the breakdown is delayed since the reduction is more efficient during the post-breakdown.**
- **We also showed no chemical activity in the time off between two pulses, the final solution conductivity is more decreased when the reduction is increased may due to the reaction of (Cr(III) with the sulfate ions).** We also observed the blue-black precipitates appearing at the bottom of the reactor after the treatment, which may correspond to a kind of Cr(III)-sulfate**. The pH of the solution is slightly increased due to the consumption of hydronium ions to reduce Cr(VI). However**, this variation is not huge since we do not observe the significant change after the process.

8.2.2 Production of H_2O_2 in Cr(VI) solution

The study of the formation of H_2O_2 in Cr(VI) solution aims to identify the relationship between the variations of [H_2O_2] and [Cr(VI)], in order to better understand the mechanisms responsible for the reduction process of Cr(VI). The analytical method is based on measuring the absorbance at 440 nm of the complex formed by the reaction of H_2O_2 and NH_4VO_3. The results have shown that we successfully measured the concentration of Cr(VI) and H_2O_2 simultaneously during the treatment process.

These results also showed a relationship between H_2O_2 and Cr(VI) concentrations: when Cr(VI) is more reduced, H_2O_2 is more produced. However, we also found that H_2O_2 is not the only factor leading to reducing Cr(VI) during the PLI process.

8.3 Improvement of the detection method

Finally, in the frame of the second aim of this work, we develop a new optical system for real-time and *in situ* analysis of Cr(VI) concentrations during the treatment process. The principle of this method is based on the measurement of the transmitted power of incoming light through the Cr(VI) solution and follows the Beer-Lambert law. We noted that **we successfully measured *in situ* the concentration of Cr(VI) in real-time and with this new system**. Moreover, the other advantage of this method is to indicate precisely when Cr(VI) is completely reduced. This campaign has studied two different path lengths of 5 cm and 10 cm. We concluded that a path length of 5 cm is appropriate for *in situ* measurements of Cr(VI) concentration in our experimental configuration. We have found that at low Cr(VI) concentrations, the use of 10 cm path length for the *in situ* measurements proves to be effective.

8.4 Outlook

From the results presented, it can be concluded that pulsed electrical discharges in liquids promise a novel technique for water and wastewater treatment, especially for the removal of Cr(VI) pollutants. The main advantage of this system is the direct generation of reactive species within the pollutant solution, resulting in high efficiency as the reactive species can react directly with the pollutant.

However, more studies are required to better understand the reduction process. For example, the pulse duration influences the reduction efficiency, but the mechanism is still not completely understood. Therefore, more accurate measurements of discharge properties in the liquid phase and the mechanism of initiation and propagation of streamer discharge during the process are needed to better understand the effect. For example, an optical emission spectrometer is required to identify the excited species.

In addition, the study of the reactive species formed in the solution after plasma discharge is also one of the goals to be achieved. The study of reactive species such as OH can support a better understanding of the plasma processes in solution and, in particular, the influence on the reduction process of Cr(VI) by the PLI method.

Moreover, additional study is required to develop the system to improve the process to make it cheaper and scale it up to be competitive with conventional methods.

For example, some of the problems remain in our system:

- The electrode erosion during the process
- The volume of the reactor is small
- The reactive zone is small due to the small channel between two electrodes

To solve these problems, some of the solutions are present:

- By changing the electrode configuration to enable the chromium plating of metal surfaces during the chromium(VI) reduction process. Thus can avoid the damage of the electrodes and capillary during the treatment process.
- By changing to the use of multi electrodes and a cycler reactor in order to increase the reactor volume
- By allowing a gas flow through of the electrodes to promote the production of reducing species in the reactive zone.

Annex

Annex Chapter 3

Calibration curves for chemical analysis

This appendix presents how to calculate the concentrations of substances such as Cr(VI), H_2O_2, and OH by using a calibration curve. We note that by following the literature [201], we calculate the calibration curves' statistical treatment random errors (for all of the measurements by UV-vis measurement).

Annex 3.1: Concentration of Cr(VI) by Direct ex situ measurement

It is based on the original color of Cr(VI) ions at the wavelength of 350-375 nm. The absorbance is measured using an Avaspec DHC2048XL spectrometer. A cuvette with a path length of l cm is used to measure the absorbance of the samples.

Preparation of standard Cr(VI) solution

The Cr(VI) stock solutions are prepared by dissolving a given amount of potassium dichromate in distilled water: 50 mg/L Cr (VI) ions are prepared by dissolving 0.1414 g (±2 %) of potassium dichromate ($K_2Cr_2O_7$) in distilled water, and the volume is made up to the mark with distilled water in a 1 L volumetric flask.

The calibration curve of Cr(VI) is made from solutions with concentrations ranging from 1 to 47 mg/L in an acidic environment. The 47 mg/L Cr(VI) standard solution is prepared by mixing 94 mL of 50 mg/L Cr(VI) stock solution with 6 mL of acid H_2SO_4 0.1 M. The working range of the Cr(VI) solution is shown in **Table A 1**

Analysis with UV-Vis spectroscopy

We remind that, in this work, the treatment of Cr(VI) by the PLI is completed in an acidic medium, so it should be considered in the protocol for the calibration curve (blank solution). The blank reference is obtained by mixing 1.88 mL of H_2O + 0.12 mL of H_2SO_4. The volume of sulfuric acid is calculated to have the same concentration of sulfuric acid as used in the working solution of Cr(VI). The calibration curve is performed by measuring the absorbance at 350 nm for 2 mL of each solution containing different Cr(VI) concentrations. The final absorbance value is calculated as the average of 3 measurements for each concentration.

Results

The results of 3 different measurements and the average are shown in **Table A 1**. We present the uncertainty of standard Cr(VI) solutions concentration and the standard deviation error of three different measurements. The maximum uncertainty value of 0.1 % would represent the high accuracy of the Avaspec DHC2048XL spectrometer.

[Cr(VI)] mg/L	Absorbance at 350 nm				Standard deviation	Uncertainties %
	Time 1	Time 2	Time 3	Average		
1.00 ± 0.03 (0.6%)	0.02524	0.02523	0.02519	0.02522	2.6E-05	0.1
5.00 ± 0.03 (0.6%)	0.1524	0.1526	0.1525	0.1525	1.00E-04	0.07
10.00 ± 0.06 (0.6%)	0.304	0.3041	0.3039	0.3040	1.00E-04	0.03
20.00 ± 0.12 (0.6%)	0.6054	0.6055	0.6057	0.6055	1.53E-04	0.03
30.00 ± 0.18 (0.6%)	0.8891	0.8890	0.8892	0.8891	1.00E-04	0.01
40.00 ± 0.24 (0.6%)	1.1968	1.1962	1.1967	1.1966	3.21E-04	0.03
47.00 ± 0.28 (0.5%)	1.4143	1.4141	1.4142	1.4142	1.00E-04	0.01

Table A 1 Absorbance at 350 nm of different concentrations of Cr(VI)

Figure A 1 shows the linear relationship existing between the concentrations of Cr(VI) solution and its absorbance.

The linear equation is: Y = 33.4 X + 0.1 with a correlation factor R^2 = 0.9999; with Y, the Cr(VI) concentration, and X the absorbance of the solution.

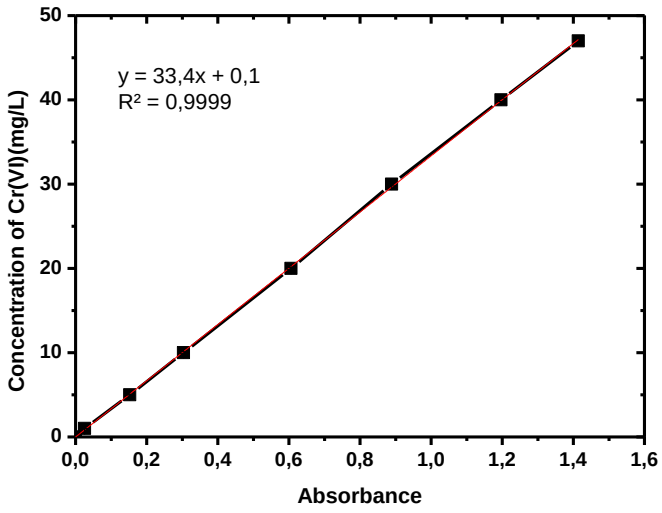

Figure A 1 Calibration curve of different concentrations of Cr(VI) at 350 nm. The uncertainty of [Cr(VI)] (1 %) is not discernable

Annex 3.2: Concentration of Cr(VI) by Indirect ex situ measurement

This method is based on the measurement of the absorbance of the complex of Cr(VI) with DPC in an acidic environment. The absorbance is measured as its maximum, obtained at 540 nm. This method is used to measure the concentration of Cr(VI) below ***1 mg/L.***

The absorbance is measured using an Avaspec DHC2048XL spectrometer. A cuvette with a path length of l cm was used to measure the absorbance of the samples.

Preparation of standard Cr(VI) solution

The calibration curve of Cr(VI) is made from 0.1 to 1 mg/L in an acidic environment. The Cr(VI) solutions are prepared by dilution with distilled water from the 47 mg/L standard solution (94 mL of 50 mg/L Cr(VI) solution with 6 mL of acid H_2SO_4 0.1 M). We prepare a series of Cr(VI) solutions of different concentrations of: 0.1; 0.2; 0.4; 0.6; 0.8; 1 mg/L.

Analysis with UV-Vis spectroscopy

The blank reference is obtained by mixing 2 mL H_2O + 0.1 mL H_2SO_4 0.1 M + 0.1 mL DPC 0.02 M. The volume of sulfuric acid is calculated to have the same concentration of sulfuric acid as used as the working solution of Cr(VI). In order to be sure that all the Cr(VI) ions present in the solution react with the DPC, the volume of DPC used is chosen to have an excess concentration according to the reaction stoechiometry.

The calibration curve is performed by measuring the absorbance at 540 nm of 2 mL of each solution containing different Cr(VI) concentrations + 0.1 mL H_2SO_4 0.1 M and + 0.1 mL DPC 0.02 M. After mixing the complex, we let it stand for 15 minutes to develop the resulting complexe. The final absorbance value is calculated as the average of 3 measurements for each concentration.

Results

The results of 3 different measurements and the average is shown in **Table A 2**.

[Cr(VI)] mg/L	**Absorbance at 540 nm**				**Standard deviation**	**Uncertainty %**
	Time 1	Time 2	Time 3	Average		
0.10 ± 0.01 (3 %)	0.0728	0.07271	0.07311	0.0728	2,10E-04	0.3
0.20 ± 0.01 (3 %)	0.1463	0.1467	0.1465	0.1465	2,00E-04	0.1
0.40 ± 0.01 (3 %)	0.2893	0.2911	0.2914	0.2890	1,14E-03	0.4
0.60 ± 0.02 (3 %)	0.4428	0.4363	0.4355	0.4376	4,00E-03	0.9
0.80 ± 0.02 (3 %)	0.5649	0.5614	0.5592	0.5612	2,87E-03	0.5
1.00± 0.03 (3 %)	0.70887	0.7108	0.7092	0.7094	1,03E-03	0.1

Table A 2 Absorpbance at 540 nm of the complex of different concentrations of Cr(VI) with DPC

Figure A 2 shows the linear relationship existing between the concentrations of Cr(VI) solution and its absorbance.

The linear equation is: Y = 1.41 X + 0.01 with a correlation factor R^2 = 0.9996, with Y the Cr(VI) concentration, X the absorbance of the solution.

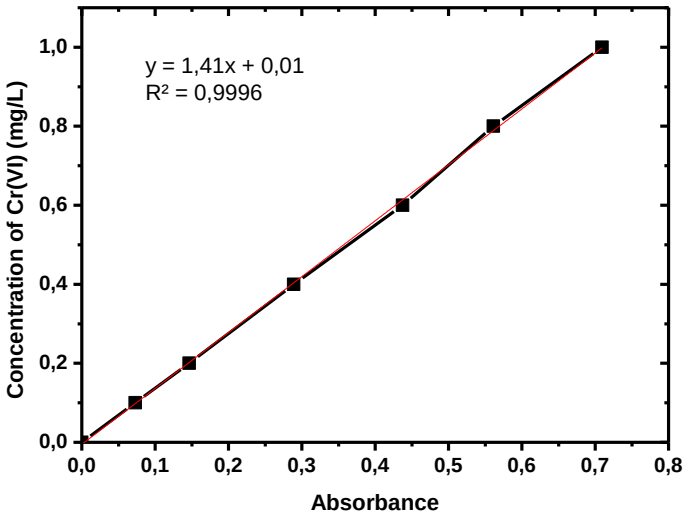

Figure A 2 Calibration curve of different concentrations of Cr(VI) at 540 nm. The uncertainty of [Cr(VI)] (3 %) is not discernible

Annex 3.3: Concentration of Cr(VI) by *in situ* measurement

The principle of this method is based on the changes in the transmitted power of incoming light through the Cr(VI) solution during the treatment process.

Preparation of standard Cr(VI) solution

A solution of concentration ~100 mg/L Cr (VI) ions is prepared by dissolving 0.2828 g (±2%) potassium dichromate ($K_2Cr_2O_7$) in distilled water, and the volume is made up to the mark with distilled water in a 1 L volumetric flask.

To make the calibration curve using this method, we measure the absorbance over a wide range of different concentrations of Cr(VI) from 1 to 50 mg/L. The 100 mL of the working solution is prepared from a ~100 mg/L stock solution mixing with acid H_2SO_4 0.1 M.

Samples and data process

a) Samples

The 100 mL of the working solution is transferred into the rectangular quartz vessel (10×5×5 cm). In this study, we present two different calibration curves corresponding to two different path lengths of the reactor: 10 cm (the length of the reactor), and 5 cm (the width of the reactor), respectively. We note that the path length of the reactor in this work corresponds with the distance traveled by the light.

b) Data processesing

In contrast to the direct measurement of the absorbance of Cr(VI) solutions with a spectrophotometer, the method for *in situ* measurements of the concentration of Cr(VI) solutions is based on the change in the power of the transmitted light. It is noted that the LED should be switched on 15 minutes before starting the measurement to ensure stability. Although the mechanism is related to Cr(VI) absorption, this method requires several steps to obtain the final result:

- We measure the initial power of the laser light going through the solution of water + acid H_2SO_4 0.1 M (as a reference intensity) I_0 (µW)
- We measure the power of three different acquisitions with the same Cr(VI) solution. For example, **Figure A 3** shows three Cr(VI) measurements at 1 mg/L that give very similar results (variations lower than 1 %). Since power is recorded as a function of time, we need to calculate an average value of each measurement's output power.

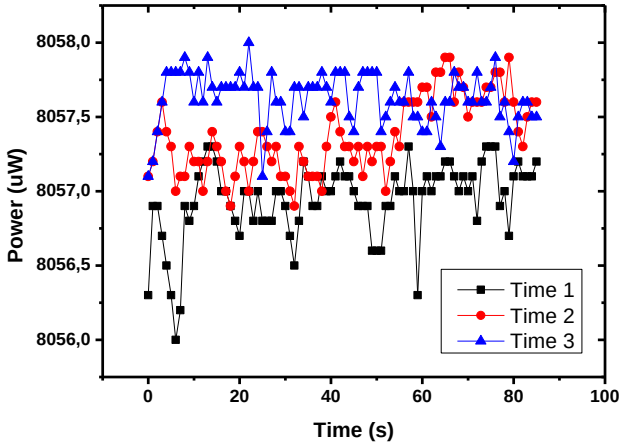

Figure A 3 Three different measurements with the same concentration of Cr(VI) (1 mg/L)

- The final value I is calculated as the average of 3 measurements for each concentration.
- The absorbance value is calculated by following the equation Equation A 1:

$$A = -\log_{10} T = \log_{10} \frac{I}{I_0} \qquad \textbf{Equation A 1}$$

I_0 (µW) is the power of incoming light (measured in water solution), and I (µW) is the power of light after passing through the Cr(VI) solution.

Results

- ***10 cm path length***

Table A 3 shows the values of output power and absorbance after the calibration process for different solutions of concentrations of Cr(VI) from 1 – 50 mg/L in a 10 cm path length reactor. It is worth noting that the I_0 = 8150 µW is used to calculate the transmittance (T) and the absorbance (A). The uncertainty calculated by standard deviation is below 1 %, then it is not presented.

Figure A 4 and **Figure A 5** show the relation between absorbance and Cr(VI) solutions in two different concentration ranges. Linearity is observed between 1 and 10 mg/L (**Figure A 4)**, defining the validity interval of the Beer-Lambert law. The linear equation is Y = 5.45X + 0.85 with a correlation factor R^2 of 0.9967.

Figure A 5 shows that a non-linear behavior is observed between 10 and 50 mg/L, which is certainly related to the high absorbance of these solutions, meaning that the Beer-Lambert law is not valid at these high concentrations. The non-linear equation can be given by $Y = 2.32\times10^{-5} \times . e^{\frac{x}{0.19072}} + 9.84$ with a correlation factor R^2 of 0.99947

Concentration (mg/L)	Time 1 (µW)	Time 2 (µW)	Time 3 (%W)	Average (µW)	T	Abs
1.00 ± 0.01 (1 %)	7184.0	7185.0	7187.0	7185.3	0.8819	0.05460
2.00 ± 0.02 (1 %)	5578.0	5577.0	5578.0	5577. 7	0.6845	0.1646
3.00 ± 0.03 (1 %)	3418.0	3425.0	3430.0	3424.3	0.4202	0.3765
4.00 ± 0.04 (1 %)	2071.0	2071.0	2072.0	2071.3	0.2541	0.5950
5.00 ± 0.05 (1 %)	1277.0	1279.0	1280.0	1278. 7	0.1569	0.8043
10.0 ± 0.1 (1 %)	177.20	177.30	177.50	177.3	0.02177	1.6622
15.0 ± 0.2 (1 %)	56.50	56.50	56.60	56.5	0.00694	2.1589
20.0 ± 0.2 (1 %)	32.10	32.10	32.10	32.1	0.00394	2.4046
25.0 ± 0.3 (1 %)	23.60	23.60	23.60	23.6	0.00289	2.5384
30.0 ± 0.3 (1 %)	19.60	19.60	19.70	19.6	0.00241	2.6182
35.0 ± 0.4 (1 %)	17.50	17.50	17.50	17.5	0.00215	2.6681
40.0 ± 0.4 (1 %)	16.20	16.20	16.20	16.2	0.00199	2.7015
45.0 ± 0.5 (1 %)	15.40	15.40	15.40	15.4	0.00189	2.7235
50.0 ± 0.5 (1 %)	14.90	14.90	14.90	14.9	0.00183	2.7380

Table A 3 Absorbance of different concentrations of Cr(VI) measured in 10 cm path length.

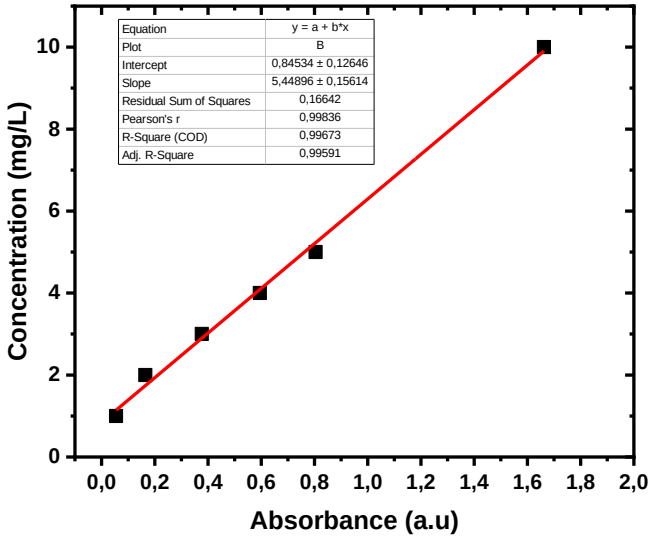

Figure A 4 Standard curve of Cr(VI) in range 1 - 10 mg/L. Measured in 10 cm path length reactor. The uncertainty of [Cr(VI)] (1 %) is not present.

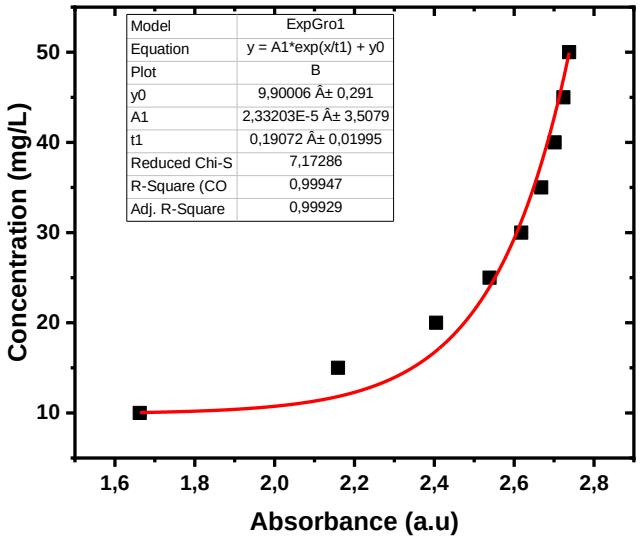

Figure A 5 Standard curve of Cr(VI) in range 10 - 50 mg/L. Measured in 10 cm path length reactor. The uncertainty of [Cr(VI)] (1 %) is not present

- ***5 cm path length***

Table A 4 shows the values after the calibration process for different concentrations of Cr(VI) from 1 – 50 mg/L. It is worth noting that the I_0 = 8697 µW is used to calculate the transmittance (*T*) and the absorbance (A). The uncertainty calculated by standard deviation is below 1 %. then it is not presented.

Figure A 6 and **Figure A 7** show the relation between absorbance and Cr(VI) solutions in two different concentration ranges. Linearity is observed between 1 and 10 mg/L (**Figure A 6**) defining the validity interval of the Beer-Lambert law. The linear equation is y = 11.04x + 1.18 with a correlation factor R^2 of 0.9922.

Figure A 7 shows that a non-linear behavior is observed between 10 and 50 mg/L, which is certainly related to the high absorbance of these solutions, meaning that the Beer-Lambert law is not valid at these high concentrations

The non-linear equation is given by $Y = 3.44\times10^{-6} \times e^{\frac{x}{0.16932}} + 13.39 \times e^{\frac{x}{1.964}} - 10.16$ with a correlation factor R^2 of 0.9997

Concentration (mg/L)	Time 1 (uW)	Time 2 (uW)	Time 3 (uW)	Average (uW)	T	Abs
1.00 ± 0.01 (1 %)	8181.0	8181.0	8181.0	8181.0	0.940669	0.02656
2.00 ± 0.02 (1 %)	7359.0	7359.0	7259.0	7325.7	0.84231	0.07453
3.00 ± 0.03 (1 %)	6182.0	6152.0	6142.0	6158.7	0.708137	0.1499
4.00 ± 0.04 (1 %)	5106.0	5106.0	5016.0	5076.0	0.583696	0.2338
5.00 ± 0.05 (1 %)	4112.40	4112.40	4112.40	4112.4	0.472853	0.3253
10.0 ± 0.1 (1 %)	1329.70	1329.70	1329.70	1329.7	0.152892	0.8156
15.0 ± 0.2 (1 %)	524.00	525.00	526.00	525.0	0.060387	1.2191
20.0 ± 0.2 (1 %)	206.00	202.00	210.00	206.0	0.023684	1.6255
25.0 ± 0.3 (1 %)	116.00	113.00	113.00	114.0	0.01311	1.8824
30.0 ± 0.3 (1 %)	69.60	66.60	66.00	67.4	0.007747	2.1109
35.0 ± 0.4 (1 %)	46.70	45.60	45.30	45.9	0.005272	2.278
40.0 ± 0.4 (1 %)	34.70	34.70	34.70	34.7	0.003992	2.3988
45.0 ± 0.5 (1 %)	28.90	28.80	28.80	28.8	0.003315	2.4796
50.0 ± 0.5 (1 %)	25.00	25.00	25.00	25.0	0.002874	2.5414

Table A 4 Absorbance of different concentrations of Cr(VI) measured in 5cm path length.

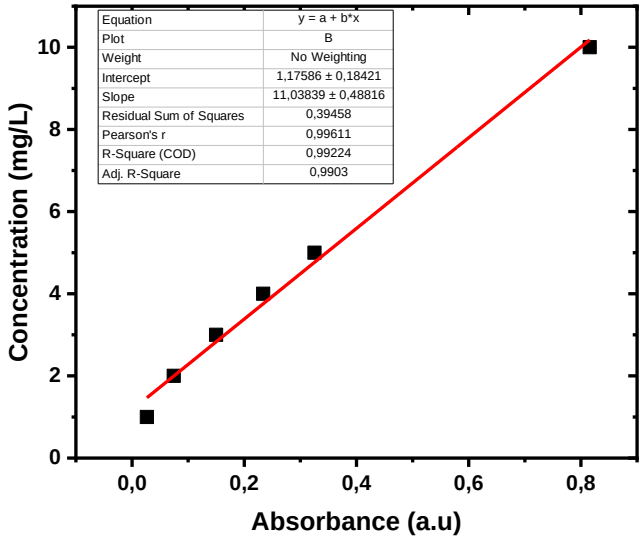

Figure A 6 Standard curve of Cr(VI) in range 1 - 10 mg/L. Measured in 5 cm path length reactor. The uncertainty of [Cr(VI)] (1 %) is not present

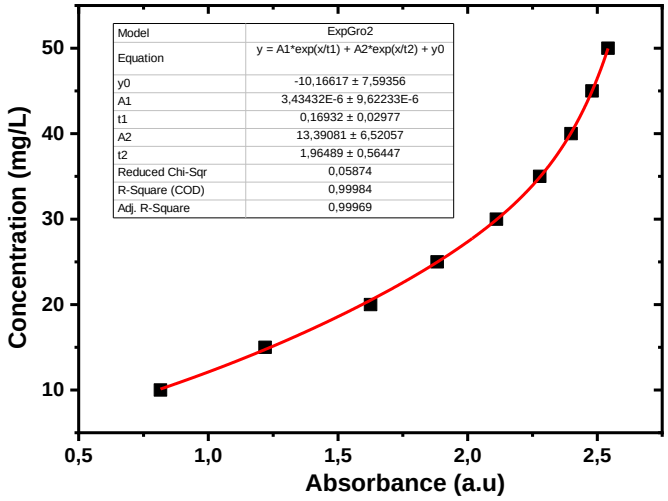

Figure A 7 Standard curve of Cr(VI) in range 10 - 50 mg/L. Measured in 5 cm path length reactor. The uncertainty of [Cr(VI)] (1 %) is not present

Annex 3.4 Protocol for the titration of H_2O_2 in the stock solution

To determine the concentration of H_2O_2 in a solution by UV-visible absorption. we have to perform a dedicated calibration (present in **annex 3.5**). This calibration requires the titration of H_2O_2 by potassium permanganate ($KMnO_4$). Moreover the potassium permanganate solution is standardized by titration with pure sodium oxalate ($Na_2C_2O_4$).

Standardization of the $KMnO_4$ solution

In the first step we need to prepare two different working solutions: $KMnO_4$ and $Na_2C_2O_4$

Preparation of the $KMnO_4$ and $Na_2C_2O_4$ solutions

- The $KMnO_4$ solution is prepared by dissolving 0.2984 g (±2%) of $KMnO_4$ powder in 400 mL of distilled water. Note that this solution has to be titrated afterward to determine its exact molarity.
- The $Na_2C_2O_4$ solution is prepared by dissolving 0.2016 g (±2%) of $Na_2C_2O_4$ powder in 100 mL of H_2SO_4 1 M solution (150 mL of H_2SO_4 1 M solution is prepared by mixing 100 mL of distilled water with 50 mL of H_2SO_4 3 M). The concentration $C_{Na_2C_2O_4}$ can be calculated by **Equation A 2**:

$$C_{Na_2C_2O_4} = \frac{m}{M \times V} = \frac{0.2016}{133.96 \times 100 \times 10^{-3}} = \mathbf{0.0151 \pm 0.0002\ M} \qquad \textbf{Equation A 2}$$

Titration of $KMnO_4$ solution

- Transfer 20 mL of the $Na_2C_2O_4$ solution to clean 250 mL flasks
- Take a 50 mL burette, clean it, and rinse it a few times with distilled water. Rinse the burette twice with about 10 mL of $KMnO_4$ solution (discard the rinse water) and then fill the burette with the solution, ensuring that the tip does not contain any air bubbles. Note the initial volume of $KMnO_4$ in the burette.
- Warm the flasks with 20 mL of the $Na_2C_2O_4$ solution to 70°C and start magnetic stirring
- Titrate the solution by slowly dropping the $KMnO_4$ solution until to a faint pink, after that record the volume of $KMnO_4$ added to the $Na_2C_2O_4$ solution
- Repeat the titration for two other samples
- The reaction of $Na_2C_2O_4$ with $KMnO_4$ is presented by **Reaction A 1** :

$$5Na_2C_2O_4 + 2KMnO_4 + 8H_2SO_4 \rightarrow K_2SO_4 + 5Na_2SO_4 + 2MnSO_4 + 10CO_2 + 8H_2O \qquad \textbf{Reaction A 2}$$

Results

Table A 5 shows the volume of $KMnO_4$ for three-time titration

The volume of $KMnO_4$ (mL)	Time 1	Time 2	Time 3	Average
	25.7 ± 0.1	25.7 ± 0.1	25.5 ± 0.1	25.6 ± 0.1

Table A 5 Volume of $KMnO_4$ solution consume for three times of titration

Following **Reaction A 2** and **Table A 5** we can calculate the initial concentration of $KMnO_4$ solution by two steps:

From **Reaction A 2** we know the chemical reaction balance of $KMnO_4$ with $Na_2C_2O_4$ present by **Equation A 3**:

$$\frac{n(KMnO_4)}{5} = \frac{n(Na_2C_2O_4)}{2} \qquad \textbf{Equation A 3}$$

Thus the concentration of $KMnO_4$ solution is calculated by **Equation A 4,** with for this example $C_{Na_2C_2O_4} = 0.0151$ mol/L and $V_{Na_2C_2O_4} = 20$ mL:

$$C_{KMnO_4} = \frac{5}{2} \times C_{Na_2C_2O_4} \times \frac{V_{Na_2C_2O_4}}{V_{KMnO_4}} = \mathbf{0.0047 \pm 0.0002\ M} \qquad \textbf{Equation A 4}$$

Titration of H_2O_2 solution

The dark purple MnO_4^- oxidizes hydrogen peroxide in an acid solution. forming oxygen gas and very pale pink Mn^{2+} ions [261]. Thus. when a solution of $KMnO_4$ is added dropwise to an acidified hydrogen peroxide solution. each drop is decolorized until all the H_2O_2 is used up. The next drop of permanganate solution is added to color and signals the end-point of the titration. The principle is following **Reaction A 3** [261].

$$2MnO_4^- + 6H^+ + 5H_2O_2 \rightarrow 5O_2 + 8H_2O + 2Mn_2^+ \qquad \textbf{Reaction A 3}$$

The H_2O_2 solution is prepared by following the steps bellow

Preparation of standard H_2O_2 solution

The 100 mL of standard H_2O_2 solution is prepared by mixing 0.114 ± 0.001 mL of H_2O_2. (wt50%) stock solution with 99.884 ± 0.009 mL of distilled water

Preparation of H_2O_2 working solution for titration

A 75 mL of H_2O_2 working solution is prepared by mixing a complex solution of 10 mL standard H_2O_2 solution + 50 mL of distilled water + 15 mL of the H_2SO_4 1 M

Titration of the H_2O_2 solution

It is noted that the procedure to titration of H_2O_2 is similar to the titration of $KMnO_4$

- Transfer 75 mL of the working solution of H_2O_2 into 250 mL flasks
- Take a 50 mL burette. clean it. and rinse it a few times with distilled water. Rinse the burette twice with about 10 mL of $KMnO_4$ solution (discard the rinse water) and then fill the burette with the solution, ensuring that the tip does not contain any air bubbles. Note the initial volume of $KMnO_4$ in the burette
- Titrate the acidic hydrogen peroxide solution by a slow drop of $KMnO_4$ solution, swirling continuously. Continue until one drop produces a pink color and then wait for the solution stable for at least 1 minute. Then record the value of the remaining solution in the burette.
- Refill the burette. Repeat the titration with two other samples

Results

After the titration. **Table A 6** shows the volume of $KMnO_4$ solution used for the three times titration of the H_2O_2 solution

V_{KMnO4} (mL)	V1	V2	V3	Average
	16.6 ± 0.1	16.7 ± 0.1	16.5 ± 0.1	16.6 ± 0.1

Table A 6 Volume of $KMnO_4$ consume for titration of H_2O_2 solution

We first calculate the concentration of H_2O_2 in the working solution by two steps below:

From reaction **Reaction A 3** we know the chemical reaction balance of H_2O_2 and $KMnO_4$ as presented in **Equation A 5 :**

$$\frac{n(H_2O_2)}{2} = \frac{n(KMnO_4)}{5} \qquad \textbf{Equation A 5}$$

Then we can calculate the concentration of H_2O_2 in the working solution by **Equation A 6**:

$$C_{Working\ H_2O_2} = \frac{5}{2} \times C_{KMnO_4} \times \frac{V_{KMnO_4}}{V_{Working\ H_2O_2}} = \mathbf{0.0026 \pm 0.0003\ M} \qquad \textbf{Equation A 6}$$

After that. we can calculate the concentration of H_2O_2 in the standard solution by:

$$C_{Standard\ H_2O_2} = \frac{V_{Working\ H_2O_2}}{V_{H_2O_2}} \times C_{Working\ H_2O_2} = \mathbf{0.0195 \pm 0.0002\ M} \qquad \textbf{Equation A 7}$$

Finally we can calculate the concentration of H_2O_2 in the stock solution:

$$C_{Stock\ H_2O_2} = \frac{V_{Working\ H_2O_2}}{V_{H_2O_2}} \times C_{Standard\ H_2O_2} = \mathbf{17.11 \pm 0.34\ M} \qquad \textbf{Equation A 8}$$

By following [201,210] we also calculate the uncertainties following all of the previous steps and the final uncertainties in the concentration of H_2O_2 are about 2 %. *i.e.* $[H_2O_2]$ = 17.1 ± 0.3 M

Annex 3.5: Concentration of Hydrogen peroxide by Eisenberg method (in water)

The absorbance is measured using an Avaspec DHC2048XL spectrometer. A cuvette with a path length of l cm is used to measure the absorbance of the samples.

Preparation of solution

The stock solution of H_2O_2 is prepared from the marketed H_2O_2 solution (wt 50 %) of 17.1±0.3 M. which is titrated by the permanganate solution (in **annex 3.4**).

We prepare a series of H_2O_2 solutions of different concentration: 0.07; 0.1; 0.2; 0.3; 0.5; 1 mM by diluting with water the H_2O_2 stock solution.

Samples for analysis in spectroscopy UV-Vis

The blank reference is obtained by mixing 2 mL H_2O + 1 mL TiOSO4 0.0125 M (Sigma Aldrich).

The calibration curve is performed by measuring the absorbance at 410 nm of 2 ml of each solution containing the different H_2O_2 solutions + 1 mL $TiOSO_4$ 0.0125 M. After mixing we let it stand for 15 minutes to develop the complex. The final absorbance value is calculated as the average of 3 measurements for each concentration.

Results

Table A 7 shows absorbance of the complex of H_2O_2 with $TiOSO_4$ measured at 410 nm

[H_2O_2] mM	**Absorbance at 410 nm**				**Standard deviation**	**Uncertainty %**
	Time 1	Time 2	Time 3	Average		
0.070 ± 0.002 (3 %)	0.00915	0.00921	0.00905	0.00914	8.08E-05	0.9
0.100 ± 0.003 (3 %)	0.01546	0.01556	0.01536	0.01546	1.00E-04	0.6
0.200 ± 0.006 (3 %)	0.03281	0.03173	0.03211	0.03222	5.48E-04	1.7
0.300 ± 0.009 (3 %)	0.04892	0.04897	0.048778	0.04889	9.96E-05	0.2
0.50 ± 0.02 (3 %)	0.08387	0.08647	0.08437	0.08490	1.38E-03	1.6
1.00 ± 0.01 (3 %)	0.18424	0.18414	0.18362	0.18400	3.33E-04	0.2

Table A 7 Absorbance of the complex measured at 410 nm

Figure A 8 shows the relation between absorbance and H_2O_2 concentration measured in a 1 cm path length cuvette. Linearity is observed between 0.07 and 1 mM defining the validity interval of the Beer-Lambert law. The linear equation is $Y = 5.40X + 0.02$ with a correlation factor R^2 of 0.9981

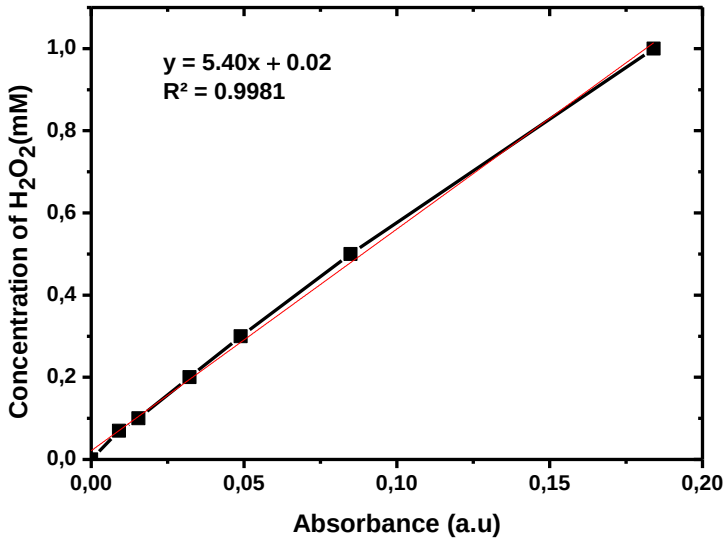

Figure A 8 Standard curve of H_2O_2 in range 0.07 - 1 mM. Measured at 410 nm. The uncertainty of [H_2O_2)] (3 %) is not present

Annex 3.6: Concentration of Hydrogen peroxide by Christopher Andreas Vasko method

The principle of this method is based on the absorption at 440 nm of the [VO_2^{3+}] ion as a product of the reaction between H_2O_2 with NH_4VO_3 in an acidic environment as presented in

$$VO^{3-} + 4\ H^+ + H_2O_2 \rightarrow VO_2^{\ 3+} + 3\ H_2O \qquad \textbf{Reaction A 4}$$

To verify its reliability before using it to measure [H_2O_2] in a Cr(VI) solution we use this method to check the concentration of H_2O_2 formed in water.

The absorbance is measured using an Avaspec DHC2048XL spectrometer. A cuvette with a path length of l cm is used to measure the absorbance of the samples.

Preparation of solution

The stock solution of H_2O_2 is prepared from the marketed H_2O_2 solution (wt 50%) of 17.1±0.3 M.

We prepare a series of different concentrations of H_2O_2 solution: 0.2; 0.4; 0.6; 0.8; 1 mg/L by diluted from the H_2O_2 stock solution.

NH_4VO_3 0.06 M solution is prepared by dissolving 1.40484 ± 0.14048 g of powder NH_4VO_3 in 200 mL of the acid H_2SO_4 0.5 M solution.

Samples for analysis in spectroscopy UV-Vis

The blank reference is obtained by mixing 2 mL H_2O + 1 mL NH_4VO_3 0.06 M.

The calibration curve is performed by measuring the absorbance at 440 nm of 2 mL of each solution containing different H_2O_2 concentrations + 1 mL NH_4VO_3 0.06 M. After mixing the solutions we let it stand for 15 minutes to develop the complex. The final absorbance value is calculated as the average of 3 measurements for each concentration.

Results

Table A 8 shows the absorbance of the complex of H_2O_2 with NH_4VO_3 measured at 440 nm

[H_2O_2] mM	**Absorbance at 440 nm**				**Standard deviation**	**Uncertainty %**
	Time 1	Time 2	Time 3	Average		
0.200 ± 0.006 (3 %)	0.04163	0.04176	0.04159	0.04166	8.89E-05	0.2
0.40 ± 0.01 (3 %)	0.08813	0.08814	0.08814	0.08814	5.77E-06	0.01
0.60 ± 0.02 (3 %)	0.1284	0.1282	0.1284	0.12833	1.15E-04	0.1
0.80 ± 0.02 (3 %)	0.1807	0.1801	0.1807	0.1805	3.46E-04	0.2
1.00 ± 0.03 (3 %)	0.2351	0.2357	0.2353	0.2354	3.06E-04	0.1

Table A 8 Absorbance of the complex measured at 440nm

Figure A 9 shows the relation between absorbance and H_2O_2 concentration measured in 1 cm path length. Linearity is observed between 1 and 10 mg/L defining the validity interval of the Beer-Lambert law. The linear equation is Y = 4.27X + 0.02 with a correlation factor R^2 of 0.9969

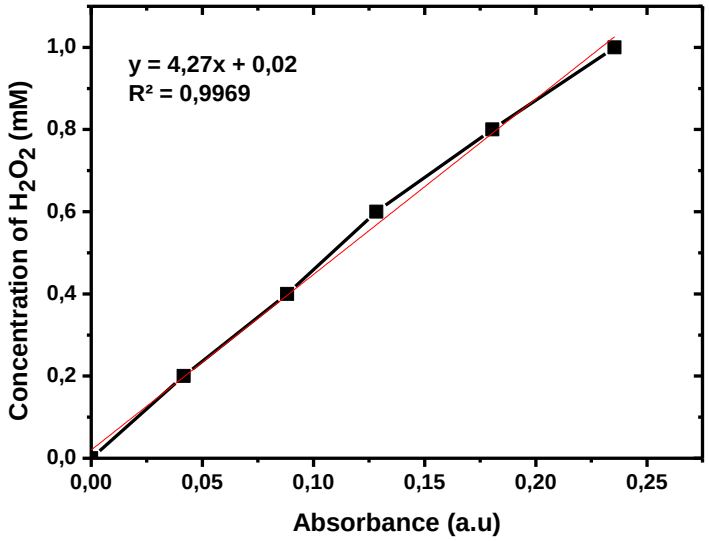

Figure A 9 Standard curve of H_2O_2 in range 0.2 - 1 mM. Measured at 440 nm. The uncertainty of [H_2O_2)] (3 %) is not present

Annex 3.7: Concentration of Hydrogen peroxide by Christopher Andreas Vasko method & Cr(VI) by direct measurement

The objective is to measure simultaneously [Cr(VI)] and [H_2O_2]. For that we will use direct absorption measurement for Cr(VI) and Vasko method for H_2O_2 (with NH_4VO_3). As mentioned previously, direct Cr(VI) maximum absorption is about 350 nm. We observe that by measuring the absorbance of a Cr(VI) solution containing some NH_4VO_3, the maximum of absorbance shifts to 360 nm and there is also a non-negligible absorption band at 440 nm (pink curve in **Figure A 10**).Figure A 10 UV-vis spectrum of Cr(VI) and the complex [VO23+] in Cr (VI) solution

This absorption at 440 nm affects the measurement of H_2O_2 concentration by both the Enseiberg and Vasko methods. Thus the measurements of [H_2O_2] and [Cr(VI)] in Cr(VI) solution by UV-Vis spectroscopy absorption are not direct.

The method used to estimate the concentrations is detailed below:

Step 1: Influence of the [VO_2^{3+}] complex on the absorption peak of Cr(VI).

Figure A 10 shows the spectra obtained for two different Cr(VI) solutions:

- the pink curve illustrates the absorption of: 2 ml Cr(VI) 50 mg/L + 1 ml NH_4VO_3 0.06 M (**Solution 1-no complex**)

- the blue curve illustrates the absorption of: 2 ml Cr(VI) 50 mg/L + 1 ml NH_4VO_3 0.06 M + few drops of H_2O_2 1 M (**Solution 2-with complex** VO_2^{3+})

As presented in **Figure A 10** the intensity in the maximum absorbance of chromium does not change with the presence of the [VO_2^{3+}] ion.

Step 2: Analysis of the double absorbance at 440 nm

The increase in the intensity of the band at 440 nm in the blue curve compared with the pink curve is due to the absorption of [VO_2^{3+}] ion. Because the reaction of H_2O_2 with NH_4VO_3 has a ratio of 1:1. we can conclude that the increase observed at 440 nm in the blue curve is the absorption of [VO_2^{3+}] in Cr(VI) solution.

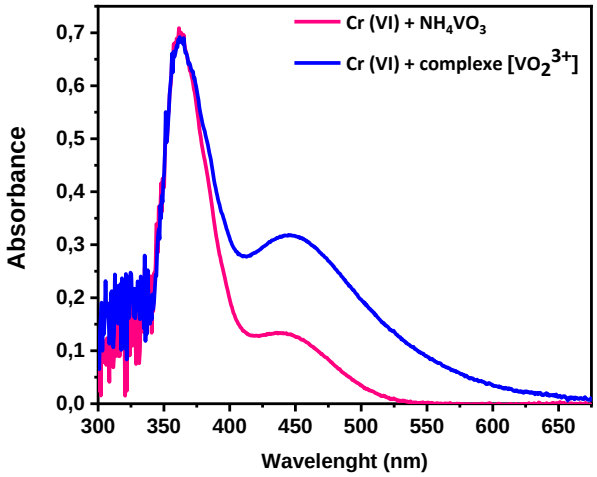

Figure A 10 UV-vis spectrum of Cr(VI) and the complex $[VO_2^{3+}]$ in Cr (VI) solution

In this case the equation used to calculate the absolute absorbance of $[H_2O_2]$ from the UV-spectrum is:

Abs **$[VO_2^{3+}]$ = [Abs @ 440 nm of solution 2] - [Abs @ 440 nm of solution 1]**

However the absorbance at 440 nm of solutions also depends on the Cr(VI) concentration which will change during the PLI process.

To measure the concentration of H_2O_2 in Cr(VI) we need to use a combination of **three different** calibration curves (detailed in the next steps):

1. *Calibration curve of the different concentrations of Cr(VI) with NH_4VO_3 at 360 nm (1st calibration curve) => to calculate the concentration of Cr(VI) after the treatment process and to know the absorbance at 440 nm (as a baseline)*
2. *From the 1st curve => we can have the 2nd calibration curve for absorbance at 440 nm (baseline calibration curve)*
3. *Calibration curve of the different concentrations of H_2O_2 with NH_4VO_3 at 440 nm (3rd calibration curve)*

Step 3: 1st and 2nd calibration curve for Cr(VI)

From the 100 mg/L stock solution (Annex 3.3) we prepare a series of working solutions with different Cr(VI) concentrations ranging from 1 to 50 mg/L. The reference for the UV-Visible spectrometer is prepared from 2 mL of water and 1 mL of 0.06 M NH_4VO_3. To measure the absorbance of the samples, 2 mL of Cr(VI) solution is added to 1 mL of NH_4VO_3 0.06 M in the cuvette. Then the absorbance is measured three times at 360 nm and 440 nm. The final value is calculated by taking the average of the three different measurements. **Table A 9** shows the absorbance at 360 nm and 440 nm of different concentrations of Cr(VI) with NH_4VO_3

[Cr (VI)] mg/L	Absorbance at 360 nm				Absorbance at 440 nm			
	Time 1	Time 2	Time 3	Average	Time 1	Time 2	Time 3	Average
1.00 ± 0.03 (0.6%)	0.0392	0.0355	0.0358	0.0368	0.00724	0.0075	0.007	0.0073
5.00 ± 0.03 (0.6%)	0.0786	0.0787	0.07894	0.0785	0.00138	0.00139	0.0137	0.0138
10.00 ± 0.06 (0.6%)	0.1654	0.1632	0.1612	0.1633	0.03336	0.03367	0.03305	0.0334
15.00 ± 0.09 (0.6 %)	0.2315	0.2315	0.2318	0.2316	0.04587	0.04587	0.04563	0.0458
25.00 ± 0.15 (0.6 %)	0.3956	0.4025	0.3959	0.398	0.07393	0.07428	0.07382	0.074
35.00 ± 0.021 (0.6 %)	0.55	0.5311	0.5369	0.5393	0.1054	0.1048	0.1044	0.1049
50.00 ± 0.15 (0.3 %)	0.7481	0.7373	0.7371	0.7408	0.1445	0.1441	0.1442	0.1443

Table A 9 Absorpbance of different concentrations of Cr(VI). measured with NH_4VO_3 at 360 nm and 440 nm

From this **Table A 9**. we present two different calibration curves (1st and 2nd calibration curves).

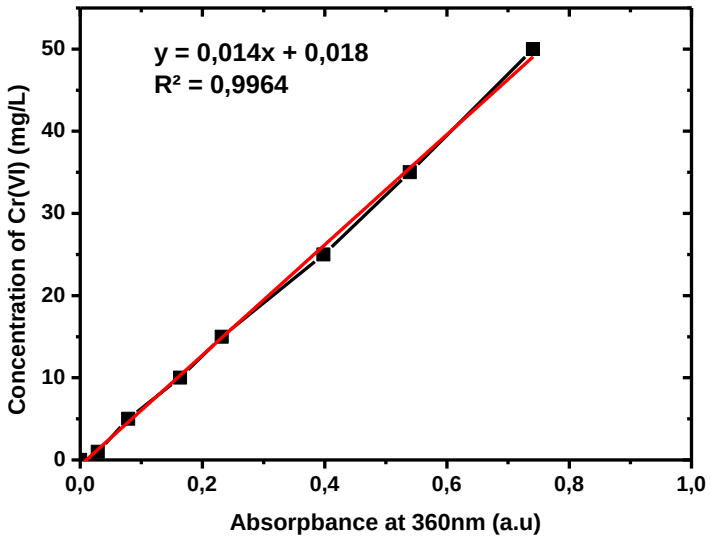

Figure A 11 Standard concentrations of Cr(VI). measured at 360 nm with NH_4VO_3

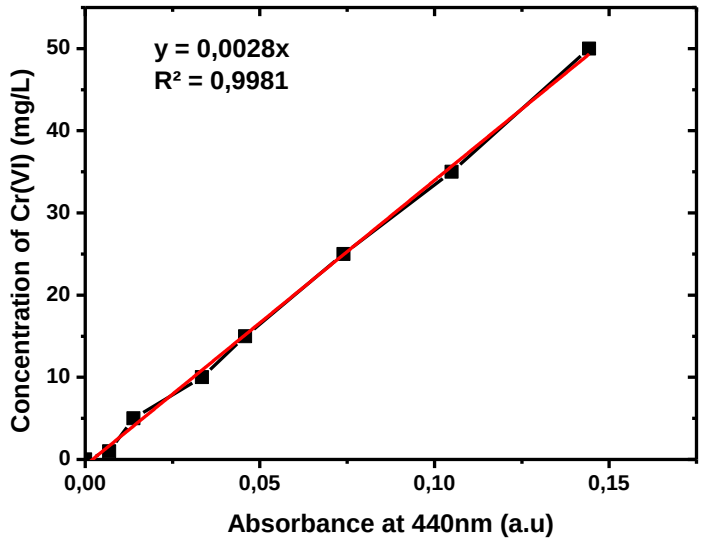

Figure A 12 Standard concentrations of Cr(VI). measured at 440 nm with NH_4VO_3

Figure A 11 shows the relation between absorbance and Cr(VI) concentration measured in 1 cm path length cuvette at 360 nm. Linearity is observed between 1 and 50 mg/L defining the validity interval of the Beer-Lambert law. The linear equation is Y = 0.014X + 0.018 with a correlation factor R^2 of 0.9964.

Figure A 12 shows the relation between absorbance and Cr(VI) concentration measured in 1 cm path length at 440 nm. The linear eqution is Y = 0.0028X with a correlation factor R^2 of 0.9981.

Step 4: Influence of different concentrations of the [VO_2^{3+}] complex on the absorption peak at 440nm for different concentrations of Cr(VI).

Three calibration curves of H_2O_2 in 3 different Cr(VI) solutions at 1 - 25 - 50 mg/L are carried out. The range of H_2O_2 concentrations in the solutions is from 0.2 to 1 mM. The solutions are then mixed with 1 mL of NH_4VO_3 0.06 M to measure the absorbance at 440 nm. The reference for the UV-Visible spectrometer is prepared from 2 mL of water and 1 mL of 0.06 M NH_4VO_3.

To measure the absorbance of the samples 2 mL of each Cr(VI) solution containing different concentrations of H_2O_2 is added to 1 mL of 0.06 M NH_4VO_3 in the cuvette. As an example. **Figure A 13** shows the absorbance of different concentrations of H_2O_2 in a 50 mg/L Cr(VI) solution. These results show first that the absorbance of Cr(VI) at 360 nm does not depend on the concentrations of H_2O_2.

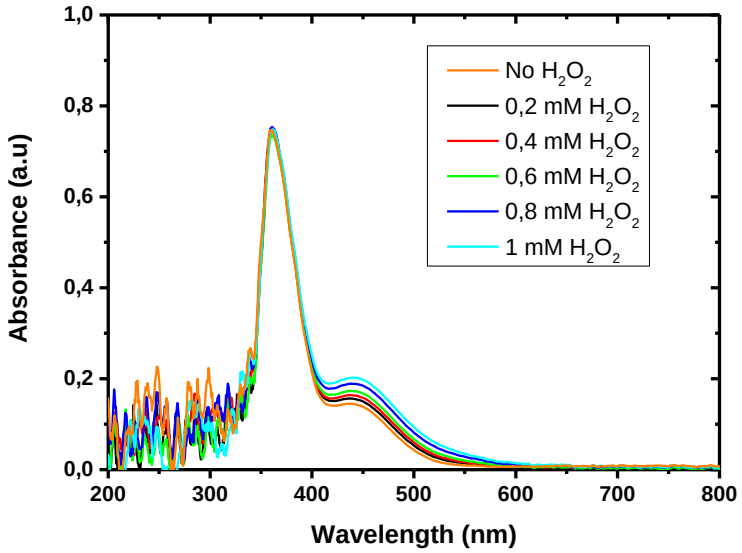

Figure A 13 Standard concentrations of H_2O_2. measured at 440 nm with NH_4VO_3 in 50 mg/L Cr(VI) solution

The steps for creating a calibration curve for different concentrations of H_2O_2 in this 50 mg/L Cr(VI) solution are:

- To measure absorbance at 440 nm of: 2 mL of Cr(VI) 50 mg/L + 1 mL NH_4VO_3 0.06 M (orange curve in . **Figure A 13**). This value is used as the baseline value (***1st value***)
- To measure absorbance at 440 nm of: 2 mL of Cr(VI) 50 mg/L containing different concentrations of H_2O_2 + 1ml NH_4VO_3 0.06 M (***2nd value***)
- Finally the exact absorbance value of $[VO_2^{3+}]$ is calculated by using: ***2nd value – 1st value***

By following the steps above we do three different calibration curves of H_2O_2 in 3 different Cr(VI) solutions 1-25-50 mg/L respectively as shown in **Figure A 14**.

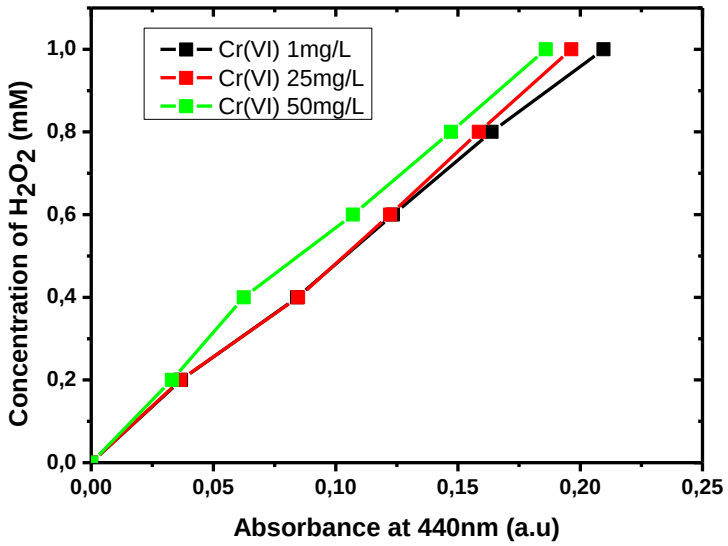

Figure A 14 Standard concentrations of H_2O_2 in Cr(VI) solutions with known concentrations measured at 440 nm with NH_4VO_3. Black curve presents the absorbance in [Cr(VI)]=1 mg/L. Red curve presents the absorbance in [Cr(VI)]=25 mg/L. Green curve presents the absorbance in [Cr(VI)]=50 mg/L

The three curves have the same tendency and show a 15 % of discrepancy. We can conclude that the Cr(VI) concentrations do not significantly affect the calibration curve of H_2O_2 in Cr (VI) solution considering an uncertainty of 15%

Step 5: 3rd Calibration curve of H_2O_2

The average of the three curvess is calculated and used as the calibration curve for the H_2O_2 measurement in the experiments on Cr(VI) reduction by electric discharge as shown in **Figure A 15**. The linear equation is Y = 5.04X with a correlation factor R^2 of 0.9996

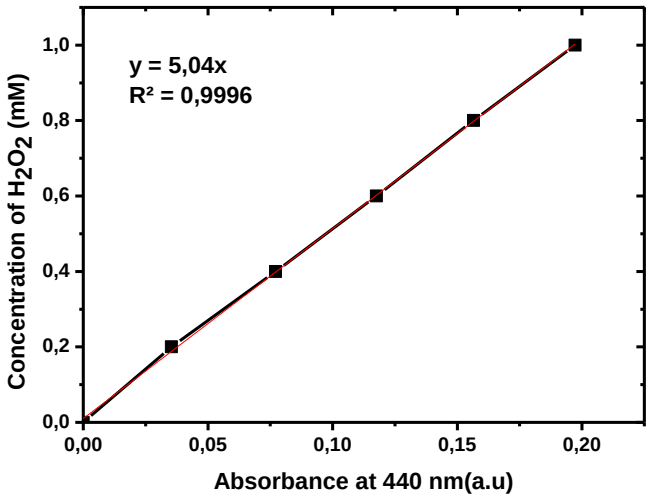

Figure A 15 Calibration curve for H_2O_2 measurement by a used average of 3 calibration curves

Step 6: Measurement process of a solution

This section presents an example of estimating Cr(VI) and H_2O_2 concentration after the PLI process.

First we perform the blank reference for UV-Vis using 2 mL H_2O + 1 mL NH_4VO_3 0.06 M.

Then we perform the absorption measurement of the sample using 2 mL of the treated solution + 1 mL NH_4VO_3 0.06 M. The spectrum is presented in Figure 16.

1. The absorbance at 360 nm is measured (A1 as presented in **Figure A 16**), then [Cr(VI)] is calculated thanks to curve 1 (**Figure A 11**).

From **Figure A 16** we can also take the value (A2) as the absorbance of both baseline of Cr(VI) + complex of H_2O_2 with VO_2^{3+}

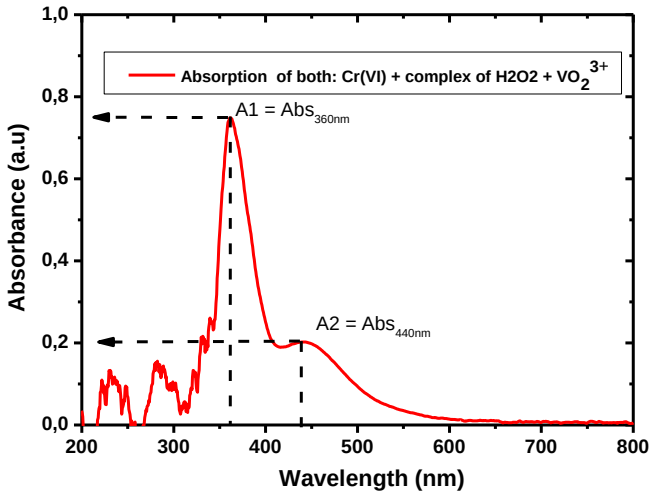

Figure A 16 Absorption spectrum of the working solution containing Cr(VI) and the H_2O_2 + [VO_2^{3+}] complex.

Following the previous protocol step we need to calculate the absorbance at 440 nm of only Cr(VI) as we called "baseline."

2. Baseline calculation: From [Cr(VI)] and curve 2 (**Figure A 12**) we can estimate the baseline absorbance at 440 nm ABS_{440nm} as A3 (it is noted that the value of A3 present in the graph can not be directly taken from the curve)

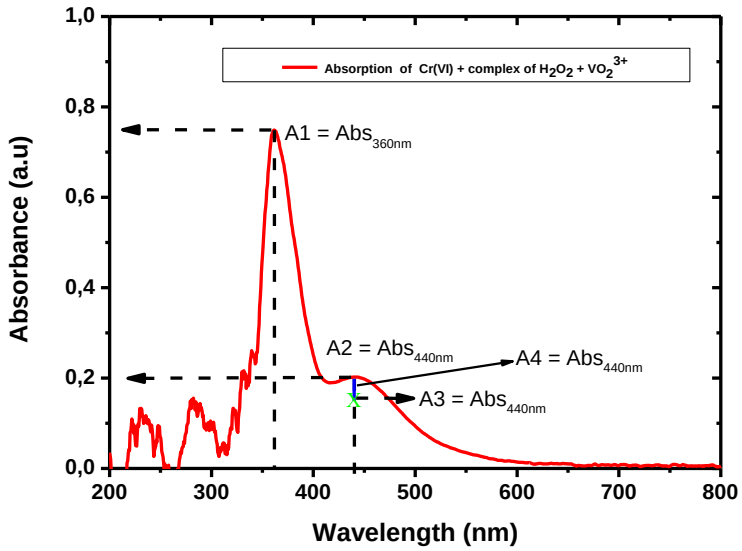

Figure A 17 An example to calculate the final concentration of H_2O_2 in Cr(VI) solution

3. Finally we calculate the absorbance of complex H_2O_2 with VO_2^{3+} at 440 nm A4 by using value A2 minus value A3 (blue line shown in **Figure A 17**). From A4 we can calculate the concentration of H_2O_2 by using curve 3 (the equation presented in **Figure A 15**).

Step 7: Test to validate the calibration curve for H_2O_2 & Cr (VI) measurement.

This method is complex so we check its validity with reference solutions

- **Method**

- We prepare three different solutions containing Cr(VI) and H_2O_2. (the concentrations of each species are known) :

  Sample 1 contains: Cr(VI) 5 mg/L + H_2O_2 0.1 mM

  Sample 2 contains: Cr(VI) 20 mg/L + H_2O_2 0.5 mM

  Sample 3 contains: Cr(VI) 40 mg/L + H_2O_2 0.7 mM

- We measure the absorbances at 360 nm and 440 nm for the three solutions and calculate the concentration of H_2O_2 and Cr (VI) using the three calibration curves

- We cCompare the results with the known concentrations of the 3 samples

- **Results**

By use of the three calibration curves done previously we obtain the results shown in **Table A 10**.

[Cr(VI)] Prepared (mg/L)	**[Cr (VI)] Calculated from measurement (mg/L)**	***Error (%)***
5	5.12 ± 0.05	*2*
20	21.00 ± 0.21	*5*
40	43.97 ± 0.44	***9***
[H_2O_2] Prepared (mM)	**[H_2O_2] Calculated from measurement (mM)**	***Error (%)***
0.1	0.0998 ± 0.0149	***0.2***
0.5	0.5268 ± 0.0790	***5***
0.7	0.7547 ± 0.1132	***7***

Table A 10 Comparison of the concentration of Cr(VI) and H_2O_2 after using three different calibration curves with a know concentration

The maximum error indicating the difference between the theoretical and experimental concentrations is 9 %. This uncertainty is within the uncertainty of the calibration curve (15 %). We confirm that this method can be used to measure H_2O_2 and Cr (VI) concentrations in the treatment process.

CONCLUSION

This method can be used to measure both the concentration of Cr(VI) and H_2O_2 in the solution during the treatment process; however. we also have some drawbacks. The advantages and disadvantages of this method are presented in the table below:

Advantages	**Disadvantages**
- Able to measure at the same time both concentrations of Cr(VI) and H_2O_2 during the treatment process - Do not require a complex system - Do not require a lot of chemical compounds	- Having to use three different calibrations lead to difficulty in the calculation - Not able to measure a low concentration of Cr(VI) - High uncertainties (15%)

Annex Chapter 4

Annex 4.2.2 Effect of applied voltage

a. In the case of NOBK

Figure A 18 shows the electrical signals for different applied voltages measured using different time resolutions, (a) 0.5 µs and (b) 0.001 µs. The signals show a similar shape and maximum intensity.

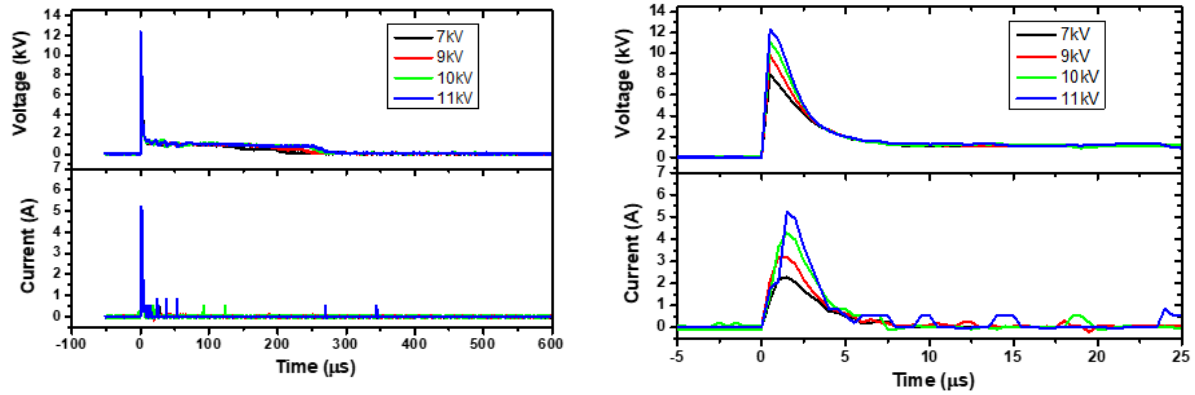

(a)

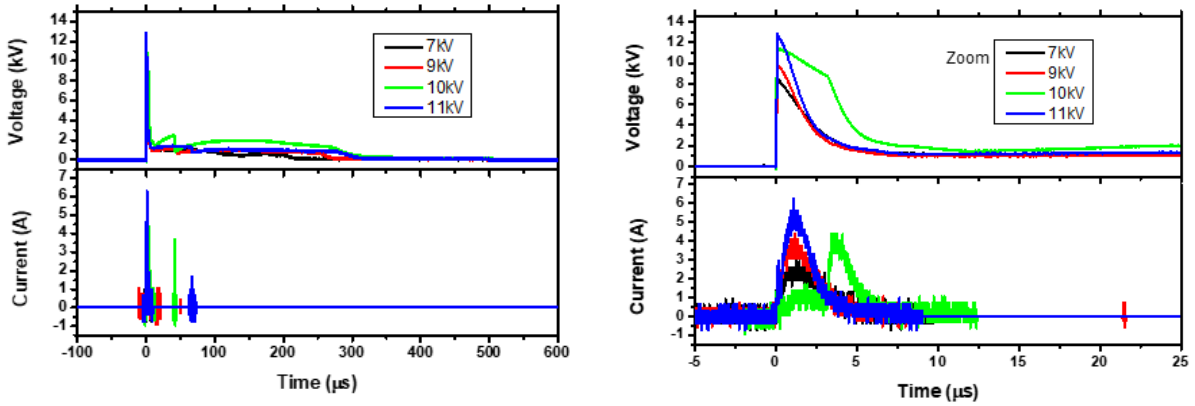

(b)

Figure A 18 Voltage and current signals and a zoom of a pin-to-pin discharge for case NOBK in Cr(VI) solution (47 mg/L,σ=4 mS/cm,pH=2.4) for 7, 9, 10, and 11 kV. V = 100 mL, Δt = 500 µs, gap = 2 mm, electrodes length = 0±10 µm, f = 50 Hz. The signals were monitored with a time resolution of (a) 0.5 µs and (b) 0.001 µs

b. In the case of BK

Figure A 19 shows the electrical signals for different applied voltages measured using different time resolutions, (a) 0.5 µs and (b) 0.001 µs. The signals show a similar shape, the difference in the maximum current is due to the random distribution (described previously in **Chapter 4)**.

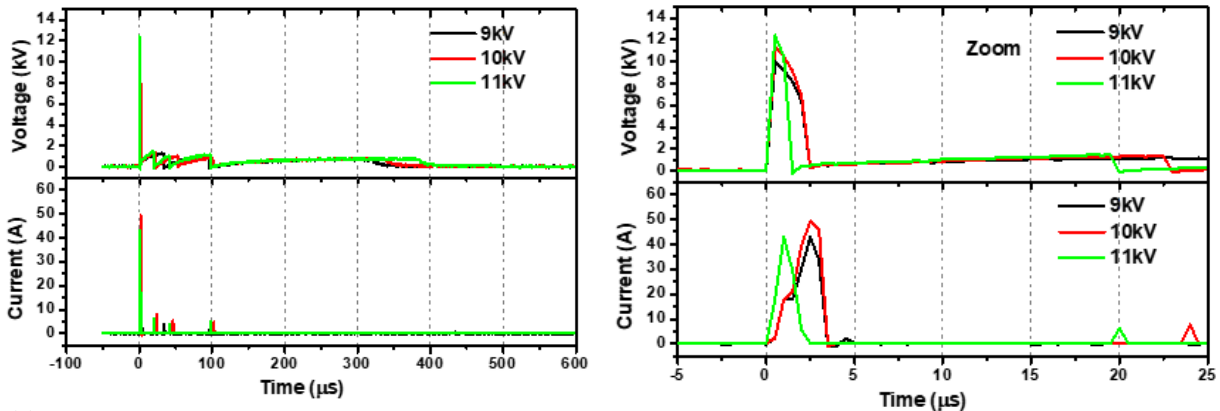

(a)

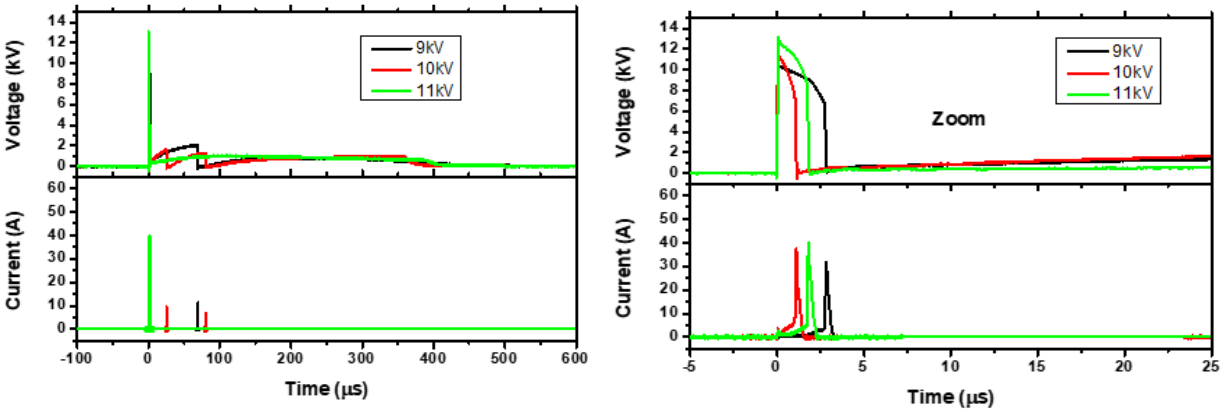

(b)

Figure A 19 Voltage and current signals and a zoom of a pin-to-pin discharge for case BK in Cr(VI) solution (47 mg/L,σ=4 mS/cm,pH=2.4) for 9, 10, and 11 kV. V = 100 mL, Δt = 500 µs, gap = 2 mm, electrodes length = 0±10 µm, f = 50 Hz. The signals were monitored with a time resolution of (a) 0.5 µs and (b) 0.001 µs

Annex 4.2.3 Effect of the interelectrode gap

Figure A 20 shows the electrical signals for different applied voltages measured using different time resolutions, (a) 0.5 µs and (b) 0.001 µs. The figures show a similar shape of the electrical waveforms.

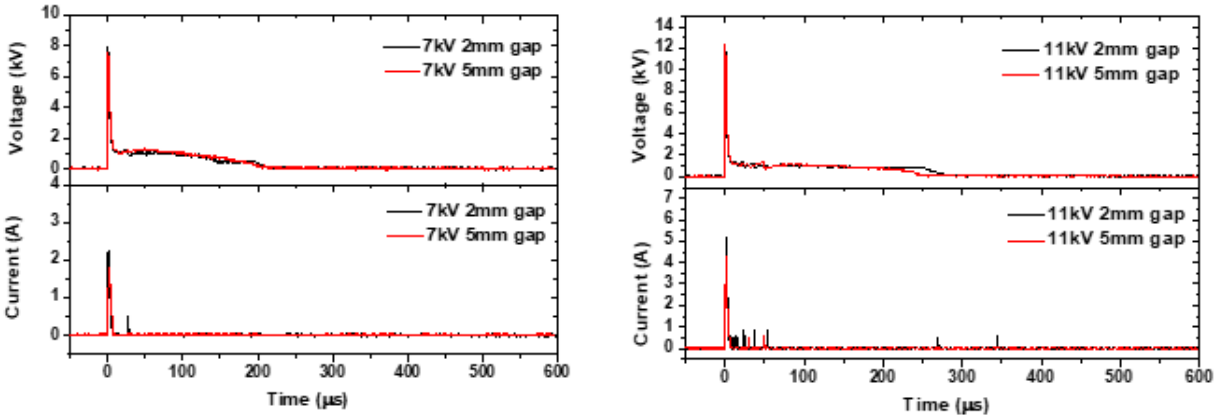

(a)

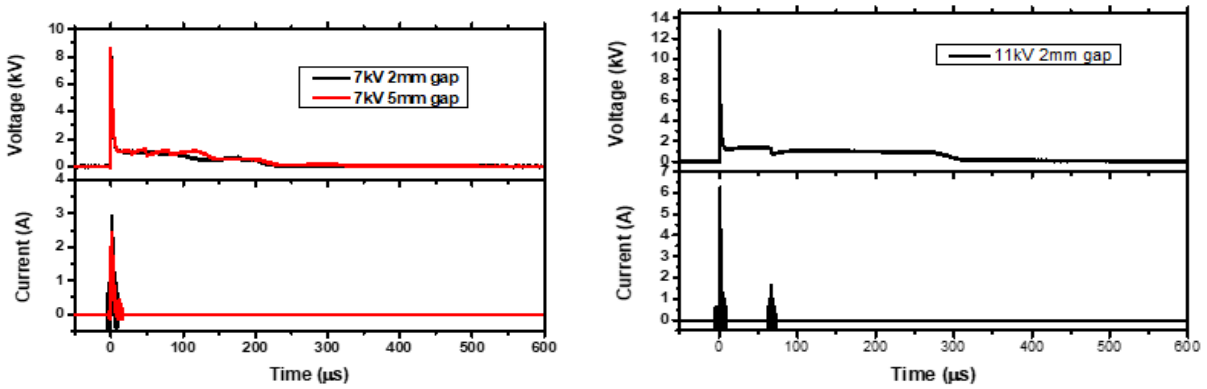

(b)

Figure A 20 Voltage and current signals and a zoom of a pin-to-pin discharge for case BK in Cr(VI) solution (47 mg/L,σ=4 mS/cm, pH=2.4) for gaps of 2 and 5 mm. V = 100 mL, Δt = 500 µs, electrodes length = 0±10 µm, f = 50 Hz. The signals were monitored with a time resolution of (a) 0.5 µs and (b) 0.001 µs. No signal for the discharge at 11 kV with a 5 mm gap.

Annex 4.2.4 Effect of the pulse duration

In this study, we do not present the signal in the case BK for 11 kV with a different pulse duration

Figure A 21 shows the electrical signals for different pulse durations measured using different time resolutions, (a) 0.5 µs and (b) 0.001 µs. The figures show a similar shape of the electrical waveforms.

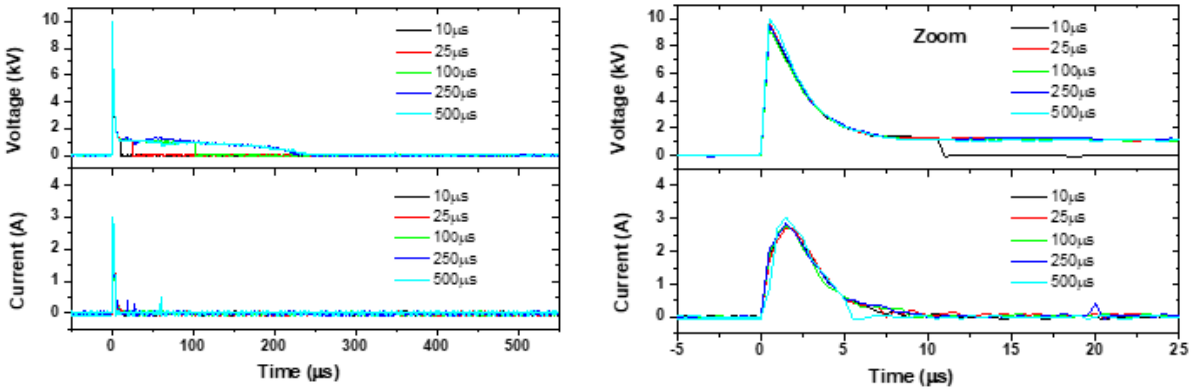

(a)

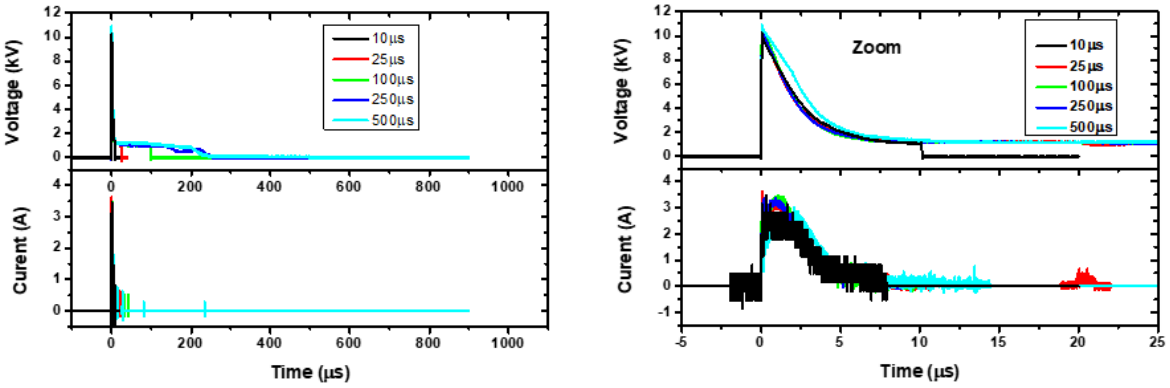

(b)

Figure A 21 Voltage and current signals and a zoom of 9 kV discharge in Cr(VI) solution (47 mg/L,σ=4 mS/cm,pH=2.4) for different pulse durations with U = 9 kV, V = 100 mL, gap = 5 mm, electrodes length = 0±10 µm, f = 50 Hz. The signals were monitored with a time resolution of (a) 0.5 µs and (b) 0.001 µs.

.

Annex Chapter 5

Annex 5.1 Effect of the pulse frequency on the H_2O_2 production

Figure A 22 presents the electrical signals obtained for the 3 conditions involving only case 2. The characteristics of the waveforms are similar and consistent to previous comments performed for case 2 in water .

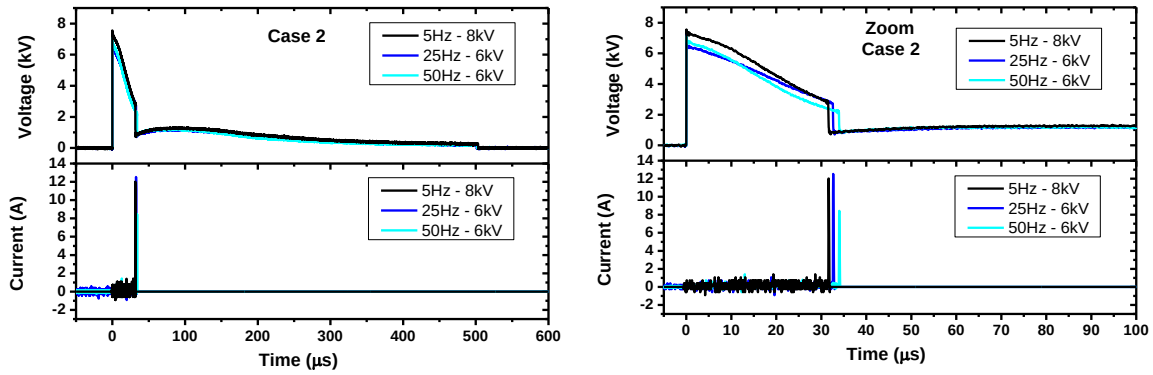

(a) (b)

Figure A 22 Electrical waveforms of pin-to-pin discharge for case 2 generated in water for different frequencies and voltages , V = 200 mL, Δt = 500 µs, 2 mm of gap, and σ = 200 µS/cm); (a) Voltage and Current signals and (b) a zoom of these signals.

Figure A 23 presents the electrical signals obtained for the three conditions involving only case 3.Case 3 is observed for 50 Hz-9 kV but a mix of case 2 and case 3 appears for 25 Hz-9 kV and 5 Hz-9 kV. Then, as we did for Case 2, we adjust the applied voltage to ensure that only case 3 is present and it leads to the additional conditions 25 Hz-10 kV- and 5 Hz-11 kV. This means that the frequency decrease has to be compensated by increasing the applied voltage to keep the same case. The characteristics of the waveforms are similar and consistent with previous comments performed for case 3 in water. In particular, we observe that the breakdown occurs earlier, and the current peak is higher for case 3 than for case 2.

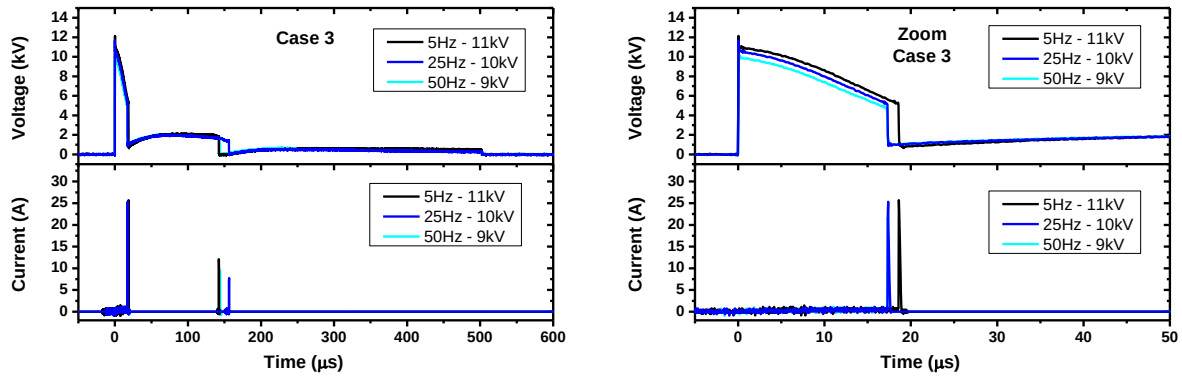

(a) (b)

Figure A 23 Electrical waveforms of pin-to-pin discharge for case 3 generated in water for different frequencies and voltages, V = 200 mL, Δt = 500 µs, 2 mm of gap, and σ = 200 µS/cm); (a) Voltage and Current signals (b) a zoom of these signals.

Figure A 24presents the energy per pulse for case 2 and case 3 for different frequencies. In **Figure A 24**(a) we obtain about 23 mJ of energy per pulse for 50 Hz-6 kV while it is about 20 mJ for 25 Hz-6 kV and 27 mJ for 5 Hz-8 kV. We observe that the energy per pulse increases when the applied voltage increases despite decreasing the frequency. In the same way, in **Figure A 24**(b), we obtain about 45 mJ of energy per pulse for 50 Hz-9 kV while it is about 48 mJ for 25 Hz-10 kV and 58 mJ for 5 Hz-11 kV.

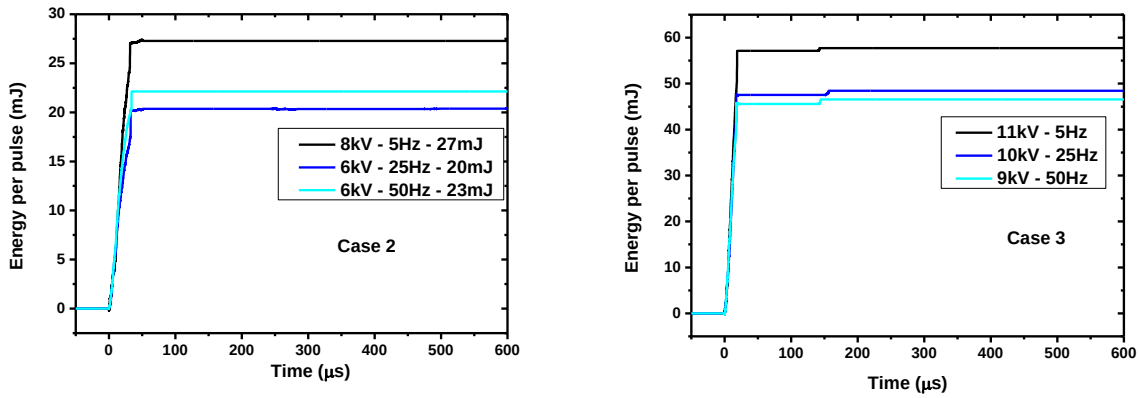

(a) (b)

Figure A 24 Time evolution of energy per pulse for (a) case 2 (b) for case 3 for different frequencies and voltages, V = 200 mL, Δt = 500 µs, 2 mm of gap, and σ = 200 µS/cm)

Annex 5.2 Effect of pulse duration on the H_2O_2 production

Figure A 25 shows the electrical signal of case 2 ((a) for 6 kV) and case 3 ((b) for 9 kV) with different pulse durations. There is no significant modification in the electrical waveforms for case 2 and case 3 with changing the pulse duration. However, regarding case 3, the number of breakdowns decreases with decreasing the pulse duration since the secondary breakdowns used to occur after 50µs. For example, we obtain two breakdowns in case 3, 9kV-500 µs, but only one breakdown is obtained for 50 and 100 µs (as presented in **Figure A 25** (b)).

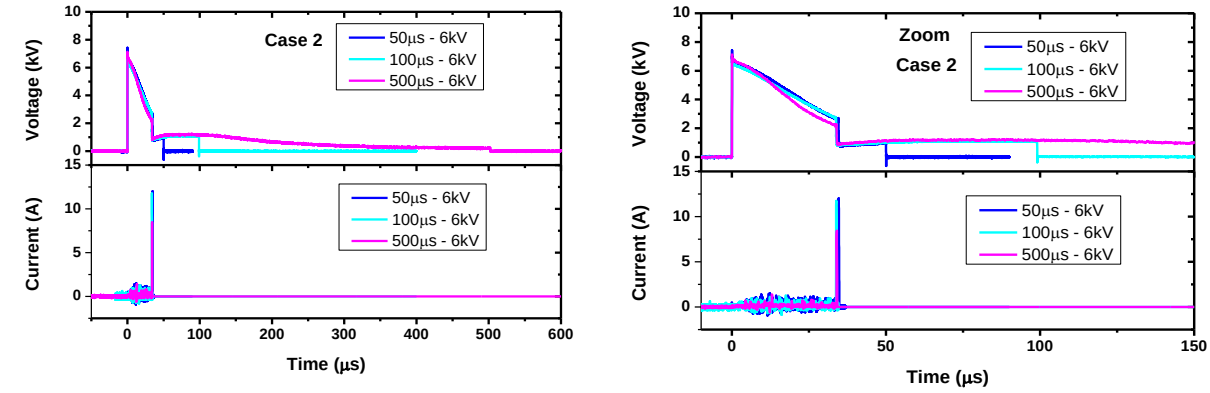

(a)

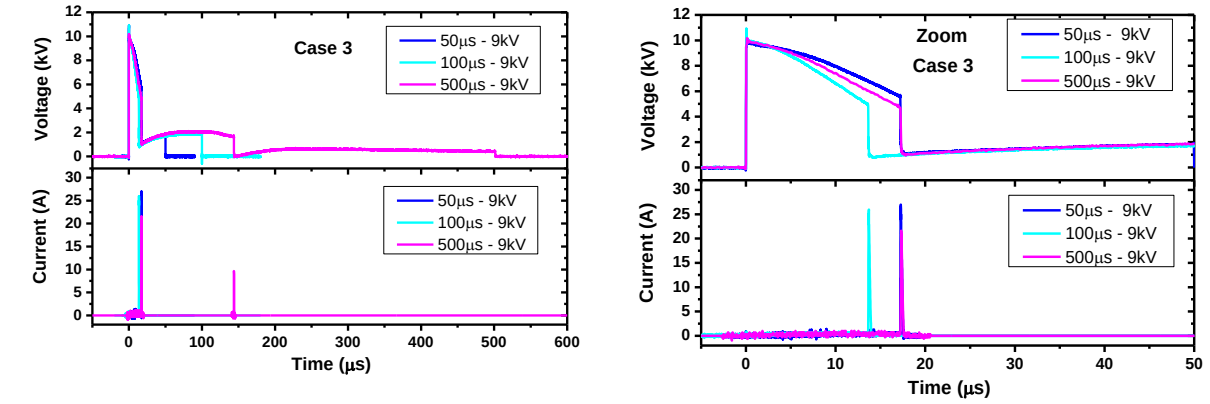

(b)

Figure A 25 Electrical waveforms of pin-to-pin discharge generated in water for different pulse durations V = 200 mL, Δt = 500 µs, 2 mm of gap, and σ = 200 µS/cm); (a) Voltage and Current signals of case 2 - 6 kV with different pulse durations (b) Voltage and Current signals of case 3 - 9 kV with different pulse durations

As illustrated in **Figure A 26**, most energy is deposited before 50 µs (before the first breakdown). Considering the uncertainties in the measurement (10 %), the energy per pulse does not depend significantly on the pulse duration.

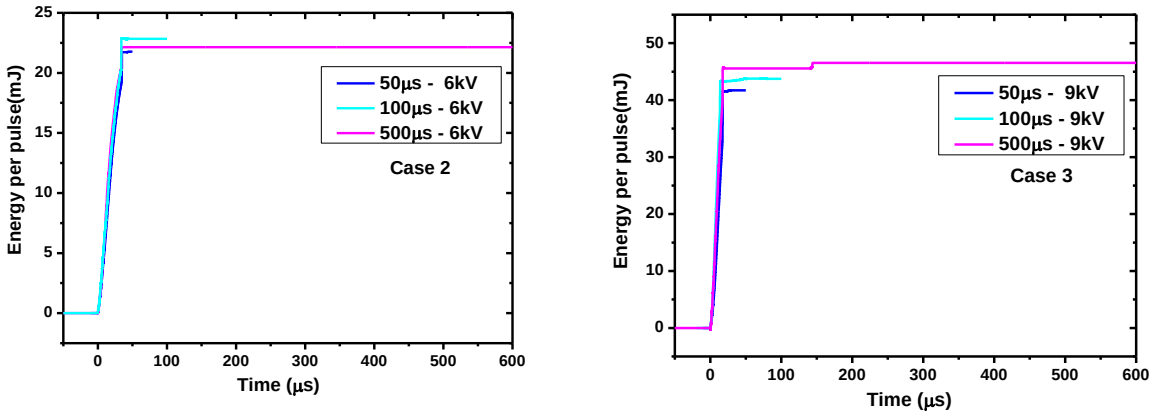

(a) (b)

Figure A 26 Time evolution of energy per pulse of (a) case 2 - 6 kV with different pulse durations (b) case 3 9 kV with a different pulse durations V = 200 mL, f = 50 Hz, 2 mm of gap, and σ = 200 µS/cm

Annex 5.3 Effect of different electrode materials on H_2O_2 formation

Figure A 27 shows the electrical waveforms and the energy delivered for three cases for different materials of the electrodes. There is no significant modification in the electrical waveforms for all of the case with changing the electrode materials. The uncertainties of about 10 % on the energy, for example in case 2 6 kV the maximum variations on the energy from 23 mJ to 26 mJ.

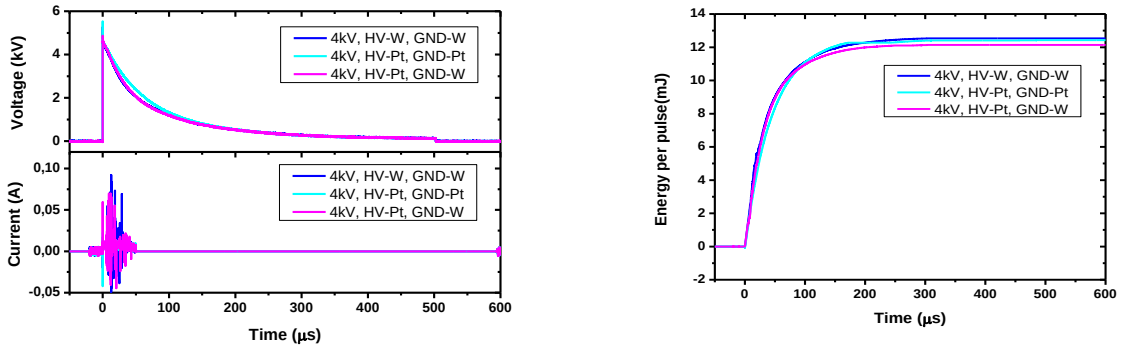

(a)

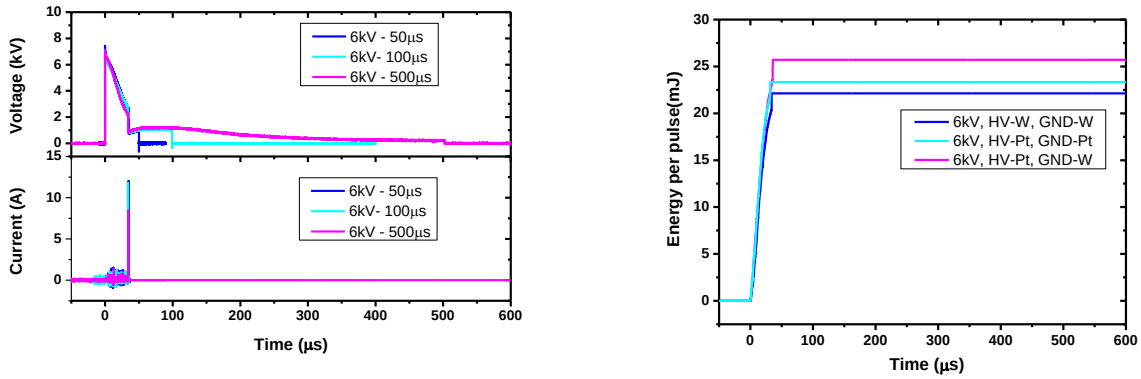

(b)

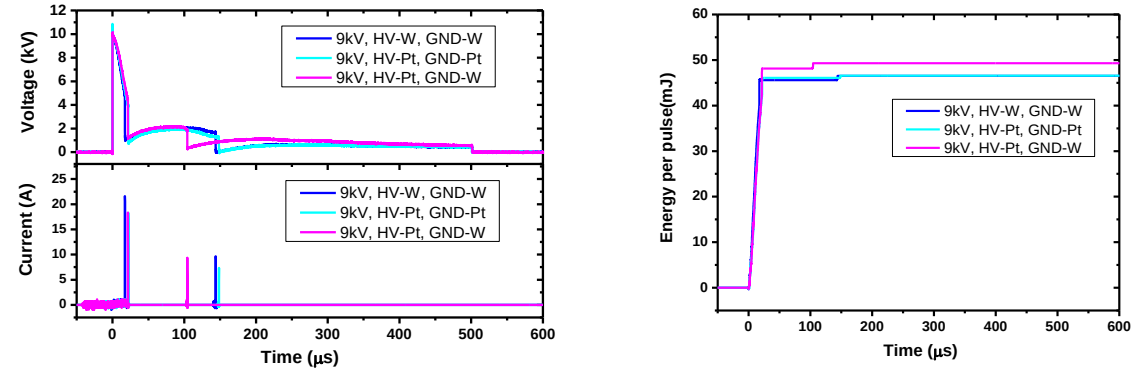

(c)

Figure A 27 Electrical waveforms and energy per pulse of pin-to-pin discharge generated in water for different electrodes material. (a) case 1- 4 kV (b) case 2 -6 kV and (c) case 3-9 kV. V = 200 mL, Δt = 500 µs, 2 mm of gap, and σ = 200 µS/cm. HV means anode and GND is for the cathode

Annex 5.4 Effect of electrodes parameters on H_2O_2 formation

Figure A 28 shows the electrical waveforms and the time evolution of the energy per pulse for 6 and 9 kV with the electrodes' differences in length and diameter. There is no significant modification in the electrical waveforms for all of the case with changing the electrode parameters. The uncertainties of about 10 % on the energy, for example in case 2 6 kV the maximum variations on the energy from 22 mJ to 25 mJ

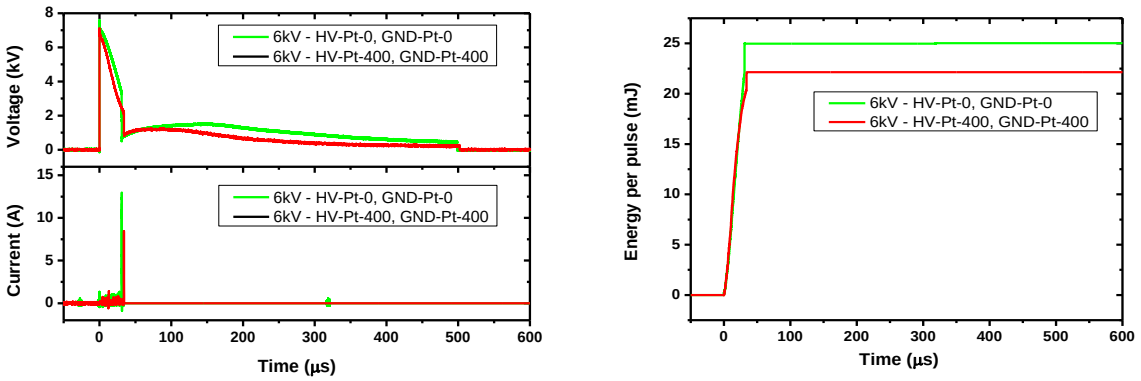

(a)

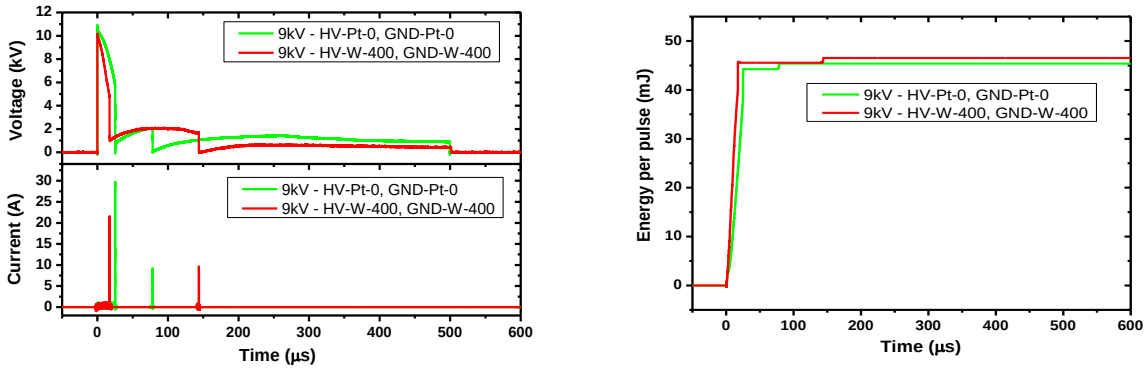

(b)

Figure A 28 Electrical waveforms and energy per pulse of pin-to-pin discharge generated in water for different electrodes length and diameters. (a) 6 kV (b) 9 kV. V = 200 mL, Δt = 500 µs, 2 mm of gap, and σ = 200 µS/cm). HV means anode, and GND is for the cathode. The green curve presented the signal of discharge with the electrode's diameter = 200 µm, and the red curve presented the signal of discharge with the electrode's diameter = 100 µm

Annex 5.5 Effect of electrolytes on H_2O_2 formation

Figure A 29 shows the electrical waveforms of NOBK for different electrolytes at the same 4 mS/cm of solution conductivity.

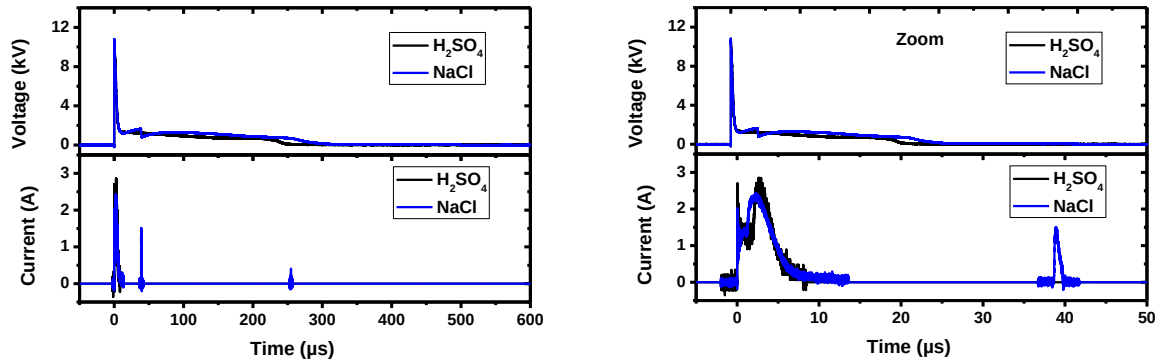

(a) (b)

Figure A 29 Electrical waveforms and zoom of pin-to-pin discharge generated in water for different electrolytes. U= 9 kV, V = 100 mL, Δt = 500 µs, 2 mm of gap, and σ = 4 mS/cm.

Annex Chapter 6

Annex 6.1 Effect of pulse frequency on the reduction of Cr(VI)

For U = 8 kV

Table A 11 shows the pH and the conductivity of the solution before and after plasma discharge for the different pulse frequencies for the applied voltage of 8 k. We do not observe any significant change in the final pH values for an increase in the pulse frequency of plasma discharge despite different durations of the process. The solution conductivity change is irregular because the time of the process and the number of pulses is very different. For example, at the pulse frequency of 70 Hz, after 105 minutes with the number of pulses being 441 K, the solution conductivity is decreased by about 26 % (from 4.08 to 3.04 mS/cm). In comparison, at 25 Hz, the time of process increased up to 300 minutes, and we obtained the same order of magnitude in the number of pulses (450 K), but the solution conductivity is decreased by about 21 % (from 4.07 to 3.43 mS/cm). We noted that the phenomena are similar when we compared the change of solution conductivity for discharge at pulse frequencies of 50 Hz and 10 Hz. However, it is not easy to draw an accurate conclusion about the effect of pulse frequency on the change in conductivity of the solution because a change in pulse frequency leads to a change in many parameters such as the processing time and the number of pulses.

Pulse frequency (Hz)	Duration of the process (minutes) -*number of pulses*	pH		Conductivity (mS/cm)	
		Initial	Final	Initial	Final
10	540 – *324K*	2.4	2.4	4.07	3.60
25	300 – *450K*	2.4	2.4	4.07	3.20
50	120 – *360K*	2.4	2.4	4.07	3.43
70	105 – *441K*	2.4	2.4	4.08	3.04

Table A 11 Initial and final solution parameters obtained from ex situ pH and conductivity measurements for the different pulse frequency. Cr(VI) solution (47 mg/L, σ=4 mS/cm, pH=2.4) U = 8 kV, V = 100 mL, Δt = 500 µs, gap = 2 mm, electrodes length = 0±10 µm

For U = 9 kV

Due to the limitations of the device, it is not able to operate at 70 Hz at 9 kV; therefore, the pulse frequency is changed from 10 Hz to 50 Hz. We note that in this study, we always keep the same duration of the process (*i.e.*, 120 minutes) to confirm the influence of a number of pulses on reduction efficiency.

Figure A 30 presents the concentration of Cr(VI) as a function of the number of pulses. We obtain a linear Cr(VI) reduction behavior for a given pulse frequency. We also obtain the same reduction rate for the same number of pulses as presented previously at 8 kV. For example, we have the same 13 % on reducing Cr(VI) when the number of pulses is 45 000 for all pulse frequencies. The same phenomenon is obtained for 25 Hz and 50 Hz at the pulse rate of 180 000. However, we can see that for the same process duration of 120 minutes, a low applied frequency is the worst case for the reduction of Cr(VI), because the number of pulses decreases.

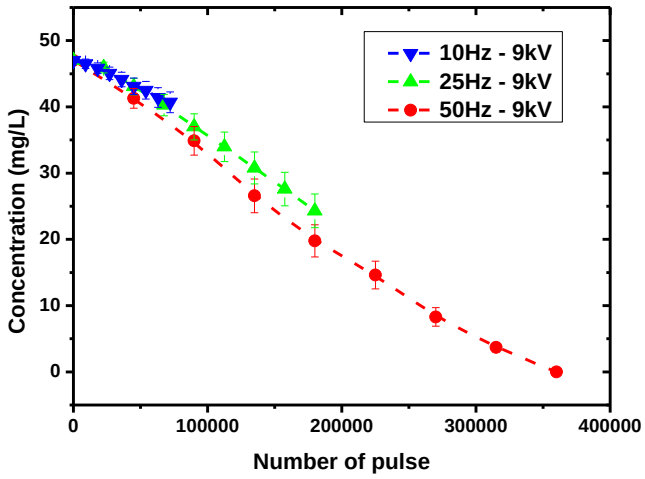

Figure A 30 Concentration of Cr(VI) as a function of number of pulses of a pin-to-pin discharge obtained in Cr(VI) solution (47 mg/L, σ=4 mS/cm, pH=2.4) U = 9 kV, V = 100 mL, Δt = 500 µs, f = 50 Hz, gap = 2 mm, electrodes length = 0±10 µm.

We also observe that the number of BK increases with an increase in pulse frequency (**Figure A 31**). For example, the number of BK increases from 8 % to 15 % for increased pulse frequency from 10 Hz to 50 Hz. A slight increase in injected energy is obtained when the pulse rate is increased from 10 Hz to 25 Hz. However, this increase is not obtained when the pulse frequency is increased from 25 Hz to 50 Hz (**Figure A 31** and **Table A 12**).

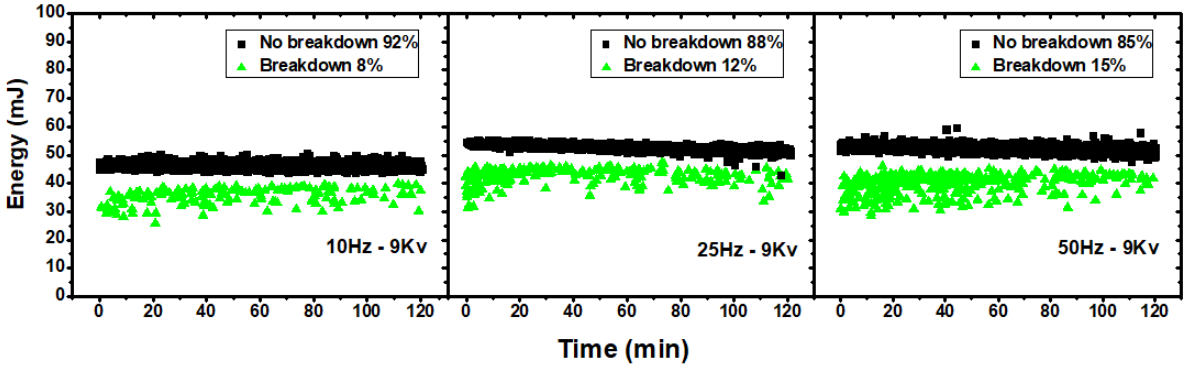

Figure A 31 Time evolution of the injected energy per pulse for the different frequencies (10 Hz, 25 Hz, and 50 Hz). Cr(VI) solution (47 mg/L, σ=4 mS/cm, pH=2.4) U = 9 kV, V = 100 mL, f = 50 Hz, Δt = 500 µs, gap = 2 mm, electrodes length = 0±10 µm. The time of the process is 120 minutes.

Table A 12 shows the influence of pulse frequency on the reduction efficiency and the discharge characteristics. We obtain that reducing the pulse frequency from 50 Hz to 10 Hz leads to a decrease in reduction efficiency from 100 % to 13 %, and also, the total injected energy decreases from 18.4 to 3.2 kJ, respectively. This decrease leads to variations in the energy yield, which is slightly decreasing from 2.6×10^{-4} to 1.9×10^{-4} g/kJ. However, we note that the decreased pulse frequency from 50 Hz to 25 Hz does not significantly change the energy yield due to the proportional decrease of reduction efficiency and the total injected energy, as shown in **Table A 12**. Regardless, the main goal of this work is to reduce 100 % of the Cr(VI) in the solution; therefore, it is not interesting to work at low frequencies.

	10 Hz	**25 Hz**	**50 Hz**
Reduction efficiency	13 %	48 %	100 %
Number of BK/NOBK	8 / 92	12 / 88	15 / 85
Energy per pulse BK / NOBK (mJ)	34 / 46	40 / 53	42 / 54
Total Energy (kJ)	3.2	9.0	18.8
Energy yield (g/kJ)	1.9×10^{-4}	2.5×10^{-4}	2.5×10^{-4}

Table A 12 Influence of applied pulse frequencies on Cr(VI) reduction efficiency and the discharge characteristic. Cr(VI) solution (47 mg/L, σ=4 mS/cm, pH=2.4) U = 9 kV, V = 100 mL, Δt = 500 µs, f = 50 Hz, gap = 2 mm, electrodes length = 0±10 µm. The time of the process is 120 minutes.

As shown in **Table A 13**, the pH of the solution does not change at the end of the process for a given pulse frequency. The conductivity of the solution decreases more when the pulse frequency is increased (or the number of pulses is increased). For example, when discharging at 10 Hz (or a pulse number of 75 K), we obtained a decrease of only 4 % from 4.07 to 3.89 mS/cm, while when discharging at 50 Hz (or a pulse number of 360 K), we obtained a decrease of 23 % (from 4.01 to 3.08 mS/cm).

Pulse frequency (Hz)	Time of the process (minutes) -number of pulses	pH		Conductivity (mS/cm)	
		Initial	Final	Initial	Final
10	120 – 75 K	2.4	2.4	4.07	3.89
25	120 – 180 K	2.4	2.4	4.07	3.70
50	120 – 360 K	2.4	2.4	4.01	3.08

Table A 13 Initial and final solution parameters obtained from ex situ pH and conductivity measurements for the different pulse frequencies. Cr(VI) solution (47 mg/L, σ=4 mS/cm, pH=2.4) U = 9 kV, V = 100 mL, f = 50 Hz, Δt = 500 μs, gap = 2 mm, electrodes length = 0±10 μm.

Annex 6.2 *In situ* measurement of Cr(VI)

As presented in **Chapter 3**, the advantage of this *in situ* method is that there is no need to sample solutions or use any reagents, and above all, this method can accurately determine when Cr(VI) is completely reduced. The principle of this method is based on the changes in the transmitted power of incoming light through the Cr(VI) solution during the process, which follows the Beer-Lambert law. Thus the path length is one of the parameters that have an influence on the output signal.

In this section, we study the influence of path length on the measurement of Cr(VI) concentration during the treatment process. The path length will be changed from 5 to 10 cm. We note that in this work, the path length corresponds to the length and width of the reactor. The quartz reactor is used with a length of 10 cm and a width of 5 cm. The conditions used for this section are: the length of both platinum electrodes is HV-0-GND-0 with a diameter of 200 µm; Δt = 500 µs, 2 mm gap. The volume of the working solution is 100 mL, with the initial concentration of Cr(VI) equal to 47 mg/L. The initial pH of the solution is 2.4, and the initial conductivity of the solution is about 4 mS/cm. The applied voltage is kept the same for all of the experiments at 9 kV. The Cr(VI) concentrations are obtained from the measured output power of the solution during the treatment process compared with the established calibration curve (**Annex 3.3**).

5 cm path length

Figure A 32 (a) shows the change in the output power during the 120 minutes of the treatment process. We obtain a slight increase in the output power from beginning up to 80 minutes (<500 µW) due to the high absorbance of the Cr(VI) solution. After that, when Cr(VI) concentration is more reduced, we obtain a very high transmittance from 90 minutes to the end of the process. However, we note that this change does not evaluate the speed of the reduction process. We observe that the power reaches a maximum at 118 minutes and then decreases (as shown in **Figure A 32** (b)). We noted that this maximum peak corresponds to the complete reduction of Cr(VI). To verify the concentration of Cr(VI) at this time, we sample 2 mL of the solution and mix it with 1 mL of DPC solution. The UV-vis spectrum analysis results does not show any absorption of Cr(VI) complexe with DPC. This means that Cr(VI) has been completely reduced.

We also obtain that the power is slightly decreased after 118 minutes. We noted that the discharge is still active for up to 120 minutes, then many species are still produced in solution. This species can absorb the incoming light, thus leading to the decrease of the output power. After 120 min, when the plasma is turned off, these species are no longer formed, resulting in a constant of output power (**Figure A 32**(b)). Several investigations have reported this phenomenon [262–265]. By analyzing the results of plasma-activated water, they obtained the absorbances of several species such as H_2O_2, O_2, O_3, H_2 at wavelengths from 200 nm to 400 nm.

To demonstrate this, we also perform some experiments with discharge in water to obtain the change in power during discharge and after discharge. The results of this experiment are consistent with the given explanations. We also note that it is difficult to distinguish precisely the species that affect the output power.

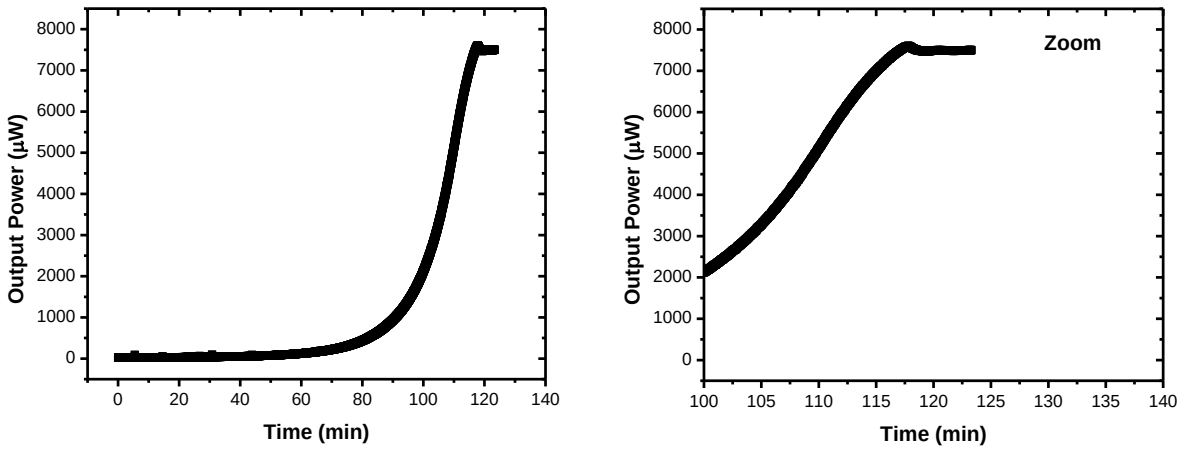

(a) (b)

Figure A 32 Output power as a function of time (a) and a zoom (b) of a pin-to-pin discharge obtained in Cr(VI) solution (47 mg/L, σ=4 mS/cm, pH=2.4) U = 9 kV, V = 100 mL, Δt = 500 µs ,f = 50 Hz, gap = 2 mm, electrodes length = 0±10 µm. 5 cm path length. 5 cm path length

Figure A 33 shows the Cr(VI) concentration as a function of time obtained by two different measurement methods. We note that the green curve is obtained by the direct ex situ measurement, which is used to measure the absorbance of Cr(VI) in this thesis. The black curve presents the Cr(VI) concentration results measured by the new *in situ* method. We observe a similar Cr(VI) concentration behavior for both methods. The black curve shows that the Cr(VI) concentration is reduced to zero at about 118 minutes instead of the 120 minutes obtained with the ex situ method. This result confirms the approximation discussed in chapter VI concerning the determination of the total injected energy used for the total reduction of Cr(VI).

We can first conclude that it is possible to measure *in situ* the concentration of Cr(VI) with more time accuracy by using this experimental setup. This method allow identifying when Cr(VI) is completely reduced.

In the next section, we will present the influence of the path length on the output signal when the path length is increased to 10 cm. This study aims to improve the technique about the concentration sensitivity.

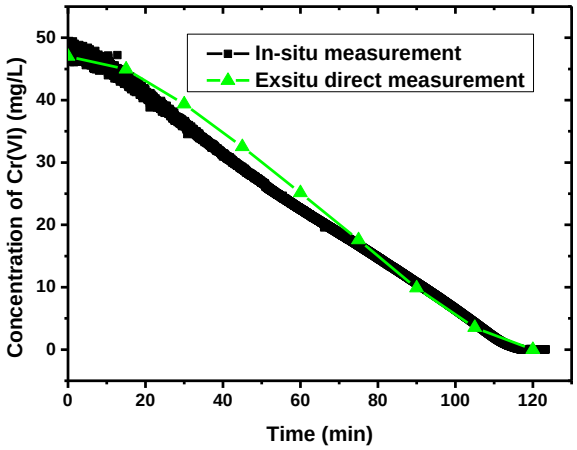

Figure A 33 Concentration of Cr(VI) as a function of time measured by two different methods of a pin-to-pin discharge obtained in Cr(VI) solution (47 mg/L, σ=4 mS/cm, pH=2.4) U = 9 kV, V = 100 mL, Δt = 500 μs, f = 50 Hz, gap = 2 mm, electrodes length = 0±10 μm. 5 cm path length.

10 cm path length

Figure A 34 (a) shows the change in the output power during the 120 minutes of the treatment process. We obtain a slow increase in the output power from beginning up to 90 minutes (<250 µW) due to the high absorbance of the Cr(VI) solution. After that, we obtain a very high transmittance from 100 minutes to the end of the process. Similar to the 5 cm path length results, we also obtain a maximum on the output power at about 116 minutes, then after the output power slightly decreases up to the end of the process. The maximum output power also corresponds to the complete reduction of Cr(VI).

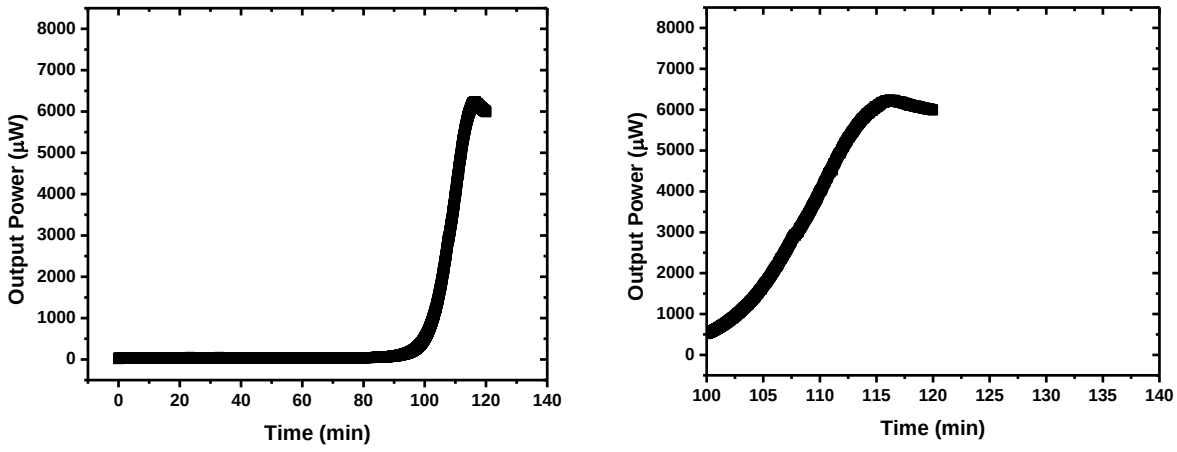

(a) (b)

Figure A 34 Output power as a function of time (a) and a zoom (b) of a pin-to-pin discharge obtained in Cr(VI) solution (47 mg/L, σ=4 mS/cm, pH=2.4) U = 9 kV, V = 100 mL, Δt = 500 µs, f = 50 Hz, gap = 2 mm, electrodes length = 0±10 µm. 10 cm path length

However, as shown in **Annex 3.3**, we obtain the break of Beer-Lambert law ffor high concentrations of Cr(VI) when the path length increases to 10 cm. This method, dedicated to low concentration measurements, does nnot allow the calculation of the high concentration of Cr(VI), as shown in **Figure A 35**. We note that the green curve is obtained by the direct ex situ measurement, and the black curve presents the Cr(VI) concentration results measured by the new *in situ* method. We obtain huge variations on calculating the high Cr(VI) concentration in the first 60 minutes for concentrations higher than 25 mg/L. Then after 60 minutes, for lower concentrations, we obtain similar concentration of Cr(VI) for both measurement methods. We also obtain the total reduction of Cr(VI) at around 116 minutes instead of 120 min by the ex situ method and 118 min using 5cm-length.

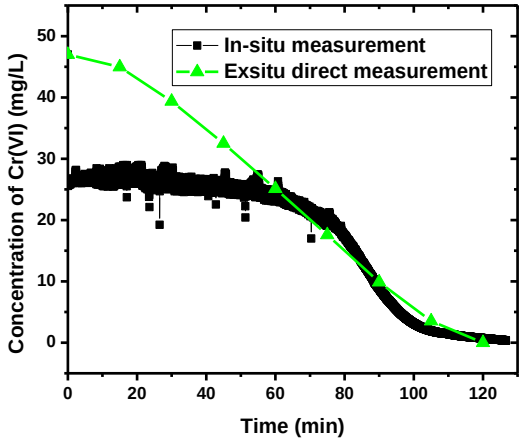

Figure A 35 Concentration of Cr(VI) as a function of time, measured by two different methods of a pin-to-pin discharge obtained in Cr(VI) solution (47 mg/L, σ=4 mS/cm, pH=2.4) U = 9 kV, V = 100 mL, Δt = 500 µs, f = 50 Hz, gap = 2 mm, electrodes length = 0±10 µm. 10 cm path length.

In conclusion, we note that the in situ method is easy to use and very powerful to monitor in real-time the Cr(VI) concentration. Moreover increasing the path length allows improving the detection threshold. Obviously, the path length has to be adapted to the range of the target concentrations in order to not break the Beer-Lambert law

Annex 6.3 *In situ* measurement of the discharge in water

Figure A 36 shows the output power as a function of time for discharge in water with 5 cm path length. We obtained two phases: Phase 1 corresponds to the output power during the plasma discharge. We can see that during the discharge, the production of many species leads to a decrease in the output power. Phase 2 corresponds to the output power after 120 minutes of discharge. As we can see, when there is no plasma discharge, the species that remain in solution disappear slowly, such as H_2O_2, leading to increasing the output power.

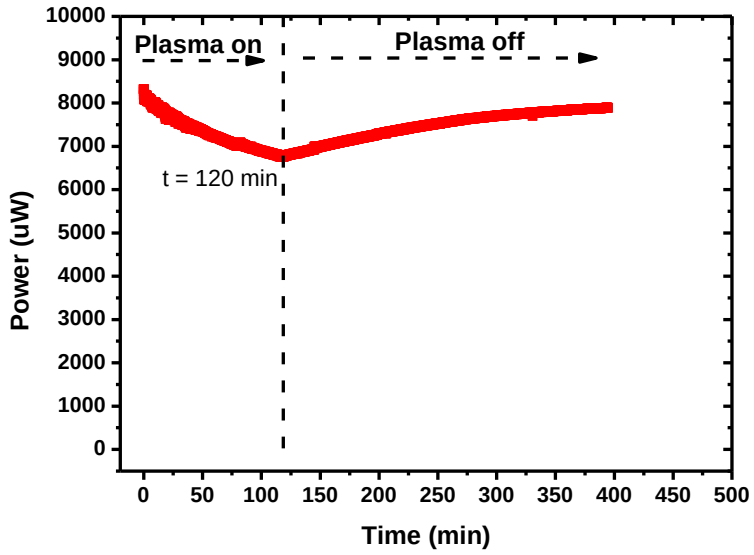

Figure A 36 Output power as a function of time of a pin-to-pin discharge obtained in water (σ=4 mS/cm adjust by H_2SO_4 0.1 M) for 9 kV, V = 100 mL, Δt = 500 µs, gap = 2 mm, electrodes length = 0±10 µm, f = 50 Hz. 5 cm path length

Annex Chapter 7

Annex 7. Comparison of the measurements of Cr(VI) concentration using two methods, the ex situ direct method and Vasko's method

Figure A 37 compares the concentration of Cr(VI) during the treatment process, measured by two methods: ex situ direct method and Vasko's method for three different applied voltages. As we can see, the results of both methods are similar.

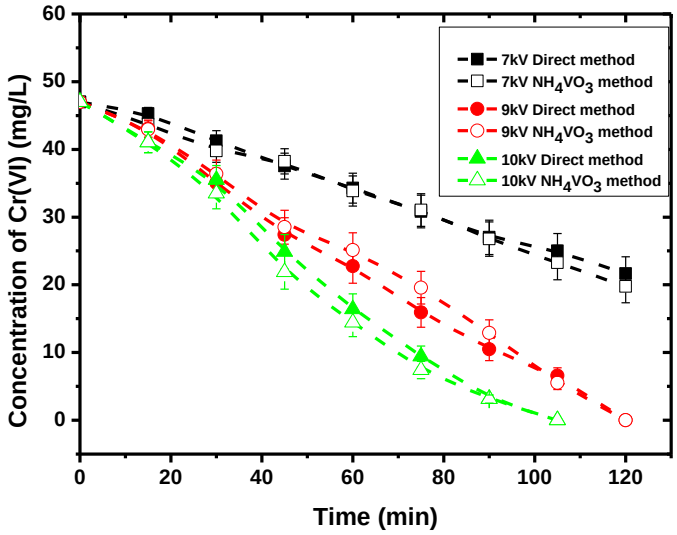

Figure A 37 Concentration of Cr(VI) as a function of time of a pin-to-pin discharge obtained in a pin-to-pin discharge obtained in Cr(VI) solution (47 mg/L, σ = 4 mS/cm, pH = 2.4) for 7, 9, and 10 kV, V = 100 mL, Δt = 500 µs, gap = 2 mm, electrodes length = 0±10 µm, f = 50 Hz. Measurements by two different methods.

References

(1) Https://Www.Actu-Environnement.Com/Ae/News/Marseille-Eaux-Souterraines-Risques-Sanitaires-ChromeVI-35032.Php4.

(2) Https://France3-Regions.Francetvinfo.Fr/Provence-Alpes-Cote-d-Azur/Bouches-Du-Rhone/Marseille/Pollution-Historique-Au-Chrome-Inquiete-Toujours-Riverains-Du-Quartier-Saint-Louis-Marseille-1784241.Html.

(3) Wang, L.; Jiang, X. Plasma-Induced Reduction of Chromium (VI) in an Aqueous Solution. *Environ. Sci. Technol.* **2008**, *42* (22), 8492–8497.

(4) Jiang, B.; Guo, J.; Wang, Z.; Zheng, X.; Zheng, J.; Wu, W.; Wu, M.; Xue, Q. A Green Approach towards Simultaneous Remediations of Chromium(VI) and Arsenic(III) in Aqueous Solution. *Chem. Eng. J.* **2015**, *262*, 1144–1151. https://doi.org/10.1016/j.cej.2014.10.064.

(5) Du, C.; Yan, J. Reduction and Removal of Cr(VI) from Aqueous Solution by Microplasma. In *Plasma Remediation Technology for Environmental Protection*; Advanced Topics in Science and Technology in China; Springer Singapore: Singapore, 2017; pp 41–59. https://doi.org/10.1007/978-981-10-3656-9_4.

(6) Ke, Z.; Huang, Q.; Zhang, H.; Yu, Z. Reduction and Removal of Aqueous Cr(VI) by Glow Discharge Plasma at the Gas–Solution Interface. *Environ. Sci. Technol.* **2011**, *45* (18), 7841–7847. https://doi.org/10.1021/es201680m.

(7) Burns, V. M.; Burns, R. G. Mineralogy of Chromium. In *Chromium: its Physicochemical Behavior and Petrologic Significance*; Irvine, T. N., Ed.; Pergamon, 1976; pp 903–910. https://doi.org/10.1016/B978-0-08-019954-2.50015-9.

(8) Https://Www.Chemguide.Co.Uk/Inorganic/Transition/Chromium.Html.

(9) Tumolo, M.; Ancona, V.; De Paola, D.; Losacco, D.; Campanale, C.; Massarelli, C.; Uricchio, V. F. Chromium Pollution in European Water, Sources, Health Risk, and Remediation Strategies: An Overview. *Int. J. Environ. Res. Public. Health* **2020**, *17* (15), 5438. https://doi.org/10.3390/ijerph17155438.

(10) Wilbur, S. B. *Toxicological Profile for Chromium*; US Department of Health and Human Services, Public Health Service, Agency, 2000.

(11) Hua, Y.; Clark, S.; Ren, J.; Sreejayan, N. Molecular Mechanisms of Chromium in Alleviating Insulin Resistance. *J. Nutr. Biochem.* **2012**, *23* (4), 313–319.

(12) Yatera, K.; Morimoto, Y.; Ueno, S.; Noguchi, S.; Kawaguchi, T.; Tanaka, F.; Suzuki, H.; Higashi, T. Cancer Risks of Hexavalent Chromium in the Respiratory Tract. *J. UOEH* **2018**, *40* (2), 157–172.

(13) Tao, M.; Chen, L.; Xiong, X.; Zhang, M.; Ma, P.; Tao, J.; Wang, Z. Formation Process of the Widespread Extreme Haze Pollution over Northern China in January 2013: Implications for Regional Air Quality and Climate. *Atmos. Environ.* **2014**, *98*, 417–425. https://doi.org/10.1016/j.atmosenv.2014.09.026.

(14) Järup, L. Hazards of Heavy Metal Contamination. *Br. Med. Bull.* **2003**, *68* (1), 167–182. https://doi.org/10.1093/bmb/ldg032.

(15) Ferreira, L. M.; Cunha-Oliveira, T.; Sobral, M. C.; Abreu, P. L.; Alpoim, M. C.; Urbano, A. M. Impact of Carcinogenic Chromium on the Cellular Response to Proteotoxic Stress. *Int. J. Mol. Sci.* **2019**, *20* (19), 4901.

(16) https://www.osha.gov/SLTC/hexavalentchromium/healtheffects.html (accessed 2020 -04 -07).

(17) Mesbah, F. H. G.; Zewail, T. M.; Farag, H. A. Equilibrium and Kinetic Studies of Cr (VI) Removal from Aqueous Solution Using DiaionSA20A Exchange Resin. *environment* **2015**, *1* (2).

(18) Fan, X.; Ding, S.; Chen, M.; Gao, S.; Fu, Z.; Gong, M.; Tsang, D. C. W.; Wang, Y.; Zhang, C. Peak Chromium Pollution in Summer and Winter Caused by High Mobility of Chromium in

Sediment of a Eutrophic Lake: In Situ Evidence from High Spatiotemporal Sampling. *Environ. Sci. Technol.* **2019**, *53* (9), 4755–4764. https://doi.org/10.1021/acs.est.8b07060.
(19) Lindberg, E.; Hedenstierna, G. Chrome Plating: Symptoms, Findings in the Upper Airways, and Effects on Lung Function. *Arch. Environ. Health Int. J.* **1983**, *38* (6), 367–374. https://doi.org/10.1080/00039896.1983.10545822.
(20) Zhang, J. D.; Li, X. L. [Chromium pollution of soil and water in Jinzhou]. *Zhonghua Yu Fang Yi Xue Za Zhi* **1987**, *21* (5), 262–264.
(21) Linos, A.; Petralias, A.; Christophi, C. A.; Christoforidou, E.; Kouroutou, P.; Stoltidis, M.; Veloudaki, A.; Tzala, E.; Makris, K. C.; Karagas, M. R. Oral Ingestion of Hexavalent Chromium through Drinking Water and Cancer Mortality in an Industrial Area of Greece - An Ecological Study. *Environ. Health* **2011**, *10* (1), 50. https://doi.org/10.1186/1476-069X-10-50.
(22) Sazakli, E.; Villanueva, C.; Kogevinas, M.; Maltezis, K.; Mouzaki, A.; Leotsinidis, M. Chromium in Drinking Water: Association with Biomarkers of Exposure and Effect. *Int. J. Environ. Res. Public. Health* **2014**, *11* (10), 10125–10145. https://doi.org/10.3390/ijerph111010125.
(23) Sharma, P.; Bihari, V.; Agarwal, S. K.; Verma, V.; Kesavachandran, C. N.; Pangtey, B. S.; Mathur, N.; Singh, K. P.; Srivastava, M.; Goel, S. K. Groundwater Contaminated with Hexavalent Chromium [Cr (VI)]: A Health Survey and Clinical Examination of Community Inhabitants (Kanpur, India). *PLoS ONE* **2012**, *7* (10), e47877. https://doi.org/10.1371/journal.pone.0047877.
(24) http://www.who.int/water_sanitation_health/publications/chromium/en/ (accessed 2020 -03 -31).
(25) https://www.waterboards.ca.gov/drinking_water/certlic/drinkingwater/Chromium6.html (accessed 2020 -04 -08).
(26) Saponaro, S.; Brizzi, L.; Galbusera, F.; Mastorgio, A. F.; Sezenna, E. In Situ Hexavalent Chromium Reduction by Injection of Organic Substrates in the Aquifer; USA, 2016; pp 1–7.
(27) Kumar, P. S.; Kirthika, K.; Kumar, K. S. Removal of Hexavalent Chromium Ions from Aqueous Solutions by an Anion-Exchange Resin. *Adsorpt. Sci. Technol.* **2008**, *26* (9), 693–703. https://doi.org/10.1260/026361708788251402.
(28) Fu, F.; Wang, Q. Removal of Heavy Metal Ions from Wastewaters: A Review. *J. Environ. Manage.* **2011**, *92* (3), 407–418. https://doi.org/10.1016/j.jenvman.2010.11.011.
(29) Zewail, T. M.; Yousef, N. S. Kinetic Study of Heavy Metal Ions Removal by Ion Exchange in Batch Conical Air Spouted Bed. *Alex. Eng. J.* **2015**, *54* (1), 83–90. https://doi.org/10.1016/j.aej.2014.11.008.
(30) https://www.iwapublishing.com/news/removal-technologies-wastewater-treatment (accessed 2020 -04 -09).
(31) Kang, S.-Y.; Lee, J.-U.; Moon, S.-H.; Kim, K.-W. Competitive Adsorption Characteristics of Co2+, Ni2+, and Cr3+ by IRN-77 Cation Exchange Resin in Synthesized Wastewater. *Chemosphere* **2004**, *56* (2), 141–147. https://doi.org/10.1016/j.chemosphere.2004.02.004.
(32) Petruzzelli, D.; Passino, R.; Tiravanti, G. Ion Exchange Process for Chromium Removal and Recovery from Tannery Wastes. *Ind. Eng. Chem. Res.* **1995**, *34* (8), 2612–2617. https://doi.org/10.1021/ie00047a009.
(33) Shi, T.; Wang, Z.; Liu, Y.; Jia, S.; Changming, D. Removal of Hexavalent Chromium from Aqueous Solutions by D301, D314 and D354 Anion-Exchange Resins. *J. Hazard. Mater.* **2009**, *161* (2–3), 900–906. https://doi.org/10.1016/j.jhazmat.2008.04.041.
(34) Lyubchik, S.; Lyubchik, A.; Lygina, O.; Lyubchik, S.; Fonsec, I. Comparison of the Thermodynamic Parameters Estimation for the Adsorption Process of the Metals from Liquid Phase on Activated Carbons. In *Thermodynamics - Interaction Studies - Solids, Liquids and Gases*; Moreno Pirajn, J. C., Ed.; InTech, 2011. https://doi.org/10.5772/19514.
(35) Chingombe, P.; Saha, B.; Wakeman, R. J. Surface Modification and Characterisation of a Coal-Based Activated Carbon. *Carbon* **2005**, *43* (15), 3132–3143. https://doi.org/10.1016/j.carbon.2005.06.021.

(36) Mohan, D.; Pittman, C. U. Activated Carbons and Low Cost Adsorbents for Remediation of Tri- and Hexavalent Chromium from Water. *J. Hazard. Mater.* **2006**, *137* (2), 762–811. https://doi.org/10.1016/j.jhazmat.2006.06.060.

(37) Jusoh, A.; Su Shiung, L.; Ali, N.; Noor, M. J. M. M. A Simulation Study of the Removal Efficiency of Granular Activated Carbon on Cadmium and Lead. *Desalination* **2007**, *206* (1–3), 9–16. https://doi.org/10.1016/j.desal.2006.04.048.

(38) Pérez-Candela, M.; Martín-Martínez, M. José.; Torregrosa-Maciá, R. Chromium(VI) Removal with Activated Carbons. *Water Res.* **1995**, *29* (9), 2174–2180. https://doi.org/10.1016/0043-1354(95)00035-J.

(39) Hamadi, N. Adsorption Kinetics for the Removal of Chromium(VI) from Aqueous Solution by Adsorbents Derived from Used Tyres and Sawdust. *Chem. Eng. J.* **2001**, *84* (2), 95–105. https://doi.org/10.1016/S1385-8947(01)00194-2.

(40) Park, S.-J.; Jung, W.-Y. Removal of Chromium by Activated Carbon Fibers Plated with Copper Metal. *Carbon Lett.* **2001**, *2* (1), 15–21.

(41) Chopra, A. K.; Sharma, A. K.; Kumar, V. Overview of Electrolytic Treatment: An Alternative Technology for Purification of Wastewater. *Arch. Appl. Sci. Res.* **2011**, *3* (5), 191–206.

(42) Owlad, M.; Aroua, M. K.; Daud, W. A. W.; Baroutian, S. Removal of Hexavalent Chromium-Contaminated Water and Wastewater: A Review. *Water. Air. Soil Pollut.* **2009**, *200* (1–4), 59–77.

(43) Jin, W.; Du, H.; Yan, K.; Zheng, S.; Zhang, Y. Improved Electrochemical Cr(VI) Detoxification by Integrating the Direct and Indirect Pathways. *J. Electroanal. Chem.* **2016**, *775*, 325–328. https://doi.org/10.1016/j.jelechem.2016.06.030.

(44) Martínez-Huitle, C. A.; Ferro, S. Electrochemical Oxidation of Organic Pollutants for the Wastewater Treatment: Direct and Indirect Processes. *Chem Soc Rev* **2006**, *35* (12), 1324–1340. https://doi.org/10.1039/B517632H.

(45) Garcia-Segura, S.; Eiband, M. M. S. G.; de Melo, J. V.; Martínez-Huitle, C. A. Electrocoagulation and Advanced Electrocoagulation Processes: A General Review about the Fundamentals, Emerging Applications and Its Association with Other Technologies. *J. Electroanal. Chem.* **2017**, *801*, 267–299. https://doi.org/10.1016/j.jelechem.2017.07.047.

(46) Chen, G. Electrochemical Technologies in Wastewater Treatment. *Sep. Purif. Technol.* **2004**, *38* (1), 11–41. https://doi.org/10.1016/j.seppur.2003.10.006.

(47) Sahu, O.; Mazumdar, B.; Chaudhari, P. K. Treatment of Wastewater by Electrocoagulation: A Review. *Environ. Sci. Pollut. Res.* **2014**, *21* (4), 2397–2413. https://doi.org/10.1007/s11356-013-2208-6.

(48) Lu, J.; Wang, Z.-R.; Liu, Y.-L.; Tang, Q. Removal of Cr Ions from Aqueous Solution Using Batch Electrocoagulation: Cr Removal Mechanism and Utilization Rate of in Situ Generated Metal Ions. *Process Saf. Environ. Prot.* **2016**, *104*, 436–443. https://doi.org/10.1016/j.psep.2016.04.023.

(49) Kurniawan, T. A.; Chan, G. Y. S.; Lo, W.-H.; Babel, S. Physico–Chemical Treatment Techniques for Wastewater Laden with Heavy Metals. *Chem. Eng. J.* **2006**, *118* (1–2), 83–98. https://doi.org/10.1016/j.cej.2006.01.015.

(50) Rana, P.; Mohan, N.; Rajagopal, C. Electrochemical Removal of Chromium from Wastewater by Using Carbon Aerogel Electrodes. *Water Res.* **2004**, *38* (12), 2811–2820. https://doi.org/10.1016/j.watres.2004.02.029.

(51) Kongsricharoern, N.; Polprasert, C. Chromium Removal by a Bipolar Electro-Chemical Precipitation Process. *Water Sci. Technol.* **1996**, *34* (9), 109–116. https://doi.org/10.2166/wst.1996.0189.

(52) Noller, B. N.; Woods, P. H.; Ross, B. J. Case Studies of Wetland Filtration of Mine Waste Water in Constructed and Naturally Occurring Systems in Northern Australia. *Water Sci. Technol.* **1994**, *29* (4), 257–265. https://doi.org/10.2166/wst.1994.0205.

(53) Minas, F.; Chandravanshi, B. S.; Leta, S. Chemical Precipitation Method for Chromium Removal and Its Recovery from Tannery Wastewater in Ethiopia. *Chem. Int.* **2017**, *3* (4), 392–405.

(54) Jobby, R.; Jha, P.; Yadav, A. K.; Desai, N. Biosorption and Biotransformation of Hexavalent Chromium [Cr(VI)]: A Comprehensive Review. *Chemosphere* **2018**, *207*, 255–266. https://doi.org/10.1016/j.chemosphere.2018.05.050.
(55) https://www.elsevier.com/books/atomic-absorption-spectrometry/cantle/978-0-444-42015-2 (accessed 2020 -04 -10).
(56) Markiewicz, B.; Komorowicz, I.; Sajnóg, A.; Belter, M.; Barałkiewicz, D. Chromium and Its Speciation in Water Samples by HPLC/ICP-MS – Technique Establishing Metrological Traceability: A Review since 2000. *Talanta* **2015**, *132*, 814–828. https://doi.org/10.1016/j.talanta.2014.10.002.
(57) Andrle, C. M.; Broekaert, J. A. C. Speciation of Cr(III) and Cr(VI) by Reversed Phase High-Performance Liquid Chromatography Using UV-Detection. *Fresenius J. Anal. Chem.* **1993**, *346* (6–9), 653–658. https://doi.org/10.1007/BF00321265.
(58) Barałkiewicz, D.; Pikosz, B.; Belter, M.; Marcinkowska, M. Speciation Analysis of Chromium in Drinking Water Samples by Ion-Pair Reversed-Phase HPLC–ICP-MS: Validation of the Analytical Method and Evaluation of the Uncertainty Budget. *Accreditation Qual. Assur.* **2013**, *18* (5), 391–401. https://doi.org/10.1007/s00769-013-1002-y.
(59) Barnowski, C.; Jakubowski, N.; Stuewer, D.; Broekaert, J. A. C. Speciation of Chromium by Direct Coupling of Ion Exchange Chromatography With Inductively Coupled Plasma Mass Spectrometry. *J. Anal. At. Spectrom.* **1997**, *12* (10), 1155–1161. https://doi.org/10.1039/a702120h.
(60) Frois, S. R.; Tadeu Grassi, M.; de Campos, M. S.; Abate, G. Determination of Cr(vi) in Water Samples by ICP-OES after Separation of Cr(Iii) by Montmorillonite. *Anal. Methods* **2012**, *4* (12), 4389. https://doi.org/10.1039/c2ay26125a.
(61) Zewdu, F.; Amare, M. Determination of the Level of Hexavalent, Trivalent, and Total Chromium in the Discharged Effluent of Bahir Dar Tannery Using ICP-OES and UV–Visible Spectrometry. *Cogent Chem.* **2018**, *4* (1). https://doi.org/10.1080/23312009.2018.1534566.
(62) Miyazaki, Akira.; Barnes, R. M. Differential Determination of Chromium(VI)-Chromium(III) with Poly(Dithiocarbamate) Chelating Resin and Inductively Coupled Plasma-Atomic Emission Spectrometry. *Anal. Chem.* **1981**, *53* (2), 364–366. https://doi.org/10.1021/ac00225a058.
(63) Jyothi, N. R.; Mohammad Farook, N. A.; Cho, M.; Shim, J. Analysis and Speciation of Chromium in Environmental Matrices by Various Analytical Techniques. *Asian J. Chem.* **2013**, *25* (8), 4125–4136. https://doi.org/10.14233/ajchem.2013.14625.
(64) *Https://Www.Iitk.Ac.in/Che/Pdf/Resources/AAS-GTA-Reading-Material.Pdf*.
(65) Oti Wilberforce et al. Review of Principles and Application of AAS, PIXE and XRF and Their Usefulness in Environmental Analysis of Heavy Metals. *Volume 9* (6 Ver. II (Jun. 2016)). https://doi.org/10.9790/5736-0906021517.
(66) West, M.; Ellis, A. T.; Kregsamer, P.; Potts, P. J.; Streli, C.; Vanhoof, C.; Wobrauschek, P. Atomic Spectrometry Update. X-Ray Fluorescence Spectrometry. *J. Anal. At. Spectrom.* **2008**, *23* (10), 1409. https://doi.org/10.1039/b813039f.
(67) Potts, P. J.; Ellis, A. T.; Kregsamer, P.; Marshall, J.; Streli, C.; Weste, M.; Wobrauschekc, P. Atomic Spectrometry Update. X-Ray Fluorescence Spectrometry. *J Anal Spectrom* **2003**, *18*, 1297–1316.
(68) Unceta, N.; Séby, F.; Malherbe, J.; Donard, O. F. X. Chromium Speciation in Solid Matrices and Regulation: A Review. *Anal. Bioanal. Chem.* **2010**, *397* (3), 1097–1111. https://doi.org/10.1007/s00216-009-3417-1.
(69) CORAZZA et al, M. Measurement of Nickel, Cobalt and Chromium in Toy Make-up by Atomic Absorption Spectroscopy. *Acta Derm Venereol* **2009**, *89*, 130–133.
(70) Belay, K.; Tadesse, A. Comparison of Digestion Methods for Determination of Pb (II), Cr (VI) and Cd (II) Contents in Some Ethiopia Spices Using Atomic Absorption Spectroscopy. *Int. J. Acad. Sci. Res.* **2014**, *2* (3), 42–53.

(71) Nagaraj, P.; Aradhana, N.; Shivakumar, A.; Shrestha, A. K.; k Gowda, A. Spectrophotometric Method for the Determination of Chromium (VI) in Water Samples. *Environ. Monit. Assess.* **2009**, *157* (1–4), 575–582. https://doi.org/10.1007/s10661-008-0557-2.

(72) Bansal et al, V. High Performance Liquid Chromatography: A Short Review; 2010. https://doi.org/10.1234/jgpt.v2i5.208.

(73) Thammana, M. A Review on High Performance Liquid Chromatography (HPLC). *Res Rev J Pharm Anal RRJPA* **2016**, *5* (2), 22–28.

(74) Xiang, Y.; Liu, Y.; Lee, M. L. Ultrahigh Pressure Liquid Chromatography Using Elevated Temperature. *J. Chromatogr. A* **2006**, *1104* (1–2), 198–202. https://doi.org/10.1016/j.chroma.2005.11.118.

(75) Abidi, S. L. High-Performance Liquid Chromatography of Phosphatidic Acids and Related Polar Lipids. *J. Chromatogr. A* **1991**, *587* (2), 193–203. https://doi.org/10.1016/0021-9673(91)85156-A.

(76) Akan, J. C.; Sodipo, O. A.; Mohammed, Z.; Abdulrahman, F. I. Determination of Organochlorine, Organophosphorus and Pyrethroid Pesticide Residues in Water and Sediment Samples by High Performance Liquid Chromatography (HPLC) with UV/Visible Detector. *J Anal Bioanal Tech* **2014**, *5* (6).

(77) Parbhunath, O. L.; Rautenbach, F.; Davison, G.; Marnewick, J. L. Optimization and Validation of a Reverse-Phase High Performance Liquid Chromatography Assay with Ultra-Violet Detection for Measuring Total L-Ascorbic Acid in Food and Beverage Products. *J. Anal. Bioanal. Tech.* **2014**, *5* (4), 1.

(78) Szterk, A.; Roszko, M.; Najman, K.; Kruk, M.; Mroczek, E.; Zarodkiewicz, M.; Rogalski, M.; Waszkiewicz-Robak, B. Comparison of Various Detection Systems Coupled to High Performance Liquid Chromatography for Determination of Tocopherols in Meat. The Influence and Comparison of the Most Popular Sample Preparation Method. *J Anal Bioanal Tech S* **2013**, *2*, 2.

(79) Lories, I. B.; Mostafa, A. A.; Girges, M. A. High Performance Liquid Chromatography, TLC Densitometry, First Derivative and First Derivative Ratio Spectrophotometry for Determination of Rivaroxaban and Its Alkaline Degradates in Bulk Powder and Its Tablets. *J Chromatogr Sep Tech* **2013**, *4*, 1–6.

(80) Chierentin, L.; Salgado, H. R. N. Development and Validation of a Simple, Rapid and Stability-Indicating High Performance Liquid Chromatography Method for Quantification of Norfloxacin in a Pharmaceutical Product. *J Chromatogr Sep Tech* **2013**, *4* (2), 171–175.

(81) Srinivasarao et al, K. Validated Method Development for Estimation of Formoterol Fumarate and Mometasone Furoate in Metered Dose Inhalation Form by High Performance Liquid Chromatography. *J Anal Bioanal Tech* **2012**, *3* (7).

(82) Gugulothu, D. B.; Fernandes, C. B.; Patravale, V. B. A Versatile High Performance Liquid Chromatography Method for Simultaneous Determination of Three Curcuminoids in Pharmaceutical Dosage Forms. *Pharm Anal Acta* **2012**, *3* (4).

(83) Ying, L.-Y.; Jiang, H.-L.; Zhou, S.; Zhou, Y. Ionic Liquid as a Complexation and Extraction Medium Combined with High-Performance Liquid Chromatography in the Evaluation of Chromium(VI) and Chromium(III) Speciation in Wastewater Samples. *Microchem. J.* **2011**, *98* (2), 200–203. https://doi.org/10.1016/j.microc.2011.01.010.

(84) https://www.waters.com/waters/fr_FR/How-Does-High-Performance-Liquid-Chromatography-Work%3F/nav.htm?locale=fr_FR&cid=10049055 (accessed 2020 -04 -28).

(85) Wang, L.-L.; Wang, J.-Q.; Zheng, Z.-X.; Xiao, P. Cloud Point Extraction Combined with High-Performance Liquid Chromatography for Speciation of Chromium(III) and Chromium(VI) in Environmental Sediment Samples. *J. Hazard. Mater.* **2010**, *177* (1–3), 114–118. https://doi.org/10.1016/j.jhazmat.2009.12.003.

(86) Rakhunde, R.; Deshpande, L.; Juneja, H. D. Chemical Speciation of Chromium in Water: A Review. *Crit. Rev. Environ. Sci. Technol.* **2012**, *42* (7), 776–810. https://doi.org/10.1080/10643389.2010.534029.
(87) Syty, A.; Christensen, R. G.; Rains, T. C. Determination of Added Chromium(III) and Chromium(VI) in Natural Water by Ion-Pairing High-Performance Liquid Chromatography with Detection by Atomic Absorption Spectrometry. *J. Anal. At. Spectrom.* **1988**, *3* (1), 193. https://doi.org/10.1039/ja9880300193.
(88) https://sciencing.com/disadvantages-advantages-hplc-5911530.html (accessed 2020 -04 -10).
(89) https://www.sciencedirect.com/topics/biochemistry-genetics-and-molecular-biology/inductively-coupled-plasma (accessed 2020 -04 -10).
(90) Kamat, S. S.; Suryawanshi, R. P. Quantitative Analysis of Trace Elements in Herbal Tablets by ICP-MS. *J. Acad. Ind. Res. JAIR* **2015**, *3* (11), 577.
(91) Tokalıoğlu, Ş. Determination of Trace Elements in Commonly Consumed Medicinal Herbs by ICP-MS and Multivariate Analysis. *Food Chem.* **2012**, *134* (4), 2504–2508. https://doi.org/10.1016/j.foodchem.2012.04.093.
(92) Jia, L.-H.; Li, Y.; Li, Y.-Z. Determination of Wholesome Elements and Heavy Metals in Safflower (Carthamus Tinctorius L.) from Xinjiang and Henan by ICP-MS/ICP-AES. *J. Pharm. Anal.* **2011**, *1* (2), 100–103. https://doi.org/10.1016/S2095-1779(11)70017-X.
(93) Beauchemin, D. Inductively Coupled Plasma Mass Spectrometry Methods. In *Encyclopedia of Spectroscopy and Spectrometry*; Elsevier, 2017; pp 236–245. https://doi.org/10.1016/B978-0-12-409547-2.11222-3.
(94) Holmes, L. Determination of Thorium by ICP-MS and ICP-OES. *Radiat. Prot. Dosimetry* **2001**, *97* (2), 117–122. https://doi.org/10.1093/oxfordjournals.rpd.a006647.
(95) Thomas, R. *Practical Guide to ICP-MS*; Practical spectroscopy; M. Dekker: New York, NY, 2004.
(96) https://www.agilent.com/cs/library/applications/5990-9366EN_AppNote_7700x_Cr.pdf (accessed 2020 -04 -10).
(97) Tikkanen, M. W. Development of a Drinking Water Regulation for Perchlorate in California. *Anal. Chim. Acta* **2006**, *567* (1), 20–25. https://doi.org/10.1016/j.aca.2006.03.087.
(98) Donard et al, O. F. X. Development of Analytical Procedures for Determination of Total Chromium by Quadrupole ICP-MS and High-Resolution ICP-MS, and Hexavalent Chromium by HPLC-ICP-MS, in Different Materials Used in the Automotive Industry. *Anal. Bioanal. Chem.* **2003**, *377* (4), 685–694. https://doi.org/10.1007/s00216-003-2133-5.
(99) Zhang, N.; Suleiman, J. S.; He, M.; Hu, B. Chromium(III)-Imprinted Silica Gel for Speciation Analysis of Chromium in Environmental Water Samples with ICP-MS Detection. *Talanta* **2008**, *75* (2), 536–543. https://doi.org/10.1016/j.talanta.2007.11.059.
(100) Sacher, F.; Raue, B.; Klinger, J.; Brauch, H.-J. Simultaneous Determination of Cr(III) and Cr(VI) in Ground and Drinking Waters by IC-ICP-MS. *Int. J. Environ. Anal. Chem.* **1999**, *74* (1–4), 191–201. https://doi.org/10.1080/03067319908031425.
(101) Long, X.; Miró, M.; Hansen, E. H. Universal Approach for Selective Trace Metal Determinations via Sequential Injection−Bead Injection−Lab-on-Valve Using Renewable Hydrophobic Bead Surfaces as Reagent Carriers. *Anal. Chem.* **2005**, *77* (18), 6032–6040. https://doi.org/10.1021/ac050710t.
(102) Singer Pressman, M. A.; Aldstadt, III, J. H. A Remote in Situ Monitor Based on Continuous Flow Analysis for the Quantitation of Sub-Micromolar Levels of Hexavalent Chromium in Natural Waters. *J. Environ. Monit.* **2005**, *7* (8), 809. https://doi.org/10.1039/b503754a.
(103) Bardiya, N.; Hwang, Y.-W.; Bae, J.-H. Interference of Thiosulfate during Colorimetric Analysis of Hexavalent Chromium Using 1,5-Diphenylcarbazide Method. *Anaerobe* **2004**, *10* (1), 7–11. https://doi.org/10.1016/j.anaerobe.2003.10.001.

(104) Rajesh, N.; Agarwal, V.; Aarthy, S. Solid Phase Extraction of Chromium (VI) from Aqueous Solutions by Adsorption of Its Diphenylcarbazide Complex on an Alumina Column. *Can. J. Chem. Eng.* **2008**, *86* (1), 72–76. https://doi.org/10.1002/cjce.20006.
(105) Sanchez-Hachair, A.; Hofmann, A. Hexavalent Chromium Quantification in Solution: Comparing Direct UV–Visible Spectrometry with 1,5-Diphenylcarbazide Colorimetry. *Comptes Rendus Chim.* **2018**, *21* (9), 890–896. https://doi.org/10.1016/j.crci.2018.05.002.
(106) Stancheva, K. A.; Bogdanov, B. I.; Georgiev, D. P.; Hristov, Y. H.; Markovska, I. G. Spectrophotometric Determination of Hexavalent Chromium Content in Commercial Cement – an Assessment of the Optimal Conditions for the Analysis of Chromium (VI). *Eurasian J Anal Chem* **2013**, 8.
(107) Lazo, P. Determination of Cr (VI) in Environmental Samples Evaluating Cr (VI) Impact in a Contaminated Area. *J. Int. Environ. Appl. Sci.* **2009**, *4* (2), 207–213.
(108) Memon, J.-R.; Memon, S. Q.; Bhanger, M. I.; Khuhawar, M. Y. Use of Modified Sorbent for the Separation and Preconcentration of Chromium Species from Industrial Waste Water. *J. Hazard. Mater.* **2009**, *163* (2–3), 511–516. https://doi.org/10.1016/j.jhazmat.2008.07.001.
(109) Freidberg, J. P. *Plasma Physics and Fusion Energy*; Cambridge university press, 2008.
(110) Chen, F. F. *Introduction to Plasma Physics and Controlled Fusion*; Springer, 1984; Vol. 1.
(111) d'Agostino, R.; Favia, P.; Kawai, Y.; Ikegami, H.; Sato, N.; Arefi-Khonsari, F. *Advanced Plasma Technology*; John Wiley & Sons, 2008.
(112) Bogaerts, A.; Neyts, E.; Gijbels, R.; van der Mullen, J. Gas Discharge Plasmas and Their Applications. *Spectrochim. Acta Part B At. Spectrosc.* **2002**, *57* (4), 609–658. https://doi.org/10.1016/S0584-8547(01)00406-2.
(113) Petitpas, G.; Rollier, J.; Darmon, A.; Gonzalezaguilar, J.; Metkemeijer, R.; Fulcheri, L. A Comparative Study of Non-Thermal Plasma Assisted Reforming Technologies. *Int. J. Hydrog. Energy* **2007**, *32* (14), 2848–2867. https://doi.org/10.1016/j.ijhydene.2007.03.026.
(114) von Woedtke, Th.; Reuter, S.; Masur, K.; Weltmann, K.-D. Plasmas for Medicine. *Phys. Rep.* **2013**, *530* (4), 291–320. https://doi.org/10.1016/j.physrep.2013.05.005.
(115) Foster, J. E. Plasma-Based Water Purification: Challenges and Prospects for the Future. *Phys. Plasmas* **2017**, *24* (5), 055501.
(116) Fridman, A.; Gutsol, A.; Cho, Y. I. Non-Thermal Atmospheric Pressure Plasma. In *Advances in Heat Transfer*; Elsevier, 2007; Vol. 40, pp 1–142. https://doi.org/10.1016/S0065-2717(07)40001-6.
(117) Nijdam, S.; van Veldhuizen, E.; Bruggeman, P.; Ebert, U. An Introduction to Nonequilibrium Plasmas at Atmospheric Pressure. *Plasma Chem. Catal. Gases Liq.* **2012**, 1–44.
(118) Griem, H. R. High-Density Corrections in Plasma Spectroscopy. *Phys. Rev.* **1962**, *128* (3), 997.
(119) Calzada, M. D.; Moisan, M.; Gamero, A.; Sola, A. Experimental Investigation and Characterization of the Departure from Local Thermodynamic Equilibrium along a Surface-Wave-Sustained Discharge at Atmospheric Pressure. *J. Appl. Phys.* **1996**, *80* (1), 46–55.
(120) Boulos, M. I.; Fauchais, P.; Pfender, E. *Thermal Plasmas: Fundamentals and Applications*; Springer Science & Business Media, 2013.
(121) Firdaus Zainal, M. N.; Redzuan, N.; Misnal, M. F. I. Brief Review: Cold Plasma. *J. Teknol.* **2015**, *74* (10). https://doi.org/10.11113/jt.v74.4834.
(122) Czernichowski, A. Gliding Arc: Applications to Engineering and Environment Control. *Pure Appl. Chem.* **1994**, *66* (6), 1301–1310. https://doi.org/10.1351/pac199466061301.
(123) Conrads, H.; Schmidt, M. Plasma Generation and Plasma Sources. *Plasma Sources Sci. Technol.* **2000**, *9* (4), 441–454. https://doi.org/10.1088/0963-0252/9/4/301.
(124) Gomez, E.; Rani, D. A.; Cheeseman, C. R.; Deegan, D.; Wise, M.; Boccaccini, A. R. Thermal Plasma Technology for the Treatment of Wastes: A Critical Review. *J. Hazard. Mater.* **2009**, *161* (2–3), 614–626. https://doi.org/10.1016/j.jhazmat.2008.04.017.

(125) Smith, R. W.; Wei, D.; Apelian, D. Thermal Plasma Materials Processing and Applications and Opportunities. *Plasma Chem. Plasma Process.* **1989**, *9* (S1), 135S-165S. https://doi.org/10.1007/BF01015877.
(126) Sato, M. Degradation of Organic Contaminants in Water by Plasma. **2009**, 7.
(127) Nehra, V.; Kumar, A.; Dwivedi, H. K. Atmospheric Non-Thermal Plasma Sources. *Int. J. Eng.* **2008**, *2* (1), 53–68.
(128) Denes, F. Macromolecular Plasma-Chemistry: An Emerging Field of Polymer Science. *Prog. Polym. Sci.* **2004**, *29* (8), 815–885. https://doi.org/10.1016/j.progpolymsci.2004.05.001.
(129) Samir, U.; Wright Jr, K. H.; Stone, N. H. The Expansion of a Plasma into a Vacuum: Basic Phenomena and Processes and Applications to Space Plasma Physics. *Rev. Geophys.* **1983**, *21* (7), 1631–1646.
(130) Dyakonov, M. I.; Shur, M. S. Plasma Wave Electronics: Novel Terahertz Devices Using Two Dimensional Electron Fluid. *IEEE Trans. Electron Devices* **1996**, *43* (10), 1640–1645.
(131) Fridman, A. *Plasma Chemistry*; Cambridge University Press, 2008.
(132) Haertel, B.; Woedtke, T. von; Weltmann, K.-D.; Lindequist, U. Non-Thermal Atmospheric-Pressure Plasma Possible Application in Wound Healing. *Biomol. Ther.* **2014**, *22* (6), 477–490. https://doi.org/10.4062/biomolther.2014.105.
(133) Vandenbroucke, A. M.; Morent, R.; De Geyter, N.; Leys, C. Non-Thermal Plasmas for Non-Catalytic and Catalytic VOC Abatement. *J. Hazard. Mater.* **2011**, *195*, 30–54. https://doi.org/10.1016/j.jhazmat.2011.08.060.
(134) Lukes et al, P. Non-Thermal Plasma Induced Decomposition of 2-Chlorophenol in Water. *Acta Phys. Slovaca* **2003**, *53* (6), 423–428.
(135) Foster, J.; Sommers, B. S.; Gucker, S. N.; Blankson, I. M.; Adamovsky, G. Perspectives on the Interaction of Plasmas with Liquid Water for Water Purification. *IEEE Trans. Plasma Sci.* **2012**, *40* (5), 1311–1323.
(136) Brault, P.; Abraham, M.; Bensebaa, A.; Aubry, O.; Hong, D.; Rabat, H.; Magureanu, M. Insight into Plasma Degradation of Paracetamol in Water Using a Reactive Molecular Dynamics Approach. *J. Appl. Phys.* **2021**, *129* (18), 183304. https://doi.org/10.1063/5.0043944.
(137) Magureanu, M.; Piroi, D.; Mandache, N. B.; David, V.; Medvedovici, A.; Parvulescu, V. I. Degradation of Pharmaceutical Compound Pentoxifylline in Water by Non-Thermal Plasma Treatment. *Water Res.* **2010**, *44* (11), 3445–3453. https://doi.org/10.1016/j.watres.2010.03.020.
(138) Tian, T.; Rabat, H.; Magureanu, M.; Aubry, O.; Hong, D. Electrical Investigation of a Pin-to-Plane Dielectric Barrier Discharge in Contact with Water. *J. Appl. Phys.* **2021**, *130* (11), 113301. https://doi.org/10.1063/5.0056654.
(139) Hamdan, A.; Gagnon, C.; Aykul, M.; Profili, J. Characterization of a Microwave Plasma Jet (TIAGO) In-contact with Water: Application in Degradation of Methylene Blue Dye. *Plasma Process. Polym.* **2020**, *17* (3), 1900157. https://doi.org/10.1002/ppap.201900157.
(140) Diamond, J.; Profili, J.; Hamdan, A. Characterization of Various Air Plasma Discharge Modes in Contact with Water and Their Effect on the Degradation of Reactive Dyes. *Plasma Chem. Plasma Process.* **2019**, *39* (6), 1483–1498. https://doi.org/10.1007/s11090-019-10014-9.
(141) Bruggeman, P.; Leys, C. Non-Thermal Plasmas in and in Contact with Liquids. *J. Phys. Appl. Phys.* **2009**, *42* (5), 053001. https://doi.org/10.1088/0022-3727/42/5/053001.
(142) Bruggeman, P. J.; Kushner, M. J.; Locke, B. R.; Gardeniers, J. G. E.; Graham, W. G.; Graves, D. B.; Hofman-Caris, R. C. H. M.; Maric, D.; Reid, J. P.; Ceriani, E.; Fernandez Rivas, D.; Foster, J. E.; Garrick, S. C.; Gorbanev, Y.; Hamaguchi, S.; Iza, F.; Jablonowski, H.; Klimova, E.; Kolb, J.; Krcma, F.; Lukes, P.; Machala, Z.; Marinov, I.; Mariotti, D.; Mededovic Thagard, S.; Minakata, D.; Neyts, E. C.; Pawlat, J.; Petrovic, Z. L.; Pflieger, R.; Reuter, S.; Schram, D. C.; Schröter, S.; Shiraiwa, M.; Tarabová, B.; Tsai, P. A.; Verlet, J. R. R.; von Woedtke, T.; Wilson, K. R.; Yasui, K.; Zvereva, G. Plasma–Liquid Interactions: A Review and Roadmap. *Plasma Sources Sci. Technol.* **2016**, *25* (5), 053002. https://doi.org/10.1088/0963-0252/25/5/053002.

(143) Vanraes, P.; Nikiforov, A. Y.; Leys, C. Electrical Discharge in Water Treatment Technology for Micropollutant Decomposition. *Plasma Sci. Technol. Phys. States Chem. React.* **2016**, *429*.
(144) Bruggeman et al, P. Characteristics of Atmospheric Pressure Air Discharges with a Liquid Cathode and a Metal Anode. *Plasma Sources Sci. Technol.* **2008**, *17* (2), 025012. https://doi.org/10.1088/0963-0252/17/2/025012.
(145) Titov, V. A.; Rybkin, V. V.; Smirnov, S. A.; Kulentsan, A. N.; Choi, H.-S. Experimental and Theoretical Studies on the Characteristics of Atmospheric Pressure Glow Discharge with Liquid Cathode. *Plasma Chem. Plasma Process.* **2006**, *26* (6), 543–555.
(146) Lisitsyn, I. V.; Nomlyama, H.; Katsuki, S.; Akiyama, H. Thermal Processes in a Streamer Discharge in Water. *IEEE Trans. Dielectr. Electr. Insul.* **1999**, *6* (3), 351–356. https://doi.org/10.1109/94.775622.
(147) An, W.; Baumung, K.; Bluhm, H. Underwater Streamer Propagation Analyzed from Detailed Measurements of Pressure Release. *J. Appl. Phys.* **2007**, *101* (5), 053302.
(148) Marinov, I.; Guaitella, O.; Rousseau, A.; Starikovskaia, S. M. Modes of Underwater Discharge Propagation in a Series of Nanosecond Successive Pulses. *J. Phys. Appl. Phys.* **2013**, *46* (46), 464013. https://doi.org/10.1088/0022-3727/46/46/464013.
(149) Pootawang, P. Solution Plasma Synthesis and Characteristic for Mesoporous Silica and Metal Nanoparticles System. PhD Thesis, Dissertation, Nagoya University, Nagoya, 2011.
(150) Siefermann, K. R.; Liu, Y.; Lugovoy, E.; Link, O.; Faubel, M.; Buck, U.; Winter, B.; Abel, B. Binding Energies, Lifetimes and Implications of Bulk and Interface Solvated Electrons in Water. *Nat. Chem.* **2010**, *2* (4), 274.
(151) Lukes, P.; Locke, B. R. Plasmachemical Oxidation Processes in a Hybrid Gas–Liquid Electrical Discharge Reactor. *J. Phys. Appl. Phys.* **2005**, *38* (22), 4074.
(152) Gao, J.; Wang, X.; Hu, Z.; Deng, H.; Hou, J.; Lu, X.; Kang, J. Plasma Degradation of Dyes in Water with Contact Glow Discharge Electrolysis. *Water Res.* **2003**, *37* (2), 267–272. https://doi.org/10.1016/S0043-1354(02)00273-7.
(153) Magureanu, M.; Piroi, D.; Gherendi, F.; Mandache, N. B.; Parvulescu, V. Decomposition of Methylene Blue in Water by Corona Discharges. *Plasma Chem. Plasma Process.* **2008**, *28* (6), 677–688. https://doi.org/10.1007/s11090-008-9155-x.
(154) Secu, L.; Magureanu, M.; Mandache, N. B.; Parvulescu, V. I. Decomposition of Methylene Blue in Water by Corona Discharges. In *Proc. 28th Int. Conf. on Phenomena in Ionized Gases (Prague, Czech Republic)*; 2007; pp 1348–1.
(155) Locke, B. R.; Sato, M.; Sunka, P.; Hoffmann, M. R.; Chang, J.-S. Electrohydraulic Discharge and Nonthermal Plasma for Water Treatment. *Ind. Eng. Chem. Res.* **2006**, *45* (3), 882–905. https://doi.org/10.1021/ie050981u.
(156) Lesaint, O. Propagation of Positive Discharges in Long Liquid Gaps. In *ICDL'96. 12th International Conference on Conduction and Breakdown in Dielectric Liquids*; IEEE: Roma, Italy, 1996; pp 161–166. https://doi.org/10.1109/ICDL.1996.565406.
(157) Hebner, R. E.; Kelley, E. F.; Forster, E. O.; Fitzpatrick, G. J. Observation of Prebreakdown and Breakdown Phenomena in Liquid Hydrocarbons. *J. Electrost.* **1982**, *12*, 265–283. https://doi.org/10.1016/0304-3886(82)90093-6.
(158) Sun, A.; Huo, C.; Zhuang, J. Formation Mechanism of Streamer Discharges in Liquids: A Review. *High Volt.* **2016**, *1* (2), 74–80.
(159) Nomura, S.; Mukasa, S.; Toyota, H.; Miyake, H.; Yamashita, H.; Maehara, T.; Kawashima, A.; Abe, F. Characteristics of In-Liquid Plasma in Water under Higher Pressure than Atmospheric Pressure. *Plasma Sources Sci. Technol.* **2011**, *20* (3), 034012. https://doi.org/10.1088/0963-0252/20/3/034012.
(160) Lesaint, O.; Gournay, P.; Tobazeon, R. Investigations on Transient Currents Associated with Streamer Propagation in Dielectric Liquids. *IEEE Trans. Electr. Insul.* **1991**, *26* (4), 699–707. https://doi.org/10.1109/14.83692.

(161) Hebner, R. E. Measurement of Electrical Breakdown in Liquids. In *The Liquid State and Its Electrical Properties*; Kunhardt, E. E., Christophorou, L. G., Luessen, L. H., Eds.; NATO ASI Series; Springer US: Boston, MA, 1988; Vol. 193, pp 519–537. https://doi.org/10.1007/978-1-4684-8023-8_21.
(162) Korobeinikov, S. M.; Melekhov, A. V.; Besov, A. S. Breakdown Initiation in Water with the Aid of Bubbles. *High Temp.* **2002**, *40* (5), 652–659. https://doi.org/10.1023/A:1020420216579.
(163) Ishijima, T.; Sugiura, H.; Saito, R.; Toyoda, H.; Sugai, H. Efficient Production of Microwave Bubble Plasma in Water for Plasma Processing in Liquid. *Plasma Sources Sci. Technol.* **2010**, *19* (1), 015010. https://doi.org/10.1088/0963-0252/19/1/015010.
(164) Maehara, T.; Toyota, H.; Kuramoto, M.; Iwamae, A.; Tadokoro, A.; Mukasa, S.; Yamashita, H.; Kawashima, A.; Nomura, S. Radio Frequency Plasma in Water. *Jpn. J. Appl. Phys.* **2006**, *45* (11), 8864–8868. https://doi.org/10.1143/JJAP.45.8864.
(165) Kocik, M.; Dors, M.; Podlinski, J.; Mizeraczyk, J.; Kanazawa, S.; Ichiki, R.; Sato, T. Characterisation of Pulsed Discharge in Water. *Eur. Phys. J.-Appl. Phys.* **2013**, *64* (1).
(166) Lesaint, O.; Massala, G. Positive Streamer Propagation in Large Oil Gaps: Experimental Characterization of Propagation Modes. *IEEE Trans. Dielectr. Electr. Insul.* **1998**, *5* (3), 360–370. https://doi.org/10.1109/94.689425.
(167) Fujita, H.; Kanazawa, S.; Ohtani, K.; Komiya, A.; Kaneko, T.; Sato, T. Initiation Process and Propagation Mechanism of Positive Streamer Discharge in Water. *J. Appl. Phys.* **2014**, *116* (21), 213301. https://doi.org/10.1063/1.4902862.
(168) Lesaint, O. "Streamers" in Liquids: Relation with Practical High Voltage Insulation and Testing of Liquids. In *2008 IEEE International Conference on Dielectric Liquids*; IEEE: Futuroscope-Chasseneuil, 2008; pp 1–6. https://doi.org/10.1109/ICDL.2008.4622543.
(169) Lesaint, O. Prebreakdown Phenomena in Liquids: Propagation 'Modes' and Basic Physical Properties. *J. Phys. Appl. Phys.* **2016**, *49* (14), 144001. https://doi.org/10.1088/0022-3727/49/14/144001.
(170) Beroual, A.; Tobazeon, R. Prebreakdown Phenomena in Liquid Dielectrics. *IEEE Trans. Electr. Insul.* **1986**, *EI-21* (4), 613–627. https://doi.org/10.1109/TEI.1986.348967.
(171) Beroual, A.; Zahn, M.; Badent, A.; Kist, K.; Schwabe, A. J.; Yamashita, H.; Yamazawa, K.; Danikas, M.; Chadband, W. D.; Torshin, Y. Propagation and Structure of Streamers in Liquid Dielectrics. *IEEE Electr. Insul. Mag.* **1998**, *14* (2), 6–17. https://doi.org/10.1109/57.662781.
(172) Habib, M. A.; Islam, M. N.; Hosseini, S. H. R.; Akiyama, H. Physical and Chemical Effects of Underwater Discharge with a Variation in Solution Conductivity and Input Voltage. *DUET* **2017**, *3* (1), 6.
(173) Takai, O. Solution plasma processing (SPP). *Pure Appl. Chem.* **2008**, *80* (9), 2003–2011. https://doi.org/10.1351/pac200880092003.
(174) Bratescu, M. A.; Saito, N.; Takai, O. Redox Reactions in Liquid Plasma during Iron Oxide and Oxide-Hydroxide Nanoparticles Synthesis. *Curr. Appl. Phys.* **2011**, *11* (5), S30–S34. https://doi.org/10.1016/j.cap.2011.06.007.
(175) Rond, C.; Desse, J. M.; Fagnon, N.; Aubert, X.; Er, M.; Vega, A.; Duten, X. Time-Resolved Diagnostics of a Pin-to-Pin Pulsed Discharge in Water: Pre-Breakdown and Breakdown Analysis. *J. Phys. Appl. Phys.* **2018**, *51* (33), 335201. https://doi.org/10.1088/1361-6463/aad175.
(176) Rond, C.; Desse, J. M.; Fagnon, N.; Aubert, X.; Vega, A.; Duten, X. Influence of Applied Voltage and Electrical Conductivity on Underwater Pin-to-Pin Pulsed Discharge. *J. Phys. Appl. Phys.* **2019**, *52* (2), 025202. https://doi.org/10.1088/1361-6463/aae681.
(177) Rond, C.; Fagnon, N.; Vega, A.; Duten, X. Statistical Analysis of a Micro-Pulsed Electrical Discharge in Water. *J. Phys. Appl. Phys.* **2020**, *53* (33), 335204. https://doi.org/10.1088/1361-6463/ab8b03.
(178) Sunka, P.; Babický, V.; Clupek, M.; Lukes, P.; Simek, M.; Schmidt, J.; Cernák, M. Generation of Chemically Active Species by Electrical Discharges in Water. *Plasma Sources Sci. Technol.* **1999**, *8* (2), 258–265. https://doi.org/10.1088/0963-0252/8/2/006.

(179) Mozumder, A. *Fundamentals of Radiation Chemistry*; Elsevier, 1999.
(180) Itikawa, Y.; Mason, N. Cross Sections for Electron Collisions with Water Molecules. *J. Phys. Chem. Ref. Data* **2005**, *34* (1), 1–22. https://doi.org/10.1063/1.1799251.
(181) Yousfi, M.; Benabdessadok, M. D. Boltzmann Equation Analysis of Electron-molecule Collision Cross Sections in Water Vapor and Ammonia. *J. Appl. Phys.* **1996**, *80* (12), 6619–6630. https://doi.org/10.1063/1.363785.
(182) Zheng, W.; Jewitt, D.; Kaiser, R. I. Formation of Hydrogen, Oxygen, and Hydrogen Peroxide in Electron-irradiated Crystalline Water Ice. *Astrophys. J.* **2006**, *639* (1), 534–548. https://doi.org/10.1086/499231.
(183) Liu, Y.; Liu, D.; Zhang, J.; Sun, B.; Luo, S.; Zhang, H.; Guo, L.; Rong, M.; Kong, M. G. Fluid Model of Plasma–Liquid Interaction: The Effect of Interfacial Boundary Conditions and Henry's Law Constants. *AIP Adv.* **2021**, *11* (5), 055019. https://doi.org/10.1063/5.0042945.
(184) Joshi, R. P.; Thagard, S. M. Streamer-Like Electrical Discharges in Water: Part II. Environmental Applications. *Plasma Chem. Plasma Process.* **2013**, *33* (1), 17–49. https://doi.org/10.1007/s11090-013-9436-x.
(185) Yasui, K.; Tuziuti, T.; Iida, Y.; Mitome, H. Theoretical Study of the Ambient-Pressure Dependence of Sonochemical Reactions. *J. Chem. Phys.* **2003**, *119* (1), 346–356. https://doi.org/10.1063/1.1576375.
(186) Locke, B. R.; Thagard, S. M. Analysis and Review of Chemical Reactions and Transport Processes in Pulsed Electrical Discharge Plasma Formed Directly in Liquid Water. *Plasma Chem. Plasma Process.* **2012**, *32* (5), 875–917. https://doi.org/10.1007/s11090-012-9403-y.
(187) Garrett, B. C.; Dixon, D. A.; Camaioni, D. M.; Chipman, D. M.; Johnson, M. A.; Jonah, C. D.; Kimmel, G. A.; Miller, J. H.; Rescigno, T. N.; Rossky, P. J.; Xantheas, S. S.; Colson, S. D.; Laufer, A. H.; Ray, D.; Barbara, P. F.; Bartels, D. M.; Becker, K. H.; Bowen, K. H.; Bradforth, S. E.; Carmichael, I.; Coe, J. V.; Corrales, L. R.; Cowin, J. P.; Dupuis, M.; Eisenthal, K. B.; Franz, J. A.; Gutowski, M. S.; Jordan, K. D.; Kay, B. D.; LaVerne, J. A.; Lymar, S. V.; Madey, T. E.; McCurdy, C. W.; Meisel, D.; Mukamel, S.; Nilsson, A. R.; Orlando, T. M.; Petrik, N. G.; Pimblott, S. M.; Rustad, J. R.; Schenter, G. K.; Singer, S. J.; Tokmakoff, A.; Wang, L.-S.; Zwier, T. S. Role of Water in Electron-Initiated Processes and Radical Chemistry: Issues and Scientific Advances. *Chem. Rev.* **2005**, *105* (1), 355–390. https://doi.org/10.1021/cr030453x.
(188) Pastina, B.; LaVerne, J. A. Effect of Molecular Hydrogen on Hydrogen Peroxide in Water Radiolysis. *J. Phys. Chem. A* **2001**, *105* (40), 9316–9322. https://doi.org/10.1021/jp012245j.
(189) Locke, B. R.; Shih, K.-Y. Review of the Methods to Form Hydrogen Peroxide in Electrical Discharge Plasma with Liquid Water. *Plasma Sources Sci. Technol.* **2011**, *20* (3), 034006. https://doi.org/10.1088/0963-0252/20/3/034006.
(190) Pettine, M.; Campanella, L.; Millero, F. J. Reduction of Hexavalent Chromium by H2O2 in Acidic Solutions. *Environ. Sci. Technol.* **2002**, *36* (5), 901–907. https://doi.org/10.1021/es010086b.
(191) Chandana, L.; Lakshminarayana, B.; Subrahmanyam, Ch. Influence of Hydrogen Peroxide on the Simultaneous Removal of Cr(VI) and Methylene Blue from Aqueous Medium under Atmospheric Pressure Plasma Jet. *J. Environ. Chem. Eng.* **2015**, *3* (4), 2760–2767. https://doi.org/10.1016/j.jece.2015.09.030.
(192) Harianti, A. R.; Saksono, N. Application of Plasma Electrolysis Method for Simultaneous Phenol and Cr(VI) Wastewater Degradation Using Na2SO4 Electrolyte; Jakarta, Indonesia, 2017; p 020041. https://doi.org/10.1063/1.5011898.
(193) Zhang, C.; Sun, Y.; Yu, Z.; Zhang, G.; Feng, J. Simultaneous Removal of Cr(VI) and Acid Orange 7 from Water Solution by Dielectric Barrier Discharge Plasma. *Chemosphere* **2018**, *191*, 527–536. https://doi.org/10.1016/j.chemosphere.2017.10.087.
(194) Shutov, D. A.; Sungurova, A. V.; Smirnova, K. V.; Rybkin, V. V. Kinetic Features of Chromium (VI) Reduction and Phenol Degradation in Aqueous Solution by Treatment in Atmospheric-Pressure Air Direct-Current Discharge. *High Energy Chem.* **2018**, *52* (1), 95–98.

(195) Bobkova, E. S.; Sungurova, A. V.; Rybkin, V. V. Reduction of Chromium(VI) in Aqueous Solution by Treatment with Direct-Current Discharge at Atmospheric-Pressure in Air. *High Energy Chem.* **2016**, *50* (3), 209–212. https://doi.org/10.1134/S0018143916030048.
(196) Chen, Z.; Ponraj, S. B.; Dai, X. J. Reduction of Aqueous Chromium (VI) by Plasma Treatment of Wastewater.
(197) Jamróz, P.; Gręda, K.; Pohl, P.; Żyrnicki, W. Atmospheric Pressure Glow Discharges Generated in Contact with Flowing Liquid Cathode: Production of Active Species and Application in Wastewater Purification Processes. *Plasma Chem. Plasma Process.* **2014**, *34* (1), 25–37. https://doi.org/10.1007/s11090-013-9503-3.
(198) Anderson, A. R.; Farhataziz. 60Co Radiolysis of Potassium Dichromate in Acid Solution. *Trans. Faraday Soc.* **1963**, *59*, 1299. https://doi.org/10.1039/tf9635901299.
(199) Van Niekerk, W.; Pienaar, J. J.; Lachmann, G.; Van Eldik, R.; Hamza, M. A Kinetic and Mechanistic Study of the Chromium (VI) Reduction by Hydrogen Peroxide in Acidic Aqueous Solutions. *Water SA* **2019**, *33* (5). https://doi.org/10.4314/wsa.v33i5.184022.
(200) Https://Www.Behlke.Com/Pdf/301-03-Gsm.Pdf.
(201) Http://www.utc.fr/~avalle/dossiers-pdf/Incertitudes-version2002.PDF.
(202) Nguyen, T. S.; Rond, C.; Vega, A.; Duten, X.; Forget, S. Investigation of Hydrogen Peroxide Formation After Underwater Plasma Discharge. *Plasma Chem. Plasma Process.* **2020**, *40* (4), 955–969. https://doi.org/10.1007/s11090-020-10084-0.
(203) Inkson, B. J. Scanning Electron Microscopy (SEM) and Transmission Electron Microscopy (TEM) for Materials Characterization. In *Materials Characterization Using Nondestructive Evaluation (NDE) Methods*; Elsevier, 2016; pp 17–43. https://doi.org/10.1016/B978-0-08-100040-3.00002-X.
(204) http://www.aps.org/publications/apsnews/201108/physicshistory.cfm (accessed 2020 -03 -31).
(205) Eisenberg, G. Colorimetric Determination of Hydrogen Peroxide. *Ind. Eng. Chem. Anal. Ed.* **1943**, *15* (5), 327–328. https://doi.org/10.1021/i560117a011.
(206) Vasko, C. A. *Microplasmas for Gas Phase Hydrogen Peroxide Production*; Technische Universiteit Eindhoven, 2015.
(207) Hadwan, M. H.; Ali, S. kadhum. New Spectrophotometric Assay for Assessments of Catalase Activity in Biological Samples. *Anal. Biochem.* **2018**, *542*, 29–33. https://doi.org/10.1016/j.ab.2017.11.013.
(208) Mahadevaiah; Abdul Galil, M. S.; Yogendra Kumar, M. S.; Sathish, M. A.; Nagendrappa, G. Simple Spectrophotometric Method for the Determination of Sulfur Dioxide by Its Decolorizing Effect on the Peroxovanadate Complex. *J. Anal. Chem.* **2008**, *63* (3), 239–243. https://doi.org/10.1134/S1061934808030088.
(209) Nogueira, R.; Oliveira, M.; Paterlini, W. Simple and Fast Spectrophotometric Determination of H2O2 in Photo-Fenton Reactions Using Metavanadate. *Talanta* **2005**, *66* (1), 86–91. https://doi.org/10.1016/j.talanta.2004.10.001.
(210) Http://Www.Physics.Hmc.Edu/Courses/P053/Manual/2008/Intro_to_uncert_v4.Pdf. 22.
(211) Https://Lcn.People.Uic.Edu/Classes/Che205s17/Docs/Che205s17_reading_12a.Pdf.
(212) Rond, C.; Fagnon, N.; Dufour, B.; Nguyen, S. T.; Vega, A.; Duten, X. Microsecond Electrical Breakdown in Water: Advances Using Emission Analysis and Cavitation Bubble Theory. *Molecules* **2022**, *27* (3), 662. https://doi.org/10.3390/molecules27030662.
(213) Dufour, B.; Fagnon, N.; Vega, A.; Duten, X.; Rond, C. Analysis of Discharge Regimes Obtained by Microsecond Underwater Electrical Breakdown in Regard to Energy Balance. *J. Phys. Appl. Phys.* **2021**, *54* (36), 365202. https://doi.org/10.1088/1361-6463/ac09ba.
(214) Kim, H.; Teramoto, Y.; Hirakawa, T.; Negishi, N.; Ogata, A. Microbubble Formation in Underwater Pulsed Streamer Discharge.
(215) Korobeynikov, S. M.; Melekhov, A. V. Microbubbles and Breakdown Initiation in Water. In *Proceedings of 2002 IEEE 14th International Conference on Dielectric Liquids. ICDL 2002 (Cat. No. 02CH37319)*; IEEE, 2002; pp 127–130.

(216) Hayashi, Y.; Takada, N.; Kanda, H.; Goto, M. Effect of Fine Bubbles on Electric Discharge in Water. *Plasma Sources Sci. Technol.* **2015**, *24* (5), 055023. https://doi.org/10.1088/0963-0252/24/5/055023.
(217) Gamaleev, V.; Britun, N.; Hori, M. Control and Stabilization of Centimeter Scale Glow Discharge in Ambient Air Using Pulse-Width Modulation. *IEEE Access* **2020**, *8*, 201486–201497. https://doi.org/10.1109/ACCESS.2020.3035534.
(218) Https://Digital.Library.Unt.Edu/Ark:/67531/Metadc829180/M2/1/High_res_d/1096464.Pdf.
(219) Namihira, T.; Yamaguchi, T.; Yamamoto, K.; Choi, J.; Kiyan, T.; Sakugawa, T.; Katsuki, S.; Akiyama, H. Characteristics of Pulsed Discharge Plasma in Water. In *2005 IEEE Pulsed Power Conference*; IEEE: Monterey, CA, USA, 2005; pp 1013–1016. https://doi.org/10.1109/PPC.2005.300473.
(220) Tao, S.; Guangsheng, S.; Ping, Y.; Jue, W.; Weiqun, Y.; Yaohong, S.; Shichang, Z. An Experimental Investigation of Repetitive Nanosecond-Pulse Breakdown in Air. *J. Phys. Appl. Phys.* **2006**, *39* (10), 2192–2197. https://doi.org/10.1088/0022-3727/39/10/030.
(221) Yang, Y.; Zhang, H.; Gong, C.; Huang, G.; Tu, Y. Effect of Pulse Width on Streamer Propagation of Underwater Corona Discharge. *Plasma Process. Polym.* **2018**, *15* (6), 1800028. https://doi.org/10.1002/ppap.201800028.
(222) Locke, B. R.; Shih, K.-Y. Review of the Methods to Form Hydrogen Peroxide in Electrical Discharge Plasma with Liquid Water. *Plasma Sources Sci. Technol.* **2011**, *20* (3), 034006. https://doi.org/10.1088/0963-0252/20/3/034006.
(223) Bruggeman, P. J.; Kushner, M. J.; Locke, B. R.; Gardeniers, J. G.; Graham, W. G.; Graves, D. B.; Hofman-Caris, R.; Maric, D.; Reid, J. P.; Ceriani, E. Plasma–Liquid Interactions: A Review and Roadmap. *Plasma Sources Sci. Technol.* **2016**, *25* (5), 053002.
(224) Lukeš, P. Water Treatment by Pulsed Streamer Corona Discharge. *Inst. Plasma Phys. CR Prague Czech Repub.* **2001**.
(225) Yang, Y.; Cho, Y. I.; Fridman, A. *Plasma Discharge in Liquid: Water Treatment and Applications*; CRC Press, 2017.
(226) Https://Www.Lenntech.Com/Processes/Disinfection/Chemical/Disinfectants-Hydrogen-Peroxide.Htm.
(227) Kirkpatrick, M. J.; Locke, B. R. Hydrogen, Oxygen, and Hydrogen Peroxide Formation in Aqueous Phase Pulsed Corona Electrical Discharge. *Ind. Eng. Chem. Res.* **2005**, *44* (12), 4243–4248. https://doi.org/10.1021/ie048807d.
(228) Joshi, A. A.; Locke, B. R.; Arce, P.; Finney, W. C. Formation of Hydroxyl Radicals, Hydrogen Peroxide and Aqueous Electrons by Pulsed Streamer Corona Discharge in Aqueous Solution. *J. Hazard. Mater.* **1995**, *41* (1), 3–30. https://doi.org/10.1016/0304-3894(94)00099-3.
(229) Mededovic, S.; Locke, B. R. Primary Chemical Reactions in Pulsed Electrical Discharge Channels in Water. *J. Phys. Appl. Phys.* **2007**, *40* (24), 7734–7746. https://doi.org/10.1088/0022-3727/40/24/021.
(230) Grymonpré, D. R.; Finney, W. C.; Clark, R. J.; Locke, B. R. Hybrid Gas−Liquid Electrical Discharge Reactors for Organic Compound Degradation. *Ind. Eng. Chem. Res.* **2004**, *43* (9), 1975–1989. https://doi.org/10.1021/ie030620j.
(231) Holzer, F.; Locke, B. R. Influence of High Voltage Needle Electrode Material on Hydrogen Peroxide Formation and Electrode Erosion in a Hybrid Gas–Liquid Series Electrical Discharge Reactor. *Plasma Chem. Plasma Process.* **2008**, *28* (1), 1–13. https://doi.org/10.1007/s11090-007-9107-x.
(232) Potocký, Š.; Saito, N.; Takai, O. Needle Electrode Erosion in Water Plasma Discharge. *Thin Solid Films* **2009**, *518* (3), 918–923. https://doi.org/10.1016/j.tsf.2009.07.172.
(233) Akolkar, R.; Sankaran, R. M. Charge Transfer Processes at the Interface between Plasmas and Liquids. *J. Vac. Sci. Technol. Vac. Surf. Films* **2013**, *31* (5), 050811. https://doi.org/10.1116/1.4810786.

(234) Goryachev, V. L.; Ufimtsev, A. A.; Khodakovskii, A. M. Mechanism of Electrode Erosion in Pulsed Discharges in Water with a Pulse Energy of ∼ 1 J. *Tech. Phys. Lett.* **1997**, *23* (5), 386–387. https://doi.org/10.1134/1.1261862.

(235) Lukes, P.; Clupek, M.; Babicky, V.; Sisrova, I.; Janda, V. The Catalytic Role of Tungsten Electrode Material in the Plasmachemical Activity of a Pulsed Corona Discharge in Water. *Plasma Sources Sci. Technol.* **2011**, *20* (3), 034011. https://doi.org/10.1088/0963-0252/20/3/034011.

(236) Mededovic, S.; Locke, B. Platinum Catalysed Decomposition of Hydrogen Peroxide in Aqueous-Phase Pulsed Corona Electrical Discharge. *Appl. Catal. B Environ.* **2006**, *67* (3–4), 149–159. https://doi.org/10.1016/j.apcatb.2006.05.001.

(237) Alteri, G. B.; Bonomo, M.; Decker, F.; Dini, D. Contact Glow Discharge Electrolysis: Effect of Electrolyte Conductivity on Discharge Voltage. *Catalysts* **2020**, *10* (10), 1104. https://doi.org/10.3390/catal10101104.

(238) Liu, Y.; Li, Z.; Luo, Q.; Han, Y.; Zhang, Q.; Lin, F. Comparison and Evaluation of Electrode Erosion Under High-Pulsed Current Discharges in Air and Water Mediums. *IEEE Trans. Plasma Sci.* **2016**, *44* (7), 1169–1177. https://doi.org/10.1109/TPS.2016.2578343.

(239) Lukeš, P.; Člupek, M.; Babický, V.; Šunka, P.; Skalný, J. D.; Štefečka, M.; Novák, J.; Málková, Z. Erosion of Needle Electrodes in Pulsed Corona Discharge in Water. *Czechoslov. J. Phys.* **2006**, *56* (S2), B916–B924. https://doi.org/10.1007/s10582-006-0304-2.

(240) Depetris-Wery, M.; Catonné, J.-C. Potentiels standards d'oxydo-réduction en solution aqueuse - Application aux traitements de surface en voie humide. *Étude Propr. Métaux* **2015**. https://doi.org/10.51257/a-v1-m1430.

(241) Anik, M.; Osseo-Asare, K. Effect of PH on the Anodic Behavior of Tungsten. *J. Electrochem. Soc.* **2002**, *149* (6), B224. https://doi.org/10.1149/1.1471544.

(242) Matsuoka, K.; Sakamoto, S.; Nakato, K.; Hamada, A.; Itoh, Y. Degradation of Polymer Electrolyte Fuel Cells under the Existence of Anion Species. *J. Power Sources* **2008**, *179* (2), 560–565. https://doi.org/10.1016/j.jpowsour.2008.01.027.

(243) Ceccato, P. Filamentary Plasma Discharge inside Water: Initiation and Propagation of a Plasma in a Dense Medium. **2009**.

(244) Wang, S.; Peng, Y. Natural Zeolites as Effective Adsorbents in Water and Wastewater Treatment. *Chem. Eng. J.* **2010**, *156* (1), 11–24. https://doi.org/10.1016/j.cej.2009.10.029.

(245) Kachoosangi, R. T.; Compton, R. G. Voltammetric Determination of Chromium(VI) Using a Gold Film Modified Carbon Composite Electrode. *Sens. Actuators B Chem.* **2013**, *178*, 555–562. https://doi.org/10.1016/j.snb.2012.12.122.

(246) Https://Vminteq.Lwr.Kth.Se/.

(247) Buxton, G. V.; Greenstock, C. L.; Helman, W. P.; Ross, A. B. Critical Review of Rate Constants for Reactions of Hydrated Electrons, Hydrogen Atoms and Hydroxyl Radicals (·OH/·O⁻ in Aqueous Solution. *J. Phys. Chem. Ref. Data* **1988**, *17* (2), 513–886. https://doi.org/10.1063/1.555805.

(248) Pivovarov, O.; Derkach, T.; Department of Industrial Pharmacy, Kyiv National University of Technologies and Design, 2, Nemirovicha-Danchenko St., 01011 Kyiv, Ukraine; Skiba, M.; Department of Inorganic Substances and Ecology, Ukrainian State University of Chemical Technology, 8, Gagarina Ave., 49005 Dnipro, Ukraine. Low-Pressure Discharge Plasma Treatment of Aqueous Solutions with Mn, Cr and Fe. *Chem. Chem. Technol.* **2019**, *13* (3), 317–325. https://doi.org/10.23939/chcht13.03.317.

(249) Jiang, B.; Zheng, J.; Qiu, S.; Wu, M.; Zhang, Q.; Yan, Z.; Xue, Q. Review on Electrical Discharge Plasma Technology for Wastewater Remediation. *Chem. Eng. J.* **2014**, *236*, 348–368. https://doi.org/10.1016/j.cej.2013.09.090.

(250) Thomas, D. K.; Maass, O. ELECTROLYTIC CONDUCTANCE IN HYDROGEN PEROXIDE – WATER MIXTURES: PART II. SOME MONOBASIC AND DIBASIC ACIDS. *Can. J. Chem.* **1958**, *36* (5), 744–749. https://doi.org/10.1139/v58-108.

(251) Fogel, Norman.; Tai, J. M. Jen.; Yarborough, Jean. Chromium(III) Sulfate in Acid Sulfate Solutions. *J. Am. Chem. Soc.* **1962**, *84* (7), 1145–1151. https://doi.org/10.1021/ja00866a017.
(252) Baroch, P.; Potocky, S.; Saito, N. Generation of Plasmas in Water: Utilization of a High-Frequency, Low-Voltage Bipolar Pulse Power Supply with Impedance Control. *Plasma Sources Sci. Technol.* **2011**, *20* (3), 034017. https://doi.org/10.1088/0963-0252/20/3/034017.
(253) Chang, H.; Hsu, C. Plasmas in Saline Solutions Sustained Using Rectified Ac Voltages: Polarity and Frequency Effects on the Discharge Behaviour. *J. Phys. Appl. Phys.* **2012**, *45* (25), 255203. https://doi.org/10.1088/0022-3727/45/25/255203.
(254) Chang, H.; Hsu, C. Diagnostic Studies of Ac-Driven Plasmas in Saline Solutions: The Effect of Frequency on the Plasma Behavior. *Plasma Sources Sci. Technol.* **2011**, *20* (4), 045001. https://doi.org/10.1088/0963-0252/20/4/045001.
(255) Ruma; Lukes, P.; Aoki, N.; Spetlikova, E.; Hosseini, S. H. R.; Sakugawa, T.; Akiyama, H. Effects of Pulse Frequency of Input Power on the Physical and Chemical Properties of Pulsed Streamer Discharge Plasmas in Water. *J. Phys. Appl. Phys.* **2013**, *46* (12), 125202. https://doi.org/10.1088/0022-3727/46/12/125202.
(256) Lu, X.; Kolb, J. F.; Xiao, S.; Laroussi, M.; Schoenbach, K. H.; Schamiloglu, E. Dielectric Strength of Sub-Millimeter Water Gaps Subjected to Microsecond and Sub-Microsecond Voltage Pulses. In *2005 IEEE Pulsed Power Conference*; IEEE: Monterey, CA, USA, 2005; pp 600–603. https://doi.org/10.1109/PPC.2005.300730.
(257) Kawano, S.; Wada, K.; Kakuta, T.; Takaki, K.; Satta, N.; Takahashi, K. Influence of Pulse Width on Decolorization Efficiency of Organic Dye by Discharge inside Bubble in Water. *J. Phys. Conf. Ser.* **2013**, *441*, 012007. https://doi.org/10.1088/1742-6596/441/1/012007.
(258) Tamaribuchi, H.; Wang, D.; Namihira, T.; Katsuki, S.; Akiyama, H. Effect of Pulse Width on Generation of Ozone by Pulsed Streamer Discharge. In *2007 16th IEEE International Pulsed Power Conference*; IEEE: Albuquerque, NM, 2007; pp 407–410. https://doi.org/10.1109/PPPS.2007.4651869.
(259) Mizuno, T.; Akimoto, T.; Azumi, K.; Ohmori, T.; Aoki, Y.; Takahashi, A. Hydrogen Evolution by Plasma Electrolysis in Aqueous Solution. *Jpn. J. Appl. Phys.* **2005**, *44* (1A), 396–401. https://doi.org/10.1143/JJAP.44.396.
(260) Bokare, A. D.; Choi, W. Advanced Oxidation Process Based on the Cr(III)/Cr(VI) Redox Cycle. *Environ. Sci. Technol.* **2011**, *45* (21), 9332–9338. https://doi.org/10.1021/es2021704.
(261) Http://Studylib.Net/Doc/7641234/Permanganate-Oxalate-Titration.
(262) Oh, J.-S.; Szili, E. J.; Ogawa, K.; Short, R. D.; Ito, M.; Furuta, H.; Hatta, A. UV–Vis Spectroscopy Study of Plasma-Activated Water: Dependence of the Chemical Composition on Plasma Exposure Time and Treatment Distance. *Jpn. J. Appl. Phys.* **2018**, *57* (1), 0102B9. https://doi.org/10.7567/JJAP.57.0102B9.
(263) Mai-Prochnow, A.; Zhou, R.; Zhang, T.; Ostrikov, K. (Ken); Mugunthan, S.; Rice, S. A.; Cullen, P. J. Interactions of Plasma-Activated Water with Biofilms: Inactivation, Dispersal Effects and Mechanisms of Action. *Npj Biofilms Microbiomes* **2021**, *7* (1), 11. https://doi.org/10.1038/s41522-020-00180-6.
(264) Gorbanev, Y.; Privat-Maldonado, A.; Bogaerts, A. Analysis of Short-Lived Reactive Species in Plasma–Air–Water Systems: The Dos and the Do Nots. *Anal. Chem.* **2018**, *90* (22), 13151–13158. https://doi.org/10.1021/acs.analchem.8b03336.
(265) Oinuma, G.; Nayak, G.; Du, Y.; Bruggeman, P. J. Controlled Plasma–Droplet Interactions: A Quantitative Study of OH Transfer in Plasma–Liquid Interaction. *Plasma Sources Sci. Technol.* **2020**, *29* (9), 095002. https://doi.org/10.1088/1361-6595/aba988.

Abstract

This project aims to develop a green method for reducing Cr(VI) in an aqueous solution and a high-performance and economical technology to determine [Cr(VI)].

First, we develop a plasma-liquid process to efficiently reduce Cr(VI). It consists of a pin-to-pin electrodes system under high pulsed voltage (about 9 kV, 500 µs, 50 Hz) immersed in the solution to be treated. The experimental setup has been first tested in water to study the production of H_2O_2. Then the reduction of Cr(VI) is studied by varying different physical parameters (applied voltage, inter-electrode distance, applied frequency, and pulse duration). The reduction of Cr(VI) increases with the increase of injected energy (by increasing applied voltage), the number of pulses, the number of breakdowns and the pulse duration.

The second objective of this thesis is to develop an innovative method for measuring Cr(VI) at low concentrations. The results show that using this method allows analyzing the concentration of Cr(VI) in real-time and in-situ during the treatment process. Moreover, this method can also define when Cr(VI) is completely reduced.

Resume

Ce projet vise à développer une méthode verte pour réduire le Cr(VI) dans une solution aqueuse et une technologie performante et économique pour déterminer le [Cr(VI)].

Tout d'abord, nous développons un procédé plasma-liquide pour réduire efficacement le Cr(VI). Il consiste en un système d'électrodes pin-to-pin sous haute tension pulsée (environ 9 kV, 500 µs, 50 Hz) immergé dans la solution à traiter. Le dispositif expérimental a d'abord été testé dans l'eau pour étudier la production de H_2O_2. Ensuite, la réduction du Cr(VI) est étudiée en faisant varier différents paramètres physiques (tension appliquée, distance inter-électrodes, fréquence appliquée et durée d'impulsion). La réduction du Cr(VI) augmente avec l'augmentation de l'énergie injectée (en augmentant la tension appliquée), le nombre d'impulsions, le nombre de pannes et la durée des impulsions.

Le deuxième objectif de cette thèse est de développer une méthode innovante pour mesurer le Cr(VI) à de faibles concentrations. Les résultats montrent que l'utilisation de cette méthode permet d'analyser la concentration de Cr(VI) en temps réel et in-situ pendant le processus de traitement. De plus, cette méthode permet également de définir le moment où le Cr(VI) est complètement réduit.